Trinity College Dublin
Coláiste na Tríonóide, Baile Átha Cliath
The University of Dublin

Investigating Molluscum Contagiosum Virus Protein MC009 as a Novel Inhibitor of Human Innate Immune Signalling

This thesis is submitted to Trinity College Dublin, The University of Dublin, for the degree of Doctor of Philosophy (Ph.D.)

By

Aleksandra Kusiak

16306153

Supervisor: Dr. Gareth Brady

School of Medicine

March 2024

Declaration

I, Aleksandra Kusiak, declare that this thesis has not been submitted as an exercise for a degree at this or any other university and it is entirely my own work.

I agree to deposit this thesis in the University's open access institutional repository or allow the library to do so on my behalf, subject to Irish Copyright Legislation and Trinity College Library conditions of use and acknowledgement.

I consent to the examiner retaining a copy of the thesis beyond the examining period, should they so wish (EU GDPR May 2018).

I have read and understood the plagiarism provisions in the General Regulations of the University Calendar for the current year, found at http://www.tcd.ie/calendar.

I have also read and understood the guide and completed the 'Ready Steady Write' Tutorial on avoiding plagiarism, located at https://libguides.tcd.ie/academic-integrity/ready-steady-write.

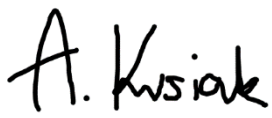

PhD Candidate Signature

Table of Contents

Declaration ..... **ii**

Acknowledgements ..... **vi**

Abstract ..... **viii**

Lay Abstract ..... **x**

Project Outputs ..... **xii**

Abbreviations ..... **xiv**

List of Figures and Tables ..... **xviii**

Chapter 1: Introduction **1**

1.1 Molluscum contagiosum virus **2**

1.1.1 Poxviruses 2

1.1.2 Molluscum contagiosum 3

1.1.3 Molluscum contagiosum virus 6

1.2 Innate immune signalling **9**

1.2.1 The innate immune response 9

1.2.2 The NF-κB family 11

1.2.3 The IRF family 13

1.2.4 Toll-like receptor signalling 16

1.2.5 RIG-I receptor signalling 28

1.2.6 cGAS-STING signalling axis 31

1.2.7 The importin family 33

1.3 MCV immune evasion **36**

1.4 Thesis aims **42**

Chapter 2: Materials and Methods **43**

2.1 Materials **44**

2.1.1 List of materials 44

2.2.2 Buffers and solutions 50

2.2 Methods 53

2.2.1 Cell culture techniques 53

2.2.2 $LiNO_2$ cell storage 54

2.2.3 Plasmids and oligonucleotides 54

2.2.4 Bacterial transformation 55

2.2.5 Plasmid purification 56

2.2.6 Generation of MC009-expressing stable cell lines 57

2.2.7 Reporter gene assay 57

2.2.8 Immunoblotting 61

2.2.9 Immunoprecipitation 63

2.2.10 Confocal microscopy (coverslip method) 65

2.2.11 Confocal microscopy (chamber slide method) 66

2.2.12 Sandwich ELISA 68

2.2.13 IFNα/β bioassay 70

2.2.14 siRNA optimisation 72

2.2.15 Statistical analysis 72

Chapter 3: Involvement of MC009 in NK-κB and IRF Signalling. 74

3.1 Introduction 75

3.2 MCV ORF plasmid screen identifies MC009 as an inhibitor of NF-κB and IRF activation. 76

3.3 MC020 identified as inhibitor control. 81

3.4 MC009 does not inhibit a Ras-activated Elk1 control pathway. 83

3.5 MC009 is an inhibitor of NF-κB activation by pro-inflammatory and innate sensing pathways. 84

3.6 MC009 is an inhibitor of IRF activation. 90

3.7 MC009 impairs cytokine and IFN-α/β release. 95

3.8 Identification of functional regions of MC009.....99

3.9 Discussion.....101

3.10 Conclusion.....108

Chapter 4: MC009 Inhibits TNFα-induced p65 Nuclear Translocation. 110

4.1 Introduction.....111

4.2 Confocal microscopy protocol optimisation. 112

4.3 MC009 inhibits TNFα-stimulated p65 nuclear translocation. 117

4.4 MC009 does not inhibit NF-κB signalling through direct interaction with p65 or IκB degradation. 123

4.5 Discussion.....125

4.6 Conclusion.....128

Chapter 5: MC009 Interacts with Karyopherin Proteins to Inhibit Signal Transduction. 129

5.1 Introduction.....130

5.2 MC009 does not interact with importin IPO5. 131

5.3 MC009 interacts with karyopherin KPNA6. 134

5.4 MC009 forms a complex with KPNA6 and p65. 143

5.5 KPNA6 siRNA knockdown optimisation. 152

5.6 Discussion.....155

5.7 Conclusion.....161

Chapter 6: Discussion.....162

References.....167

Acknowledgements

Firstly, I want to thank my supervisor Dr. Gareth Brady for giving me the opportunity of the last three (and a half) years. Thank you for your knowledge, help and support during the project. More importantly, thank you for being kind and understanding when life got in the way. I have been told that having a good PhD supervisor is half of the success and I could not agree more.

To my lab fam…Tom, for being my ultimate MCV guide and for not making me come in at crazy hours the first week of my PhD. Clara, for showing me the power of a label maker, for not judging me that time I cried doing blots, for always listening and looking out for me. Carla and Ryan (Carlos and Rachel) I could not imagine the Brady bunch without the pen thievery and constant movie references, you guys made the long days 'mucho' better (the days probably would have been shorter without you though). Mariya, for the late-night lab chats and the deep-heat when I couldn't move my neck. To my lab fam, thank you for all the laughs. I could not have asked for a better team.

To the TTMI gang, Izzy, Derv, Arlena, Conor, Matt, Emma, Amrita, Ailbhe, Tara, Julie, Sarah, Jordy and to so many others, thanks for making TTMI such an amazing place to work, for 1pm lunch, for office chats and for taking Halloween so seriously.

Thank you to Prof. Andrew Bowie, Dr. Andreas Pichlmair and Gavin McManus without whom the project would not have been possible.

To my mum, Grażyna Kusiak, thank you for being the most amazing and caring mum, and for supporting me in everything I do. To the rest of my family, thank you for asking

about science but also for taking my mind off of it when I needed it. [Mojej mamie, Grażynie Kusiak, dziękuje, że jesteś najcudowniejszą i troskliwą mamą, oraz za ciągłe wsparcie. Reszcie mojej rodziny, dziękuje za pytanie o świat nauki ale także za to, że mogłam o nim zapomnieć kiedy tego potrzebowałam.]

Finally to my pre-PhD friends, thank you for the hugs, the laughs, the candles and the bops. Thank you for the supportive messages, words of encouragement and for still sending memes even though I wouldn't see them until the weekend.

Thank you all for being part of my PhD journey.

Abstract

Molluscum contagiosum virus (MCV) is a human-adapted poxvirus that causes mild, raised skin lesions which are highly contagious. The lesions are notable for exerting minimal to no inflammation but can persist for long durations of time without an effective anti-viral response from the host. Human innate signalling pathways are targeted by MCV encoded immunomodulators, such as MC005 and MC132. These cascades regulate two major transcription factor families responsible for driving an anti-viral immune response, the nuclear factor kappa B (NF-κB) and the interferon regulatory factor (IRF) members. These transcription factors require an importin/karyopherin shuttle to translocate into the nucleus in order to upregulate inflammatory and gene expression in response to infection. To date, less than 15 MCV proteins have been thoroughly researched and their immunomodulatory function understood. Furthermore, the role of karyopherin proteins is not well described during MCV pathogenesis and immune evasion.

MC009 was previously identified as a *Molluscipoxvirus* specific protein by the lab, however its mechanism of action had not been defined. Pathway mapping conducted using gene reporter assays determined MC009 to be an inhibitor of pattern recognition receptor (PRR)- and cytokine-induced κB- and IRF-luciferase activity. MC009-driven inhibition resulted in reduced IL-8, IP-10 and IFN-β production and IFN-β-luciferase activity. Following this discovery, the mechanism of function was investigated. Three hypotheses were studied to understand the diminished pro-inflammatory cytokine and type I IFN production. Firstly, an MC009-p65 interaction was investigated, however, there was no indication of the two proteins directly interacting with each other. The phosphorylation of IκB was examined next which was not altered in cells expressing MC009. Lastly, transcription factor nuclear translocation was studied. MC009 detained

p65 within the cytoplasm after TNFα induction, preventing p65 from translocating into the nucleus.

NF-κB members depend on karyopherin proteins to transport across the nuclear membrane. Using confocal microscopy and co-immunoprecipitation (Co-IP) techniques, MC009 was observed to interact with overexpressed and endogenous karyopherin subunit α 6 (KPNA6). A strong interaction between MC009 and KPNA5 and a weaker interaction with KPNA1 were also observed. MC009 disrupts p65-mediated immune responses through KPNA function interference. Furthermore, the interaction between MC009 and KPNA6 did not inhibit KPNA6-p65 binding, but rather formed a p65-KPNA6-MC009 complex. The protein complex likely sequesters within the cytoplasm as MC009 was not observed translocating into the cell nucleus with endogenous KPNA6.

In this thesis, I present MC009 as a potent inhibitor of both NF-κB and IRF3/7 signalling, a mechanism through which MCV inhibits the activation of pro-inflammatory and anti-viral immune responses. The inhibitor causes major disturbances to human immune gene regulation by p65 cytoplasmic sequestration. I report MC009 as the first MCV-derived immunosuppressor and only second known poxviral protein capable of signal inhibition by directly targeting karyopherin proteins. MC009 offers novel insights into human innate signalling whilst broadening our understanding of MCV immune evasion strategies.

Lay Abstract

Molluscum contagiosum virus (MCV) is a human-specific poxvirus that causes mild, raised skin lesions which are highly contagious. The lesions are notable for not causing redness or swelling which are key signs of inflammation. The infection can last for long durations of time without being detected by the host. The human innate immune system is composed of complex signalling pathways activated in response to the virus. MCV uses special proteins (called immunomodulators) to dampen or completely block the signal, similarly to a dam blocking a river, interfering with virus clearance. The pathways regulate two major protein families found at the end of each pathway: the nuclear factor kappa B (NF-κB) and the interferon regulatory factor (IRF) members. NF-κB and IRF proteins require a shuttle (called karyopherin proteins) to move from the cytoplasm of the cell into the nucleus. NF-κB and IRF members need to access the nucleus for the virus to be detected and fought. To date, less than 15 MCV proteins have been thoroughly researched and their function understood. Furthermore, the role of karyopherin proteins is not well described during not only MCV infections. This thesis focuses on the MCV protein, called MC009.

MC009 was previously identified as an MCV immunomodulator by the lab, however, it was not understood where and how it stopped the immune signal. Key proteins involved in innate pathways were tested which determined MC009 to be an inhibitor of NF-κB and IRF activity. Diminished NF-κB and IRF activity resulted in reduced IL-8, IP-10 and IFN-β production all necessary to fight the viral infection. Following this discovery, the mechanism of function was investigated. Three ideas were studied to understand the diminished pro-inflammatory cytokine and type I IFN production. Firstly, I investigated if MC009 interacts with p65 (an NF-κB family member), however, there was no

indication of the two proteins directly interacting with each other. Changes to the IκB proteins were examined next but were not altered in cells with MC009. Lastly, the movement of p65 from the cytoplasm into the nucleus was studied. MC009 forced p65 to remain within the cytoplasm after stimulation with the pro-inflammatory protein TNFα, preventing p65 from moving into the nucleus.

NF-κB and IRF members depend on karyopherin proteins to transport across the wall of the nucleus. Using confocal microscopy and co-immunoprecipitation (Co-IP) experiments, MC009 was seen to interact with karyopherin subunit α 6 (KPNA6). A strong interaction between MC009 and KPNA5 and a weaker interaction with KPNA1 were also observed. MC009 disrupts p65-dependent immune responses through KPNA function interference. Furthermore, the interaction between MC009 and KPNA6 did not stop KPNA6-p65 binding. Instead, MC009, KPNA6 and p65 formed a protein complex. The protein complex likely remains within the cytoplasm as MC009 was not observed moving into the nucleus with KPNA6 produced by the cells.

In this thesis, I present MC009 as a strong inhibitor of both NF-κB and IRF3 signalling, a mechanism through which MCV inhibits the activation of inflammatory and anti-viral immune responses. The inhibitor causes major disturbances to human immune gene regulation by stopping p65 from entering the nucleus. I report MC009 as the first MCV protein and second poxviral protein capable of signal inhibition by directly targeting karyopherin proteins. Thus, MC009 offers novel insights into human innate signalling whilst broadening our understanding of MCV immune evasion strategies.

Project Outputs

Awards

- *How to out-con a con artist: Molluscum contagiosum virus inhibitor MC009.* TTMI Conference PhD Blitz. Awarded 2nd place prize for best oral presentation. Dublin, 11th of March 2022.
- *Molluscum Contagiosum Virus Protein MC009 as a Novel Inhibitor of NF-κB and Interferon Regulatory Factor Signalling.* Awarded travel grant for research abstract for the 2024 Host-Pathogen Communication Conference in Aarhus, Denmark.

Oral Presentations

- *Investigation of Molluscum Contagiosum Viral Protein MC009 as a Novel Inhibitor of Innate Signalling.* TTMI Immunology Meeting, Trinity Translational Medicine Institute, Dublin, 13th of July 2021.
- *Molluscum Contagiosum Virus protein MC009 is a novel bifunctional inhibitor of NF-κB and IRF activation.* TTMI Immunology Meeting, Trinity Translational Medicine Institute, Dublin, 15th of March 2022.
- *Investigation of the Molluscum Contagiosum Virus Protein MC009 as a Novel Inhibitor of Innate Signalling.* TTMI Immunology Meeting, Trinity Translational Medicine Institute, Dublin, 2nd of March 2023.
- *Investigation of the Molluscum Contagiosum Virus Protein MC009 as a Novel Innate Signalling Inhibitor.* TTMI Immunology Meeting, Trinity Translational Medicine Institute, Dublin, 24th of October 2023.

- *Investigation of the Molluscum Contagiosum Virus Protein MC009 as a Novel Innate Signalling Inhibitor.* IRF Meeting, Trinity Biomedical Science Institute, Dublin, 15th of December 2023.

Poster Presentation

- *Investigation of Molluscum Contagiosum Viral Protein MC009 as a Novel Inhibitor of Innate Signalling.* Host-Pathogen Communications Conference, Trinity Biomedical Science Institute, Dublin, 11th of November 2021.
- *Investigation of the Molluscum Contagiosum Virus Protein MC009 as a Novel Inhibitor of Innate Signalling*. Irish Society for Immunology, Maynooth, 1st-2nd September 2023.
- *The importin-ce of MC009: Molluscum contagiosum virus protein MC009 as a novel inhibitor of NF-κB and IRF family signalling*. British Society for Immunology, Belfast, 4th-7th December 2023.

Publications

- Kusiak, A. and Brady, G., *Bifurcation of signalling in human innate immune pathways to NF-κB and IRF family activation.* Biochem Pharmacol. 2022 Nov;205:115246. doi: 10.1016/j.bcp.2022.115246. Epub 2022 Sep 8. PMID: 36088989.
- Kusiak, A. and Brady, G., *Molluscum Contagiosum Virus Protein MC009 is a novel inhibitor of Nuclear Factor-κB and Interferon Regulatory Factor 3*. Manuscript in progress.

Abbreviations

AIDS: Acquired Immunodeficiency Syndrome

APC: Antigen-Presenting Cell

cGAS: Cyclic GMP-AMP Synthase

cIAP1: Cellular Inhibitor of Apoptosis Protein 1

CTTP: Cytoplasmic Transduction Transcriptional Processor

DAMP: Damage-Associated Molecular Pattern

DC: Dendritic Cell

DD: Death Domain

dsRNA: Double-Stranded Ribonucleic Acid

EMCLV: Equine Molluscum Contagiosum-like Virus

ER: Endoplasmic Reticulum

ERGIC: ER-Golgi Intermediate Compartment

FADD: Fas-Associated Death Domain

HIV: Human Immunodeficiency Virus

HSV: Herpes Simplex Virus

IFN: Type I Interferon

IFNAR: IFN receptor

IL-1: Interleukin 1

IL-1R: Interleukin-1 Receptor

IKK: IκB Kinase

IPS-1: IFNβ Promoter Stimulator 1

IRAK: Interleukin-1 Receptor-Associated Kinase

IRF: Interferon Regulatory Factor

ISG: IFN-Stimulated Gene

ISRE: Interferon-Stimulated Response Element

IκB: Inhibitory Kappa B

KPNA: Karyopherin α (Importin subunit α)

KPNB: Karyopherin β (Importin subunit β)

LGP2: Laboratory of Genetics and Physiology 2

LPS: Lipopolysaccharide

LRR: Leucine-Rich Repeats

MAL: MyD88 Adaptor-Like Protein

MAP3K: Mitogen-Activated Protein Kinase Kinase Kinase

MAVS: Mitochondrial Anti-viral Signalling Protein

MCV: Molluscum contagiosum virus

MDA5: Melanoma Differentiation-Associated Gene 5

MD-2: Myeloid Differentiation Protein 2

MEF: Mouse Embryonic Fibroblast

MHC-I: Major Histocompatibility Complex Class I

MyD88: Myeloid Differentiation Factor 88

NAP1: NAK-Associated Protein 1

NEMO: NF-κB Essential Modulator

NF-κB: Nuclear Factor Kappa-Light-Chain-Enhancer of Activated B Cells

NLS: Nuclear Localisation Sequence

NPC: Nuclear Pore Complex

NTD: N-Terminal Domain

PAMP: Pathogen-Associated Molecular Pattern

PARP-1: Poly (ADP-ribose) Polymerase 1

pDCs: Plasmacytoid DCs

Poly(dA:dT): Poly(deoxyadenylic-deoxythymidylic) Acid

PPARγ: Peroxisome Proliferator Activated Receptor Gamma

PRD: Positive Regulatory Domains

PRR: Pattern Recognition Receptor

PTM: Post-Translational Modification

RIG-I: Retinoic Acid-Inducible Gene 1

RIP-1: Receptor-Interacting Serine/Threonine-Protein Kinase 1

RLR: RIG-I-like Receptor

STING: Stimulator of Interferon Genes

TAK1: Transforming Growth Factor-β (TGF-β)-Activated Kinase 1

TANK: TRAF-Associated NF-κB Activator

TBD: TBK1/IKKε-Binding Domain

TBK1: TANK-Binding Kinase 1

TIM: TRAF-Interaction Motif

TIR: Toll/IL-1 Receptor Domain

TIRAP: TIR-Containing Adaptor Protein

TF: Transcription Factor

TLR: Toll-Like Receptors

TNFα: Tumour Necrosis Factor α

TNFR: Tumour Necrosis Factor Receptor

TRADD: TNF-Receptor Type 1-Associated Death Domain Protein

TRAF: TNFR-Associated Factor

TRAM: TRIF-Related Adaptor Molecule

TRIF: TIR-Domain-Containing Adaptor-Inducing Interferon-b

TRIM25: Tripartite Motif Containing 25

VACV: Vaccinia virus

VAR: Variola virus

List of Figures and Tables

Figure 1.1 Molluscum contagiosum lesions in hosts.

Figure 1.2 Electron microscope imaging of MCV viral particles.

Figure 1.3 Simplified comparison of the canonical and noncanonical NF-κB pathways.

Table 1.1 Roles of IRF family members.

Figure 1.4 TLR signalling to NF-κB and IRF family members.

Figure 1.5 TLR signalling to NF-κB and IRF family members through MyD88.

Figure 1.6 TLR-TRIF signalling to IRF family members.

Figure 1.7 RIG-I signalling to NF-κB and IRF family members.

Figure 1.8 Bifurcation of cGAS-STING signalling into NF-κB and IRF members.

Table 1.2 KPNA isoform homology represented as percentage.

Table 1.3 Comprehensive description of MCV-derived protein roles in immune system evasion.

Table 2.1 Cell seeding density for all vessel types used.

Table 2.2 Representative table of luciferase assay transfection plate additions.

Figure 2.1 Graphic representation of luciferase regulation during reporter gene assays.

Table 2.3 Recipes for resolving and stacking gels for denaturing SDS-PAGE

Table 2.4 Primary and secondary antibody description for immunoblotting.

Figure 2.2 Graphical representation of immunoprecipitation

Table 2.5 Immunofluorescence assay antibody description

Figure 2.3 Graphical representation of ELISA standards preparation for IL-8 DuoSet® kit

Table 2.6 IL-8 and IP-10 ELISA reagent dilutions.

Figure 3.1 Multiple sequence alignment of MCV subtype 1, subtype 2 and EMCLV010L.

Figure 3.2 MC009 plasmid activity and expression comparison.

Figure 3.3 Identification of negative control MCV ORF.

Figure 3.4 Mitogenic Elk1 pathway used as a control for MC009 inhibitory properties.

Figure 3.5 MC009 inhibits early stages of TLR, RLR and cGAS-mediated NF-κB signalling.

Figure 3.6 MC009 inhibits TRAF2, TRAF6 and TAB2 mediated NF-κB signalling.

Figure 3.7 MC009 inhibits NF-κB signalling mediated through the IKK complex.

Figure 3.8 MC009 inhibits direct κB-luciferase reporter activation by p65 inhibition like the p65-targetting MCV inhibitor MC132.

Figure 3.9 MC009 inhibits IRF activation by TLR, RLR and cGAS pathways.

Figure 3.10 MC009 inhibits IRF family signalling by TBK1 and IKKε.

Figure 3.11 MC009 inhibits direct ISRE-luciferase activation by IRF3 and IRF7 signalling.

Figure 3.12 Induction of MC009 expression leads to diminished IL-8 and IP-10 cytokine production.

Figure 3.13 IFN-α/β response is weakened in the presence of MC009.

Figure 3.14 MC009 inhibitory function is held in the N-terminal of the genetic sequence.

Figure 3.15 MC009 inhibition of signalling pathways activating NF-κB and IRF transcription factors.

Figure 4.1 HEK293T cells did not maintain a 2D *in vitro* model morphology when using 'Confocal Microscopy (Coverslip method)' protocol.

Figure 4.2 Nunc™ Lab-Tek™ II Chamber Slide™ System supports HEK293T cell adhesion.

Figure 4.3 Nunc™ Lab-Tek™ II Chamber Slide™ System provides a suitable HEK293T cell transfection environment.

Figure 4.4 MC009 localises in the cytoplasm of HEK293T cells.

Figure 4.5 MC009 inhibits TNFα-induced p65 nuclear translocation.

Figure 4.6 MC009 does not interact with endogenous p65.

Figure 4.7 MC009 inhibits key upstream events in TNFα-induced NF-κB activation.

Figure 5.1 Affinity purification-mass spectrometry analysis of MC009 immunoprecipitants.

Figure 5.2 IPO5 does not interact with MC009.

Figure 5.3 Endogenous KPNA6 interacts with MC009.

Figure 5.4 MC009 interacts with karyopherins KPNA1, KPNA5 and KPNA6.

Figure 5.5 Multiple sequence alignment of human KPNA1-7 amino acid sequence.

Figure 5.6 Confocal Microscopy visualising endogenous KPNA6 and MC009 or MC020.

Figure 5.7 MC009 co-localises in HEK293T cell nucleus with overexpressed KPNA1, KPNA5 and KPNA6.

Figure 5.8 Overexpressed KPNA proteins show weak interaction with unstimulated p65.

Figure 5.9 Poly(dA:dT) stimulation does not induce a KPNA6-IRF3 protein-protein interaction.

Figure 5.10 MC009 does not disrupt TNFα-induced KPNA6 and p65 interaction.

Figure 5.11 KPNA6 co-localises with p65 in HEK293T cell cytoplasm.

Figure 5.12 KPNA6 and p65 co-localise in the cytoplasm in MC009 expressing cells.

Figure 5.13 KPNA6 siRNA protocol optimisation.

Chapter 1: Introduction

This chapter contains extracts originally published in Biochemical Pharmacology. Kusiak, A. and Brady, G. Bifurcation of signalling in human innate immune pathways to NF-κB and IRF family activation. doi: 10.1016/j.bcp.2022.115246

1.1 Molluscum contagiosum virus

1.1.1 Poxviruses

Poxviruses are 200-450 nm long, brick-shaped viruses with a linear, double-stranded DNA (dsDNA) genome ranging from 130,000 to 300,000 base pairs (bp) (1–3). The *Poxviridae* family is divided into two subfamilies, *Chordopoxvirinae* and *Entomopoxvirinae*, which infect vertebrates and insects respectively. The *Chordopoxvirinae* subfamily is further subdivides into multiple genera*: Avipoxvirus*, *Capripoxvirus*, *Centapoxvirus*, *Cervidpoxvirus*, *Crocodylipoxvirus*, *Leporipoxvirus*, *Macropopoxvirus*, *Molluscipoxvirus*, *Mustlepoxvirus*, *Orthopoxvirus*, *Oryzopoxvirus*, *Parapoxvirus*, *Pteropopoxvirus*, *Salmonpoxvirus*, *Sciuripoxvirus*, *Suipoxvirus*, *Vespertilionpoxvirus and Yatapoxvirus* (3,4). The species found in the *Chordopoxvirinae* genus affect a wide range of animals such as monkeys, swine, and humans (4).

Variola virus (VAR), a member of the *Orthopoxvirus* genus, is one of the most commonly well-known viruses. VAR infections were responsible for smallpox epidemics with a 30% fatality rate causing millions of deaths worldwide (5). The virus was highly contagious with 85% infectivity rate in non-vaccinated individuals with humans being the only documented host (6–9). The infection manifested in a rash found on the tongue in the early stage of disease eventually spreading to the rest of the body as firm raised pustules (10). Immunisation against VAR was first described by Edward Jenner in 1796 using the cowpox virus (11). The disease was officially declared eradicated by the World Health Organisation (WHO) in 1980 due to a strict global immunisation campaign (12).

The vaccination against VAR used globally no longer uses cowpox but rather vaccinia virus (VACV) (13). VACV has been since used as a tool for research to further understand poxviral infections (14). Other poxvirus-induced human disease include monkeypox, sore mouth infection (orf virus) and molluscum contagiosum (3).

1.1.2 Molluscum contagiosum

Molluscum contagiosum (MC) is a dermatological infection caused by Molluscum contagiosum virus (MCV). MC is characterised by waxy, raised, often flesh-coloured skin lesions with a dimple or depression in the centre of the papule (15,16). The lesions, referred to as Mollusca, are filled with live MCV particles and as such make MC easily contagious. The infection can be passed on from person-to-person through physical touch as well as through contact with contaminated surfaces. A contained infection can also be spread to other body parts through self- or auto-inoculation. Self-inoculation occurs when Mollusca are scratched or irritated by friction caused by clothes, towels, or bedsheets. Release of live viral particles allows for their transfer to other body parts. The papules can be found all over the body however, they are most often found on the lower abdomen and genital regions in immunocompetent adults in contrast to immunocompromised patients with more lesions observed on the face and upper body (17–22). As MCV is enclosed in Henderson-Peterson bodies within the epidermis the viral particles do not circulate within the host therefore airborne or droplet transmission cannot occur (16). Additionally, it is unclear if contaminated water sources can lead to the spread of the virus.

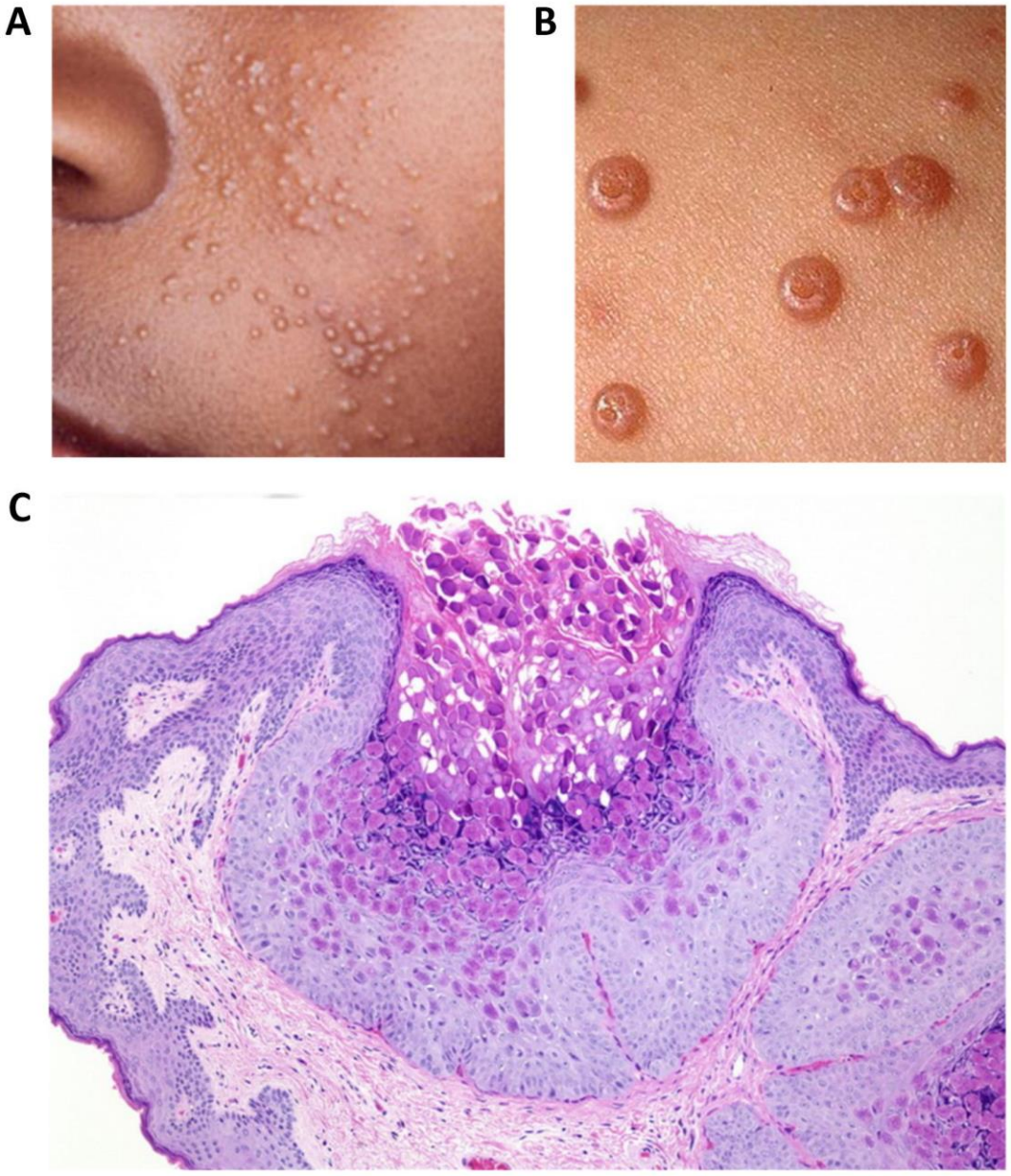

Figure 1.1. Molluscum contagiosum lesions in hosts. A-B. Images presenting active MCV infections on face (**A**) and body (**B**). **C.** Histopathology of a Mollusca lesion section with a central depression. The image shows Henderson-Patterson bodies characteristic to MCV infections. Images obtained from Centres for Disease Control and Prevention (15) (**A**), MedBullets (23) (**B**), WebPathology (24) (**C**).

Molluscum contagiosum can affect children and adults with immunocompromised individuals being more susceptible (25–27). The majority of infection cases are noted in pre-pubescent children, young immunocompetent adults and immunocompromised patients of any age (22,26). The incidence rate of infection rises from 1.5-11% in healthy hosts to 18% in immunodeficient individuals, with 10-20% of human immunodeficiency virus (HIV) patients contracting the infection (22,27,28). Mollusca tend to remain small, 2-5 millimetres in width, in individuals without any co-morbidities or co-infections. However, lesion size, intensity and morphology has been shown to vary in immunocompromised hosts where the lesions can reach up to multiple centimetres in size (19,29,30). Changes in lesion morphology and quantity are not the only observed difference in MCV infection between immunocompetent and immunocompromised patients. In hosts with no other co-morbidities the infection is generally self-limiting and resolves within a few months past initial exposure (16,29). The period over which the infection is resolved in immunocompromised patients is prolonged from a few months to several years (16).

Although the infection can be self-limiting, various molluscum contagiosum treatment options are available including oral, topical, and mechanistic methods. The type of treatment used highly depends on infection severity, host type and area affected (31). Cimetidine is the main oral treatment favoured in MCV infections for children as the treatment option has no long-term side effects and is considered more child-friendly (32,33). The treatment has not been shown to be effective in cases where Mollusca are located on the facial region. Topical options include, but are not limited to, cantharidin, tretinoin, potassium hydroxide, podophyllotoxin or salicylic acid (34–37). Lastly, mechanical methods of extraction of the viral particles include cryotherapy, curettage and

laser therapy such as pulsed-dye laser or carbon dioxide (33,38–40). These methods have been improved since the first MCV treatments were available however, many still can be painful and can lead to long-term side effects such as scarring (33,41). Unfortunately, many treatment options on the market are not viable for immunosuppressed individuals as the patients tend to be less responsive with more favourable results observed with antiretroviral therapies (19,42).

1.1.3 Molluscum contagiosum virus

Molluscum contagiosum virus (MCV) is a double-stranded DNA (dsDNA) brick-shaped poxvirus (15,16,43). MCV shares the genus *Molluscipoxvirus* with a recently described equine molluscum contagiosum-like virus (EMCLV) (44). There are four subtypes of MCV with varying infection rates and target demographics. MCV-1 causes 75-96% of the recorded infections particularly targeting immunocompetent hosts (43,45,46). This subtype has also been shown to more frequently affect children (46). MCV-2 is more commonly found in immunocompromised patients, specifically targeting those with HIV and acquired immunodeficiency syndrome (AIDS) (19,29,33,42). Subtypes 3 and 4 are rare and mostly observed in Asia and Australia (45,47). All four MCV members have similar clinical characteristics, as a result the subtypes cannot be identified purely on the physical manifestation of the infection. The full genome has only been identified for subtypes 1 and 2, 190 kilo-bp, therefore, genotyping studies for subtypes 3 and 4 are not yet possible (48–50).

The replication cycle of MCV is not well described as viral propagation in tissue culture or animal models have not been possible. MCV shares 105 homologs with species found in the *Orthopoxvirus* genus, like VACV and VAR, including genes shown to be involved

in the viral replication cycle of other better described poxviruses (51). Thus, it is assumed that MCV follows a similar replication cycle. Poxviruses completely reproduce within the cytoplasm (52). The key events after cell attachment and entry include early gene transcription and translation, DNA replication, intermediate and late transcription and translation, virion assembly and release. A favourable replication environment is established during the early mRNA synthesis stage. Immunomodulatory proteins are produced in the early stage of replication interfering with the host immune system (53). The immature virion performs the late and intermediate synthesis stages in intracellular compartments known as virus factories (54,55). DNA factories contain elements such as a viral replication organelle or host mitochondria necessary where the complete viral genome is safely reproduced (55). Poxviruses, including MCV, can adopt one of two mature forms: enveloped extracellular virion or mature intracellular virion. Mature poxviral particles can be distinguished from the immature virions by their dumb-bell shape (**Figure 1.2C**) (56).

MCV cannot be grown in tissue culture limiting experimental studies of the virus. Although some studies have shown MCV to have cytopathic effects on human primary cells, the infection was not extended to untreated cells and most infected cells experienced cell death (57–59). Animal models used for studying host–pathogen interactions or disease progression are not available as humans are the only recorded host of MCV. Attenuated VACV has been shown to work effectively as a host for MCV-encoded genes *in vivo* (60). The model presented with little inflammation but did not produce the characteristic MCV lesions.

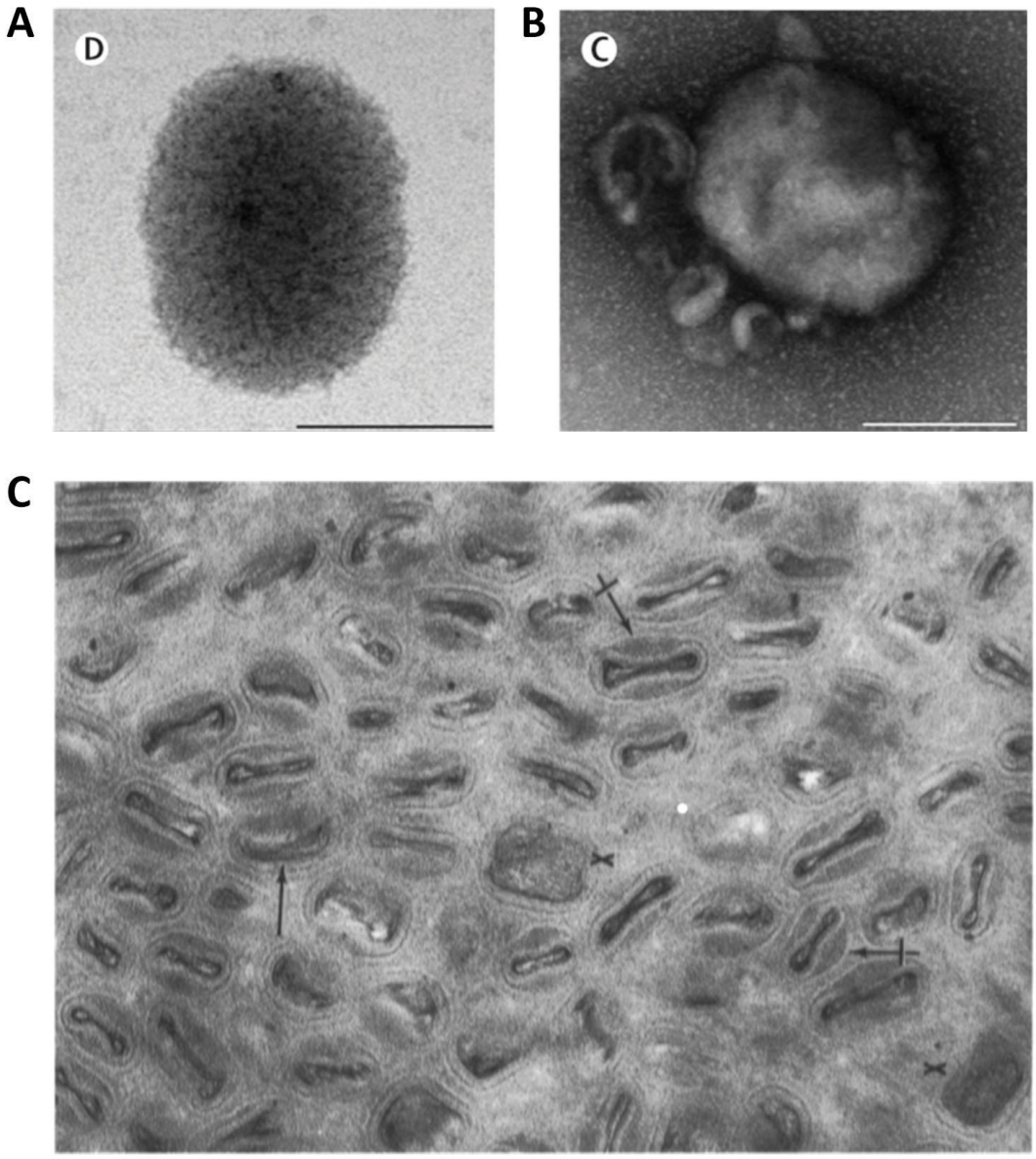

Figure 1.2. Electron microscope imaging of MCV viral particles. A-B. Electron microscope ammonium-molybdate negative staining of MCV, scale bars represent 200 nm, core protein pattern (330×260 nm; **A**) and with viral envelope (340×265 nm; **B**). **C.** Image taken as part of an electron microscope study of MCV showing section of MCV infected skin. Crossed-arrows point to lenticular-shaped lateral bodies. Rectangular mature viral particles are marked with X with electron-dense fibrillar nucleoids surrounded by a less dense capsule; x 42,000. Images obtained from The Lancet Infectious Diseases (45) (**A-B**) and The American Journal of Pathology (61) (**C**).

1.2 Innate immune signalling

1.2.1 The innate immune response

The human immune system can be broadly divided into two arms. The rapidly activated, but relatively non-specific system known as the innate immune response and the slower but highly specific adaptive immune response. Both are essential components of an effective immune response; however, their pathways and effector mechanisms are highly distinct. The innate immune system is composed of a wide range of cells from antigen-presenting cells (APCs), such as dendritic cells (DCs) and macrophages, to myeloblast-derived cells like neutrophils and eosinophils (62). These cells mediate a rapid response to immunostimulants which have entered the body with infectious agents or are derived from sterile endogenous material. Innate cells are equipped with specialised sensing mechanisms to detect these changes and activate a somewhat generic response (63,64). However, many other cell types are equipped to respond to these changes in the body. Non-immune cells, such as fibroblasts and epithelial cells also play key roles in innate immunity (65,66).

Most cells have some capacity to recognise and distinguish between pathogen-associated molecular patterns (PAMPs) derived from infectious agents, and damage-associated molecular patterns (DAMPs) derived from damaged cells and tissues (67–69). PAMPs is a broad term for exogenous, pathogen-associated molecules which can be easily identified by germline-encoded receptors (70–72). Some common PAMPs which can stimulate the release of cytokines are viral nucleic acids, lipopolysaccharides (LPS) and other structures found on or within the pathogen. Similarly, DAMPs can take various forms, yet these molecules are all derived from the host as a result of damage or other aberrant alterations to tissue like tumorigenesis (73–75). Infections and other diseases

may occur or become prolonged if the response is not adequate to the threat indicated by the two categories of signal stimulants. Additionally, autoimmune diseases can arise from excessive innate responses or aberrant recognition of self-molecules as DAMPs (74).

Innate immune cells have evolved complex and tightly regulated signal transduction pathways which help minimise excessive or dysregulated activation leading to disease. These cascades are composed of interactions between a variety of receptors, adaptor proteins, kinases, and protein complexes (76). They are dependent on distinctive post-translational modification (PTM) events without which the formation of complexes or activation of adjacent or downstream pathway components would not occur (77–79). A major outcome of innate signalling pathway activation is the transcription of target genes ultimately resulting in the release of characteristic cytokines and chemokines from the cell which orchestrate the innate response. Thus, it is crucial that the transduction of information is well calibrated and tightly controlled, yet rapid.

The transcription of innate immune response genes, in most cases, requires the translocation of activated transcription factors from the cytoplasm into the nucleus. The two major families involved in inflammation and the anti-viral immune response are NF-κB and the IRF family members (80). The NF-κB and IRF family pathways utilise similar signalling regulators at the early stages of activation. Nevertheless, the nature and degree of bifurcation in innate signalling pathways to activation of NF-κB and IRF members delivers distinct downstream immune responses.

1.2.2 The NF-κB family

The NF-κB transcription factor family is composed of five members and divided into two subgroups (81). RelA (p65), RelB and c-Rel make up group one. The second group consists of NF-κB1 (p50) and NF-κB2 (p52). p105 and p100 undergo proteolytic changes before they reach a mature state as p50 and p52, respectively. NF-κB subunits form homodimers or heterodimers, for example p65-p50 or p50-p50, each dimeric association possessing unique functionality. The activated dimers typically translocate from the cytoplasm to the nucleus and bind to accessible promoter regions of target genes containing cognate consensus sequences (82,83). NF-κB is typically cytosolic as the dimers are sequestered in the cytoplasm when in an inactive state. However, in some instances NF-κB subunits can be found in mitochondrial subcellular fractionations or pre-existing in the nucleus (84,85).

NF-κB dimers are broadly considered pro-inflammatory transcription factors as they are most commonly associated with pro-inflammatory cytokine, chemokine and adhesion molecule gene expression (86). In PRR signalling, these transcription factors can be activated via different routes and by multiple PAMPs and DAMPs. Some examples of extracellular NF-κB pathway stimulants include bacterial pathogens (*Mycobacterium tuberculosis, Neisseria gonorrhoea*), virus particle components (HIV), multicellular parasites (*Trypanosoma cruzi*) as well as interleukin 1 (IL-1), IL-18 and tumour necrosis factor α (TNFα) (87–92). NF-κB activation occurs through one of two distinct pathways, canonical or noncanonical/alternative.

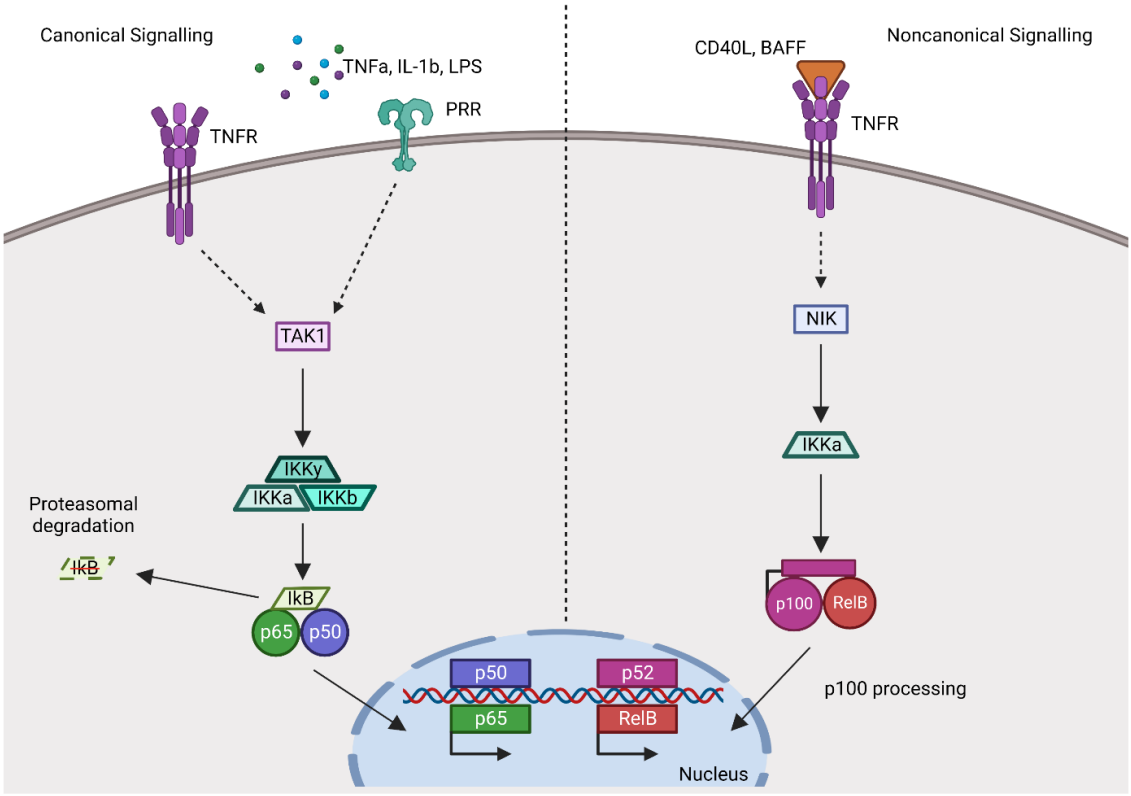

Figure 1.3. Simplified comparison of the canonical and noncanonical NF-κB pathways. The canonical pathway is activated by ligands such as TNFα, IL-1b and lipopolysaccharide (LPS). The signal is conveyed through TAK1 which feeds the information to the IKK complex: IKKα, IKKβ and IKKγ (NEMO). After the activation of the IKK complex, IKKβ phosphorylates IκB causing it to undergo proteasomal degradation and allowing NF-κB members, for example p65-p50 dimer, to translocate into the nucleus. The noncanonical pathway is activated through the TNFR family. The signal is carried through NIK to IKKα which causes p100 to undergo proteolytic changes eventually leading to NF-κB, p52-RelB, nuclear translocation. The image was created using BioRender (biorender.com).

The canonical pathway is linked to pro-inflammatory cytokines, such as IL-1β or TNFα, and PRR-signalling (93). The route primarily focuses on RelA or c-Rel-linked gene induction (94,95). The noncanonical pathway cannot be activated through TNFα, however it is regulated by specific members of the tumour necrosis factor receptor

(TNFR) family (96). The alternative pathway is closely related to adaptive immunity unlike the canonical pathway which is rooted in innate signalling and typically utilizes RelB/p52. The pathways also differentiate in their utilisation of inhibitory κB kinases (IKKs). Zandi *et al.* have shown that IKKβ and IKKγ (also known as NF-κB essential modulator or NEMO) are necessary for NF-κB canonical pathway regulation (97). IκB which restrains NF-κB dimers in the cytoplasm is phosphorylated by activated IKKβ (98–101). This phosphorylation results in IκB degradation leading to transcription factor release and nuclear translocation. Conversely, IKKα plays a more important role in noncanonical NF-κB activation (102). It is evident that the appropriate activation of the NF-κB pathway is important as it is tightly regulated by processes such as auto- and trans-phosphorylation, dimerization, and protein complex formation. The mechanism of the canonical pathway activation will be discussed in more detail throughout this section. The canonical pathway is heavily used in innate immune signalling, particularly the pro-inflammatory response. However, it also plays important roles distinct from the induction of pro-inflammatory cytokines and chemokines, including IL-8, IL-6, IP-10 and TNFα (93,103–107). Lawrence *et al.* observed that lack of NF-κB activity during an inflammatory response led to a longer resolution of inflammation time (108).

1.2.3 The IRF family

The IRF family consists of nine members in humans, IRF1-9, which play central roles in driving production of IFNs (109). A homologous DNA binding motif and five tryptophan repeats are found in all of the family members (110). Whilst in the nucleus, the IRFs bind to the interferon-stimulated response element (ISRE). The presence of IFNs, with IFNα or IFNβ being the best studied subtypes, drive IFN-stimulated gene (ISG) transcription through type I IFN receptor (IFNAR) signalling (111–113). Apart from *IFNA* and *IFNB*

genes, the type I IFN family also includes IFNκ and IFNε (113,114). ISGs code for a vast array of proteins which condition cells for incoming virus infection by inhibiting the viral life cycle at a variety of levels and enhancing virus sensing-based responses (115,116).

This project will focus on the two most prominent IRF members, IRF3 and IRF7, in sensing-driven immune signalling to highlight the differences in their activation in contrast to NF-κB members. Generation of IFNs during innate signalling requires IRF3 and/or IRF7 which are located in the cytoplasm in their inactive state (117–119). These two IRF family members regulate IFNα and IFNβ transcription in various cells (120–126). IRF7 can function in a dependant and independent manner with IRF3 depending on cell type (127–129). IRF3 drives transactivation of *IFNA* and *IFNB* recruiting IRF7 to form a positive feedback loop leading to a stronger IFN response. The transcription factors are activated through phosphorylation of serine residues found in the C-terminal region (128,130,131).

It is also important to note that NF-κB can act as a co-regulator for type I IFN production (132,133). Indeed, the combined activity of both IRFs and NF-κB are needed for robust IFNβ production (133). The *IFNB* gene contains four positive regulatory domains (PRDs), whereas *IFNA* has two PRD I- and PRD III-like elements (134,135). IRFs use different PRD sites to NF-κB members, for example PRD I is linked to IRF family members versus PRD II which is NF-κB related. Studies have shown that NF-κB activation is also required for early IFNβ expression as the rapid induction of IFNβ and initiation of the anti-viral state is reduced in the absence of NF-κB (136,137). Furthermore, Iwanaszko *et al.* observed the potential role of IRF3 as a negative regulator of NF-κB members (80).

IRF	Function
IRF1	NF-κB inhibition Anti-viral ISG regulation (e.g. *BST*2) Oncogenesis regulation
IRF2	IL-7 Cell cycle regulation Oncogenesis regulation
IRF3	IP-10 Type I IFN production
IRF4	Lymphoid, myeloid and DC cell differentiation
IRF5	IL-6, IL-12, TNFα release Type I IFN production
IRF6	Protective role in LPS-induced endotoxic shock Macrophage activation through suppressing PPARγ Embryonic development
IRF7	Type I IFN production Secondary role in positive feedback loop after IRF3 activation
IRF8	Myeloid cell differentiation
IRF9	Type I IFN response through ISGF3, STAT1 and STAT2

Table 1.1. Roles of IRF family members (138,139,148–150,140–147).

As noted previously, pathways leading to activation of the NF-κB and IRF families often share the same components at the early stages of signal transduction. These systems include receptors like toll-like receptors (TLRs) which are involved in both pro-inflammatory signalling as well as interferon induction subject to the stimulated TLR

(151–153). Cytosolic nucleic acid sensor pathways also activate both NF-κB and IRF signalling. These include retinoic acid-inducible gene 1 (RIG)-I-like receptors (RLRs) or the cyclic GMP-AMP synthase (cGAS)-stimulator of interferon genes (STING) axis (154–157).

1.2.4 Toll-like receptor signalling

One of the best studied innate immune receptor families is the TLR family. In humans, this group is composed of 10 germline-encoded pattern recognition receptors (PRRs) some of which are plasma membrane-bound while others are located intracellularly. TLRs which are located on the plasma membrane and within the cell on endosomes, the endoplasmic reticulum (ER) and lysosomes. The core structure of these PRRs is highly conserved. They can be identified by the presence of a horseshoe-like ectodomain (158). The leucine-rich repeat (LRR) motif-containing N-terminal, 22-29 amino acids, allows for PAMP and DAMP detection (158,159). Homo and hetero-dimerization is induced by ligand binding and occurs via the LRR motifs causing the other domains to neighbour each other (160). The TLRs also share a transmembrane region composed of a short chain of hydrophobic amino acid residues. This helical structure is responsible for inter-receptor interactions through the use of UNC93B in nucleic acid responsive TLRs (161). Lastly, these type I integral membrane proteins share a common cytoplasmic Toll/IL-1 receptor (TIR) domain within their C-terminal. This domain is used by the receptor dimer to recruit TIR domain-containing adaptor and bridging proteins (162). Therefore, the domain is vital for functionality as it enables the initiation of signal transduction intracellularly. The TIR domain is closely related to the signalling regions in interleukin-1 receptor (IL-1R) members. The conservation of the TIR domain throughout evolution

as well as its presence in several TLR-proximal signalling proteins further highlights its importance in innate signalling (163).

TLRs can be broadly categorised into two subfamilies: cell surface TLRs and intracellular TLRs. TLRs 1, 2, 6 and 10 target the same or similar ligands to each other. The same can be observed with TLRs 7, 8 and 9. Due to the similar homology of the TLR1/2/6/10 receptors, they are also capable of heterodimerising with each other. Heterodimerization of TLRs, outside of this subgroup, is uncommon and has been shown to have a more harmful rather than helpful effect. One exception to this rule is the heterodimerisation of TLR2 and TLR4, this rare event allows recognition of a broader range of potential PAMPs (164). An example of injury inducing heterodimerisation is the dimerization of TLR4 and TLR6 which mediates sterile inflammation in response to DAMPs (165).

TLR1/2/6 are mostly found on the cell surface and recognise lipopeptides, like lipoteichoic acid. Furthermore, TLR2 is only able to work in association with nonhomogeneous receptors meaning that TLR2 does not signal as a product of homodimerization (160). TLR4 is widely known for its association with LPS. TLR4 is unique due to its use of a co-receptor. Myeloid differentiation protein 2 (MD-2, also called LY96) is necessary for LPS signal mediation through TLR4 (166). TLR5 binds to bacterial flagellin, stimulating innate signalling during bacterial infections. The last plasma membrane-located receptor in this subgroup is TLR10. This receptor is relatively less well characterised as it was the last human-associated TLR to be discovered (167,168). TLR10 has been shown to function with TLR2, however, unlike TLR1 and TLR6, this drives anti-inflammatory responses rather than the release of pro-inflammatory cytokines (169).

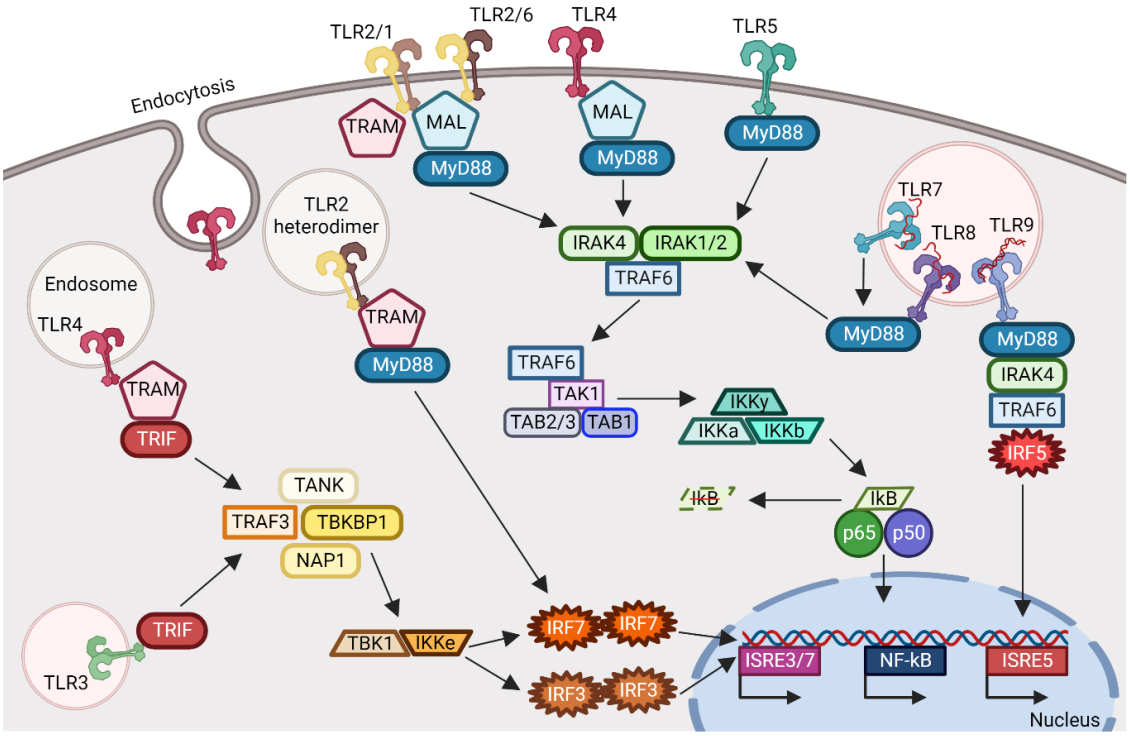

Figure 1.4. TLR signalling to NF-κB and IRF family members. TLRs found on the plasma membrane often signal through the MyD88 pathway. TLR2 heterodimers and TLR4 require MAL/TIRAP to allow for MyD88 binding to the receptors. MyD88-driven signalling induces the Myddosome which includes IRAK4, IRAK1/2 and TRAF6. The activation of the Myddosome releases TRAF6 from the complex subsequently recruiting TAK1, TAB2/3 and TAB1 to TRAF6. This allows the IKK complex to drive NF-κB translocation into the nucleus by freeing it from its IκB inhibitor. TLR2 heterodimers can also bind TRAM. This association leads to endocytosis of the receptor. Interestingly, MyD88 binds to TRAM eventually causing IRF7 dimerization and nuclear translocation. TLR7/8/9 are also able of signalling through the Myddosome similarly to the cell surface TLRs. Additionally, TLR7/8/9 can also activate IRF5 through MyD88, IRAK4 and TRAF6 binding. This subgroup of TLR receptors also regulates IRF3 and IRF7 (not depicted on the figure). Similarly to TLR2, TLR4 becomes endocytosed after activation on the cell surface. Once it is enclosed in the endosome, TLR4 signals through TRAM-TRIF to activate IRF3 and IRF7. The same pathway is used by TLR3 with the exception of TRAM, as TLR3 does not require a bridging protein to allow for TRIF binding. TRAF3 in combination with

NAP1/TBKBP1/TANK regulates TBK1 (also known as NF-κB activating kinase or NAK) and IKKε (also called IKKi) kinases which directly activate IRF transcription factors. The image was created using BioRender (biorender.com).

As mentioned previously, some TLRs have an intracellular localisation. The receptors located on the endosomal membrane are TLR3 and TLR7/8/9, although TLR3 can also be found on the cell surface (170–173). TLRs 7, 8 and 9 exist as stable dimers (174,175). TLR3 initiates inflammatory responses in the presence of double-stranded ribonucleic acid (dsRNA) produced during infection. It is important to note that TLR3 cannot be activated by ligands <40 bp providing protection against an inflammatory response to endogenous nucleic acids (176). Like TLR3, TLR7/8/9 also recognise nucleic acids. The innate immune response to viral or bacterial single-stranded RNA (ssRNA) is triggered via TLR7 and TLR8. Immune cell TLR7/8 response can also be driven through the use of synthetic immunomodulatory compounds such as imidazoquinolinone (177). Lastly, unmethylated CpG-rich DNA is the only known natural agonist of TLR9. The ligand-TLR7/8/9 complex requires an acidic environment for signalling to occur, which is provided by the endosomal compartments (178,179).

Doyle *et al.*, observed a difference in NF-κB and IRF3 roles in TLR3 and TLR4 (152). They concluded that both TLR3 and TLR4 lead to ISRE promoter binding of IRF3, however, TLR3 stimulation led to a faster and more potent IRF3 activation (152). This suggests that TLR3 and TLR4 play different roles in IRF signalling. Based on our current knowledge, it appears that the TLRs found on the cell surface focus more on NF-κB signalling and therefore are more involved in pro-inflammatory gene regulation, whereas endosomal TLRs are more prone to induce IRF activation (180–183). Although

TLR3/7/8/9 can drive inflammatory responses, they are more commonly associated with driving interferon responses. Similarly, the signalling outcome for TLR4 changes depending on its localisation. It was previously believed that TLR4 fulfilled its function from the cell surface from where it preferentially drives NF-κB activation over IRF signalling. Conversely, when endocytosed, TLR4 alters its signalling pathway leading to a more IRF-activating response (184,185).

The TIR domain, responsible for downstream signalling, also features in TLR adaptor proteins. The five accessory proteins (MyD88, MAL, TRIF, TRAM, SARM) involved in innate signalling directly downstream of the receptors all contain TIR domains. Almost all TLRs are dependent on myeloid differentiation factor 88 (MyD88) to culminate an inflammatory response (186). The only exception is TLR3 which will be discussed further later. MyD88 has a central role in downstream cascade activation culminating in NF-κB and IRF translocation into the nucleus. It binds to the receptors through TIR-TIR interaction (187). However, another important binding domain in this accessory molecule is the death domain (DD) (188,189). This domain is essential for the formation of the Myddosome which is an oligomeric complex assembled in response to MyD88 TIR domain receptor binding (190,191). MyD88 recruits members of the interleukin-1 receptor-associated kinase (IRAK) family after binding to the receptors.

The Myddosome is composed of six MyD88, four IRAK4 and four IRAK2 DDs (190). Activation of these kinases occurs through the DDs in MyD88 and the IRAKs. Myddosome formation cannot occur in TLR4 signalling without a bridging molecule called MyD88 adaptor-like protein (MAL), also known as TIR-containing adaptor protein (TIRAP) (192–194). Like MyD88 and the TLRs, MAL contains a TIR domain in its C-

terminus, allowing for strict signal regulation. MAL also forms TIR:TIR interactions with TLR2 heterodimers as well as TLR5 (193,195). IRAK1 and IRAK4 have been shown to be indispensable in interleukin-1 receptor (IL-1R)-mediated NF-κB activation (188). Loiarro *et al.* investigated the role of different DD residues in IRAK initiation. The group reported that disrupting Glu^{52} and Tyr^{58} residues in the DD halted NF-κB activation usually activated through this pathway (188). Therefore, the auto and cross phosphorylation of IRAK members aiding the assembly of the Myddosome regulates gene expression through NF-κB and IRFs.

Once in the Myddosome, IRAK1 or IRAK2 become phosphorylated. This induces conformational changes that allow for tumour necrosis factor receptor (TNFR)-associated factor 6 (TRAF6) to bind to the complex. Consequently, this mediates a release of the IRAK kinases along with TRAF6 from the oligomer. Uematsu *et al*. investigated the effects of IRAK1 deficiency in TLR7 and TLR9 signalling (196). The group observed that IRAK1 is necessary for the activation and nuclear translocation of IRF7 as it directly associates with the transcription factor, IRF7 also associates with MyD88 and TRAF6 (196,197). They also showed no effect on MyD88-dependent NF-κB activity in the absence of IRAK1 during TLR7 and TLR9 signalling. Furthermore, IRAK2 has been shown to be essential for NF-κB signalling as it drives TRAF6 ubiquitination (198). Interestingly, inhibition of the kinase proved to have no effect on IRF activation (198).

TRAF6, a ubiquitin E3 ligase, polyubiquitinates lysine-63 residues (K-63) on associated signalling proteins in the pathways through its RING domain (199). Innate signal transduction downstream of TRAF6 completely separates into two distinct pathways, NF-κB and IRF. In canonical NF-κB signalling, free TRAF6 recruits the assembly of the

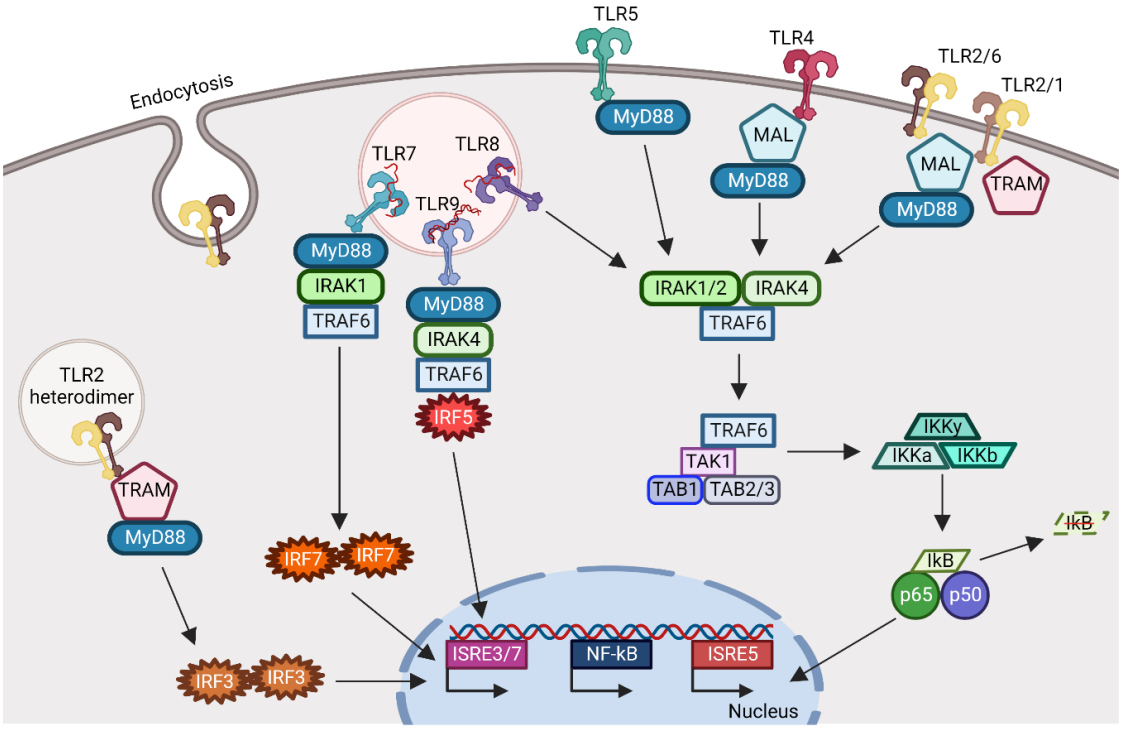

Figure 1.5. TLR signalling to NF-κB and IRF family members through MyD88. TLRs 1, 2, 4, 5, 6, 7, 8 and 9 can signal through the MyD88 adaptor protein. TLR2 heterodimers as well as TLR4 require a bridging protein, MAL or TRAM, before they can interact with MyD88. Activation of MyD88 induces the Myddosome: IRAK4, IRAK1/2 and TRAF6. This drives the release of TRAF6 which binds to TAK1, TAB1 and TAB2/3. The signal is then conveyed through the IKK complex causing IκB phosphorylation and degradation. The free NF-κB dimer translocates from the cytoplasm to the nucleus. TLR7/8/9 can also signal to the IRF family members through MyD88 by recruiting IRAK1/4 and TRAF6. Endocytosed TLR2 heterodimers drive IRF3 translocation via TRAM and MyD88. The image was created using BioRender (biorender.com).

transforming growth factor-β (TGF-β)-activated kinase 1 (TAK1) complex. The complex is composed of the serine/threonine kinase TAK1 along with TAK1-binding proteins (TAB) 1, 2 and 3. TRAF6, an E3 ligase, drives polyubiquitination of TAB2/3 leading to TAK1 activation. The formation of this complex is swiftly followed by activation of the

IKK complex. TAK1, which is a member of the mitogen-activated protein kinase kinase kinase (MAP3K) family, phosphorylates IKKβ (200). The IKK complex is made up of two catalytic subunits, IKKα and IKKβ, and a regulatory subunit, NEMO (97). NF-κB dimers are sequestered in the cytoplasm as a result of inhibitory IκB association (201). The activation of the IKK complex drives the release of NF-κB members from their inhibitor, as the activated complex phosphorylates serine 32 and 36 on IκB leading to its degradation by the 26S proteasome (202).

In addition to regulating NF-κB, TRAF6 can also play a role in IRF7 activation (197). This inflammatory response appears to involve less variables in the pathway. Unlike NF-κB, IRF7 is capable of binding to a MyD88-containing complex described as cytoplasmic transduction-transcriptional processor (CTTP) which integrates MyD88, IRAK4, TRAF6 and IRF5/7 (203). Furthermore, lack of TRAF6 during signalling to NF-κB and IRF family members reduces production of pro-inflammatory cytokines and chemokines (203). Schoenemeyer *et al.* established IRF7 as an important factor in TLR7-MyD88 signal transduction (204). IRF3-independent-IRF7 remains tightly linked to type I IFN production. Unsurprisingly, IRF7 expression can be predominantly seen in plasmacytoid DCs (pDCs), as pDCs are capable of releasing large volumes of type I IFNs in response to viral stimulants (205,206).

A second TLR-associated adaptor protein is TIR-domain-containing adaptor-inducing interferon-β (TRIF). This specialised accessory molecule plays a role in TLR3 and intracellular TLR4 signalling (184,207,208). TLR3 is the only MyD88-independent member of this receptor family and operates exclusively through TRIF. Conformational changes to the death domain in MyD88 showed no effect on TLR3-TRIF induced gene

expression (188). Conversely, TLR4 and TLR5 are the only known receptors able to induce a response through both MyD88 and TRIF (184,209). Indeed, TLR4 is the only known TLR receptor which utilises all five of the TIR-containing adaptor proteins. The receptor recruits MyD88 and MAL when associated with LPS at the plasma membrane but once it is imported into the cell through invagination it is then able to signal through TRIF and TRIF-related adaptor molecule (TRAM; or TICAM2) (210). Signalling mediated through TLR4 is therefore even more tightly regulated in comparison to some other members of this receptor family. Work by Kagan *et al.* provided insight into the importance of TRAM in prompting an IRF3-driven innate immune response (211).

In addition to the C-terminal TIR domain, the 712 amino acid accessory protein is also equipped with an N-terminal domain and a TRAF-binding motif (212). TRAF3 is another member of the TRAF kinase family, predominantly involved in IRF signalling. TRAF3 is not exclusively present in the TLR-TRIF axis (71). This E3 ligase also plays a central role in MyD88-dependant signalling as well as aiding non-TLR family PRRs. Recent studies by Fochi *et al.* have shown a link between TRAF3 presence and NF-κB activity in relation to human T-cell leukaemia virus (HTLV) Tax proteins however, this ligase has also been shown to serve a role as a negative regulator of NF-κB (213,214). Additionally, it has been studied in connection to the IRF family member activation, especially IRF3, maintaining its position as a core regulator of type I IFN production (214). TRAF3 is essential for IRF activation, as it regulates two key kinases within the IRF family pathway, IKKε and TRAF-associated NF-κB activator (TANK)-binding kinase 1 (TBK1) (215,216). The localisation of the ligase dictates the need for endosomal-based TLRs. TRAF3 conducts both MyD88- and TRIF-mediated signals, playing a significant role in IFN production (215). As mentioned previously, TRAF6

plays a major role in TLR-MyD88 driven signalling, however, it appears to be more tightly linked to cell surface receptors. In contrast, TRAF3 has been observed to closely work with endosomal TLRs including the TLR3, TLR7/8/9 as well as endocytosed TLR4.

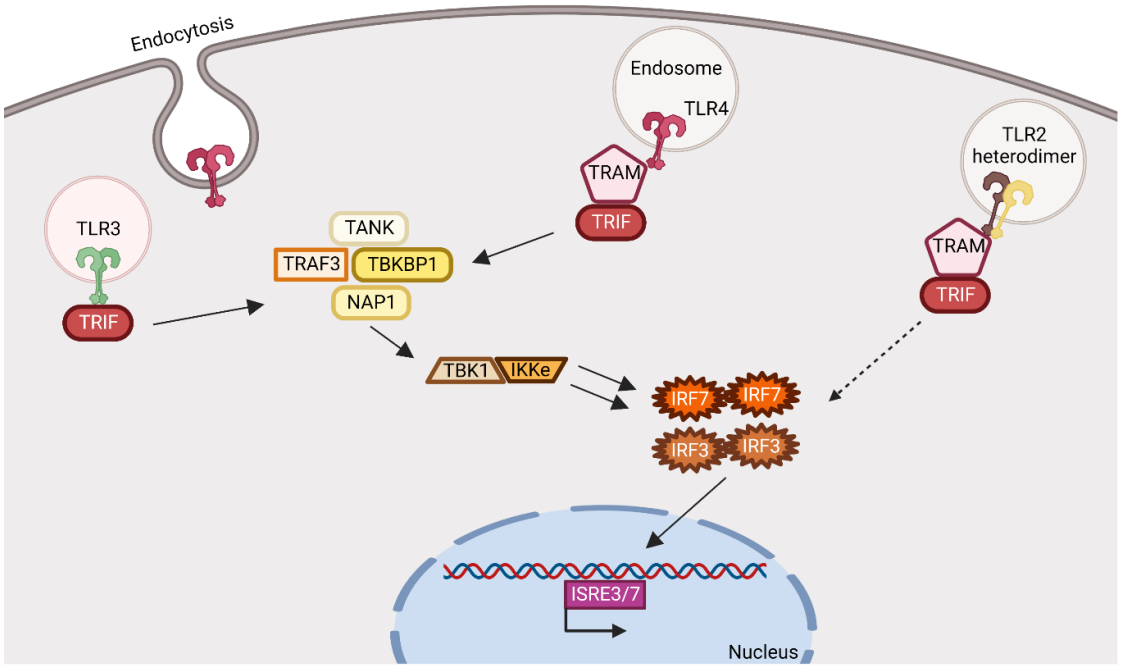

Figure 1.6. TLR-TRIF signalling to IRF family members. TRIF-driven signal transduction is typically observed with intracellular TLRs. TLR2 heterodimers can bind to the bridging protein TRAM which leads to the endocytosis of the receptor. Similarly to TLR2, TLR4 becomes endocytosed after activation on the cell surface. Endocytosed TLR2 heterodimers and TLR4 signal through TRAM-TRIF to activate IRF3 and IRF7. The full TLR2-TRIF signalling pathway is not well described. TRIF-driven TLR3 and TLR4 signalling recruits TRAF3 as well as NAP1/TBKBP1/TANK. This activates TBK1 and IKKε regulating IRF transcription factors. The image was created using BioRender (biorender.com).

It is now evident that TLR2 is also capable of signalling through TRAM-TRIF after endocytosis to drive a type I IFN response (217,218). A study has shown that a type I

IFN response can be driven through TLR2-TRAF3 (211). The team investigated the role of TRAF3 in ISRE and NF-κB activation. As expected, they recorded wild-type TRAF3 driving ISRE activation while showing no induction of NF-κB luciferase activation. Interestingly, using a plasma-membrane localised TRAF3 mutant, pleckstrin homology domain of phospholipase C-δ1(PLC- δ1) was bound to the amino terminus of the kinase, they not only noted stronger activation of ISRE but also saw a significant spike in NF-κB luciferase activation (211). Although it is still not clear if TRAF3 is involved in TLR2 signalling after endocytosis, a link between the two proteins has been made during macrophage reprogramming (219).

With regard to TLR3 signalling, the TLR3-TRIF TIR:TIR domain interaction leads to an arrangement of a protein complex incorporating two IκB kinase homologs: IKKε and TBK1 (220,221). It was previously believed that both aforementioned kinases were primarily implicated in NF-κB pathway regulation. However, it is now clear that their activity is vital to the phosphorylation of transcription factors IRF3 and IRF7, triggering an anti-microbial and anti-viral response (117,152,200,222). Perry *et al.,* demonstrated TBK1 is non-redundant for a TLR3/4-IRF3-mediated IFN response. TBK1 was initially believed to play a part in NF-κB activation. The group looked at NF-κB activity in LPS and poly I:C stimulated bone marrow derived macrophages and saw no difference between *TBK1*$^{+/+}$ and *TBK1*$^{-/-}$ cells (223). Another research group examined the subcellular localisation of IRF3 and IRF7 in the presence and absence of TBK1 or IKKε. They saw an increase in nuclear translocation of the transcription factors in the presence of either of the kinases (224). Movement of IRF3 from the cytoplasm into the nucleus appears to be related to the phosphorylation of serine residues 386 and 396. The

phosphorylation leads to dimerization allowing for transcription factor translocation (220,224).

TBK1 is associated with a number of other proteins including: TANK (I-TRAF), TBKBP1 (SINTBAD), NAP1 (TBKBP2; AZI2) (225–228). The PTM and binding of TBK1 with the various adaptors can affect its role and IFN signal response. The three proteins all contain a specially designed TBK1/IKKε-binding domain (TBD) leading to inherent competition between them to bind to the C-terminal coiled-coil 2 region of TBK1 (229). Mutations of the TBD region led to changes in interactions between the proteins and the two kinases (228). These scaffold proteins constitutively interact with the kinases working in a regulatory fashion, similar to the role NEMO plays in the IKK complex (230,231). Mouse studies have shown that TANK is used as a negative regulator of TLR-mediated NF-κB activation. Stimulation of TLR7 (synthetic R-848) in *TANK*$^{-/-}$ macrophages as well as TANK overexpression in human embryonic kidney (HEK293) cells showed a correlation between TANK and TRAF6 ubiquitination (232). Here, TRAF6 ubiquitination appears to be inhibited in the presence of TANK in TLR signalling.

TNF receptor type 1-associated death domain protein (TRADD) has also been described as a TRIF adaptor protein for TLR3 and TLR4 signalling (233,234). TRADD mediates K-63-linked polyubiquitination of receptor-interacting serine/threonine-protein kinase 1 (RIP1), a process necessary for NFκB activation (235). The use of TRADD and RIP1 by TLR3 and TLR4 is very intriguing as it leads to NF-κB signalling but not IRF3 activation (236).

1.2.5 RIG-I receptor signalling

Retinoic acid-inducible gene 1 (RIG-I)-like receptors (RLRs) are another class of PRRs that activate both NF-κB and IRFs. Unlike TLRs, this group of receptors is never found on the cell surface but rather all RLR members are exclusively found within the cytosol. The most studied member of this group is the RIG-I receptor. Other members include melanoma differentiation-associated gene 5 (MDA5) and laboratory of genetics and physiology 2 (LGP2) (237). RLR signalling is not triggered by a broad range of stimuli like the TLRs. As nucleic acid sensors, these proteins respond to viral nucleic acids meaning their primary role is to generate an anti-viral response. However, an RLR-mediated response to self-RNA has also been observed in recent studies (238–241).

RIG-I is maintained in the cytoplasm in an inactive state until a stimuli is presented (156). In the presence of short 5'-triphosphate single-stranded RNA (ssRNA) or double-stranded RNA (dsRNA) the receptor dimerises. Polyubiquitination of RIG-I at lysine-63 in the N-terminal CARD-like region by tripartite motif containing 25 (TRIM25), an E3 ubiquitin ligase, permits the receptor to bind to MAVS, a mitochondrial membrane protein (242). RIG-I can also induce IFNβ production through both NF-κB and IRF3 signalling in a TRIM25-independent manner; when the C-terminal of RIG-I undergoes ubiquitination by Riplet/RNF135 (243). Poly(dA:dT), dsDNA, has been shown to stimulate RIG-I-mediated signalling through RNA polymerase III (244). It is transcribed into 5'-triphosphate dsRNA capable of initiating an RLR signal. This is important to note as HEK293T cells are not equipped with TLR3, TLR9 or cGAS sensing machinery, therefore, Poly(dA:dT)-stimulated NF-κB or IRF activity likely occurs through this pathway.

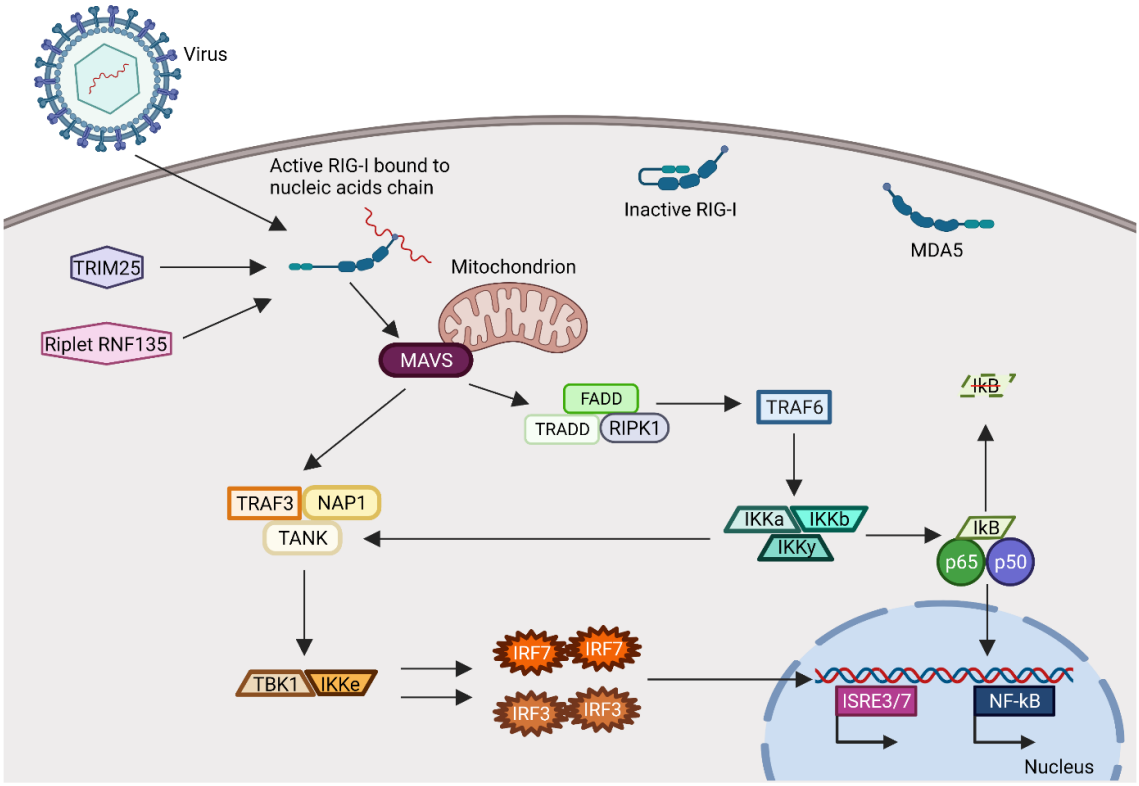

Figure 1.7. RIG-I signalling to NF-κB and IRF family members. The RLR receptor undergoes TRIM25- or Riplet/RNF135-mediated ubiquitination which activates the signalling cascade and drives MAVS to form hetero-tetramers with RIG-I on the mitochondrial surface. The signal bifurcates into NF-κB and IRF members downstream of MAVS. NF-κB activation requires the involvement of TRADD, FADD and RIPK1 in addition to TRAF6 and the IKK-complex. MAVS utilizes TRAF3, NAP1 and TANK to convey the signal to IRF3 and IRF7. The image was created using BioRender (biorender.com).

Both RIG-I and MDA5 are mitochondrial anti-viral signalling protein (MAVS) dependent (200). MAVS, formerly known as - IFNβ promoter stimulator 1 (IPS-1) and VISA, plays a similar role in RLR signal transduction as MyD88 and TRIF do in TLR signalling (245–248). MAVS contains an N-terminal CARD domain, a proline-rich region, and a C-terminal transmembrane domain. The protein is localised to mitochondrial outer membranes, peroxisome membranes and mitochondrial-associated

membranes via the transmembrane domain (249,250). The protein is necessary for the production of IFNβ through NF-κB and IRF3 in a TLR-independent manner (247). MAVS is essential for the production of IFNβ in most cell types (except pDC cells) during RLR anti-viral signalling (251). RLR activation triggers MAVS dimerization, providing a platform for subsequent adaptor proteins to bind.

Different TRAF family members can be recruited downstream of MAVS: TRAF3 and TRAF6 (247,252). The TRAF3-MAVS axis leads to IFNα induction through the binding of the TRAF domain on TRAF3 and the TRAF-interaction motif (TIM) domain on MAVS (252). Saha *et al.* showed that changes in the TIM domains altered IRF7 (*IFNA4* promoter luciferase) activity and NF-κB luciferase activity (252). The E3 ligase activity of TRAF3 eventually leads to the activation of TBK1-IKKε-driven IRF3 and IRF7 activity (220,253,254). Similarly to TLR signalling, it appears that TRAF6 is once again more tightly linked with NF-κB activation rather than IRF signalling. A study conducted on mouse embryonic fibroblasts (MEFs) investigated the role of TRAF6 in viral immune responses (255). The group showed that TRAF6-deficient MEFs had a comparable level of IRF3 translocation as that of wild-type MEFs. In contrast, p65 translocation was greatly affected in the absence of TRAF6. The study also looked at activation of IFNβ promoter with IRF3 and NF-κB in relation to TRAF6. Based on their findings, the group further demonstrated that both IRF3 and NF-κB activation, as well as ATF-2/c-Jun, are needed for the correct activation of IFNβ promoter in response to intracellular dsRNA (134,255,256).

MAVS acts upstream of the TBK1-IKKε as well as the IKK complex (249). Similar to TLR signalling, TBK1-IKKε are responsible for IRF3 activity and work with TANK and

NAP1 (227,229,231). In vitro experiments showed a direct association between NAP1 and RLR proteins (226). These studies also showed signs of binding between NAP1 and MAVS leading to IRF3 signalling and IFNβ production (226).

It has been recently determined that NEMO also plays a role in TBK1-IKKε signalling to the IRF transcription factors and is necessary for the activation of IRF3 and IRF7 (257). Zhao *et al*. showed that it was NEMO and not NF-κB that was needed for the IRF activity (257). The group investigated the relationship between NEMO and the IKK complex-related kinases. They observed that the signal passed on from NEMO to TBK1-IKKε is mediated through TANK. Furthermore, the TRAF3-TANK IRF activation in RLR signalling requires the recruitment of TRADD (258). Similarly, activation of NF-κB requires TRADD recruitment to MAVS for Fas-associated death domain (FADD) and RIP1 to form a signalling complex with MAVS, via interaction with the C-terminal domain of MAVS (245,258,259). FADD deficient MEFs showed a attenuated response to viral infection (259,260). Additionally, knockdowns of TBK1 and MAVS did not affect NF-κB activation after TNFα, peptidoglycan or PMA stimulation (228).

1.2.6 cGAS-STING signalling axis

Another route of intracellular DNA sensing is through the cyclic GMP–AMP synthase (cGAS)-stimulator of interferon gene (STING) pathway. This pathway can also lead to NF-κB and IRF activation via their corresponding kinase complexes. This is the most recently discovered sensor system signalling to NF-κB and IRF family members. Although the exact mechanism is still under investigation, it is clear that the cGAS-STING axis uses similar tools to TLR- and RLR-mediated viral responses including TRAFs and IKK/TBK1 kinases.

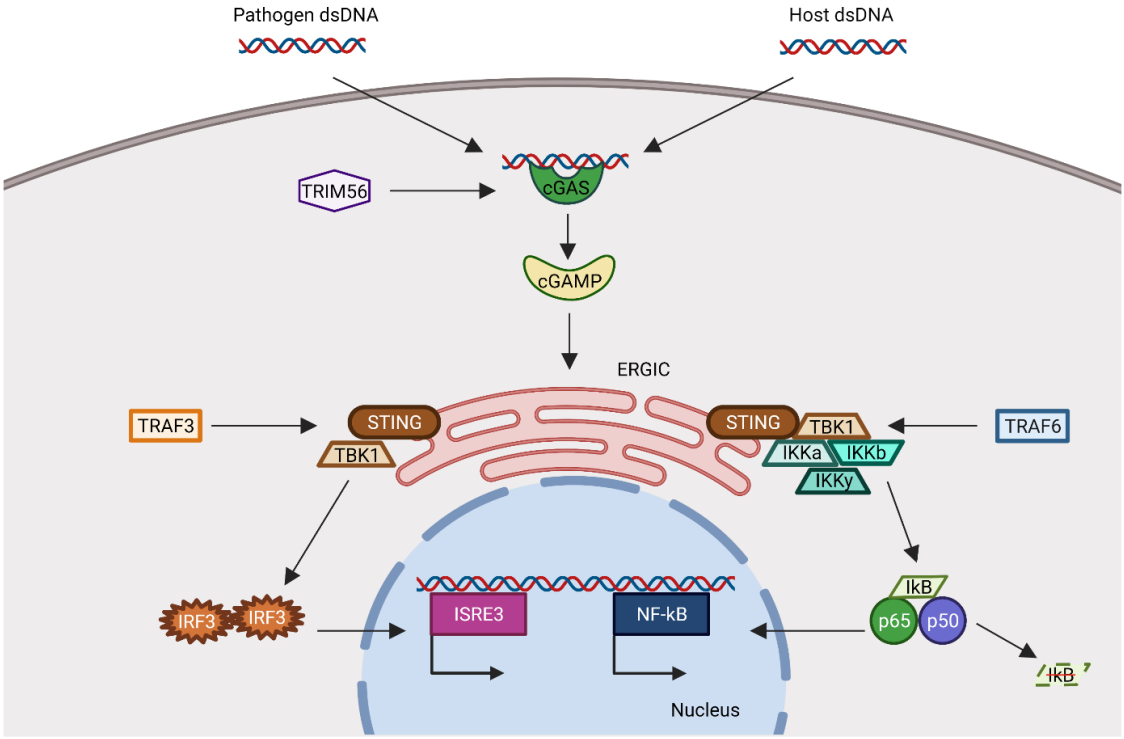

Figure 1.8. Bifurcation of cGAS-STING signalling into NF-κB and IRF members. In the presence of free dsDNA, cGAS activates STING through the upregulation of a secondary messenger called cGAMP. IRF3 dimers are formed as a result of STING-TBK1 binding which occurs in the endoplasmic reticulum-Golgi intermediate compartment (ERGIC). NF-κB requires additional aid from the IKK-complex to allow for signal transduction and eventual transcription factor translocation. The image was created using BioRender (biorender.com).

cGAS-triggered signal activity is dependent on dsDNA length as peptides <20 bp do not activate signal transduction through cGAS as well (155). Binding of the PAMP induces structural changes in cGAS allowing for better affinity for adenosine triphosphate (ATP) and guanosine triphosphate (GTP) interaction (154,261). This interaction activates a secondary messenger known as cyclic GMP-AMP (cGAMP) (262). Ubiquitination of cGAS at the Lys335 residue by TRIM56 is required for IFNα/β production during viral infections (263).

STING becomes activated in the presence of cGAMP and relays this signal to TBK1 once again leading to IRF3 oligomerisation and translocation (220,264–266). Inactive STING is found in the endoplasmic reticulum (ER) (267). Oligomerisation of STING recruits TBK1 which is used to phosphorylate STING allowing for IRF3 binding (265,266,268,269). STING activation can also drive NF-κB release however, this process is less well understood (270). TRAF3 and TRAF6 have been linked to STING-induced p65 and IRF3 activity (264). An increased luciferase activity was observed in the presence of both STING and TRAF3/6. IL-6 and IFNβ levels dropped in the absence of TRAF6, with IFNβ levels remaining stable in the absence of TRAF3. These researchers concluded that TRAF6 appears to play a greater role in dsDNA-STING-mediated NF-κB activity than in IRF3 signalling (264).

Research conducted on NF-κB signalling through this axis has shown that the transcription factor subunit p65 could be recruiting different regulatory proteins depending on the stimulant (264). IKKα and IKKβ were both involved in p65 nuclear translocation after stimulation with poly(I:C) and dsDNA. Furthermore, TBK1-deficient MEFs showed a decreased level of NF-κB nuclear translocation when stimulated with dsDNA. Additionally, stimulation of TBK1 deficient MEFs with both stimulants showed to have a massive impact on IRF3 translocation (264).

1.2.7 The importin family

NF-κB and IRF transcription factors translocate from the cytoplasm into the nucleus to convey the signal passed through the stimulated pathways. In order for this to occur, they require help from the importin family. Importin proteins, also known as karyopherins, are subdivided into two subtypes: importin subunit α (karyopherin α [KPNA]) and importin

subunit β (karyopherin β [KPNB]). There are seven importin α subunits and twenty importin β subunits found in humans (271). KPNAs are further divided into three subfamilies: α1, α2 and α3. Subfamily α1 relates to KPNA2 and KPNA7 which share 54.7% identity (272). KPNA3 and KPNA4 compose the α2 subfamily and share an 85.8% homology. Lastly, KPNA1, KPNA5 and KPNA6 make up the α3 subfamily with 80.7-84.5% similar identity (**Table 1.2**). Gabriel *et. al.* showed that virus host adaptation changes the required KPNA isotype for virion replicate within the host (273). The group observed a KPNA4 specificity in avian viruses in contrast to favoured KPNA6 after mammalian adaptation of tested virus.

	KPNA1	**KPNA2**	**KPNA3**	**KPNA4**	**KPNA5**	**KPNA6**
KPNA1	100					
KPNA2	45.7	100				
KPNA3	47.9	49.5	100			
KPNA4	47.5	50.9	85.8	100		
KPNA5	80.7	48.1	48.4	48.7	100	
KPNA6	82.1	47.3	47.8	48.2	84.5	100
KPNA7	42.6	54.7	43.7	43.7	41.4	42.5

Table 1.2. KPNA isoform homology represented as percentage. Colour legend: Blue represents importin subfamily α1, orange represents importin subfamily α2, green represents importin subfamily α3. Table modelled on figure from Kelley *et. al.* (272).

Importin α subtypes have been previously described as adaptor proteins, however, studies have shown that both subtypes can transport cargo independently or in collaboration with each other (274,275). Nevertheless, the best studied cargo transport method is nuclear localisation sequence (NLS)-dependent KPNA-KPNB complex nuclear transport. During this event, NLS-cytoplasmic cargo binds to a KPNA member. This interaction recruits a

KPNB isoform to join through the importin β binding (IBB) domain forming a cargo-KPNA-KPNB complex (276). The complex migrates through the nuclear pore complex (NPC), a large multimeric structure, approx. 60 MDa, situated within the nuclear membrane (277,278). Once in the nucleus, small RanGTP regulates KPNB detachment from the trimeric complex leading to the disassembly of the protein complex (279). Released cargo, for example p65 or IRF3, can now freely regulate gene expression in response to the initial stimulus. Conversely, KPNA and KPNB are separately exported out of the nucleus by RanGTP (280). RanGTP is converted into RanGDP while escorting KPNAs and KPNBs back into the cytoplasm, disassociating with the importin members post cytoplasmic migration, independently returning to the nucleus (279). In humans, the canonical-NLS-dependent NF-κB translocation strongly relies on the KPNA2-KPNB1 complex (281).

Host IPO5 aids porcine circovirus type 2 in translocating into host nucleus, therefore, advancing viral replication (282). KPNA2 and KPNA6 have been described as the primary nuclear transporters of p65 (281). Knockdown of KPNA2 and KPNA6 in A549 cells showed p65 sequestered within the cytoplasm in 81% and 74% of cells, respectively. To date only one poxviral protein has been identified to interact with human KPNAs. In 2019, VACV protein A55 was shown to reduce p65-KPNA2 interaction (283). Disruption of p65-KPNA2 binding blocked TNFα-stimulated p65 nuclear translocation. Pallett *et. al.* presented the adverse effects on host $CD8^+$ T cells when presented with A55. No other KPNA proteins were found to interact with A55 (283).

Recent studies have shown viruses outside of the *Poxviridae* family to interact with KPNA proteins restricting human immune responses. African swine fever virus protein

MGF360-12L competitively interacts with KPNA2, KPNA3 and KPNA4 inhibiting their interaction with p65 consequently diminishing IFN-β production (284). HIV has been observed to utilise importin α (unspecified) to migrate into the nucleus gaining access to host DNA for viral replication (285). Membrane protein found in severe acute respiratory syndrome coronavirus 2 (SARS-CoV-2) coprecipitated with both KPNA2 and KPNA6 (286). However, the interaction between the SARS-CoV-2 protein and the KPNAs had different effects on their relationship with IRF3. In the presence of membrane protein, KPNA6 could no longer bind to IRF3 disrupting the SeV-induced IRF3 nuclear translocation. This was strongly reflected in cell ability to produce IFN-β. Yu *et. al.* presented the use of host KPNA6 by influenza protein ANP32A/B to maintain efficient viral polymerase activity (287). Furthermore, KPNA6 CRISPR/Cas9 knockout inhibited viral polymerisation. The use of human KPNA and IPO proteins by pathogens is an effective solution to host immune system evasion.

1.3 MCV immune evasion

Unlike some other pathogens, such as Mycobacterium tuberculosis and Herpes simplex virus (HSV), MCV cannot remain latent or dormant in the body (15,288,289). Once the Mollusca have been cleared the virus is no longer present in the host. MCV is a prime example of a human adapted virus and a master at evading the immune system demonstrated by infection resolution time and low levels of inflammation. There are two primary ways in which MCV can do this: the infection site and the use of immunomodulatory proteins. MCV affects keratinocytes in the epidermis not crossing into the deeper layers of skin tissue and not infecting any other cell type (2). The virus encodes 182 genes some of which are involved in immune evasion (2).

Targeting of the IKK complex is commonly observed in viral immune evasion strategies as it is the key regulator of NF-κB signalling. VACV protein N1L inhibits innate signalling through direct targeting of IKK complex ultimately blocking activation of NF-κB (290). Homologs of this protein have also been encountered in other poxviruses (291). Therefore, it is not surprising that MCV would also encode open reading frames (ORFs) to target the IKK complex. Brady *et. al.* investigated the role of MC005 in human PRR- and pro-inflammatory cytokine signalling (292). The study showed that MC005 directly interacts with NEMO (292). MC005-NEMO binding inhibits a crucial conformational change in the IKK complex inhibiting signal transduction. Similarly, MC008 was also shown to target NEMO specifically inhibiting the ubiquitination of the protein (293).

MCV Protein	**Role/Function**	**Human Interacting Protein(s)**	**Reference**
MC005	Prevents IKK complex conformational changes. Inhibits NF-κB-mediated pro-inflammatory cytokine release.	IKKγ (NEMO)	(292)
MC007	Induces sequestration of tumour suppressor protein at mitochondrial membrane. Promotes cell survival.	Retinoblastoma protein	(294)
MC008	Disrupts ubiquitination of IKKγ. Inhibits NF-κB-mediated pro-inflammatory cytokine release.	IKKγ (NEMO)	(293)
MC053	Inhibits IL-18-mediated IFNγ production.	IL-18	(295)
MC054	Inhibits IL-18-mediated IFNγ production.	IL-18 Heparin	(296)

	Binds glycosaminoglycans on cell surface.		
MC080	Prevents MHC-I antigen presentation. Downregulates HLA-I and HLA-E. Impacts T cell and NK cell anti-viral response.	Tapasin	(297,298)
MC132	Induces p65 degradation. Inhibits NF-κB-mediated pro-inflammatory cytokine release.	p65 (RelA)	(299)
MC148	Inhibits cellular chemotaxis.	CXCL12α CCR8	(300–302)
MC159	Prevents IKKγ polyubiquitination. Inhibits NF-κB-mediated cell apoptosis. Inhibits TBK1 phosphorylation. IRF3 signal inhibition.	IKKγ (NEMO) TRAF2 TBK1 IKKε	(2,60,303–306)
MC160	Prevents IKKα-IKKβ interaction. Inhibits NF-κB-mediated cell apoptosis. Inhibits TBK1 phosphorylation. IRF3 and IRF7 signal inhibition.	Hsp90	(2,60,306,307)
MC163	Inhibits mitochondria-mediated cell apoptosis. Inhibits TNFα-stimulated NF-κB signalling.	IKKα	(308,309)

Table 1.3. Comprehensive description of MCV-derived protein roles in immune system evasion.

MC159 studied by Shisler *et. al.*, is another MCV immunomodulator which directly affects NEMO (303). The protein competes with cellular inhibitor of apoptosis protein 1

(cIAP1), an E3-ubiquiting ligase, for NEMO binding. MC159-NEMO interaction prevents cell apoptosis by inhibiting polyubiquitination of the kinase (305). Another well characterised viral FLICE inhibitory protein (vFLIP) is MC160. This MCV-derived inhibitor also stops virally infected cells from undergoing apoptosis. Once again, the IKK complex is affected, however, MC160 has not been shown to interact with NEMO like the previously mentioned MCV proteins. Instead, the inhibitor prevents IKKα-IKKβ interactions through induction of IKKα degradation (310). Cell apoptosis is blocked by another MCV-derived protein, MC163, as it prevents mitochondrial membrane permeabilization subsequently stopping cleavage of caspase-3 and poly(ADP-ribose) polymerase 1 (PARP-1) (309). Additionally, cell proliferation is supported by MC007 in a manner often observed in oncogenesis (294). The protein targets retinoblastoma protein through an LxCxE motif disrupting the cell cycle. Other cell surface proteins targeted by MCV include glycosaminoglycans such as heparin (296). Glycosaminoglycans regulate cell cycle events such as cell growth and proliferation, therefore, MC054-heparin binding could potentially affect these events.

Inhibitory function at a lower stage of signal transduction enables the virus to block a wider range of response stimuli. MC132 works downstream of the IKK complex as it directly interacts with NF-κB transcription factor member p65 (299). The MCV protein mediates p65-ubiquitination by the cullin-5-elongin-B/C complex leading to p65 proteasomal degradation. MCV is not the only poxvirus which exploits host ubiquitin ligases as an immune evasion strategy. VACV protein A55 interacts with cullin-3 leading to proteasomal degradation of target proteins (311).

IRF family members, primarily IRF3 and IRF7, are responsible for type I IFN responses during viral infections. IRF signalling has also been shown to be highly targeted by poxviruses, for example VACV protein N1L inhibiting TLR-mediated IRF3 activity (290). MCV-proteins MC159 and MC160 effect NF-κB and IRF signalling, however, both proteins use different domains for each type of signalling (306). These proteins prevent phosphorylation of the IKK-related kinase TBK1.

Adaptive immunity has also been shown to be impacted by MCV. MC080 is homologous to major histocompatibility complex class I (MHC-I) molecules found in wombats and wild boars (297). Surface availability of the antigen presenting molecule is reduced in cells expressing MC080 (298). Lower surface expression of MHC-I protects MCV infected cells from cytotoxic T cell and NK cell recognition. MC053 and MC054 could also impact NK cell activation and T cell response (295). The two proteins interact with pro-inflammatory cytokine IL-18 inhibiting IFNγ production. MC148R1 and MC148R2, found in MCV subtype I and II respectively, have also shown potential in deregulating a monocyte and dendritic cell response (301,302). Both MCV-encoded ORFs lead to inhibition of chemokine-mediated chemotaxis (300). Chemokine activity modulation has been seen in other poxviruses such as VACV or VAR (312–314).

As previously mentioned, MCV encodes for 182 proteins, 105 of which appear to be homologues of orthopoxviruses. Although not all may translate into immunomodulatory proteins, less than 15 MCV-derived proteins have been closely studied to uncover and understand their immune evasion properties. Protein MC009 is a small 21 kDa protein encoded for by a short 184 amino acid sequence. Senkevich *et. al.* predicted the protein to be non-globular (51). The only known homologue of MC009 comes from a closely

related *Molluscipoxvirus* member called EMCLV which is also not well characterised in literature. It is not yet understood how potently MC009 affects the immune system nor its mechanism of inhibition. MC009 is an under-studied MCV protein with potential for the development of autoimmune therapies.

1.4 Thesis aims

Based on the presented information about MCV and its use of immunomodulatory proteins this project aims to investigate the MCV protein MC009 and its role in MCV immune system evasion. Through this research, I aim to further our understanding of the host virus as well as use the immunomodulator as a tool to uncover more information about human innate signalling. Furthermore, a goal of this project is to be a stepping-stone in the development of MCV-derived anti-inflammatory therapeutic agents.

Thesis Hypothesis: MC009 is an MCV-derived immunomodulatory protein capable of inhibiting the activation of pro-inflammatory and anti-viral immune responses through targeting NF-κB and IRF signalling.

Aims:

- To investigate the effect of MC009 on NF-κB and IRF3/7 signalling using gene reporter assays.
- To examine the effect of MC009 on pro-inflammatory cytokine and type I IFN production using sandwich ELISA assays, IFNα/β bioassays and gene reporter assays.
- To determine a point of interaction between MC009 and the human innate system using confocal microscopy and co-immunoprecipitation experiments.

Chapter 2: Materials and Methods

2.1 Materials

2.1.1 List of materials

Product	**Product Code**	**Manufacturer/Supplier**
0.05% Trypsin-EDTA	25300054	Invitrogen
0.2µm Filter	83.1826.001	Sarstedt Ltd.
1,2-diaminocyclohexane-N,N,N’,N’-tetraacetic acid	319945-25G	Merck
1,4-Dithiothreitol (DTT)	10592945	Fisher Scientific
6-well Plate	10578911	Corning/Fisher
8-well Nunc Lab-Tek II Chamber Slide	16260661	Fisher Scientific
12-well Plate	3513	Corning Costar
24-well Plate	3524	Corning Costar
96-well Cell Culture Plate	10687551	Corning/Fisher Scientific
96-well Immuno ELISA Plate	10468075	Fisher Scientific
96-well Round-Bottom plate	83.3925.500	Sarstedt Ltd.
10 cm Cell Culture Dish	CLS430167-500EA	Corning/Merck
10 cm Petri Dish	82.1473.001	Sarstedt Ltd.
5 mL Stripette	13400297	Thermo Fisher
10 mL Stripette	10677341	Corning/Fisher Scientific
15 mL Falcon Tube	62.554.502	Sarstedt Ltd.
20 mL Syringe	300613	BD Biosciences
25 mL Stripette	10732742	Corning/Fisher Scientific
50 mL Falcon Tube	62.548.004	Sarstedt Ltd.
β-glycerophosphate Disodium	G9422-100G	Sigma-Aldrich
Acetyl Coenzyme A Lithium Salt	A2181-100mg	Sigma-Aldrich
Adenosine 5'-Triphosphate Disodium Salt (ATP)	A2383	Sigma-Aldrich
Alcohol Burner Wick	WHEA237071	VWR

Alexa Fluor™ 488 nm Anti-Mouse	A11029	Life Technologies
Alexa Fluor™ 488 nm Conjugated Anti-FLAG	MA1-142-A488	ThermoFisher
Alexa Fluor™ 568 nm Anti-Mouse	A11031	Invitrogen
Alexa Fluor™ 647 nm Conjugated Anti-HA	26183A647	ThermoFisher
Alexa Fluor™ 647 nm Conjugated Anti-Rabbit	A31573	Thermo Fisher
Ammonium Persulfate	A3678-25G	Sigma/Merck
Ampicillin Sodium Crystalline	A9518-25G	Sigma
Anti-β-actin Antibody	A5316	Sigma-Aldrich
Anti-DYKDDDDK (FLAG; M2) Antibody	F3165	Sigma-Aldrich
Anti-HA.11 Epitope Tag Antibody	901515	BioLegend
Anti-IκBα Antibody	4814S	Cell Signalling
Anti-KPNA6 Antibody	12366-2-AP	Proteintech
Anti-Karyopherin B3 (IPO5) Antibody	sc-17802	Santa Cruz
Anti-p65 Antibody, Rabbit	8242S	Brennan&Co
Anti-p65 Antibody, Mouse	sc-8008	Santa Cruz
Anti-phospho-IκBα, S32	2859T	Cell Signalling
Anti-phospho-p65 Antibody, S468	3039S	Cell Signalling
Anti-phospho-p65 Antibody, S536	3033S	Cell Signalling
Aprotinin	4139/10	Tocris/Bio-Techne
Autoclave Tape	15691934	Fisher Scientific
Benzonase	70746-3	Merck
Blasticidin	ant-bl-1	InvivoGen

Bromophenol Blue	32712	Riedel-de Haen
Bovine Serum Albumin (BSA)	12659-M	Merck
Cadmium Chloride ($CdCl_2$)	655198-5G	Sigma
Coelenterazine Native	10110-1	Biotium
Copper Sulfate	C8027-500g	Sigma
Cryovials	72.380.002	Sarstedt Ltd.
D-Luciferin Firefly	FL08607	Biosynth Carosynth
Dimethyl Sulfoxide (DMSO)	10213810	Fisher Scientific
Disodium Phosphate (Na_2PO_4)	S7907	Sigma-Aldrich
Dulbecco's Modified Eagle Medium (DMEM)	61965059	Gibco
DuoSet® ELISA, Human IL-8/CXCL8	DY208	R&D Systems/BioTechne
DuoSet® ELISA, Human CXCL10/IP-10	DY266	R&D Systems/BioTechne
Escherichia coli, DH5α	18265017	ThermoFisher
Eppendorf Tube, 1.5 mL	11351904	Axygen/Fisher Scientific
Ethylenediaminetetraacetic acid (EDTA)	15575020	Sigma/Fisher Scientific
Ethanol	64-17-5	TCD Estates and Facilities
Ethanol (molecular grade)	E7023-500ML	Honeywell/VWR
FLAG M2 Beads	A2220	Sigma
FLAG Peptide	F3290	Sigma
Foetal Bovine Serum	F9665-500ML	Sigma
GeneJuice® Transfection Reagent	70967-4	Merck
Glycerol	10336040	Fisher Scientific
Glycine	G8898-1KG	Sigma/Merck
HEK-Blue™ IFN-α/β Cells	hkb-ifnabv2	InvivoGen
Hemacytometer	Z359629-1EA	Merck
Hemacytometer Coverslips	Z375357-1EA	Merck

Hydrochloric Acid	15693640	Fisher Scientific
Hygromycin B Gold	ant-hg	InvivoGen
Inoculation L-Spreader	HA05088C	Microspec
Inoculation Loop	86.1562.010	Sarstedt Ltd.
IRDye® 680RD Anti-Mouse Secondary Antibody	926-68070	Li-Cor
IRDye® 680RD Goat Anti-Rabbit Secondary Antibody	926-68071	Li-Cor
IRDye® 800CW Anti-Rabbit Secondary Antibody	926-32211	Li-Cor
Isopropanol	BP2618-1	Fisher Scientific
Isopropanol, Mol. Grade	BP2618-1	Fisher Scientific
Kanamycin	K1377-1G	Sigma-Aldrich/Merck
Kimwipes	4AJ-9413021	Carl Stuart Ltd.
LB Agar	11758902	Fisher Scientific
LB Broth	12801660	Fisher Scientific
Lipofectamine™ 2000	11668019	Invitrogen/Bio-Sciences
Magnesium Carbonate Hydroxide Pentahydrate [$(MgCO_3)_4Mg(OH)_2.5H_2O$]	M5671-500G	Sigma-Aldrich
Magnesium Sulfate Heptahydrate ($MgSO_4.7H_2O$)	63138-250G	Sigma-Aldrich
Methanol	M/4000/21	TCD Estates and Facilities
Freezing Container 'Mr. Frosty'	5100-0001	Nalgene/Bio-Sciences
Nitrocellulose Membrane	10600012	Cytivia/SLS
Normocin™	ant-nr-1	InvivoGen
NP-40 (IGEPAL)	CA-630	Merck
P10 Tips	11577442	Fisher Scientific
P200 Tips	70.760.002	Sarstedt Ltd.
P1000 Tips	11548442	Fisher Scientific
Parafilm®	ASE165.15	Lennox Lab Supplies
Paraformaldehyde Solution,	15670799	ThermoFisher

4% (PFA)		
Penicillin-Streptomycin	15140122	Gibco
Phenylmethylsulfonylfluoride (PMSF) ($C_7H_7FO_2S$)	P7626-5G	Sigma-Aldrich
Phosphate Buffered Saline (PBS) (Sterile)	10010056	Invitrogen
Phosphoric Acid	15686710	Fisher Scientific
Poly(dA:dT)	P0883-10UN	Sigma/Merck
Poly-L-Lysine	P8920-100ML	Sigma-Aldrich/Merck
Potassium Chloride (KCl)	193780010	Acros Organics
Potassium Phosphate Monobasic (KH_2PO_4)	P0662-500G	Honeywell
ProLong™ Mounting Media with DAPI	P36931	Invitrogen
Protein Ladder	11852124	ThermoFisher
ProtoGel 30% Solution	NAT1260	SLS
PureLink™ Expi Endotoxin-Free Maxi Plasmid Purification Kit	A31231	Invitrogen/Bio-Sciences
Recombinant Human IFNβ	8499-IF/CF	R&D Systems/Bio-Techne
Recombinant Human TNFα	570104	BioLegend
Reservoirs, Individually Packed	E2310-1010	Starlab/Cruinn Diagnostics
Reservoirs, Multi-pack	SPL-23050	Medical Supply Co Ltd.
siRNA, KPNA6 Silencer Select Pre-designed siRNA s24241	4392420	Ambion/ThermoFisher
siRNA, KPNA6 Silencer Select Pre-designed siRNA s24242	4392420	Ambion/ThermoFisher
siRNA, Silencer Select Negative Control #1 siRNA	4390843	Ambion/ThermoFisher
Sodium Chloride (NaCl)	194090050	Acros Organics

Sodium Dodecyl Sulfate (SDS)	L4509-500G	Sigma-Aldrich
Sodium Fluoride (NaF)	GSK5130-1G	Merck
Sodium Hydrogen Phosphate, Anhydrous	13437	Alfa Aesar/ThermoFisher
Sodium Hydroxide (NaOH)	S5881-500G	Sigma-Aldrich
Sodium Orthovanadate (Na_3VO_4)	450243-10G	Sigma-Aldrich
Storage Box, 9x9	95.64.981	Sarstedt Ltd.
T175 Flask	83.3912.002	Sarstedt Ltd.
T75 Flask	15350591	Fisher Scientific
Tetramethylbenzidine (TMB) Substrate Solution	N301	Fisher Scientific
Tricine	T0377-1KG	Sigma-Aldrich
Tris Base	10376743	Fisher Scientific
Triton X-100	SIGT8787	Sigma
Trypan Blue	15250061	Invitrogen/Bio-Sciences
Tween® 20	NAT1082	SLS
QUANTI-Blue™ Solution	Rep-qbs	InvivoGen
Virkon™	12358667	Day Impex™/Fisher Scientific
Water bath Disinfectant Conditioner	4AJ-9858040	Julabo GmbH/Carl Stuart Ltd.
Wypall Paper Roll	16366158	Wypall/Fisher Scientific
Zeocin®	ant-zn-1	InvivoGen

2.2.2 Buffers and solutions

1,2-diaminocyclohexane-N,N,N',N'-tetraacetic acid

1,2-diaminocyclohexane-N,N,N',N'-tetraacetic acid powder was dissolved in 1 M sodium hydroxide. The stock was kept at room temperature until needed.

Co-immunoprecipitation lysis buffer

A stock of coimmunoprecipitation (Co-IP) lysis buffer was made using: 50 mM Tris, 150 mM NaCl, 5 mM EDTA, 10% v/v glycerol, 0.5 % v/v NP-40 (IGEPAL) and deionised H_2O (d H_2O). The stock was kept at 4°C until needed. On the day of use the following chemicals were added per 10 mL of stock buffer: 30 mM of 1M NaF, 1 mM of 200 mM Na3VO4, 1 mM of 100 mM $C_7H_7FO_4S$ (PMSF), 1% v/v of 2 mg/mL aprotinin and 40 mM of 1 M b-glycerophosphate.

Firefly luciferase substrate (Luciferase Assay Mix)

The following chemicals were added in the order in which they are listed to make up 2X luciferase assay mix (LAM): 20 mM tricine, 2.67 mM $MgSO_4.7H_2O$, 0.1 mM EDTA (pH 8.0), 33.3 mM DTT, 530 mM ATP, 270 mM acetyl coenzyme A, 30 mg luciferin. Solution was made up to the desired volume using dH_2O. After the contents were diluted in water, 2 M NaOH was added. This was followed by an addition of 50 mM magnesium carbonate hydroxide. LAM was stored in 25 mL aliquots in falcon tubes covered in tin foil at -20°C. The solution was thawed in a water bath at 37°C and diluted 1 in 2 in dH_2O before use.

Growth media

Sterile Dulbecco's Modified Eagle Medium (DMEM) media was used for all cell culturing. A 50 mL aliquot of DMEM was removed from the bottle before additions were made. This was used as serum free media (SFM) for cell transfections. Additionally, 10% foetal bovine serum (FBS) and 1% penicillin-streptomycin were added to the media. The media was kept refrigerated in between use.

Passive lysis buffer

Passive lysis buffer was made using 25 mM tris-phosphate (pH 7.8), 2 mM DTT, 2 mM 1,2-diaminocyclohexane-N,N,N',N'-tetraacetic acid, 10 % glycerol and 1% triton X-100. The ingredients were dissolved in dH_2O.

Phosphate buffered solution (PBS)

To prepare 1 L of 10x-PBS the following chemicals are needed: 80 g sodium chloride (NaCl), 2 g potassium chloride (KCl), 14.4 g disodium phosphate (Na_2PO_4) and 2.4 g monopotassium phosphate (KH_2PO_4). The chemicals were dissolved in dH_2O to make up 1 L.

Renilla luciferase substrate

Coelenterazine powder was diluted in 500µL molecular grade ethanol to make a 2 mg/mL coelenterazine solution stock. The powder and liquid forms of coelenterazine were stored at -20°C. The liquid stock of coelenterazine was diluted 1 in 1000 in PBS before use.

Running buffer

The running buffer is prepared in a 10x stock using 10 g sodium dodecyl sulphate (SDS), 30.3 g Tris base and 144.1 g glycine. The buffer is made up to 1 L using dH_2O.

Transfer buffer

Transfer buffer was prepared using running buffer. Methanol was added to the running buffer, making a 20% methanol:80% running buffer solution.

Tris-phosphate

Tris base was dissolved in dH_2O. The pH was adjusted using phosphoric acid to the required pH.

Western blot sample buffer

Sample buffer was prepared in two parts. Firstly 1 M Tris-HCl (pH6.8) was added to 2% SDS (10% stock), 10% glycerol, 0.1% bromophenol blue and made up to 20 mL with dH_2O. Before use, 10% 1M DTT and 1% Benzonase are added to the buffer.

2.2 Methods

2.2.1 Cell culture techniques

HEK293T cells were cultured in DMEM supplemented with 10% FBS and containing 1% penicillin-streptomycin. Cells were washed with pre-warmed sterile PBS and detached from the flask using 5 mL of pre-warmed 0.05% trypsin-EDTA. Cells were left to incubate with trypsin-EDTA for 2-5 minutes while the flask was placed back in the incubator at 37°C and 5% CO_2. Once trypsinisation was complete, the cells were resuspended in 10 mL of complete media, making the total volume of liquid 15 mL. The cells were centrifuged at 1,300 rpm for 5 minutes at room temperature.

To seed cells in plates shown in **Table 2.1**, after centrifugation, cells were resuspended in 20-30 mL DMEM depending on the size of the cell pellet. Cells were prepared for counting using 10 µL of resuspended cells mixed with 10 µL trypan blue dye. Half of the mixture was placed on a grid haemocytometer and a light microscope was used to count the cells. The average cell count was multiplied by two to account for the dilution caused by trypan blue.

To calculate the number of cells needed to seed a plate, the following calculation was used:

$$X\ (Average\ cell\ count \times 10^4\ cells/mL) = Total\ volume\ needed\ (mL)(Seeding\ density\ cells/mL)$$

$$X = mL\ of\ cells\ needed\ from\ resuspension$$

$$\therefore Total\ volume\ needed - X = Amount\ of\ DMEM\ needed$$

Cells were diluted accordingly in a fresh falcon tube and seeded in plates. The plates were incubated at 37°C and 5% CO_2 overnight.

Seeding Vessel	Cell Type	Surface area (cm^2)	Seeding density (cells/mL)	Growth media per well (mL)
10 cm Dish	HEK293T	56.7	$4x10^6$	10
6-well Plate	HEK293T	9.6	$5x10^5$	2
24-well Plate	HEK293T	1.9	$1x10^5$	1
96-well Plate	HEK293T	0.32	$2x10^5$	0.2
96-well Plate	HEK-Blue IFNα/β	0.32	$4x10^5$	0.12
8-well Chamber Slide	HEK293T	0.7	$1.8x10^5$	0.5

Table 2.1. Cell seeding density for all vessel types used.

2.2.2 $LiNO_2$ cell storage

A flask of cells was cultured for the purpose of freezing down healthy cell stocks. Cell culture was conducted as described. After centrifugation the cell pellet was resuspended in freezing solution. Freezing solution was made by adding 500 µL DMSO to 5 mL FBS. Resuspended cells, 500 µL, were poured into cryovials and labelled with cell type, date and initials of researcher performing the protocol. The vials were immediately moved to a -80°C freezer in a 'Mr. Frosty' container and left overnight. The cells were moved to a liquid nitrogen tank the following day. HEK293T cells were frozen down for easy accessibility when new cells were needed.

2.2.3 Plasmids and oligonucleotides

Prior to commencing this research, a library of open reading frames (ORFs) from MCV subtype 1 MC009L was custom synthesized by GenScript and subcloned into KpnI and

NotI sites of the pCEP4 expression vector (Invitrogen # V04450) with a C-terminal FLAG (DYKDDDDK) or an HA (YPYDVPDYA) epitope tag and pMEP4 (a kind gift from Professor Paul Farrell, Imperial College London) for CdCl2-inducible expression. Similarly, MCV subtype 1 MC020L was cloned in the same manner into the pCEP4 vector. MC132 and MC005 were made as previously described (292,299). MC009 truncations were constructed prior to commencement of this work by amplifying indicated regions with flanking KpnI and NotI sites (see **Figure 3.14**). Plasmids expressing IKKα-FLAG, IKKβ-FLAG, IKKε-FLAG, TAB2-FLAG, TRAF2-FLAG, and TRAF6-FLAG were from Tularik Inc. The sources of other expression plasmids were as follows: TRIF-FLAG, S. Akira (Osaka University, Osaka, Japan); and ISRE-luciferase, L. O'Neill (Trinity College Dublin, Dublin, Ireland); CD4-TLR3, R. Medzhitov (Yale University, CT); MAVS-FLAG and cGAMP synthase (cGAS), J. Chen (UT Southwestern Medical Centre); RasHa, D. Cantrell (University of Dundee, Dundee, United Kingdom). KPNA1-6-FLAG plasmids were received from C. Basler (Icahn School of Medicine at Mount Sinai, USA). The human STING coding region was amplified by PCR from full-length I.M.A.G.E. cDNA clones (IRATp970D0274D and IRAVp968F0688D; imaGenes) and cloned into the vector pCMV-myc (Clontech). The kB–luciferase reporter gene was obtained from R. Hofmeister (Universitat Regensburg, Germany), the pFR-luciferase reporter and pFA2-Elk1 were from Agilent. Full-length NEMO-FLAG and NEMO-HA were from K. Fitzgerald (University of Massachusetts, Amherst, MA). The K277A mutant NEMO was generated as previously described.(292)

2.2.4 Bacterial transformation

Plasmids for cell transfections were prepared from stocks maintained in the lab. LB broth and LB agar plates (10 cm dishes) were prepared before bacterial transformation. Both

liquids were autoclaved. In a sterile flow-hood, 5 mL of LB broth was poured into a sterile falcon tube and 50 mg/mL ampicillin was added to the LB agar and remaining LB broth.

To begin the bacterial transformation, the bench space was sterilised using 70% ethanol. A Bunsen flame was lit during the procedure. Sterile Eppendorf tubes were labelled accordingly in preparation. All plasmids and competent cells (DH5α *E. coli*) were kept on ice. Depending on plasmid concentration, 0.5-2 µL plasmid was added to 10 µL competent cells in a sterile labelled Eppendorf tube. The tubes were left on ice for 30 minutes. Following this, the cells underwent heat shock by placing them in a water bath at 42°C for 45 seconds. The tubes were then returned to ice for an additional 5 minutes. Under a Bunsen flame, 150 µL sterile LB broth (without antibiotic) was added to the Eppendorf tubes. They were placed in a shaker-incubator at 225 rpm and 37°C for 1 hour. Once ready, 50-100 µL of cells was added to previously prepared 10 cm agar plates (with ampicillin or kanamycin where appropriate) under a Bunsen flame. The cells were spread using a sterile spreader. The labelled plates were incubated overnight at 37°C in the incubator.

2.2.5 Plasmid purification

Day 1: The bench was sterilised, and a Bunsen flame was lit to allow for bacterial pre-culture preparation. Aliquots, 5 mL of LB broth with ampicillin, were prepared in 15 mL falcon tubes and the tubes were labelled accordingly. The bacterial plates were retrieved from the incubator (see section *2.2.4 Bacterial Transformation*) and one bacterial colony from the plates was added to the corresponding falcon tube. The tube cap was closed loosely and taped down. The tubes were placed in a shaker-incubator at 225 rpm for 7-8 hours at 37°C. When ready, 2 mL of pre-culture was added to 200 mL LB broth (with

ampicillin or kanamycin) in sterile 250 mL conical flasks under a Bunsen flame. The flask tops were covered in tin foil and left in a shaker at 140 rpm and 37°C overnight.

Day 2: Each conical flask was equally divided into labelled 50 mL falcon tubes and centrifuged at 4,000 rpm for 15 minutes. The medium was discarded and sterilised with virkon. The pellets were resuspended and purified as per PureLink™ Expi Endotoxin-Free Maxi Plasmid Purification Kit protocol.

2.2.6 Generation of MC009-expressing stable cell lines

HEK293T cells were used as parental cells for the generation of MC009-expressing stable inducible cells. A T75 flask of HEK293T cells was transfected with pMEP4-MC009-FLAG plasmid using GeneJuice® as the transfection reagent. The cells were selected with 100-300 ug/mL Hygromycin B Gold to obtain MC009-expressing cells. The cells were cultured as per the standard cell culture protocol with Hygromycin B Gold to maintain stable expression. Expression of pMEP4-MC009-FLAG was induced with 1 µM $CdCl_2$.

2.2.7 Reporter gene assay

Day 1: Normal cell culture protocol was carried out and HEK293T cells were seeded at $2x10^5$ cells/mL in 96-well plates. The plates were incubated at 37°C and 5% CO_2 overnight.

Day 2: Plates were inspected under a light microscope to check cell density, morphology, and lack of contamination. Plasmids and master mixes required for transfection were made outside of the hood. Stocks of 100 ng/µL were made up with sterile dH_2O for all

plasmids used for transfection to allow for easy calculation and handling. The reporter master mix contained 40 ng/mL TK Renilla luciferase and 80 ng/mL second reporter plasmid, for example NF-κB luciferase, in a 1:2 ratio respectively. The activator master mix was made using the reporter master mix. Different concentrations of reporter activators were used as indicated; the concentrations ranged between 0.1-50 ng/mL. The transfection master mix was made inside of the flow-hood, this was made in a 2:1 GeneJuice® to DNA ratio. The amount of transfection master mix needed was calculated with 1.76 µL/well GeneJuice® (220 ng DNA/well x 4 wells x 2:1 GeneJuice® to DNA ratio) and 30 µL/well serum free media (SFM; DMEM without FBS and antibiotics). The master mix was vortexed and left to incubate for 5 minutes in room temperature in the hood. The reporter master mix, activator master mix, 100 ng/mL MCV ORF plasmid, CMV empty vector and transfection master mix were added accordingly to a new sterile transfection plate. The empty vector was added to certain wells to allow for equal DNA concentration between wells. An example of transfection plate additions can be seen in **Table 2.2**. Assays using non-transfected stimulants, like TNFα or Poly(dA:dT), were not transfected with an 'activator master mix' on day 2. The plate was incubated at room temperature in the flow-hood for 15 minutes. After the incubation was complete, 8 µL of each well was transferred to the corresponding well of the 96-well plate seeded the day prior. Each well was made to allow for triplicates. The plate was incubated for 20-24 hours at 37°C and 5% CO_2.

	Reporter Master Mix	Activator Master Mix	MCV Inhibitor	Empty vector	Transfection Master Mix
	µL				
Neg. control	4.8	-	-	4	31.76
Pos. control	-	6.8	-	2	31.76
MC009 10 ng	-	6.8	0.4	1.6	31.76
MC009 25 ng	-	6.8	1	1	31.76
MC009 50 ng	-	6.8	2	-	31.76
MC020 10 ng	-	6.8	0.4	1.6	31.76
MC020 25 ng	-	6.8	1	1	31.76
MC020 50 ng	-	6.8	2	-	31.76

Table 2.2. Representative table of luciferase assay transfection plate additions. This table represents the additions made to each well for a luciferase assay experiment using 50 ng/µL activator master mix. MC009 is used as the studied inhibitor while MC005, MC132 and MC020 act as controls. The additions made of the MC009, MC005, MC020 and MC132 are represented by MC009 and MC020 in the above table. CMV HA-tagged (empty vector; EV) is used to balance the DNA concentration between wells. The negative control well only contains the reporter master mix and EV. The positive control well contains the activator master mix which includes the reporter DNA and the EV. Transfection master mix is added to all wells.

Day 3: Cells not transfected with an activator plasmid were stimulated with TNFα or Poly(dA:dT). TNFα was diluted in SFM and incubated for 5 minutes at room temperature. The final concentration of TNFα was 50 ng/mL. TNFα stimulated plates were incubated at 37°C and 5% CO_2 for 6 hours. Plates requiring Poly(dA:dT) were treated with 1 µg/mL of DNA. Lipofectamine™ 2000 was used as the transfection reagent for Poly(dA:dT) at a 1:1 ratio. Lipofectamine™ 2000 was incubated at room temperature in SFM for 5 minutes prior to the addition of DNA. The DNA-lipid complex

was incubated for a further 15 minutes at room temperature. Poly(dA:dT) was added to the transfected wells and cells were incubated at 37°C and 5% CO_2 for 24 hours.

The remainder of the protocol was carried out on the bench in non-sterile conditions. The plates were removed from the incubator and observed under a light microscope. The supernatant was discarded, and the plate was tapped lightly on tissue paper to remove excess media. Previously thawed passive lysis buffer was added to the plate wells, 50 µL/well. The plate was placed on a shaker for 15 minutes. When ready, 20 µL of lysed samples was transferred to two white 96-well white luminometer plates. One plate was used for a luciferase read-out and 40 µL of luciferase assay mix was added to each well. The plate was then inserted into the luminometer and read. Diluted coelenterazine was added to the second plate, 40 µL/well and the same procedure was repeated. The data was analysed using Microsoft Excel and graphed in GraphPad PRISM.

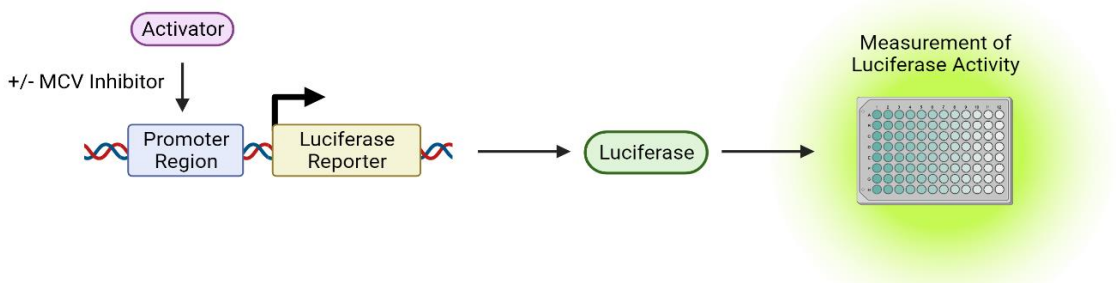

Figure 2.1. Graphic representation of luciferase regulation during reporter gene assays. A promoter region upstream of a luciferase reporter must be activated for the cell to produce luciferase. In the presence of an inhibitor of the tested pathway (activator-promoter region reporter, for example, TRIF-ISRE luciferase promoter) luciferase activity released from the cell lysate will be lower as the production of the enzyme is downregulated. Image was created using BioRender (biorender.com).

2.2.8 Immunoblotting

Sample buffer was prepared prior to retrieving the plate from the incubator (see *Western Blot Sample Buffer* in **Section 2.2.2. Buffers and Solutions**). The supernatant was aspirated from the plate and the plate was placed on ice. The plate was placed at an angle to aspirate the remainder of media. Cells were lysed using the Western blot sample buffer. The wells/plates were scraped using a sterile scraper. The samples were transferred into labelled Eppendorf tubes. The tubes were boiled at 95-100°C for 5 minutes. Samples were used thereafter or stored at -20°C until needed.

SDS-PAGE gels were prepared in the order as seen in **Table 2.3**. APS and TEMED were added immediately before pouring the gels to allow for sufficient time to mix and pour the gels before they solidified. The resolving gel was poured into the cassette first. Isopropanol was poured on top of the resolving gel while it set. Once the gel was polymerised, the isopropanol was poured off. Any remaining isopropanol was absorbed using filter paper. The stacking gel was poured directly on top of the resolving gel and a comb of adequate size was inserted into the gel immediately. The resolving and stacking gels took approximately 15-20 minutes to set. The gels were placed in the SDS-PAGE tank. The cassettes were placed, openings with combs facing each other, into the electrophoretic tank and running buffer was added to the middle chamber and allowed to run over the cassettes into the side chambers. The combs were then removed. For a 15-well comb, 1.5 µL protein ladder was used and 20 µL samples in the remaining wells. The gels were electrophoresed at 30 mA/gel for 60-95 minutes.

Nitrocellulose membrane was used for gel transfer. A western blot sandwich was made up in the following order: sponge, filter paper, gel, membrane, filter paper, sponge.

Transfer buffer was poured into the tank and an ice pack was placed inside of the filled tank. The transfer was conducted at 350 mA for 60-90 minutes. The membrane was blocked in 3% BSA dissolved in PBS for 60 minutes on a shaker at room temperature. The membrane was placed in 50 mL falcon tube with protein side facing in. Primary antibody diluted in blocking solution was added to the tube. The tube was left on a roller overnight at 4°C.

	Stacking Gel	**Resolving Gel**				
	5%	**6%**	**8%**	**10%**	**12%**	**15%**
H_2O (mL)	2.7	5.3	4.6	4.0	3.3	2.3
30% Acryl-bisacrylamide (mL)	0.67	2.0	2.7	3.3	4.0	5.0
1.5 M Tris, pH 8.8 (mL)	0.5	2.5	2.5	2.5	2.5	2.5
10% SDS (mL)	0.04	0.1	0.1	0.1	0.1	0.1
10% APS (mL)	0.04	0.1	0.1	0.1	0.1	0.1
TEMED (mL)	0.004	0.008	0.006	0.004	0.004	0.004
Total Volume (mL)	4.0	10.0	10.0	10.0	10.0	10.0

Table 2.3. Recipes for resolving and stacking gels for denaturing SDS-PAGE; as per Roche Lab FAQs 3rd edition.

Day 2: The primary antibody was removed, and the membrane was washed three times with 0.05% Tween® 20 and PBS on a roller. Secondary antibody was diluted in blocking solution and added to the tube and placed on a roller. The membrane was incubated in secondary antibody in room temperature for 1 hour. The membrane was washed again, 3 x 5 min washes, and imaged using Li-Core or Bio-Rad imaging technology. If necessary, the blot was stored in wash buffer at 4°C.

Antibody	Antibody Type	Host Species	Dilution Factor
HA Tag	Primary	Mouse	1:1,000
DYKDDDDK Tag	Primary	Mouse	1:7,000
β-actin	Primary	Mouse	1:10,000
KPNB1	Primary	Rabbit	1:1000
IκBα	Primary	Mouse	1:1000
IPO5	Primary	Mouse	1:200-1000
KPNA6	Primary	Rabbit	1:1000
p65	Primary	Mouse	1:1000
p65	Primary	Rabbit	1:1000-50,000
Phospho-p65 S536	Primary	Rabbit	1:1000
Phospho-p65 S468	Primary	Rabbit	1:1000
Phospho-IκBα	Primary	Rabbit	1:1000
UBR5	Primary	Mouse	1:1000
Anti-mouse IRDye® 680RD	Secondary	Goat	1:10,000
Anti-rabbit IRDye® 680RD	Secondary	Goat	1:10,000
Anti-rabbit IRDye® 800CW	Secondary	Goat	1:30,000

Table 2.4. Primary and secondary antibody description for immunoblotting; manufacturer name and catalogue number as seen in section 2.1.1 List of Materials.

2.2.9 Immunoprecipitation

Standard tissue culture protocol was followed. Cells were transfected with 8 µg DNA using GeneJuice® and were incubated for 24 hours. Immunoprecipitation sample preparation was conducted on ice or at 4°C. Before the protocol was begun, necessary equipment was pre-cooled: labelled Eppendorf tubes, beaker with ice water, cell scraper, co-immunoprecipitation (Co-IP) sample buffer. Cells were lysed using Co-IP buffer (see section *2.2.2 Buffers and Solutions*) and left on ice for 15 min. Samples were centrifuged

at 13,000 rpm for 10 min at 4°C. The supernatant was divided between “control lysate” samples and “beads” samples.

Anti-FLAG M2 affinity gel beads, 20 µL of affinity gel per sample, were used to bind any FLAG-tagged protein and its interactors. The beads were equilibrated with Co-IP lysis buffer. To equilibrate the beads, 1 mL of lysis buffer was added to the beads and the tube was inverted until the tube contents were homogenous. The Eppendorf tube was then centrifuged in a benchtop mini centrifuge for 20 seconds. The process was repeated three times. After the last equilibration step, the beads were resuspended in lysis buffer, 100 µL Co-IP lysis buffer x number of samples. The FLAG beads were added to ‘IP lysate’ samples and kept on a roller at 4°C overnight.

The following day, the beads were washed. The samples were centrifuged at 3,000 rpm for 5 minutes at 4°C. The centrifuged samples were place on ice and the supernatant was aspirated leaving behind the bead pellet. The beads were washed with cold Co-IP lysis buffer. The wash process was repeated three to five times. FLAG peptide was then added to the beads and rolled at 4°C for 30 min. Samples containing the beads were centrifuged and the supernatant was transferred to fresh tubes labelled “IP lysates”. The sample beads were frozen. Sample buffer was added to the “IP lysate” supernatant and “control lysate” samples. Previously described immunoblotting protocol was conducted to visualise results.

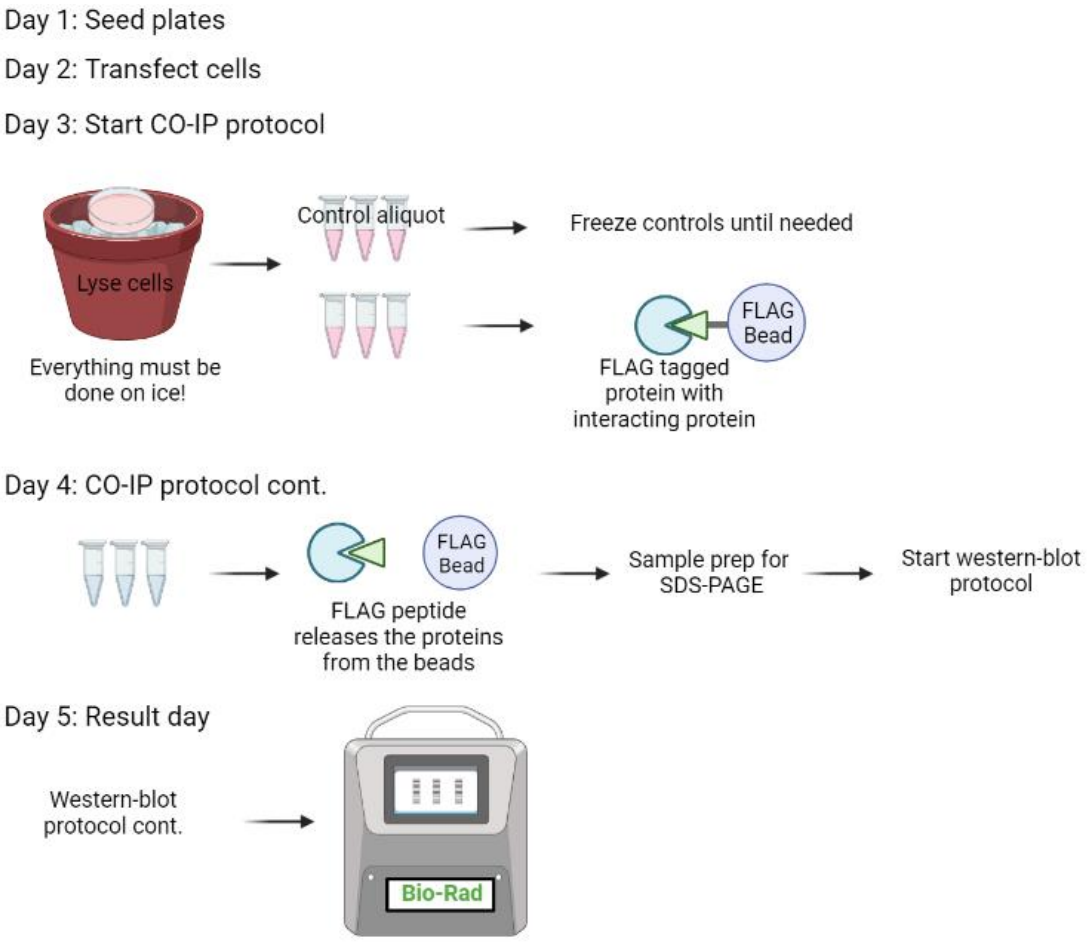

Figure 2.2. Graphical representation of immunoprecipitation; the graphic was created using BioRender (biorender.com).

2.2.10 Confocal microscopy (coverslip method)

Day 1: Cell culture was conducted as normal. Placed a single coverslip (kept in ethanol) per well of a 24-well plate. The coverslips were washed twice with 1 mL sterile PBS. Coated the coverslips in poly-L-lysine and left on for 10 minutes. Aspirated the poly-L-lysine off and allowed the coverslips to dry. The wells were seeded with $1x10^5$ cells/mL HEK293T cells. The cells were incubated overnight at 37°C and 5% CO_2.

Day 2: The wells were transfected using the same method as cell transfection for luciferase assays. Each well contained 1 µg of DNA.

Day 3: The wells were washed with non-sterile PBS twice and were fixed in 2% paraformaldehyde (PFA) in PBS for 30 minutes. The wells were washed with 1 mL PBS three times. The coverslips were then permeabilised and blocked in 2% BSA in 0.3% Triton X-100 in PBS for 30-60 minutes. Alexa Fluor™ conjugated antibodies were diluted in 2% BSA in PBS. The plate was covered with tin foil and left overnight in 4°C.

Day 4: The antibody solution was discarded. The coverslips were washed in PBS three times. Hoechst stain (blue) was used to stain the nucleus. The stain was diluted 1:1000 in PBS, 1 mg/mL, and left to incubate in room temperature for 20 minutes. The wells were washed with PBS three times. Mounting slides were labelled accordingly. A drop of mounting media, 4 µL, was placed in the centre of the slide and a coverslip was placed facedown onto the media. The slides were left to dry overnight.

Day 5: The edges of the coverslips were sealed using clear nail varnish. The slides were imaged using a Leica SP8 scanning confocal microscope and LAS X software.

2.2.11 Confocal microscopy (chamber slide method)

Cell culture was conducted following standard protocol. Cells were seeded in 8-well chamber slides at $1.8x10^5$ cells/mL. The cells were incubated overnight at 37°C and 5% CO_2. Slides were transfected using the luciferase assay transfection protocol; each well contained 1 µg of DNA. Cells were transfected for 20-24 hours. Confocal slides stimulated with TNFα were treated with 50 ng/mL of the stimulant. Stock TNFα was diluted in SFM. The cells were stimulated with TNFα for various lengths of time depending on the experiment, 0-120 minutes.

Media was gently aspirated off and the wells were washed with non-sterile PBS. The cells were fixed in 4% PFA in PBS for 15 minutes. The chambers were washed with PBS. The cells were then permeabilised and blocked in 0.3% Triton X-100 in 2% BSA in PBS for 60 minutes. The permeabilization-blocking solution was removed before slide staining was begun. Unconjugated primary antibodies were diluted in 2% BSA and left on slides for 60 minutes at room temperature.

Antibody	**Host**	**Dilution Factor**	**Alexa Fluor™ nm**	**Assigned Colour**
p65	Rabbit	1:1,000	-	-
p65	Mouse	1:1,000	-	-
KPNA6	Rabbit	1:1,000	-	-
Anti-HA Tag	Mouse	1:500	647	Red
Anti-FLAG Tag	Rat	1:1,000	488	Green
Anti-Rabbit	Donkey	1:1,000	647	Red
Anti-Mouse	Goat	1:1,000	488	Green
Anti-Mouse	Goat	1:1,000	568	Yellow

Table 2.5. Immunofluorescence assay antibody description: manufacturer name and catalogue number as seen in section 2.1.1 List of Materials.

Once the initial staining was complete, the unconjugated antibodies were aspirated off. Alexa Fluor™ conjugated antibodies were diluted in 2% BSA and added to the chambers. The slides were then wrapped in tinfoil (reducing light interaction with present fluorophores) and maintained at 4°C overnight. The antibody solution was discarded, and wells were washed with PBS. Slides were mounted using ProLong™ mounting media with DAPI. Once dry, slides were sealed. The slides were imaged using a Leica SP8 scanning confocal microscope and LAS X software.

2.2.12 Sandwich ELISA

Cell culture was carried out using the standard protocol. Stable-inducible cells were used in ELISA sample generation. The cells were seeded in 96-well plates or 6-well plates and incubated at 37°C and 5% CO_2 for 24 hours. pMEP4-MC009-FLAG containing cells were induced with 1 mM $CdCl_2$ and incubated in the same conditions for a further 24 hours. Once induced, the cells were stimulated with 50ng/mL TNFα or 1µg/mL Poly(dA:dT) for 24 hours and were maintained at 37°C and 5% CO_2. The supernatants were aspirated and transferred into pre-labelled Eppendorf tubes. Samples were kept in a -20°C freezer until needed.

Day 1: The capture antibody was reconstituted in PBS creating a stock and aliquoted. The aliquots were stored at -20°C. The stock capture antibody was further diluted to the required working concentration using PBS. A 96-well flat bottom high binding assay plate was coated with 50 µL of the desired capture antibody. The plate was wrapped in tinfoil and incubated at room temperature overnight.

Day 2: Capture antibody was discarded, and the wells were washed with 250 µL 0.05% Tween® 20 in PBS and left for 5 minutes. The wash step was repeated three times. After the last wash step was complete the plate was inverted and blotted against paper towels until all liquid was fully removed. The plate was blocked using 250 µL/well 1% BSA in PBS. During blocking the plate was covered in tinfoil and left on a shaker at room temperature for 1 hour. The wash step was repeated as previously described. Standards were reconstituted in deionised water and further diluted in 1% BSA to the working concentration range using a serial dilution. Following, 50 µL of standards or sample were

added to their respective wells. The plate was once again covered and left at 4°C overnight.

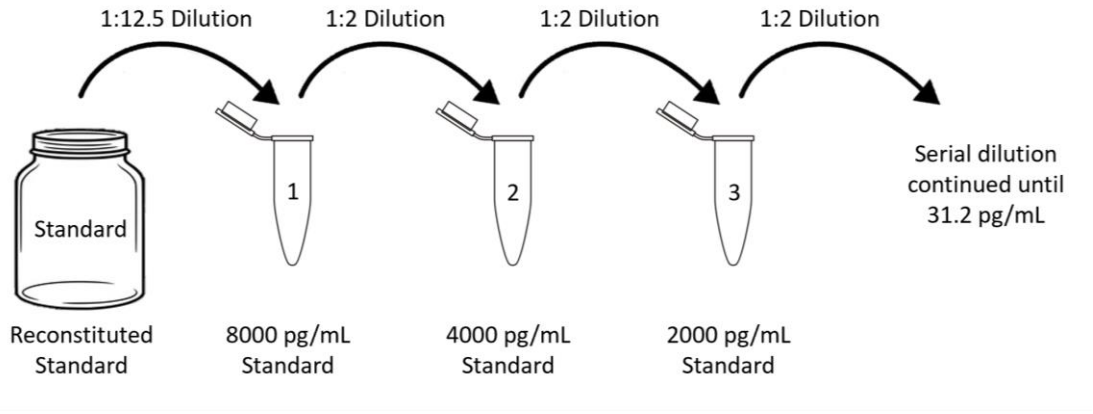

Figure 2.3. Graphical representation of ELISA standards preparation for IL-8 DuoSet® kit; the image was created using Microsoft PowerPoint.

Day 3: The wash step was repeated three times as before. Detection antibody was reconstituted and diluted in reagent diluent, 1% BSA, before 50 µL of the antibody was added to each well. The plate was sealed with tinfoil and left on a shaker at room temperature for two hours. The wells were washed and dried as previously described. Light-sensitive streptavidin horseradish-peroxidase (HRP) was diluted in reagent diluent and 100 µL was added per well. The plate was immediately covered in tinfoil and left to incubate at room temperature for 20 minutes. The aspiration and wash step were repeated for the last time. A tetramethylbenzidine (TMB) substrate solution, 100 µL, was added to all wells. Once again, the plate was sealed to and left to incubate at room temperature for 20 minutes. The reaction was stopped using 50 µL 1M H_2SO_4. The optical density (OD) was determined using a microplate spectrophotometer set to 450 nm. The data was analysed using Microsoft Excel and GraphPad PRISM software.

ELISA Type	Stock concentration	Working concentration	Dilution Factor	Dilution Liquid
Mouse Anti-Human IL-8 Capture Antibody	480 µg/mL	4 µg/mL	1:120	PBS
Recombinant Human IL-8 Standard	100 ng/mL	31.2-8000 pg/mL	1:12.5	1% BSA
Biotinylated Goat Anti-Human IL-8 Detection Antibody	0.6 µg/mL	10 ng/mL	1:60	dH_2O
Mouse Anti-Human IP-10 Capture Antibody	240 µg/mL	2 µg/mL	1:120	PBS
Recombinant Human IP-10 Standard	110 ng/mL	31.2-8000 pg/mL	1:13.75	1% BSA
Biotinylated Goat Anti-Human IP-10 Detection Antibody	1.2 µg/mL	20 ng/ml	1:60	1% BSA
Streptavidin-HRP	N/A	N/A	1:40	1% BSA

Table 2.6. IL-8 and IP-10 ELISA reagent dilutions.

2.2.13 IFNα/β bioassay

Primary samples were prepared in stable inducible MC009 cells. Cells were seeded in 6 well plates at $6x10^5$ cells/mL and incubated at 37°C and 5% CO_2 for 24 hours. $CdCl_2$ was added to the necessary wells to induce pMEP4-MC009-FLAG expression. The plate was incubated for an additional 24 hours using the same conditions. Selected wells were stimulated with 1 µg/mL Poly(dA:dT). The plate was placed back in the incubator for 24

hours. Supernatants from each well were aspirated off and transferred into pre-labelled tubes.

HEK-Blue™ IFN-α/β cells were used for the bioassay preparation and read-out. The growth media, DMEM with 10% FBS and 1% penicillin-streptomycin, was supplemented with additional antibiotics: 30 µg/mL Blasticidin, 100 µg/mL Normocin™ and 100 µg/mL Zeocin®. The supplemental antibiotics were not added into the media for plate seeding.

HEK-Blue™ IFN-α/β cells were plated in 96-well plates with 120 µL of cells resuspended in test medium, DMEM with 10% FBS and 1% penicillin-streptomycin. A serial dilution of 0.2 mg/mL recombinant human IFNβ standard stock was conducted ranging from 10,000 pg/mL to 4.9 pg/mL. An 80 µL aliquot of each standard was added per allocated well. Similarly, 80 µL of thawed primary samples from stable cells were added into the necessary wells. Additions of standards and samples were conducted in triplicates. Test medium was used as a negative control. The prepared plate was incubated at 37°C and 5% CO_2 for 24 hours. The supernatants were collected, secondary samples.

A fresh 96-well flat bottom culture plate was used for the incubation of samples with Quanti-Blue solution. Once again 200 µL of liquid was added per well: 50 µL supernatant of secondary samples and 150 µL Quanti-Blue solution. The plate was covered in tinfoil and incubated at 37°C for 10-25min. SEAP levels were quantified using a microplate spectrophotometer at 620 nm.

2.2.14 siRNA optimisation

SiRNA was resuspended in nuclease-free water and was stored at -20°C. HEK293T cells were seeded at $8x10^4$ cells/well in 24-well plates. Plates were left to incubate at 37°C and 5% CO_2 overnight. The transfection protocol used was based on the 'Silencer Select Pre-Designed, Validated, and Custom Designed siRNA' protocol (protocol publication number MAN0007836 rev. 1.0) written by Ambion by Life Technologies. Lipofectamine™ 2000 was used as the transfection reagent. Lipofectamine™ 2000 was added to SFM and incubated at room temperature for 5 minutes. SiRNA was diluted using SFM. The diluted siRNA was added to the incubated Lipofectamine™ 2000 at a 1:1 ratio. The siRNA-lipid complex was incubated at room temperature for a further 5 minutes before it was added to the plate wells. The plate was incubated at 37°C and 5% CO_2 for 24-72 hours. The samples were prepared and analysed using standard western blot protocol.

2.2.15 Statistical analysis

Gene Reporter Assay: Raw data was normalised using Microsoft Excel. First, values obtained from plate with LAM were divided by the values obtained from coelenterazine plate allowing for data normalisation of reporter gene expression against Tk Renilla. The average of the triplicates was obtained, and all results were normalised to the negative control well. Results were transferred into GraphPad PRISM software version 8.0.2 and graphed with SEM error bars. Statistical significance of results was obtained using a one-way ANOVA and Dunnett's multiple comparisons test. To conduct a one-way ANOVA each normalised average value was compared to the negative control value. The results were graphed using bar charts. The y-axis represented percentage (%) activity of the samples with the samples plotted along the x-axis. Statistical significance was indicated

by * <0.05, ** < 0.01, *** <0.001, and **** <0.0001. Replicates of the same experiment were not combined as a representative should be used to present data obtained from gene reporter assays.

ELISA and IFNα/β bioassay: The values obtained by the spectrophotometer were input into a Microsoft Excel spreadsheet and normalised by subtracting the mean value of negative control wells. This represented the background activity produced by the liquid in the wells. The normalised data was transferred into GraphPad PRISM where the standard curve was created. The data was interpolated with a second order polynomial (quadratic) standard curve. The interpolated values were graphed using bar charts showing SEM error bars. The y-axis presented the observed concentration of the investigated cytokine/IFN while the samples were plotted along the x-axis. Statistical significance was analysed through the comparison of the mean results with the stimulated control mean using one-way ANOVA. Statistical significance was indicated by * <0.05, ** < 0.01, *** <0.001, and **** <0.0001.

Chapter 3: Involvement of MC009 in NK-κB and IRF Signalling.

3.1 Introduction

Innate immunity is composed of complex pathways designed to tightly regulate a healthy response against pathogens or self-emerged molecules. Three different routes of signal induction are implicated in MCV anti-viral defences: nucleic acid-sensing TLRs, RLRs and the cGAS-STING axis (71,72,197,237,249,315). The similarities and differences between these pathways can be utilised as a guide for pathway mapping experiments in determining where MCV immunomodulators fit into human innate signalling. Gene reporter assays are a commonly used technique for pathway mapping experiments. Their efficacy and advantages can be observed in MCV literature and beyond (293,316,317).

TLR3 and TLR9 are both intracellular DNA-sensing receptors (171,318). TLR9 depends on the adaptor protein MyD88 (171,186). The signal is then transmitted to IRAK proteins and downstream TRAF6 (182,197). TRAF6 is also a vital kinase in RIG-I and cGAS-STING signalling (255,319). RIG-I signals to TRAF6 through a mitochondrial protein MAVS, whereas STING-associated TBK1 interacts directly with TRAF6 (78,248,264). In both RIG-I and cGAS-STING signalling, TRAF6 can directly regulate the IKK complex. Conversely, TLR9 signalling requires proteins such as TAK1 and TAB2 to allow for signal transduction to the IKK complex (320).

TLR3 exclusively signals through adaptor protein TRIF which in turn communicates with kinase TRAF3 (215,321). Likewise, sensing molecules RIG-I and cGAS can also induce a reaction through TRAF3. Once again, RIG-I uses an adaptor protein, in this case MAVS, to interact with the kinase whereas cGAS relies on STING to convey the information to TRAF3 (245,322,323). The signalling cascades use varied combinations of the same machinery downstream of TRAF3. TLR and RIG-I-PAMP sensing utilise

TANK, NAP1 and/or TBKBP1, individually or in conjunction with each other to regulate TBK1 and IKKε (226–228,232). The cGAS-STING axis also regulates IRF activity with help from scaffold proteins TANK, NAP1 or TBKBP1 (315,324). This signalling axis differs from its counterparts as it does not require IKKε to signal to IRF family members (325,326).

Unlike the innate signalling pathways, mitogenic pathways through RAS-ELK1 does not respond to the same ligand stimuli making it a perfect control for pathway mapping (327–329). The cascade is activated through the binding of growth factor receptor relaying the massage to RAS protein (330). Additionally, the growth factor stimulus does not lead to pro-inflammatory or type I IFN gene regulation but rather activation of ELK1 transcription factor (331–333). The mitogenic transcription factor does not regulate pro-inflammatory cytokines (such as IL-8 and IP-10) or type I IFNs (IFNα and IFNβ) released during a viral infection (331).

A limited number of MCV immunomodulators have been studied to date, multiple of which have been identified in the host lab. Studying these inhibitors has broadened not only our understanding of how MCV evades the human immune response but also of human innate signalling. This chapter concentrates on the effect of MC009 on human innate signalling pathways.

3.2 MCV ORF plasmid screen identifies MC009 as an inhibitor of NF-κB and IRF activation.

Previous work conducted in the lab involved screening expressed MCV subtype 1 ORF products against primary innate immune sensing and pro-inflammatory pathways (data

not shown). The screen was performed on 31 out of the 182 predicted MCV ORFs and identified several inhibitors of NF-κB and IRF activation from both sets of signalling pathways (51). One such inhibitor, MC009, inhibited both NF-κB and IRF activation, distinct from other inhibitors identified in this screen which targeted activation of only one transcription factor family. The MC009L ORF encodes a 184 amino acid protein with a predicted molecular weight of 21 kDa. MCV subtype 1 MC009 has a 94% similarity to its equivalent predicted protein sequence in MCV subtype 2 and a 47% similarity to EMCLV010L from the recently sequenced Equine molluscum contagiosum-like virus (**Figure 3.1**) (44).

```
EMCLV010L       -----------MEELVRAMRDFSLAESQEKVGFHCNDPYGAERWAIDELLADMVPGADNT    49
MCV1_MC009      MRLLARLLLLVMDELVFLMRNFALAQS-EPLGFHALDAFGLELWAWSDLRDSMVRTPAG-    58
MCV2_MC009      MRLLARLLLLVMDELVLLMRNFALAQS-DPLGFHALDALGLELWAWSDLRDSMVRTPAG-    58
                          *:***  **:*:**:* : :***. *  * * ** .:*  .**    .

EMCLV010L       HAPADVRAAPTLSTSEWESYVSDAVNTRMQLVTARWLTPEAPLVPEVSSDYITVLICVDC    109
MCV1_MC009      YEPATPLVSPPLCREEWTCYASDLLGARMRIVDACWLTPESPLLPRVSREHLLMLACAET    118
MCV2_MC009      YEPATPLVAPPLCREEWTCYASDLLGARMRIVDACWLTPESPLLPRVSREHLLMLACAEA    118
                : **   .:* *. .** .*.** :.:**::* * *****:**:*.** ::: :* *.:

EMCLV010L       SA-CPRLRVVSSDLSTGAMEASELWRGDVLFVSHTSKYALCAFSAR-NARFSLLSLQMRE    167
MCV1_MC009      VPENPCLRVVSSD-SNRSMEASGLRRRDLLFVSHTSDYALCVCPMSPDAIFSVAALVLSE    177
MCV2_MC009      VPESPCLRVVSSD-SNRSMEASALRRRDLLFVSHTSDYALCVFPMSQDAIFSVAALVLSE    177
                    * ******* *. :**** * * *:*******.****.     :* **: :* : *

EMCLV010L       GNKRACRRPD      177
MCV1_MC009      SNKRTRR---      184
MCV2_MC009      SNKRARR---      184
                .***: *
```

Figure 3.1. Multiple sequence alignment of MCV subtype 1, subtype 2 and EMCLV010L. EMCLV010L encoded by Equine molluscum contagiosum-like virus is the only known homolog of MC009. Key Legend: (-) gap in sequence, (.) amino acids of weakly similar properties, (:) amino acids of similar properties, (*) fully conserved amino acid. Sequence alignment was conducted using Clustal Omega (EBI-EMBL).

To begin investigating the protein, all MC009 plasmids found in the available frozen stocks collected by the host lab were tested to ensure they exhibited equivalent levels of expression and effect on innate pathways. First, MC009 ORF plasmids were tested for inhibitory ability with gene reporter assays (**Figure 3.2A**). HEK293T cells were transfected with a κB-luciferase reporter plasmid or ISRE-luciferase reporter plasmid (which parse NF-κB and IRF transcription factor activity, respectively) as well as a TK-Renilla luciferase reporter plasmid. TK-Renilla was used as a means of normalising reporter luciferase data as it possesses a broadly zero-order expression promoter and thus adjusts for transfection levels of all plasmids in the assay. The TLR3 adaptor protein TRIF was utilised to activate NF-κB and IRF3 in both reporter assays. A small concentration, 10 ng/well, of TRIF was used as overexpression of the protein can lead to cell toxicity thus leading to skewed results (318). Each MC009 plasmid was tested at two concentrations, 25 ng and 50 ng. In wells transfected with a lower dose of MC009, CMV-HA empty vector (empty vector; EV) was also added to maintain a comparable DNA concentration transfected per well.

As seen in **Figure 3.2**, the activity levels of MC009 plasmids varied greatly between the plasmid samples. Samples titled 'MP 9HA', '9 100 GB' and 'pCEP4 9F B' showed the most promising results for TRIF-mediated NF-κB signalling inhibition. This was also observed in TRIF-mediated ISRE signalling with 'MP 9HA', '9 100 GB' and 'pCEP4 9F B' having the strongest impact on activity levels even at lower MC009 doses. A ≥50% NF-κB or ISRE activity decrease can be seen in the presence of each of these plasmids (**Figure 3.2A and B**). In contrast, 'MP 9FLAG' and '9 FLAG OK' showed no inhibitory activity at either of the two MC009 amounts for both κB- and ISRE-luciferase assays.

To further investigate why there were such high discrepancies between the plasmids, protein expression from each was assessed. Once again, the MC009 plasmids were transfected at two concentrations, however, this time in 6-well plates instead of 96-well plates therefore, with plasmid amount adjusted for scale of transfection. Cell lysates were also blotted for β-actin as a loading control verifying protein level consistency per well. A notable difference was observed between the expression levels of the various MC009 plasmids which were trialled. Following the trend seen during luciferase assay testing, 'MP 9HA', '9 100 GB' and 'pCEP4 9F B' showed high levels of MC009 expression. In contrast, plasmids 'MP 9FLAG' and '9 FLAG OK' showed no MC009 expression (**Figure 3.1C**). Thus, plasmids 'MP 9HA' and '9 100 GB' (tagged with HA and FLAG respectively) were used for experimental work.

A

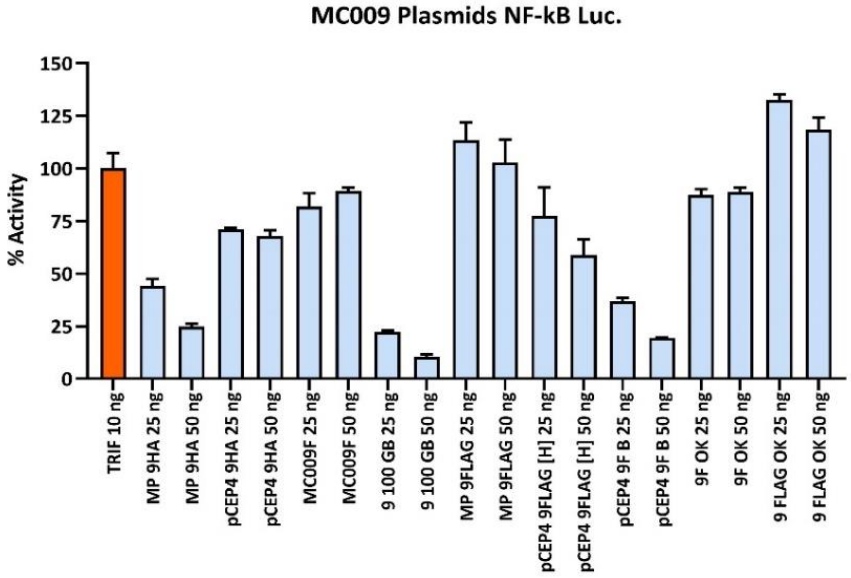

B

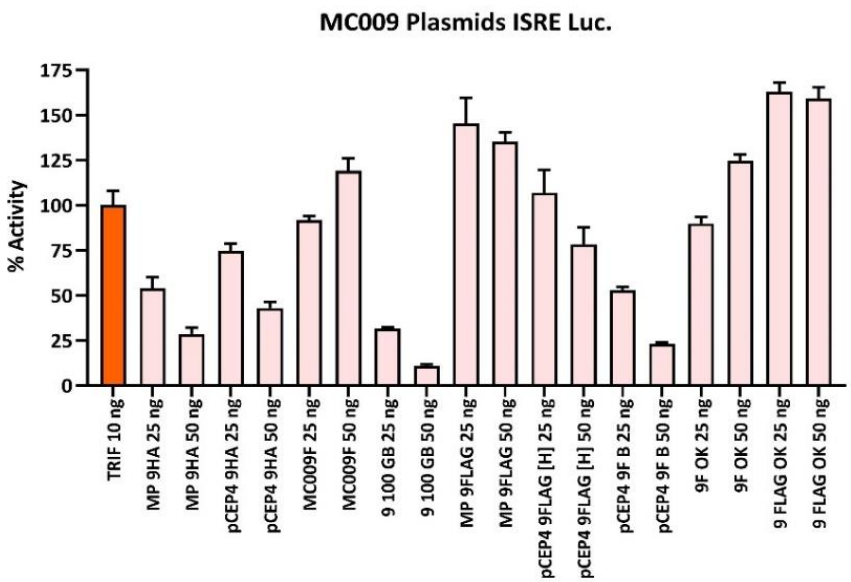

C

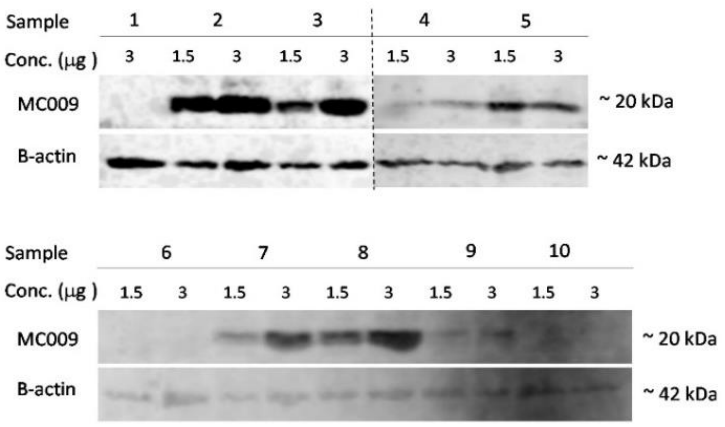

Sample Legend:
1. Empty Vector (EV)
2. MP MC009HA
3. pCEP4 9HA
4. MC009F
5. 9 100 GB
6. MP 9FLAG
7. pCEP4 9FLAG [H]
8. pCEP4 9F B
9. 9F OK
10. 9FLAG OK

Figure 3.2. MC009 plasmid activity and expression comparison. A. HEK293T cells were used to check for variability between MC009 plasmid activity. The cells were transfected with 80 ng κB-luciferase, 40 ng TK-Renilla and 10 ng TRIF. The plotted bars show the mean value of technical triplicates with SEM error bars. The graph is representative of n=1. **B.** Cells were transfected with 80 ng ISRE-luciferase, 40 ng TK-Renilla and 10 ng TRIF. The plotted bars show the mean value of technical triplicates with SEM error bars. The graph is representative of n=1. **C.** HEK293T cells were grown in 6-well plates and were transfected with 3μg DNA. They were incubated for 24h. Blots were imaged using an Odyssey Li-Cor Western blot imaging system and Odyssey software. The blots are representative of n=1.

3.3 MC020 identified as inhibitor control.

To further examine the effect of MC009 on innate signalling pathways, an MCV-ORF control expressing at an equivalent level with no effect on the investigated pathways was required. During the previously conducted MCV ORF screen, multiple ORFs showed no inhibitory properties for NF-κB or IRF activating pathways, including MC014, MC020, MC052 and MC063. Previously published work from the host lab used MC014 and MC020 as non-inhibitory controls (292,293,299).

Four MCV ORFs were tested for effects on κB- and ISRE-luciferase reporter activation. As per the MC009 plasmid screen, TRIF was used to activate both pathways and plasmids were transfected at the same two concentrations at which MC009 plasmids were previously tested. MC052 and MC063 showed moderate levels of inhibition of TRIF-mediated κB- and ISRE-luciferase activation (**Figure 3.3A and B**). Surprisingly, MC014 presented with inhibitory properties for both luciferase reporters (**Figure 3.3A and B**). In contrast, MC020 showed no significant inhibition of either pathway, and showed elevated but broadly comparable expression to MC009 at three different concentrations

(**Figure 3.3C**). Thus, MC020 was selected as the negative control for pathway mapping experiments.

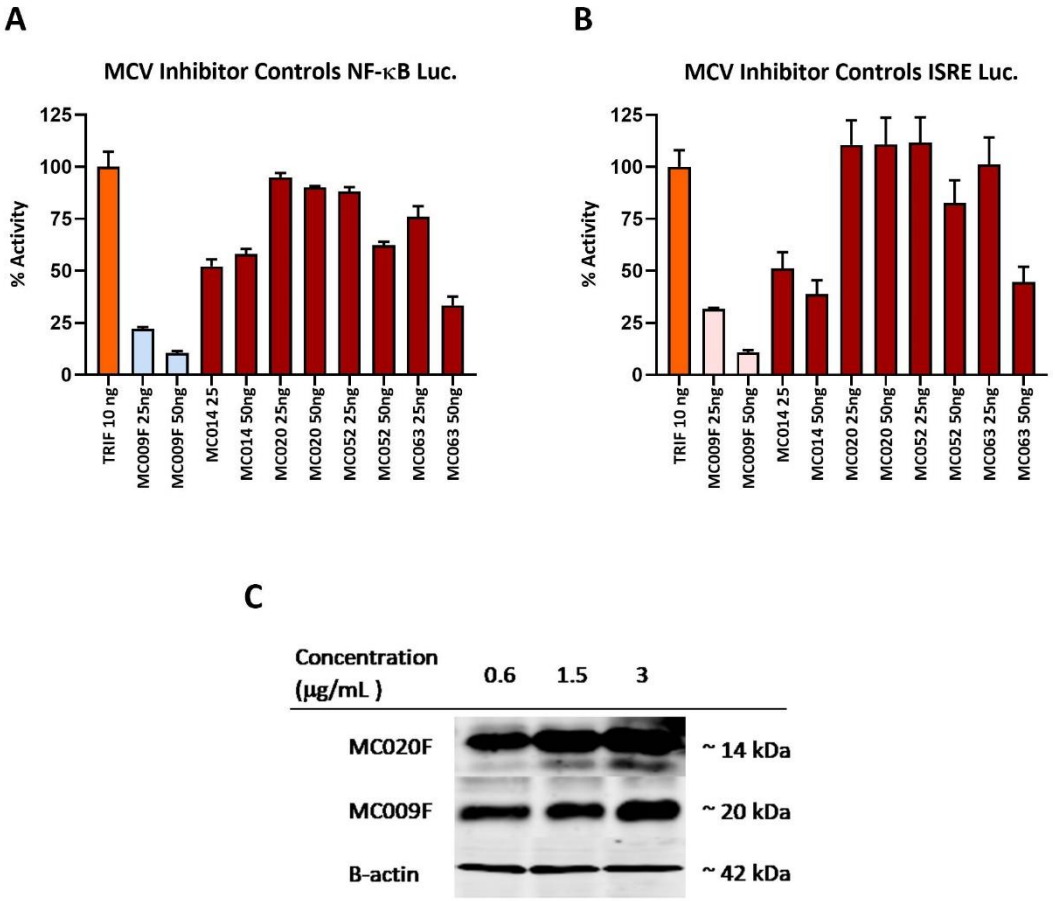

Figure 3.3. Identification of negative control MCV ORF. A-B. HEK293T cell line was used to test various MCV proteins as potential negative controls for MC009 experiments. Cells were transfected with 80 ng κB-luciferase or ISRE-luciferase, 40 ng TK-Renilla and 10 ng TRIF. Data is presented as the percentage of reporter activation with error bars representing SEM. The plotted bars show the mean value of technical triplicates. The graph is representative of n=1. **C.** HEK293T cells were grown in 6-well plates. The wells were transfected with 0.6, 1.5 or 3 µg of MCV plasmid. CMV-HA (empty vector) was used to balance the DNA concentration, 3 µg DNA per well. Cells were lysed using western blot sample buffer and resolved on a 15% SDS-PAGE

gel. Blots were imaged using an Odyssey Li-Cor Western blot imaging system and Odyssey software. The blots are representative of n=1.

3.4 MC009 does not inhibit a Ras-activated Elk1 control pathway.

As MC009 inhibited both NF-κB and IRF-activating pathways, it was necessary to determine if the MCV protein was non-specifically disrupting all cell signalling. Thus, the effect of MC009 on the Ras-activated Elk-1 mitogenic pathway was investigated. HEK293T cells were transfected with pFR-luciferase plasmid and Elk1-GAL plasmid, allowing Elk1 to bind to the luciferase plasmid through the GAL4 binding sites. The signal was stimulated using HA-tagged Ras protein. MC013 was used as a positive inhibitory control based on unpublished preliminary data observed by the host lab.

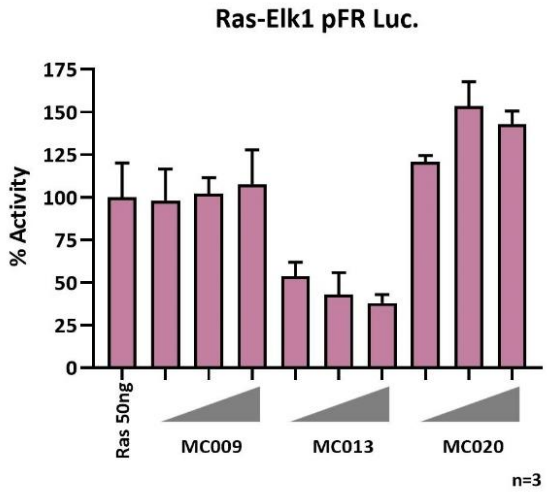

Figure 3.4. Mitogenic Elk1 pathway used as a control for MC009 inhibitory properties. HEK293T cells were transfected with 80 ng pFR-luciferase, 40 ng TK-Renilla and 5 ng Elk1 plasmid. The pathway was activated using 50 ng Ras-HA and the DNA concentration was equilibrated using an EV plasmid. Additions of MCV proteins were made at 10, 25 and 50 ng. MC013 was used as a positive control based on unpublished preliminary data from the Brady lab.

MC020 was used as a negative control. Data is presented as the percentage of reporter activation with error bars representing SEM. The graph is representative of n=3.

Ras-driven Elk1-pFR activity remained stable in the presence of MC009 at all concentrations. A clear difference in percentage activity could be observed between MC009 and MC013 treated cells, with MC013 having a strong inhibitory effect on luciferase activity even at the lowest concentration.

3.5 MC009 is an inhibitor of NF-κB activation by pro-inflammatory and innate sensing pathways.

NF-κB is activated by multiple innate pathways including pro-inflammatory (for example TNFα) and primary sensing pathways via TLRs, RLRs and the cGAS-STING axis (315,334–336). The effect of MC009 on NF-κB activation by both pro-inflammatory and sensing pathways was investigated (**Figure 3.5**). Ligand stimulation and overexpression of defined signalling proteins from innate pathways were used to drive NF-κB activation. MC132 was used as a positive control for NF-κB pathway mapping as it has been shown to target NF-κB p65 for degradation (299).

A pro-inflammatory cytokine stimulus, TNFα, was used to begin the NF-κB pathway mapping. The signal was inhibited in a dose-dependent manner by MC009 (**Figure 3.5A**). Likewise, MC009 inhibited NF-κB activation by the constitutively active CD4-TLR3 and its associated adaptor TRIF (**Figure 3.5B and C**). The MCV protein also showed great potential for inhibiting downstream TLR adaptor proteins MAL and MyD88, with >30% activity decrease after the addition of MC009 (**Figure 3.5 D and E**). To investigate the cGAS-STING axis both cGAS and STING were transfected into the system to drive

activation of this pathway. Similarly, cGAS-STING-driven κB-luciferase activity was potently inhibited by MC009 (**Figure 3.5F**). The effect of MC009 on RLR pathway activation of NF-κB were investigated by activation using transfected Poly(dA:dT), which is known to stimulate RIG-I in HEK293T cells, and overexpressed MAVS observing inhibition of both with MC009 expression (**Figure 3.5G and H**) (337).

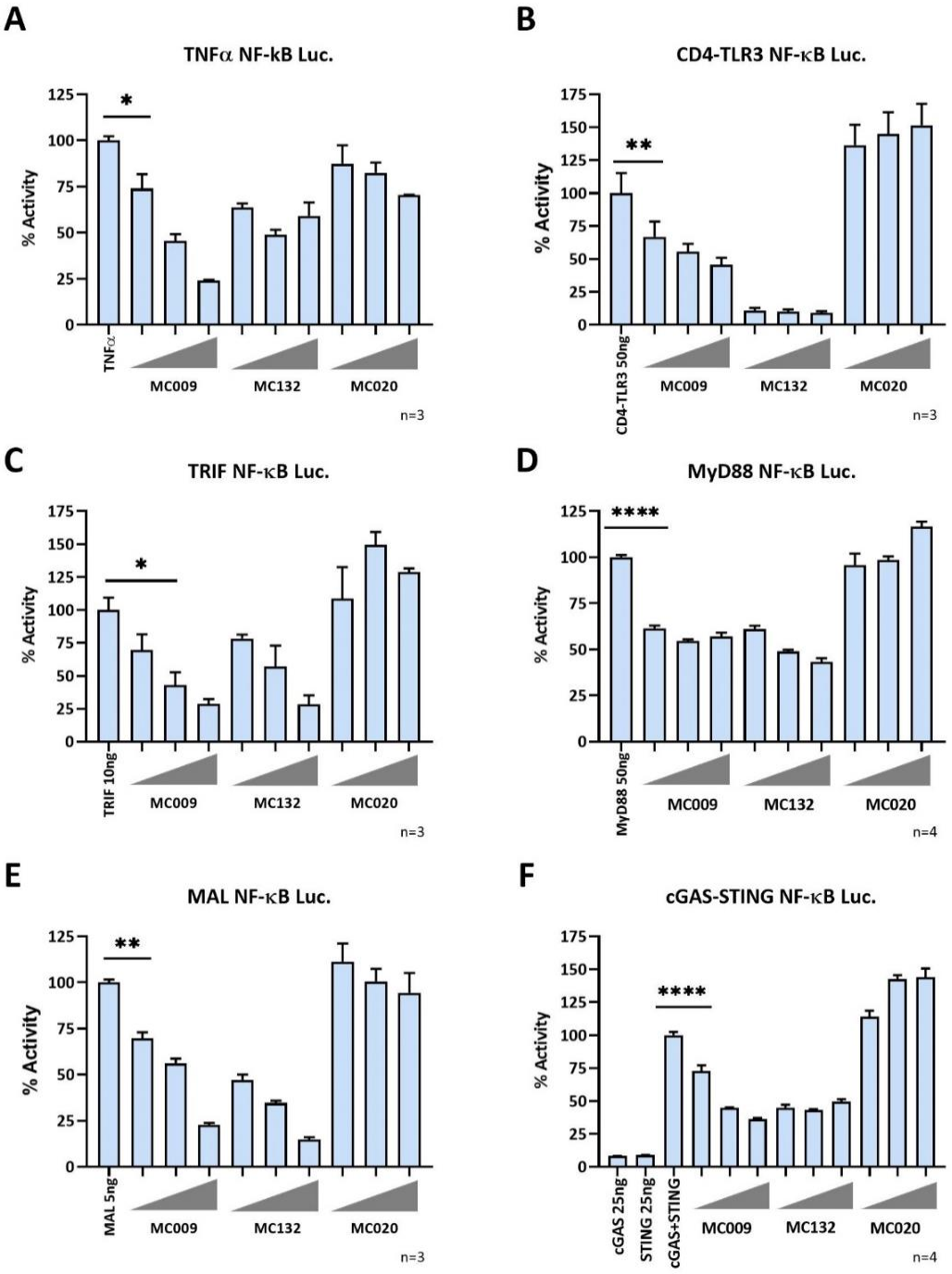

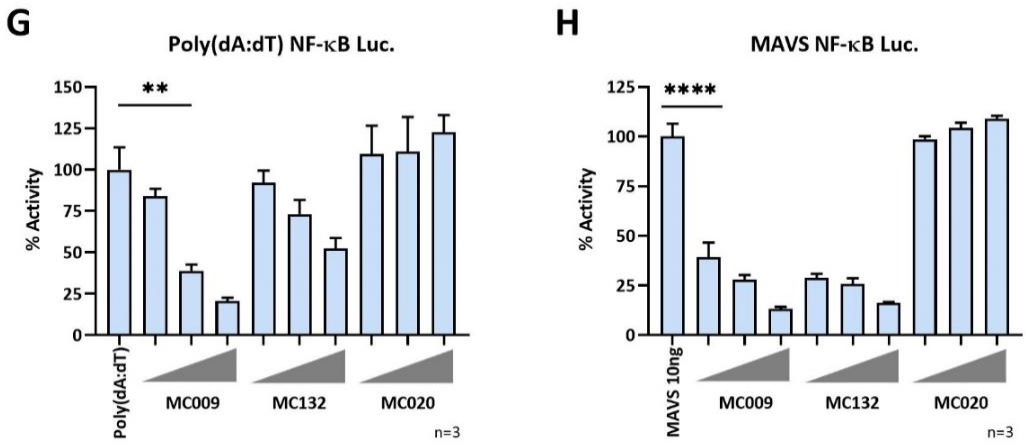

Figure 3.5. MC009 inhibits early stages of TLR, RLR and cGAS-mediated NF-κB signalling. A-H. HEK293T cells were transfected with 80 ng κB-luciferase, 40 ng TK-Renilla and EV. The signal was activated by overexpressing adaptor proteins or by stimulating with 1 μg/mL Poly(dA:dT) or 50 ng/mL TNFα . Poly(dA:dT) was transfected in using Lipofectamine 2000. The concentration of each activator was as stated on the figure panels. Additions of MCV proteins were made at 10 ng, 25 ng and 50 ng. MC132 was used as a positive control based on published data. MC020 was used as a negative control. Cells treated with TNFα were stimulated for 6 hours whereas Poly(dA:dT) stimulation lasted 24 hours. The plotted bars show the mean value of technical triplicates. Data is presented as the percentage of reporter activation with error bars representing SEM. Statistical significance was indicated by * <0.05, ** < 0.01 and **** <0.0001. All panels except panels D and F represent n=3; panels D and F are representative of n=4.

As MC009 appeared to be inhibiting NF-κB by both pro-inflammatory and sensing pathway activation of NF-κB below the level of pro-inflammatory and sensing pathways activation, I next investigated its effect on activation further down these pathways. Activation of all pathways under investigation utilise two major regulatory proteins, TRAF2 and TRAF6 (264,338). As overexpression of TRAF6 drives a strong κB-luciferase activation with 50 ng, the concentration used was reduced to 10 ng to avoid

overstimulating the system and making the interpretation of inhibitory effects more challenging. Interestingly, MC009 potently inhibited TRAF2- and TRAF6-mediated κB-luciferase activation, even more than the highly potent inhibitor MC132 in the case of TRAF6 (**Figure 3.6A and B**). Next, NF-κB activation was investigated by TAB2 which activates at the level proximal to the IKK complex (339), again observing inhibition by MC009 (**Figure 3.6C**).

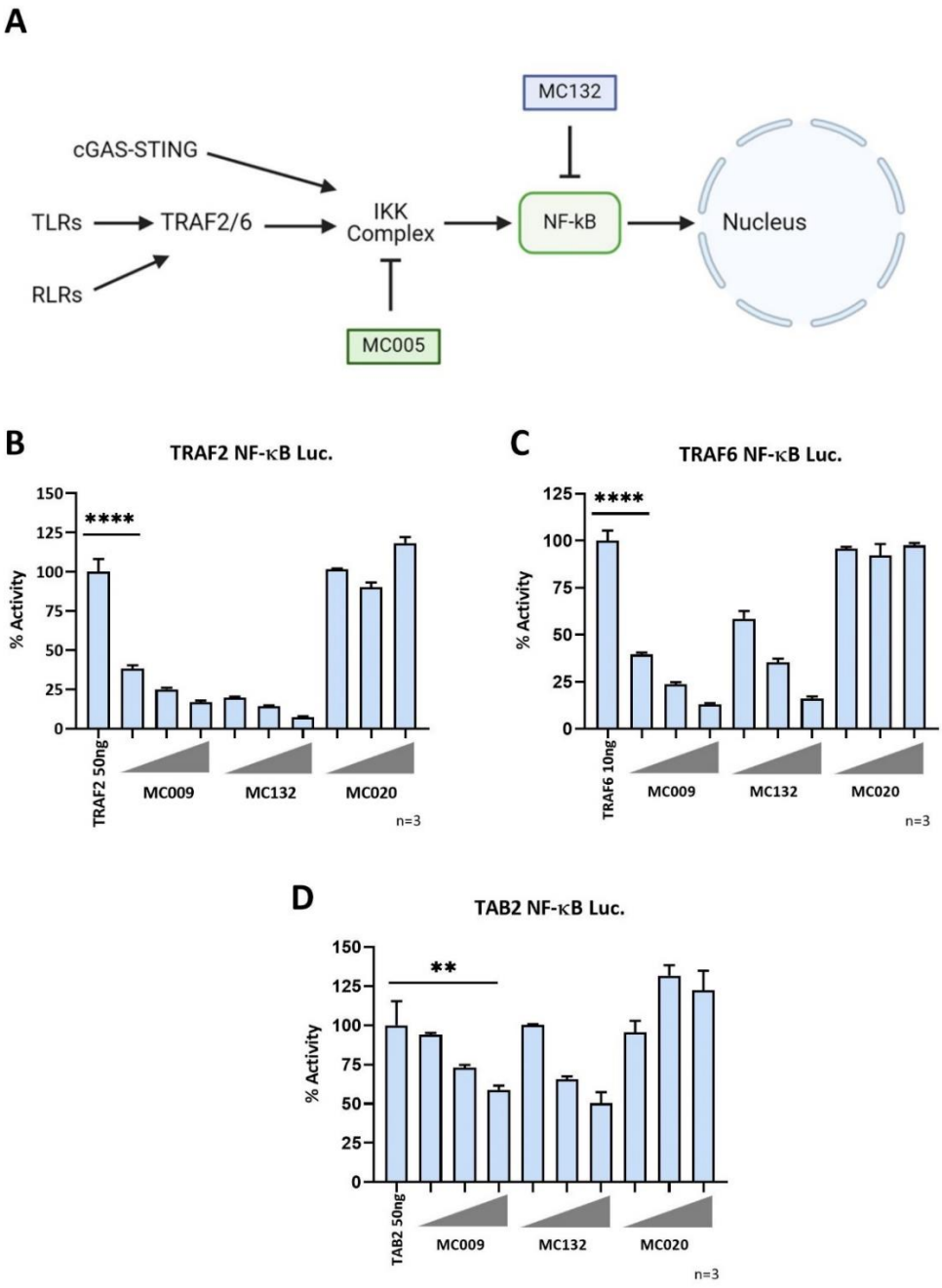

Figure 3.6. MC009 inhibits TRAF2, TRAF6 and TAB2 mediated NF-κB signalling. A. Schematic representing innate signalling pathways regulating NF-κB activity. **B-D.** HEK293T cells were transfected with 80 ng κB-luciferase, 40 ng TK-Renilla and EV. The NF-κB pathway was activated using 50 ng TRAF2, 10 ng TRAF6 or 50 ng TAB2. Additions of MCV proteins were made at 10 ng, 25 ng and 50 ng. MC132 was used as a positive control based on published data. MC020 was used as a negative control. One-way ANOVA was used to determine statistical significance. Data is presented as the percentage of reporter activation with error bars representing SEM. Statistical significance was indicated by ** < 0.01 and **** <0.0001. The plotted bars show the mean value of technical triplicates. All graphs in this figure are representative of n=3.

The IKK complex is formed from IKKα, IKKβ and NEMO. This complex is the main NF-κB activity regulator and is utilised by TLR, RLR and cGAS pathways to upregulate inflammatory responses through NF-κB members (81,97,200,340). All three kinases were initially tested at 50 ng, however, due to potent signal stimulation the concentration was decreased to 10 ng (data not shown). IKKα and IKKβ activation was, again, significantly inhibited by MC009 (**Figure 3.7A and B**). As overexpression of NEMO did not activate an κB-luciferase, a constitutively active form of NEMO (previously made in the host lab) was used to activate signalling downstream of this protein (292). MC009 virtually silenced activation of NF-κB from this activator, like MC132 and MC005 which is known to directly target NEMO (**Figure 3.7C**) (292).

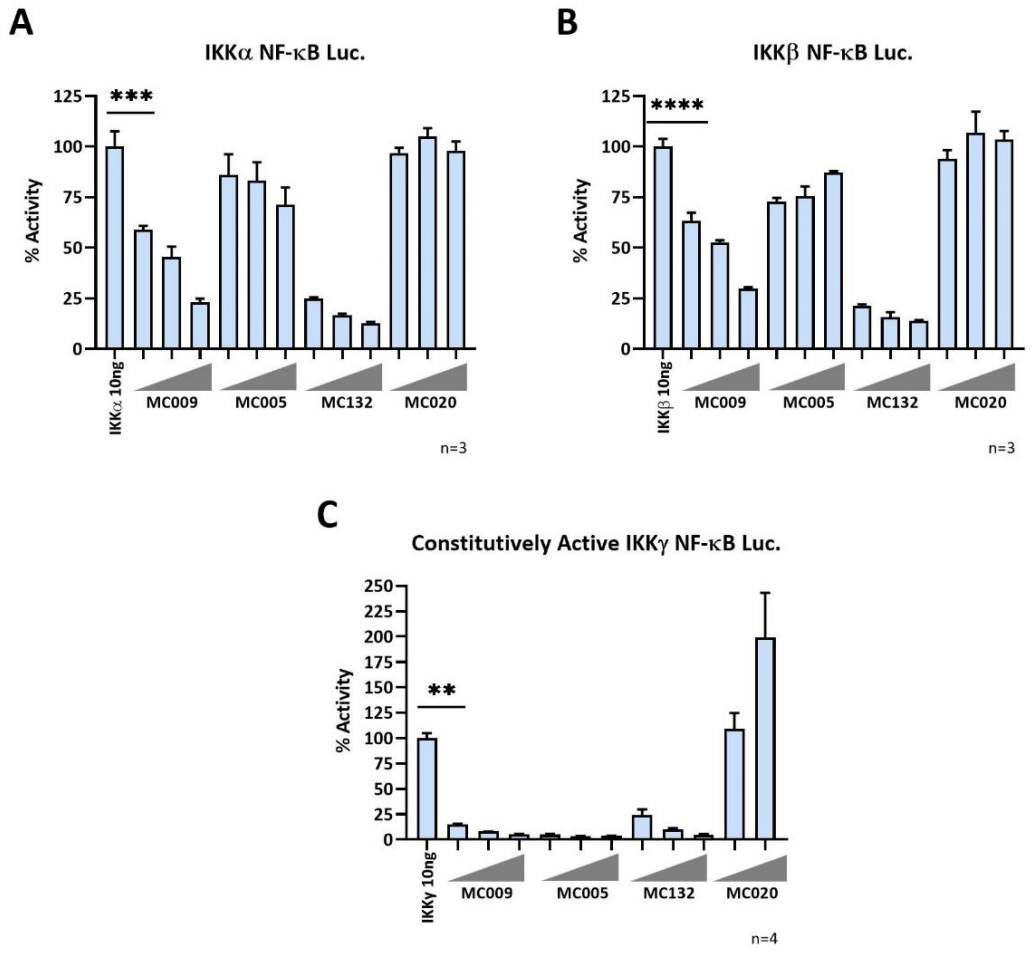

Figure 3.7. MC009 inhibits NF-κB signalling mediated through the IKK complex. A-C. HEK293T cells were transfected with 80 ng κB-luciferase, 40 ng TK-Renilla and EV. The NF-κB pathway was activated using 10 ng IKKα, 10 ng IKKβ and 10 ng mutant IKKγ. Additions of MCV proteins were made at 10 ng, 25 ng and 50 ng. MC005 and MC132 were used as a positive control based on previously published data. MC020 was used as a negative control. Data is presented as the percentage of reporter activation with error bars representing SEM. Statistical significance was indicated by ** < 0.01, *** <0.001 and **** <0.0001. The plotted bars show the mean value of technical triplicates. Panels A-B are representative of n=3; panel C is representative of n=4.

I next assessed the effect of MC009 on activation of κB-luciferase by the of NF-κB transcription factor itself by overexpressing p65/RelA. A range of concentrations were

used to observe the full effects of MC009 on overexpressed p65. Previous work in the host lab showed that MC132, which directly targets p65, inhibited at low levels of p65 expression but inhibition was bypassed at higher levels of expression (299).

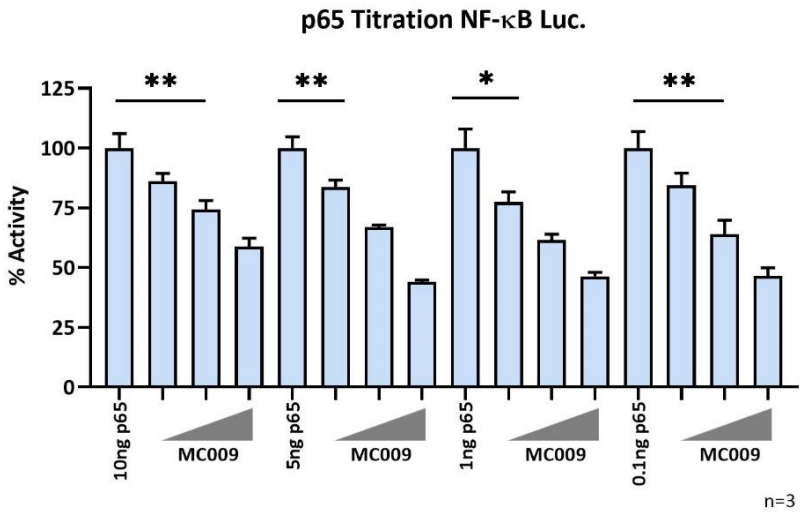

Figure 3.8. MC009 inhibits direct κB-luciferase reporter activation by p65 inhibition like the p65-targetting MCV inhibitor MC132. HEK293T cells were transfected with 80 ng κB-luciferase, 40 ng TK-Renilla and EV. The NF-κB pathway was activated using 0.1, 1, 5 and 10 ng p65. Additions of MCV proteins were made at 10 ng, 25 ng and 50 ng. One-way ANOVA was used to determine statistical significance. The plotted bars show the mean value of technical triplicates. Data is presented as the percentage of reporter activation with error bars representing SEM. Statistical significance was indicated by * <0.05 and ** < 0.01. This graph is representative of n=3.

3.6 MC009 is an inhibitor of IRF activation.

Unlike the inhibitors previously discovered in the host lab (MC005, MC008 and MC132) which were specific inhibitors of NF-κB signalling, MC009 also inhibited IRF activation.

Following the same pathway mapping protocol as for NF-κB, the investigation began with receptor adaptor proteins and an outside DNA stimulant.

The initial stages of TLR, RLR and cytosolic DNA sensing for IRF family signalling overlap with those regulating NF-κB activation (80,341). Similarly, Poly(dA:dT) and overexpressed MAVS were used to test MC009 effects on RLR-associated IRF activation. As with NF-κB activation by these stimuli, MC009 potently inhibited ISRE activation (**Figure 3.9A and B**). Unfortunately, a positive control was not used for the IRF pathway mapping as a suitable MCV protein was not available. Likewise, MC009 inhibited ISRE activation by CD4-TLR3, TRIF and cGAS-STING (**Figure 3.9 C-E**).

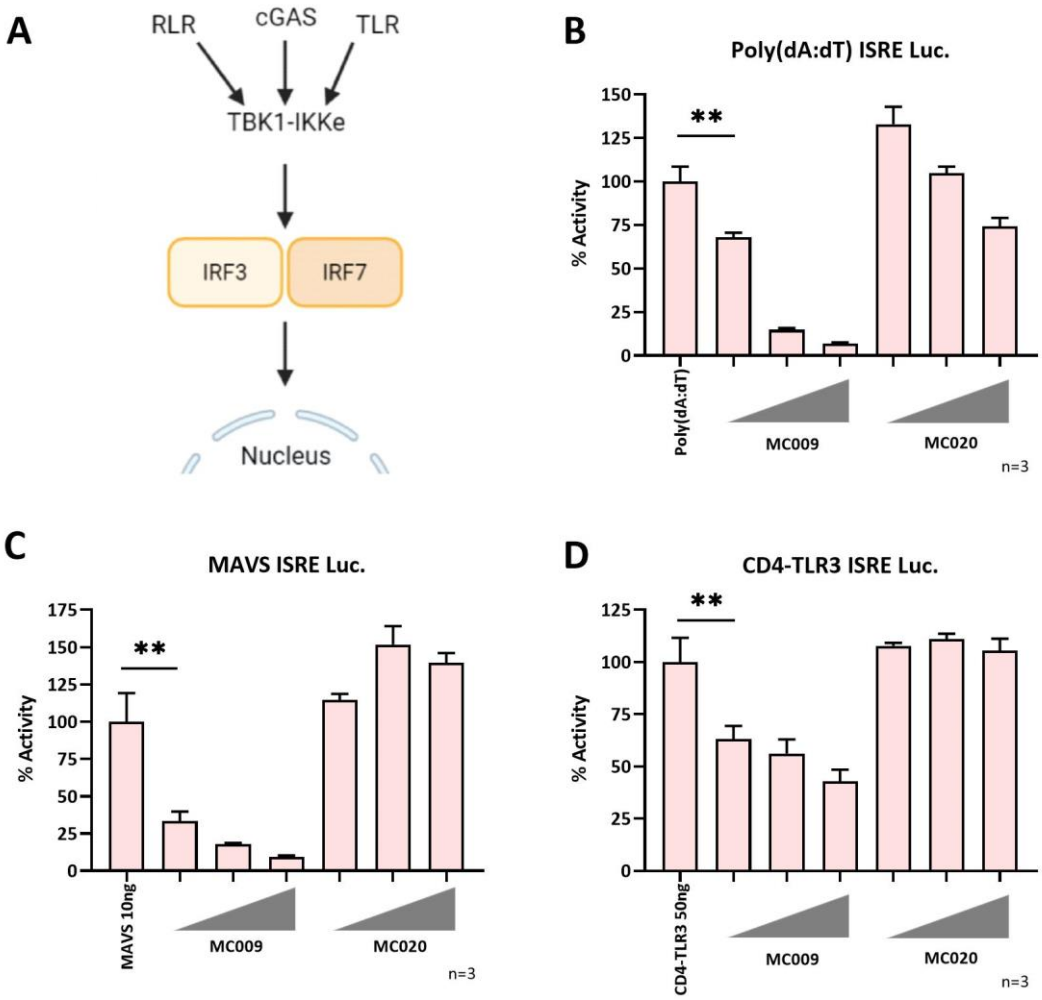

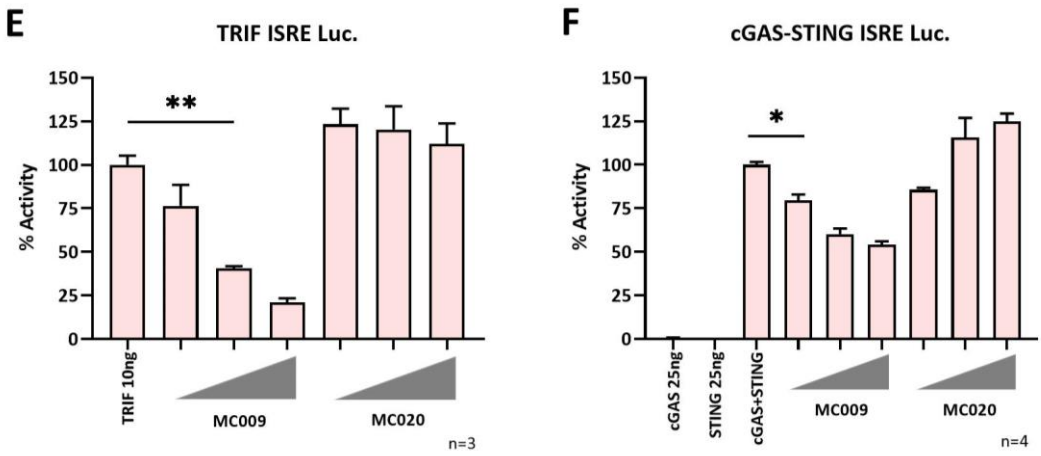

Figure 3.9. MC009 inhibits IRF activation by TLR, RLR and cGAS pathways. A. Schematic representing innate signalling pathways regulating IRF3 and IRF7 activity. **B-F.** HEK293T cells were transfected with 80 ng ISRE-luciferase, 40 ng TK-Renilla and EV. The IRF pathway was activated using 25 ng cGAS, 25 ng STING, 10 ng MAVS, 50 ng CD4 TLR3 and 10 ng TRIF. Additions of MCV proteins were made at 10 ng, 25 ng and 50 ng. The plotted bars show the mean value of technical triplicates. Data is presented as the percentage of reporter activation with error bars representing SEM. Statistical significance was indicated by * <0.05 and ** < 0.01. Panels A-E are representative of n=3; panel F is representative of n=4.

IRF activation, in contrast to NF-κB, occurs through IKK-related kinases, TBK1 and IKKε (220,230). The kinases themselves are also regulated by various combinations of upstream proteins, including TRAF3, TBKBP1, NAP1 and TANK, depending on the signal stimulus (227,228,322). Thus, activation of the pathway using TRAF3, TBKBP1, NAP1 and TANK was investigated. However, activation of ISRE-luciferase by overexpression of these proteins was not observed (data not shown). TBK1 and IKKε hold functionally equivalent roles in IRF family signal transduction as the IKK complex in NF-κB signalling. A dose dependant inhibition of TBK1 was observed (**Figure 3.10A**). A significant inhibition of signalling was also observed for IKKε-driven ISRE activation (**Figure 3.10B**).

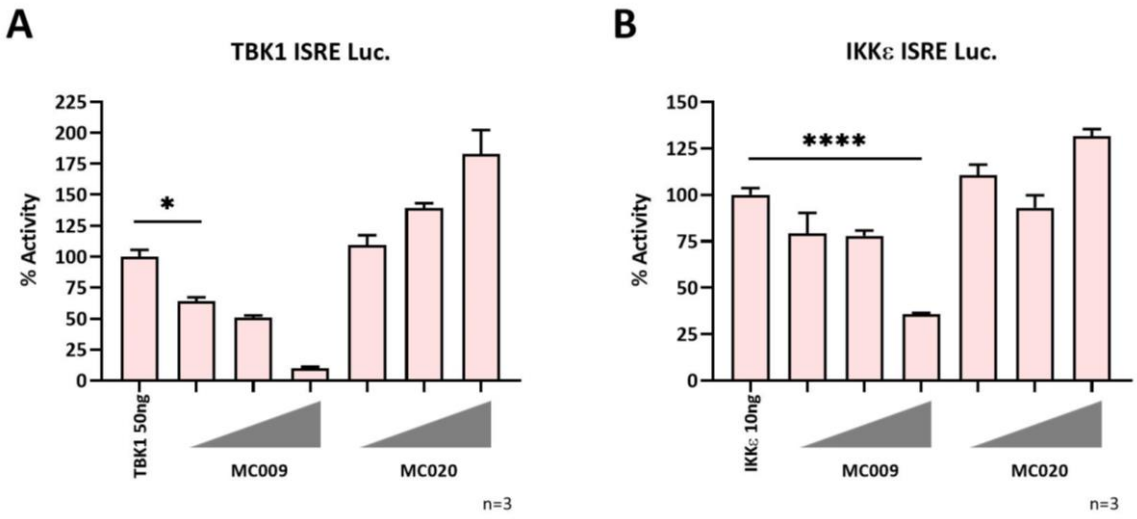

Figure 3.10. MC009 inhibits IRF family signalling by TBK1 and IKKε. A-B. HEK293T cells were transfected with 80 ng ISRE-luciferase, 40 ng TK-Renilla and EV. The IRF pathway was activated using 50 ng TBK1 or 10 ng IKKε. Additions of MCV proteins were made at 10 ng, 25 ng and 50 ng. The plotted bars show the mean value of technical triplicates. Data is presented as the percentage of reporter activation with error bars representing SEM. Statistical significance was indicated by * <0.05 and **** <0.0001. Both panels are representative of n=3.

Lastly, two IRF transcription factors were tested, IRF3 and IRF7. The IRF family members were chosen based on their involvement in pro-inflammatory responses during viral infections (72,128,152,341). Constitutively active forms of the IRFs were used to look at their ability to overcome MC009 inhibition, or lack thereof. As for p65 and κB-luciferase (**Section 3.4 Figure 3.8**), four concentrations of activator plasmids were tested. MC009 inhibited both constitutively-active IRF3 and IRF7 at every concentration used (**Figure 3.11**). Addition of MC020 showed no inhibition of the pathway (data not shown).

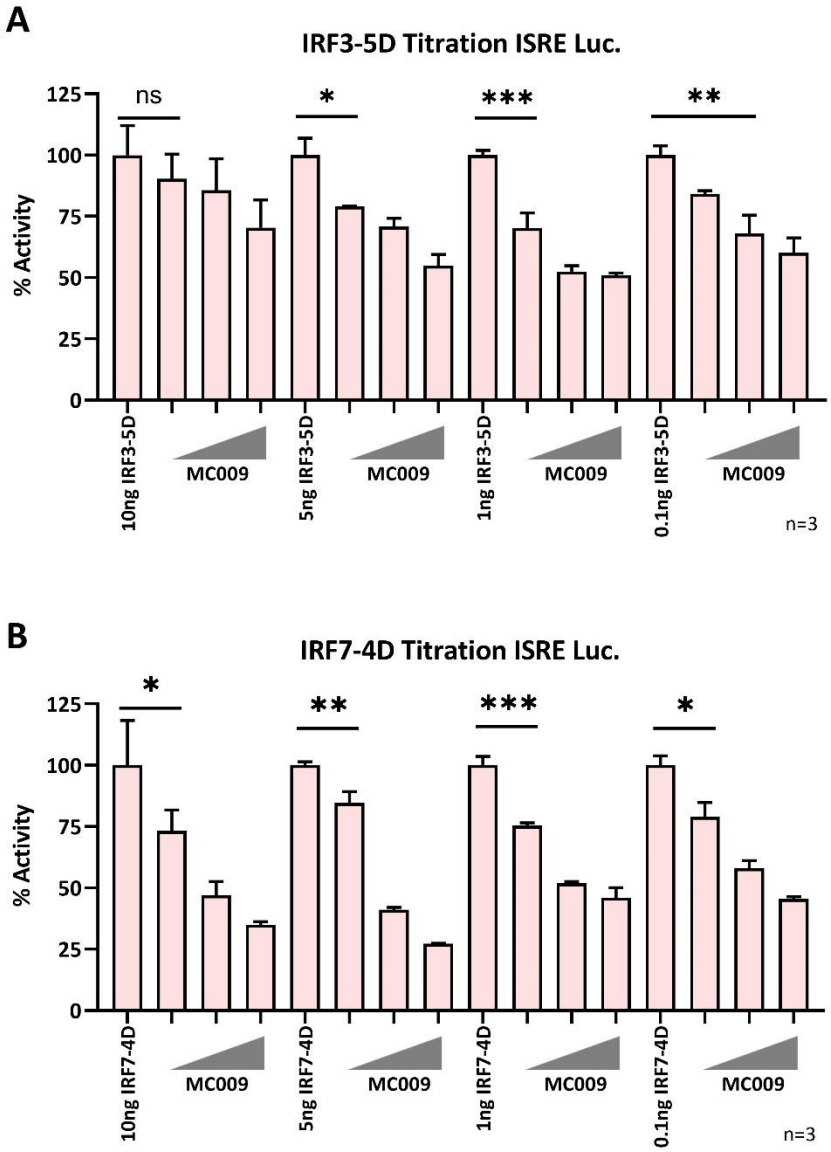

Figure 3.11. MC009 inhibits direct ISRE-luciferase activation by IRF3 and IRF7 signalling. **A-B.** HEK293T cells were transfected with 80 ng ISRE-luciferase, 40 ng TK-Renilla and EV. The IRF pathway was activated using constitutively active IRF3-5D and IRF7-4D. The experiment was trialled at four concentrations 0.1, 1, 5 and 10 ng. Additions of MCV proteins were made at 10 ng, 25 ng and 50 ng. The plotted bars show the mean value of technical triplicates. Data is presented as the percentage of reporter activation with error bars representing SEM. Statistical significance was indicated by 'ns' non-significant, * <0.05, ** < 0.01 and *** <0.001. Both panels are representative of n=3.

3.7 MC009 impairs cytokine and IFN-α/β release.

Pathway mapping not only suggested that MC009 targets downstream of NF-κB and IRF family activation, but also provided insight into the potency of the inhibitor relative to previously identified inhibitors in the case of NF-κB. Next, the consequences of MC009 inhibition on cytokine production was investigated. IL-8/CXCL8 was used as a representative NF-κB associated cytokine, whereas IP-10/CXCL10 was a representative of NF-κB and IRF family-regulated cytokine. Stable $CdCl_2$-inducible pMEP4-MC009-FLAG cells were used to prepare samples for ELISA cytokine production analysis. MC009 expression was confirmed using western immunoblotting (**Figure 3.12A**). IL-8 production was stimulated by the addition of TNFα for 24 hours. MC009 potently inhibited Poly(dA:dT)-induced IP-10 production with more modest effects on TNFα-induced IL-8 production (**Figure 3.12B and C**).

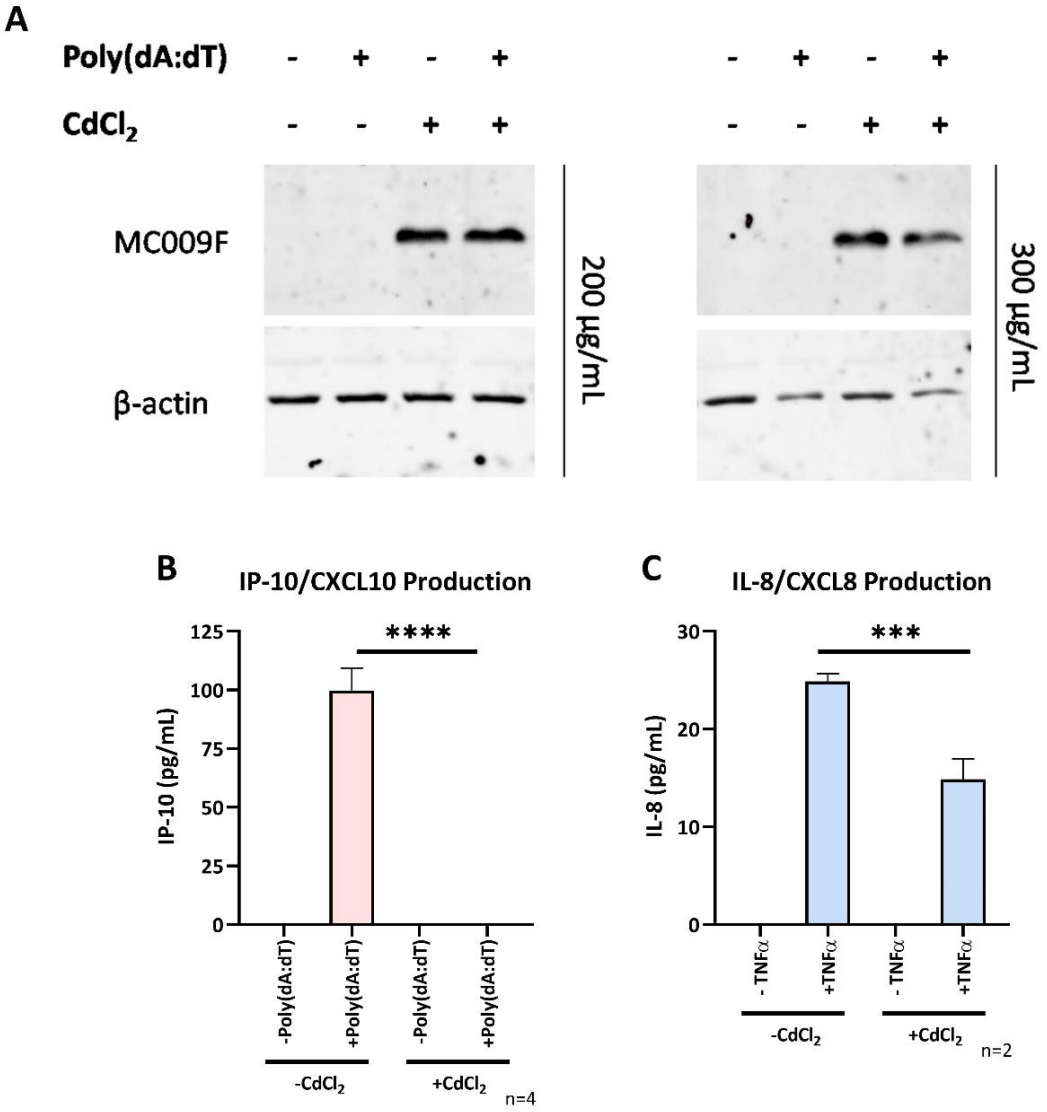

Figure 3.12. Induction of MC009 expression leads to diminished IL-8 and IP-10 cytokine production. A. HEK293T-pMEP4-MC009-FLAG cells were maintained with 200 µg/mL or 300 µg/mL of Hygromycin B Gold solution. MC009 expression was induced with 1µM $CdCl_2$ for 24 hours. **B-C.** Stable cells were seeded in 6-well plates and selected for with 200-300 µg/mL of Hygromycin B Gold solution. Protein expression was induced with 1µM $CdCl_2$ for 24 hours before stimulating with 50 ng/mL TNFα or 1 µg/mL Poly(dA:dT) for an additional 24 hours. Supernatants were probed for IL-8 or IP-10 using a sandwich ELISA; read at 450 nm. The plotted bars show the mean value of technical triplicates. Data is presented as the percentage of reporter activation with error bars representing SEM. Statistical significance was indicated by *** <0.001 and **** <0.0001. Panel B is representative of n=3; panel C is representative of n=2.

The effect of MC009 on type I IFN production was investigated with the use of IFN-β promoter luciferase assays and an IFN-α/β bioassay (**Figure 3.13**). IFN-β promoter luciferase activity mediated by cGAS-STING overexpression was inhibited in a dose dependent manner by MC009 (**Figure 3.13A**). Likewise, Poly(dA:dT)-driven IFN-β signalling was significantly reduced in the presence of MC009 in contrast to the controls MC132 and MC020 (**Figure 3.13B**). Lastly, the effect of MC009 on Poly(dA:dT)-stimulated IFN-α/β production was inspected using stable inducible pMEP4-MC009-FLAG cells. Supernatants were added to HEK-Blue IFN-α/β cells and incubated for 24 hours and measured for SEAP production (which directly correlates with IFNα/β levels). A significant reduction in the signal produced by IFN-α/β HEK-Blue cells stimulation was observed in samples expressing MC009 (**Figure 3.13C**).

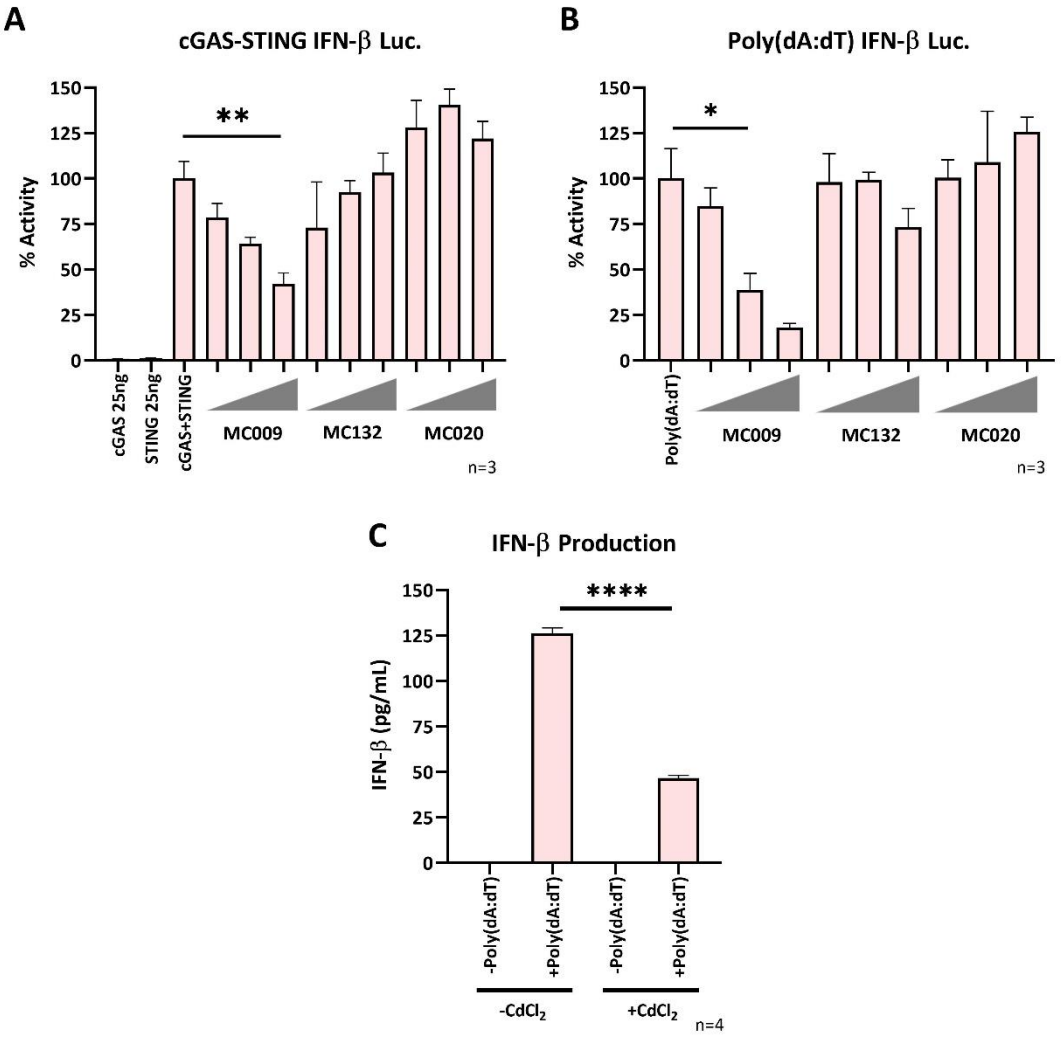

Figure 3.13. IFN-α/β response is weakened in the presence of MC009. A-B. HEK293T cells were transfected with 80 ng IFN-β-luciferase, 40 ng TK-Renilla and EV. The IRF pathway was activated with overexpressed cGAS-STING. Additions of MCV proteins were made at 10, 25 and 50 ng. **B.** Cells were stimulated with 1 µg/mL Poly(dA:dT) and incubated for an additional 24 hours. Lipofectamine 2000 was used as a transfection reagent for Poly(dA:dT). **C.** HEK293T-pMEP4-MC009-FLAG cells were maintained with 200 µg/mL of Hygromycin B Gold solution. Cells were seeded in 6-well plates. MC009 expression was induced with 1µM $CdCl_2$ for 24h before stimulating with 1 µg/mL Poly(dA:dT) for an additional 24h. Supernatants were added to HEK-Blue IFN-α/β cells and incubated for 24h. SEAP production was recorded at 620 nm. The plotted bars show the mean value of technical triplicates. The plotted bars show the mean value

of technical triplicates. Data is presented as the percentage of reporter activation (**A-B**) with error bars representing SEM (**A-C**). Statistical significance was indicated by * <0.05, ** < 0.01 and **** <0.0001. Panels A-B are representative of n=3; panel C is representative of n=4.

3.8 Identification of functional regions of MC009.

To identify important regions of MC009 for inhibition of NF-κB and IRF activation, the host lab previously generated a series of MC009 truncations. To do this, discrete regions of the MC009 nucleotide sequence were amplified and subcloned to generate ten MC009 truncations (**Figure 3.14A**). All ten truncation plasmids (M1-10) were screened using MAVS-activated κB- and ISRE-luciferase assays (**Figure 3.14B and C**). The truncations were tested at three concentrations to maintain consistency with previous experiments. Full length MC009 and MC020 were used as positive and negative controls, respectively. Truncation M1 (1-86 aa) maintained the same κB- and ISRE-luciferase inhibitory effect of full length MC009 peptide (**Figure 3.14B and C**). Inhibition was also observed with truncation M8 (1-51 aa) and M9 (1-42 aa) (**Figure 3.14C**). Expression of MC009 truncations was investigated, however, due to their size they were too small to resolve during SDS-PAGE electrophoresis (data not shown). Interestingly, M8 and M9 inhibitory function was more consistent against IRF signalling than NF-κB. Although M1, M8 and M9 share a common sequence region, M1 is 36 amino acids longer than M8 and 45 amino acids longer than M9. Truncations M4, M5 and M6 also share this common region however, they showed no inhibitory potential of NF-κB activity and moderate effects on ISRE activity.

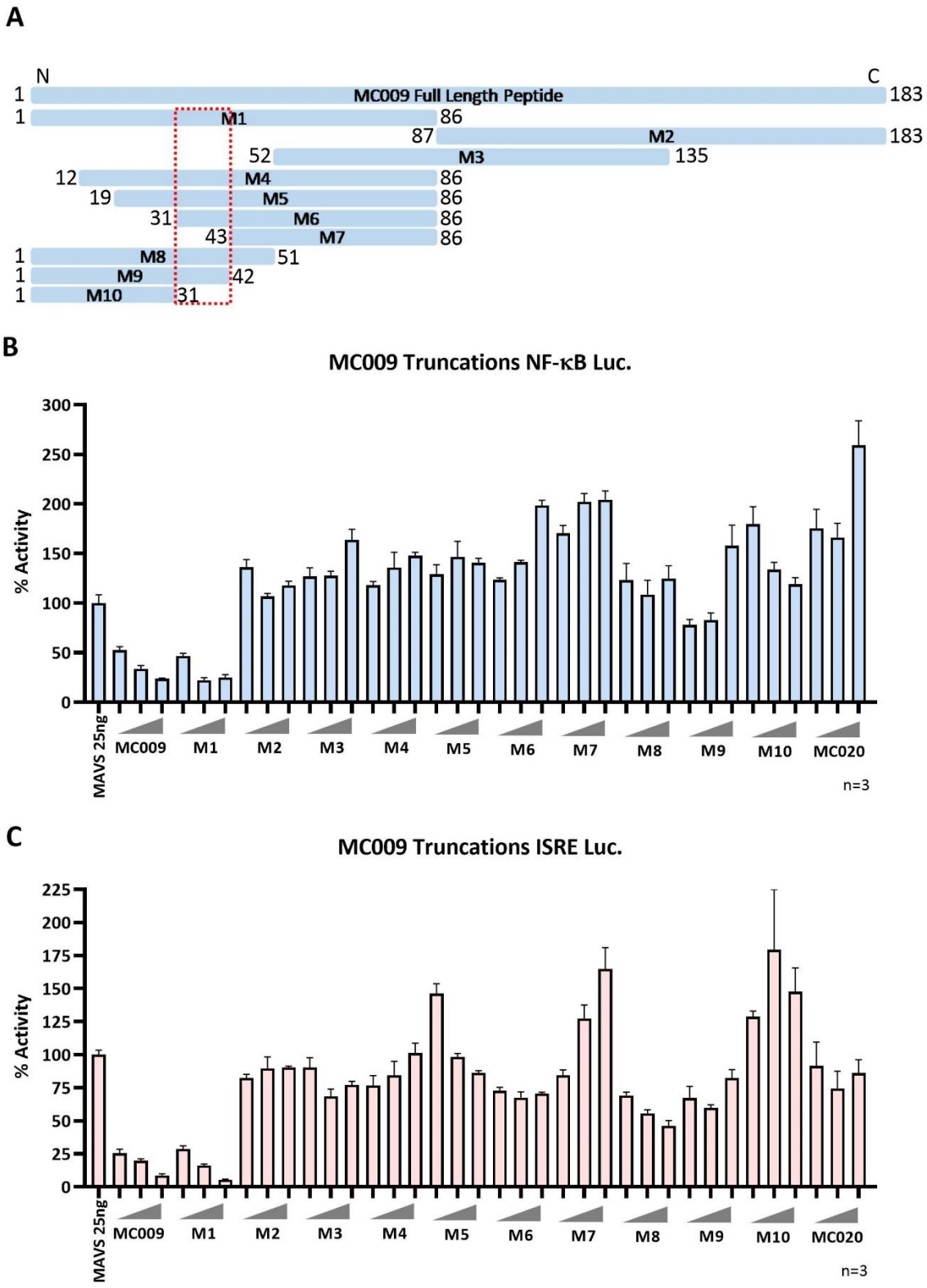

Figure 3.14. MC009 inhibitory function is held in the N-terminal of the genetic sequence. A. A visual representation of ten MC009 peptide truncations in comparison to the full length MC009. The full length MC009 peptide is 184 amino acids long. Truncations are shown in order from M1

to M9. Sequence region required for inhibitory function is highlighted in red. **B-C.** HEK293T cells were transfected with 80 ng κB- or ISRE-luciferase reporter plasmid, 40 ng TK-Renilla and EV. Both pathways were activated using 25 ng MAVS. Additions of MCV proteins were made at 10, 25 and 50 ng. The plotted bars show the mean value of technical triplicates. Data is presented as the percentage of reporter activation with error bars representing SEM. Both panels are representative of n=3.

3.9 Discussion

MCV appears to be incredibly adept at evading or inhibiting human immunity (60,292,293,299,304). Proteins such as MC005, MC132, MC159 and MC163 are just a few of the well-studied inhibitors encoded by this virus (292,299,304,308). These four ORFs all exhibit the ability to inhibit NF-κB or IRF in immune signalling using distinct mechanisms. Inhibition of transcription factor activation hampers cytokine and chemokine production necessary for a well balance inflammatory response. It is not yet clear how MCV uses these inhibitors *in vivo* or whether they act at the same time, in combination with each other or completely separately. Interestingly, like MC159 and MC160, but distinct from MC005 and MC132, the work presented in this chapter confirms that MC009 can inhibit both NF-κB and IRF activity. As the NF-κB system is better characterised than the IRF-activating pathways, new inhibitors of IRF-activation like MC009 could shed more like on this pathway and the relationship between NF-κB and IRF in response to viral infections.

All available MC009 plasmids, DYKDDDDK (FLAG) or HA tagged, were investigated for inhibitory activity (**Figure 3.2A and B**). Two plasmids, ‘MP 9HA’ and ‘9 100 GB’, were chosen for further work and as stocks for future additional MC009 plasmids as one contained a HA-tag and the other a FLAG-tag. Some tested stocks may have been

replicates of each other as original plasmids as well as 100 ng stocks were analysed. However, due to poor labelling and material transfer between multiple freezers it was not possible to distinguish which 100 ng stock aliquot was related to which original MC009 stock. Therefore, all acquired plasmids were tested. This underlined the importance for sample labelling and inventory maintenance for the MC009 project. Storage of inactive MC009 plasmids led to confusion and unnecessary use of larger quantities of reagents for the optimisation assay.

In preparation for MC009 pathway mapping, four MCV plasmids were screened as potential negative controls: MC014, MC020, MC052 and MC063 (**Figure 3.3A and B**). MC020 was chosen as the negative control as it consistently had no inhibitory effect at 'low' (25 ng) and 'high' (50ng) concentrations, showing the same trend in both κB- and ISRE-luciferase assays. Similarly to MC009 plasmids, multiple stocks of each MCV protein were found in the host lab freezers. Some plasmids were not labelled with the date of plasmid purification. Once again this highlighted the necessity for correct reagent storage and inventory.

I hypothesised MC009 to be an inhibitor of innate signalling pathways, therefore, a control signalling pathway was vital for the continuation of this project. To test this, the Ras-activated Elk1 mitogenic pathway was examined. The ternary complex factor Elk1 is a transcription factor dependent on post-translational modifications (331,342). It is downstream of a Ras protein which is inactive until bound to GTP (343). MC009 behaved in a similar manner to MC020 during Ras-mediated Elk1 activation (**Figure 3.4**) confirming the specificity of MC009 as an inhibitor of innate signalling pathways. If MC009 inhibited all types of signalling, including mitogenic pathways, the project would

no longer be specific to human innate immunity. Additionally, inhibition of all routes of signal transduction would prove to be difficult and dangerous if the MC009 peptide was investigated further as a potential therapeutic agent for autoimmune disorders. The Ras-Elk1 assay marginally varied from κB- and ISRE-luciferase assays. The control assay required the addition of a pFA-Elk1 plasmid and a pFR-luciferase reporter plasmid rather than just the addition of one luciferase reporter plasmid. In contrast to κB- and ISRE-luciferase, 80 ng of reporter plasmid was distributed among two plasmids (pFA-Elk1 and pFR-luciferase reporter) rather than one (κB- or ISRE-luciferase reporter).

Signalling cascades are composed of a plethora of proteins. Testing all proteins involved in innate signalling would have been redundant and unproductive as a larger volume of reagents would be required. Conducting more assays would also lead to an extended experimental period which was not viable due to the time restraints of a PhD degree. Therefore, only key members of TLR, RLR and cytosolic DNA sensing signalling were examined for MC009 pathway mapping. TLR-mediated NF-κB activity was tested through an artificial TLR3 dimer (CD4-TLR3), TRIF, MAL and MyD88 and a dose-dependent reduction in signal output was exhibited after the addition of MC009 (**Figure 3.5**). Unlike the other activators, the presence of two proteins was necessary for cGAS-induced luciferase activity (**Figure 3.5 D**). Strong NF-κB activation was observed after cells were transfected with both plasmids, cGAS and STING, simultaneously. TNFα, was tested as a pro-inflammatory cytokine simulating cellular response usually evoked during viral infections (**Figure 3.5A**). In all cases, signal reduction indicated that the MCV protein inhibits TLR, RLR and cGAS-STING-mediated NF-κB activity. Furthermore, it demonstrated that MC009 functions downstream of all above-mentioned proteins.

The cascades utilise common downstream proteins to regulate the IKK complex. During the NF-κB mapping stage three key proteins were chosen for the investigation of this stage of signalling (TRAF6, TRAF2 and TAB2) all of which were inhibited by MC009 (**Figure 3.6**). TRAF6 was chosen as it plays a crucial role in TLR, RLR and cGAS NF-κB signalling. TRAF2 was chosen to further our understanding of M009 effects on the TNFR pathway, while TAB2 provided more information about the TLR cascades. This narrowed down the pathway mapping at the middle stage of the cascades to optimise experimental time. If MC009 did not inhibit all three activators, other proteins such as TAK1 or TAB1 would have been investigated.

MC005 was added as an additional control during IKK kinase screens as it has been shown to interact with NEMO (**Figure 3.7**) (292). The IKK kinases are imperative to NF-κB signalling as their activity directly dictates whether NF-κB transcription factors are release by IκBα (97,344). Wild-type NEMO does not lead to signal induction as it requires a ubiquitin-mediated conformational change to move into its active state (345). To counteract the lack of signal induction by wild-type NEMO a constitutively active kinase was used. The mutant NEMO contained a point mutation in the CC2 domain of the kinase which forced the kinase to remain in its active state mediating an NF-κB signal. Inhibition of the IKK complex by MC009 inferred the inhibitor operated at the transcription factor level.

Finally, the transcription factor subunit p65 was investigated (**Figure 3.8**). P65 remains sequestered in the cytoplasm when bound to IκB in an inactive state (346). However, as the gene reporter assay uses an overexpressed p65 activator not endogenous, therefore, this did not complicate the experiment. MC132 directly inhibits p65 by forcing the

transcription factor into proteasomal degradation (299). Based on MC132 data, I understood that if MC009 inhibited p65 in a likewise pattern as MC132 then it was more likely that MC009 directly affects p65 activity. However, if MC009 was able to inhibit low and high concentrations of p65, then the inhibitor likely worked by disrupting p65 activity by proxy. MC009 similarities with MC132 indicated that the inhibitor worked alongside or downstream of the transcription factor member. Unfortunately, Brady *et. al.* also examined MC132 p65-inhibition at 25ng which was not tested during MC009 pathway mapping. Based on the data, I could conclude that MC009 inhibited NF-κB signalling at the transcription factor level. However, I could not definitively conclude if MC009 directly affected p65 or not purely based on this stage of the project.

IRF signalling was investigated using the same rationale as NF-κB pathways. cGAS-STING-driven ISRE-luciferase was inhibited by MC009 (**Figure 3.9E**). In comparison, Poly(dA:dT) and MAVS-mediated cascades saw an even more significant drop in activity levels with MC009. ISRE activity level dropped by ~75% after cell treatment with the lowest dose of MC009 (**Figure 3.9B**). TLR-related adaptor proteins were also hindered by the inhibitor (**Figure 3.9C and D**). Comparable effects of MC009 on IRF and NF-κB-activating pathways indicated that MC009 inhibited both at a further point in the signal cascade. Downstream of the adaptor proteins are TRAF3, TBKBP1, NAP1 and TANK responsible for regulating TBK1 and IKKε (341). The effect of MC009 on the signal mediated by these proteins was inconclusive as they did not drive an adequate ISRE-luciferase signal.

TBK1 and IKKε, often referred to as 'IKK-related kinases', hold an equivalent role to the IKK complex present in NF-κB signalling (**Figure 3.10**) (230,254). The two kinases are

directly upstream of IRF family members regulating transcription factor activity. IRF3 and IRF7 are the dominant IRF family members during viral infections driving a type I IFN response (128,152,347). IRF transcription factors dimerise before they translocate into the nucleus. Similarly to the constitutive NEMO mutant, phosphomimic mutants IRF3-5D and IRF7-4D were used as they did not require the phosphorylation of the serine/threonine residues by TBK1 or IKKε (**Figure 3.11**). ISRE activity was significantly reduced in HEK293T cells transfected with MC009 for both IRF3 and IRF7. This was once again indicative of MC009 directly affecting the transcription factors or interacting with proteins preventing transcription factor activity. In the future, a higher concentration of IRF activators should also be tested to determine if MC009 inhibition is bypassed.

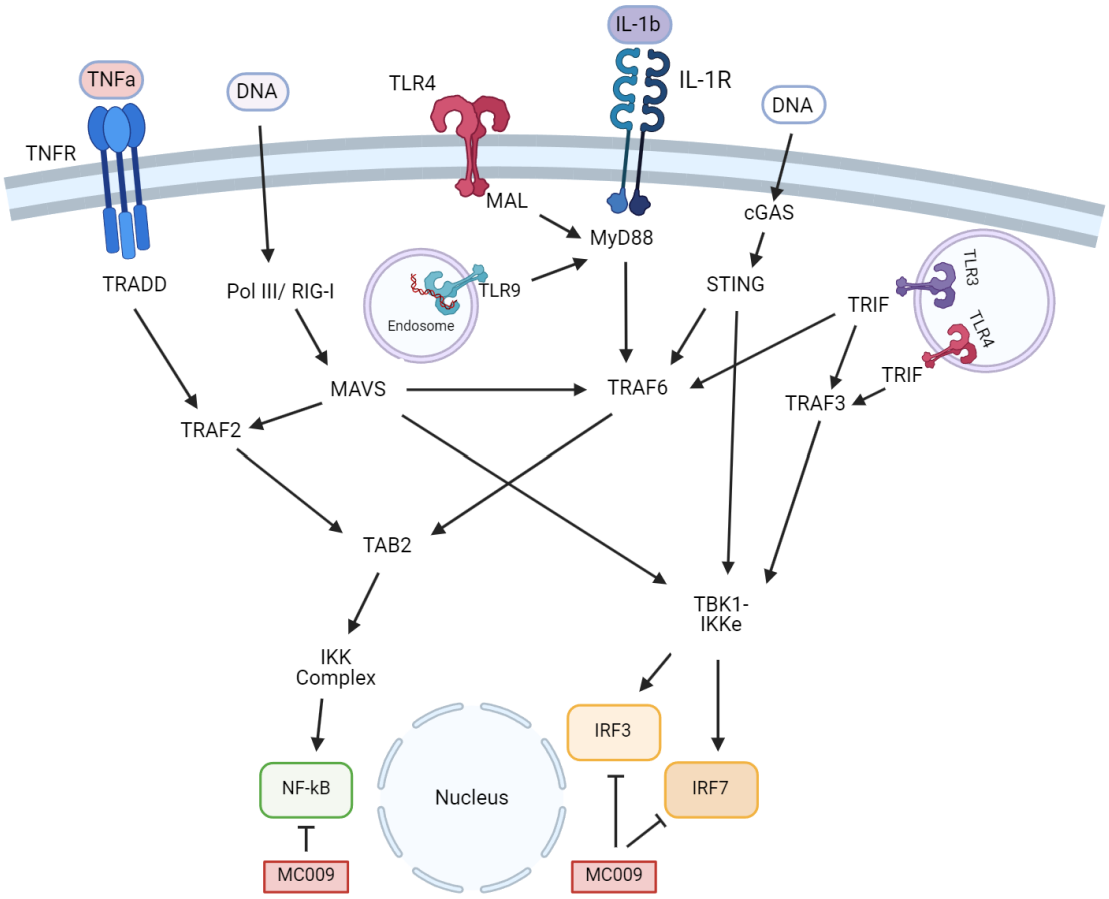

Figure 3.15 MC009 inhibition of signalling pathways activating NF-κB and IRF transcription factors. PRR- and cytokine-induced anti-viral pathways convene at the IKK complex in NF-κB signalling or the IKK-related kinases in IRF3 and IRF7 signalling. MCV-derived protein, MC009, targets innate immune signal transduction at the transccription factor level. Schematic created using Biorender (biorender.com).

MC009 demonstrated potent inhibitory function for both NF-κB and IRF signalling, it was crucial to investigate the consequences of pathway inhibition on pro-inflammatory cytokine and type I IFN production (**Figure 3.12 and Figure 3.13**). IL-8/CXCL8 and IP-10/CXCl10 were chosen as representatives of NF-κB- and IRF-governed cytokines. MC009 inhibited IL-8, IP-10 and IFN-α/β release demonstrating the effect of the inhibitor on the production of key cytokines in human innate immunity. Inhibition of pro-inflammatory cytokine and chemokine release as well as a diminished type I IFN response was complimentary to the lack of evident immune responses observed during an MCV viral infection (43). Only two experimental replicates were conducted of the IL-8 assay, a third could be conducted in future studies to confidently conclude the result. The experiments were controlled by using cells with and without $CdCl_2$. Another worthwhile example of a control for $CdCl_2$-inducible assays would have been parent cells (HEK293T cells) not transfected with pMEP4-MC009-FLAG.

Functional region(s) of MC009 were also investigated. The initial step was to compare the inhibitory potential of MC009 truncations to full length MC009 peptide. MAVS drove strong and consistent signal activity in the pathway mapping stage; therefore, it was an ideal candidate for truncation screening. Furthermore, MAVS also allowed for direct comparison of inhibitory effects on κB- and ISRE-luciferase (**Figure 3.14**). Most of the truncation sequences contained overlapping regions with one another, for example, M1

overlapped with all other nine truncations. Conversely, M10 only overlapped with 5 other sequences. Using multiple sequences for the screen allowed for the discrimination between parts of the MC009 peptide sequence necessary for its inhibitory function and parts not involved in the process. Peptide M1 showed the most potent inhibition with M8 and M9 also showing dose dependent inhibition in ISRE-luciferase screening. The three peptides share 42 amino acids found at the N terminal of the full-length sequence (**Figure 3.14A**). The screen was also conducted using IKK-β to mediate NF-κB activity which showed M9 to maintain a similar level of inhibition to full length MC009 peptide (data not shown). M4, M5 and M6 also show some inhibitory ability however, this was not consistent and was clearer in the ISRE system rather than the NF-κB screens. Importantly, truncation M10 which shares the same N terminal region with M1, M8 and M9 showed no inhibitory ability in either NF-κB or ISRE signalling. Considering the above-mentioned results, the functional region for MC009 was narrowed-down to an 11 amino acid-long region. It is important to note, while the functional region was hypothesised to be the 11 amino acid sequence, I could not conclude this finding definitively as it required more research. Short peptides can lead to misaligned protein folding disrupting protein activity and function. Additionally, due to the length of the peptides expression blots of the truncations could not be conducted. PCR testing could have been used to confirm peptide presence.

3.10 Conclusion

The project started by identifying HA- and FLAG-tagged MC009 plasmids with potent inhibitory ability. MC020 was shown to be a reliable negative control for further MC009 investigation. Pathway mapping elaborated the point at which MC009 exerts its inhibitory function on TLR, TNFR, RLR and cGAS-STING signalling all of which are

involved in an anti-viral innate response. Furthermore, the inhibitor was observed to work at the transcription factor level inhibiting p65, IRF3 and IRF7 luciferase activity. Inhibitory signalling effect was reflected in IL-8, IP-10 and IFN-β production levels shedding light as to how MCV potentially evades a strong inflammatory response during infection. Protein-protein interactions required investigation to further understand the relationship between MC009 and p65 or IRF3.

Chapter 4: MC009 Inhibits TNFα-induced p65 Nuclear Translocation.

4.1 Introduction

The localisation of MCV inhibitors pre- and post-signal induction can aid in deciphering the function and mechanism of the protein. MC005 and MC132 are exclusively observed in the cytoplasm of HEK293T cells (292,299). The same was observed by Phelan *et. al.* for MCV-derived inhibitor MC008 (293). Conversely, MC014 sequesters within the nucleus of the cell without prior cell stimulation (299). However, the localisation of MC009 remained unknown.

Phosphorylation events play a key role in controlling pro-inflammatory signalling. P65 activity is dependent on the inhibitory protein IκBα. The transcription factor member is sequestered in the cytoplasm as a result of IκBα binding. Phosphorylation of the kinase at site S32 and S36 releases p65 allowing it to translocate into the nucleus (348). Furthermore, the phosphorylation of p65 can also inhibit its role within the signalling cascade. A study presented by Lu *et. al.* underlined the importance of p65 and IRF3 phosphorylation for a healthy anti-viral response (349). The study showed a significant decrease in *TNFA* and *IFNB1* expression after PTM inhibition. Oppositely, the group observed higher cytokine production levels in cells where p65 and IRF3 phosphorylation was not disrupted.

Transcription factors are common targets of viral immunomodulators consequently inhibiting signal transduction. MC132 disrupts pro-inflammatory cytokine release by driving p65 degradation (299). The NF-κB member is recruited to the Cullin-5-Elongin B-Elongin C complex where it undergoes proteasomal degradation. Orf virus encoded protein ORFV002 also directly targets p65 inhibiting NF-κB gene regulation (350).

ORFV002 affects the acetylation of p65 disrupting the p65-p300 binding thus interfering with transcription factor activity.

The previous chapter discussed the inhibitory effect of MC009 on TLR, RIG-I and cGAS-STING anti-viral signalling as well as its consequence on cytokine, chemokine and IFN production. However, the exact mechanical effect of MC009 on transcription factors remained unknown. The aim of this chapter was to focus investigations on the relationship between MC009 and p65, as well as subsequent changes in p65-mediated signalling events, to further elucidate the molecular mechanisms of MC009 inhibition of pro-inflammatory innate signalling.

4.2 Confocal microscopy protocol optimisation.

Confocal microscopy was used to better understand where MC009 functions in cells. The protocol involved coating glass coverslips with Poly-L-Lysine for cell adhesion. HEK293T cells were seeded and transfected with MC009-FLAG as per standard cell culture and transfection protocol. The results obtained showed two major problems. The signal received in the 488 nm FLAG channel was weak while also showing a lot of background activity (**Figure 4.1**). This was especially evident in the EV control as the FLAG channel should have had no fluorescent activity. Secondly, HEK293T cells grew in clumps across the glass coverslips rather than in a single layer evenly spread over the surface.

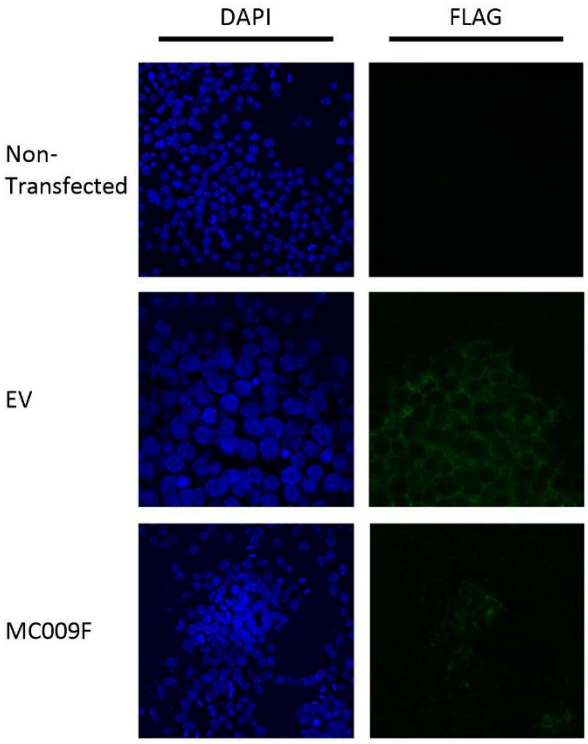

Figure 4.1. HEK293T cells did not maintain a 2D *in vitro* model morphology when using 'Confocal Microscopy (Coverslip method)' protocol. HEK293T cells were seeded at $1x10^5$ cells/mL on Poly-L-Lysine-coated glass coverslips in 24-well plates. The wells were transfected with 1 µg MC009-FLAG or EV. The slides were fixed in 2% paraformaldehyde, then blocked and permeabilised in 0.3% TritonX-100 in 2% BSA before staining. The cells were stained for FLAG (488 nm) and DAPI (405 nm). The images were taken with a 40x objective on a Leica SP8 scanning confocal microscope and LAS X software. This figure is representative of n=1.

Based on the observations made during the initial MC009 localisation attempt, the protocol for confocal microscopy required optimisation. The protocol was optimised using HEK293T cells grown in two cell culture vessel types, chamber slides and 24-well plates with coverslips, and cell growth was investigated 24 hours after cell seeding. Coverslips were treated under various conditions for cell growth optimisation. One glass coverslip was placed per well in a 24-well plate with separate plates used to accommodate different testing conditions. As the coverslips were stored in ethanol, firstly, all wells

were washed with PBS to remove any remaining ethanol still present. To test if the glass from which the coverslips were manufactured was hydrophilic and suited for cell adhesion one plate was seeded without chemical treatment. HEK293T cells attached to the coverslip surface however, compared to regular cell culture the cells were not as spread out and more cells were overlapping (**Figure 4.2A**).

Poly-L-Lysine was tested as an adhesive reagent as it accommodates stronger electrostatic interactions between the cell membrane and the culture vessel (351). Three coverslips were coated with an adhesive reagent Poly-L-Lysine which was dried in different conditions. The cells seeded on coverslips coated with Poly-L-Lysine which was dried at room temperature for 15 minutes were not evenly spread over the surface in contrast to standard cell culture (**Figure 4.2B**). Next, the Poly-L-Lysine coverslip was dried at 50°C for 60 minutes before cell seeding, however, the cells also grew in aggregates (**Figure 4.2C**). Lastly, the attachment reagent was allowed to dry overnight at room temperature. The growth of the cells was better, yet the cells were still overlapping (**Figure 4.2D**).

An acid wash was carried out prior to Poly-L-Lysine coating, which did not enhance cell adherence to the glass substrate (**Figure 4.2E**). The two last tests carried out on glass coverslips involved a PBS wash after Poly-L-Lysine coating, immediately after coating or after the reagent had fully dried. However, neither protocol involving a PBS wash showed favourable cell growth conditions (**Figure 4.2F and G**).

The 8-well Nunc^{TM} Lab-Tek^{TM} II chamber slides are also manufactured without any chemicals coating of the glass surface. Instead, the glass is prepared for cell adhesion

through a ‘multi-stage high-purity water washing process’. Two conditions were tested to investigate HEK293T cell growth on chamber slides, half of the wells were coated with Poly-L-Lysine while the remainder were left untreated. Cell growth was improved in both circumstances, with cells seeded in untreated wells resembling standard cell culture HEK293T growth (**Figure 4.2H and I**).

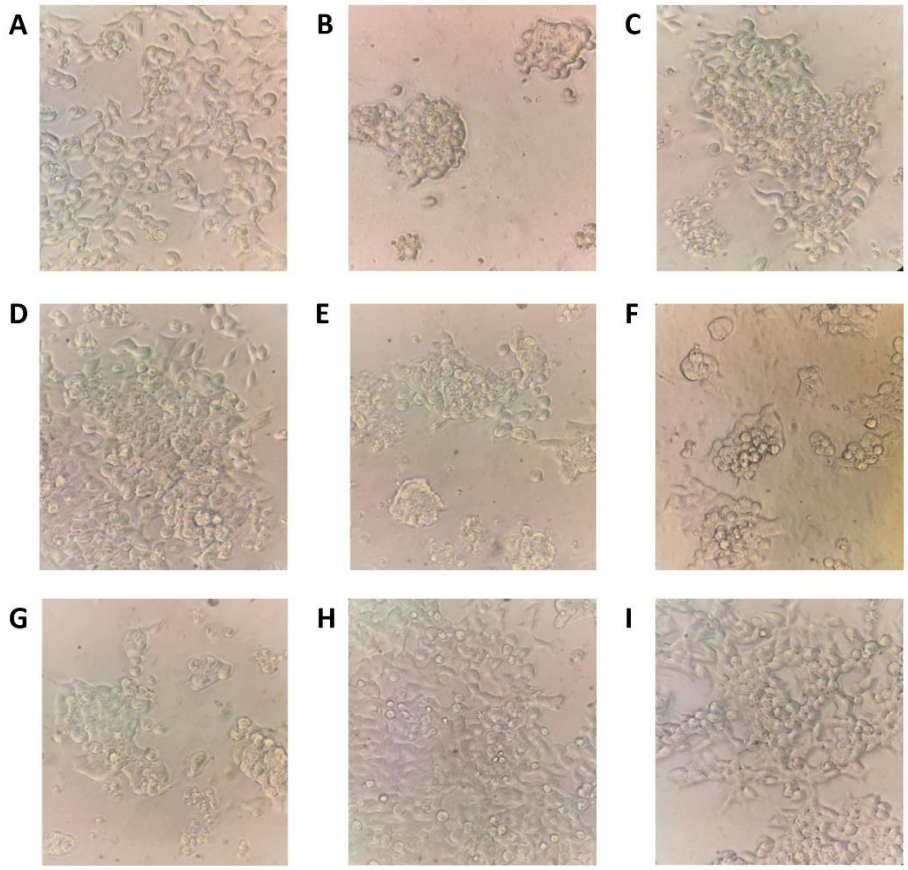

Figure 4.2. Nunc™ Lab-Tek™ II Chamber Slide™ System supports HEK293T cell adhesion. A-G. HEK293T cells were seeded $1x10^5$ cells/mL in 24-well plates. Cells were grown on glass coverslips without any treatment (**A**) or on glass coated with Poly-L-Lysine with varied protocols: coated with Poly-L-Lysine (**B**), coated with Poly-Lysine and dried at 50°C for 60 minutes prior to cell seeding (**C**), coated with Poly-Lysine and dried at room temperature overnight (**D**), washed with 1% HCl in 70% EtOH before coating with Poly-Lysine (**E**), coated with Poly-Lysine and immediately after washed with PBS (**F**) or coated with Poly-Lysine and

washed with PBS after reagent was completely dry (**G**). **H-I.** HEK293T cells were seeded 1.8x10^5 cells/mL in 8-well chamber slides. The cells were grown in untreated wells (**H**) or in Poly-L-Lysine coated wells (**I**).

The confocal microscopy slide preparation protocol was tested on four of the previously examined conditions (chamber slides with/without Poly-L-Lysine and coverslips with/without Poly-L-Lysine). The cells were prepared for confocal microscopy by fixing, permeabilising and staining, and were transfected with MC009-FLAG to test plasmid uptake. HEK293T cells grown on uncoated glass did not have a raised appearance however, the cell-surface adhesion was not as strong as with Poly-L-Lysine surfaces (**Figure 4.3**). MC009-FLAG expression was not visible in cells grown on Poly-L-Lysine coverslips.

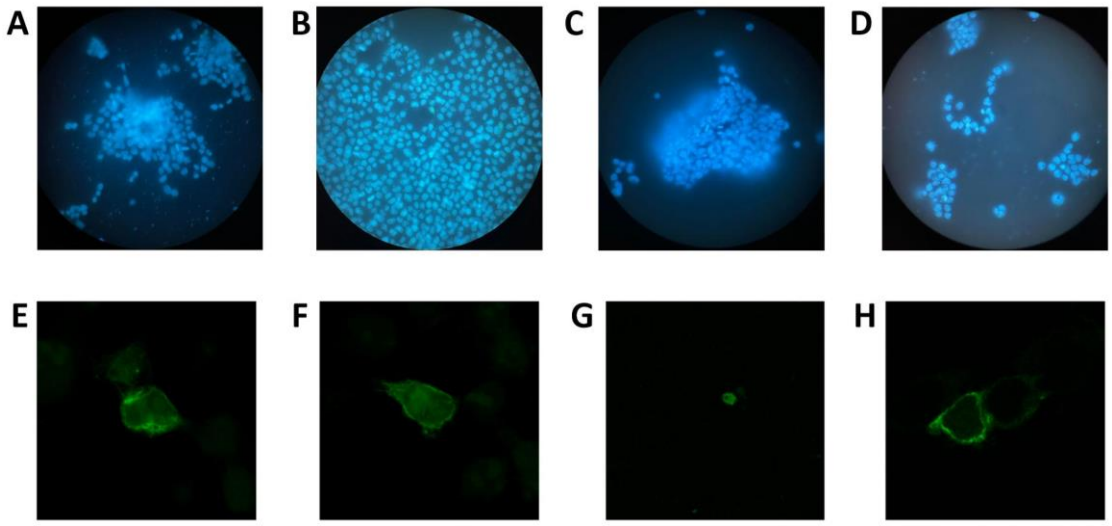

Figure 4.3. Nunc™ Lab-Tek™ II Chamber Slide™ System provides a suitable HEK293T cell transfection environment. A-B. HEK293T cells were seeded 1.8x10^5 cells/mL in 8-well chamber slides. The cells were grown on Poly-L-Lysine coated wells (**A**) or in untreated wells (**B**). **C-D.** HEK293T cells were seeded 1x10^5 cells/mL in 24-well plates. Cells were grown on glass coverslips without any treatment (**C**) or on glass coated with Poly-L-Lysine (**D**). **A-D.** HEK293T cells were transfected with 1 µg MC009-FLAG. The cultured cells were fixed in 4%

paraformaldehyde. They were permeabilised and blocked with 0.3% TritonX-100 in 2% BSA. Slides were stained with Alexa Fluor 488 nm conjugated anti-FLAG antibody and mounted using ProLong™ Gold antifade media with DAPI stain. The images were taken with a 40x objective on a Leica SP8 scanning confocal microscope and LAS X software.

4.3 MC009 inhibits TNFα-stimulated p65 nuclear translocation.

It was important to visualise where MC009 localises in the cell to better understand where it inhibited signalling pathways. HEK293T cells were transfected with MC009-FLAG or MC020-FLAG, the control MCV ORF. Confocal images showed MC009 to be evenly distributed throughout the cell cytoplasm. Although MC020 was also localised in the cytoplasm, it displayed punctate distribution (**Figure 4.4**).

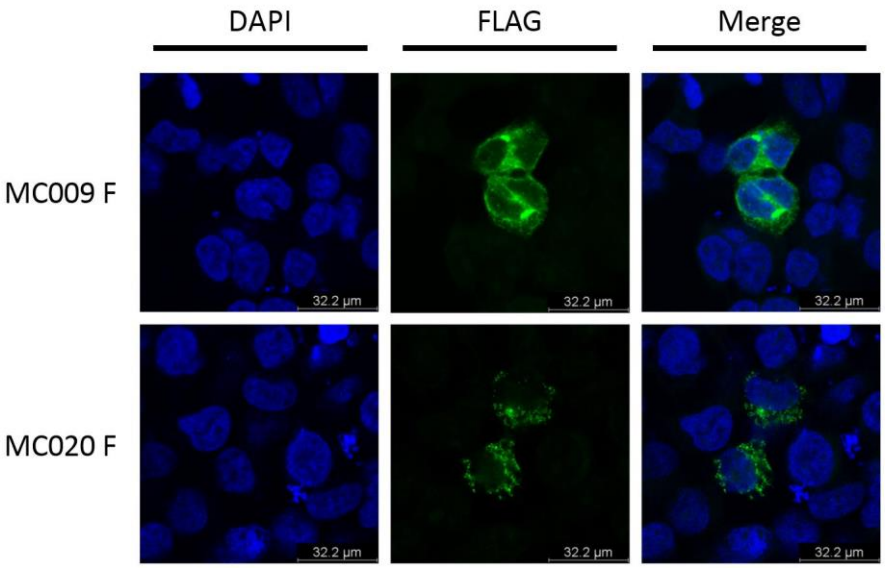

Figure 4.4. MC009 localises in the cytoplasm of HEK293T cells. HEK293T cells were seeded at $1.8x10^5$ cells/mL in 8-well chamber slides. The wells were transfected with 1 µg MC009-FLAG or MC020-FLAG. The slides were fixed in 4% paraformaldehyde, then blocked and permeabilised in 0.3% TritonX-100 in 2% BSA before staining. The cells were stained for FLAG (488 nm). ProLong™ Gold DAPI mounting solution was used for nuclear staining. The images

were taken with a 40x objective on a Leica SP8 scanning confocal microscope and LAS X software. This figure is representative of n=3.

As previously described, MC009 inhibited the induction of both NF-κB and IRF pathways, even after directly activating the system by overexpressing p65, IRF3 or IRF7 (**Figure 3.8 and Figure 3.11**). The MCV inhibitor was also shown to inhibit cytokine and IFN production (**Figure 3.12 and Figure 3.13**). NF-κB activity can be acutely stimulated by TNFα, leading to relatively rapid nuclear translocation and NF-κB-dependant gene expression (352–355). Thus, I next investigated the effect of MC009 on NF-κB nuclear translocation.

Multiple controls were utilised throughout the experimental procedure. Firstly, a CMV-HA (empty vector; EV) plasmid was used to observe background staining present in the 488 nm channel. MC020 was tested to differentiate if any changes to p65 localisation were a direct effect of MC009 expression. The p65 response to TNFα stimulation was controlled with unstimulated HEK293T cells. Lastly, a TNFα time course was conducted to visualise p65 translocation at set timepoints (**Figure 4.5**).

NF-κB subunit p65 was localised in the cytoplasm in unstimulated HEK293T cells transfected with MC009, MC020 and EV (**Figure 4.5A**). Transcription factor subunit nuclear translocation was not observed after a 10-minute TNFα stimulation but was observed from the 20-minute timepoint onward (**Figure 4.5B and C**). Notably, nuclear translocation was unaffected by EV or MC020 transfection at any timepoint of TNFα stimulation. In contrast, MC009 inhibited TNFα-induced p65 translocation past the 20-minute timepoint (**Figure 4.5C-G**).

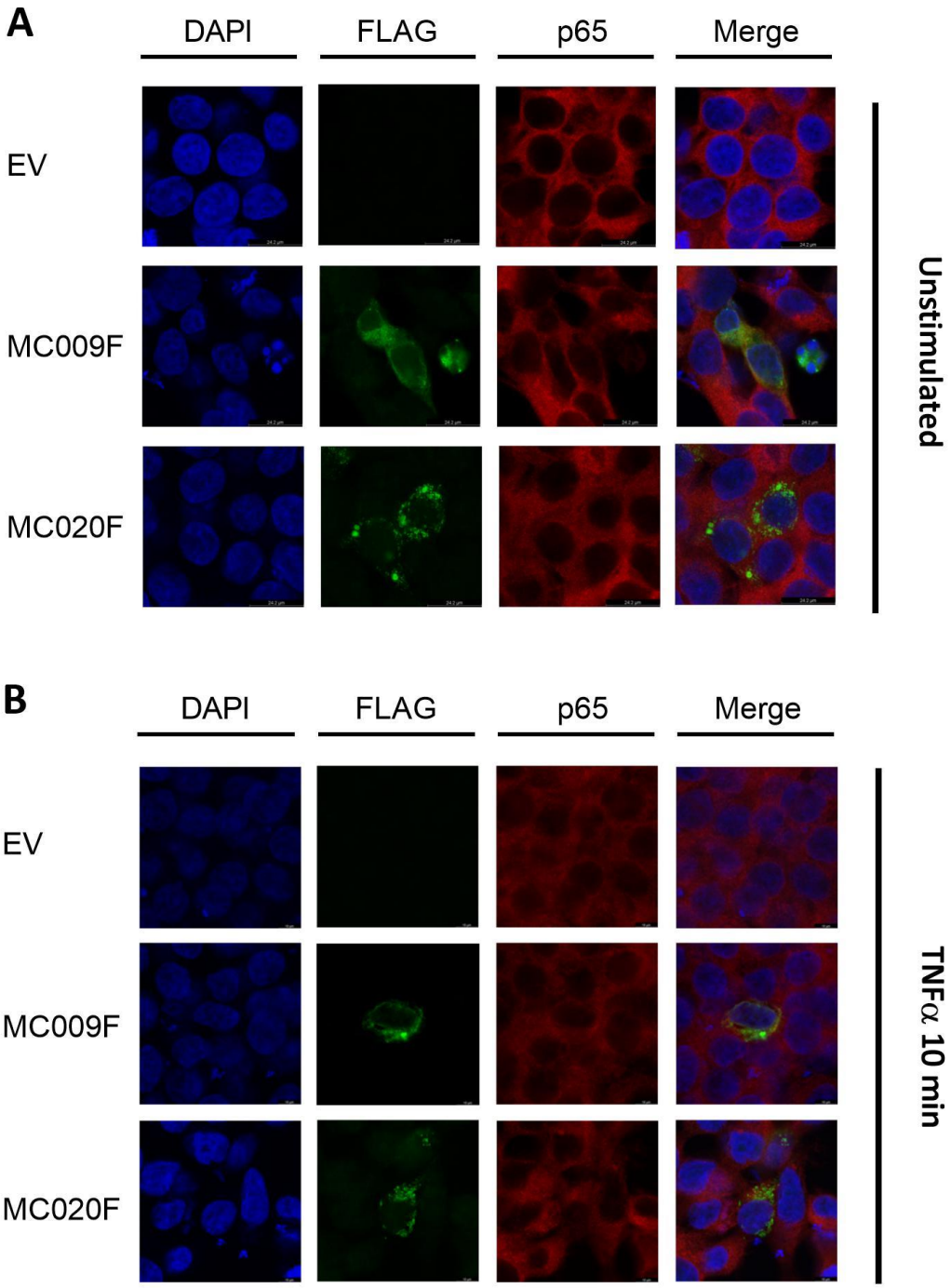
A
DAPI
FLAG
p65
Merge
EV
MC009F
MC020F
Unstimulated
B
DAPI
FLAG
p65
Merge
EV
MC009F
MC020F
TNFα 10 min

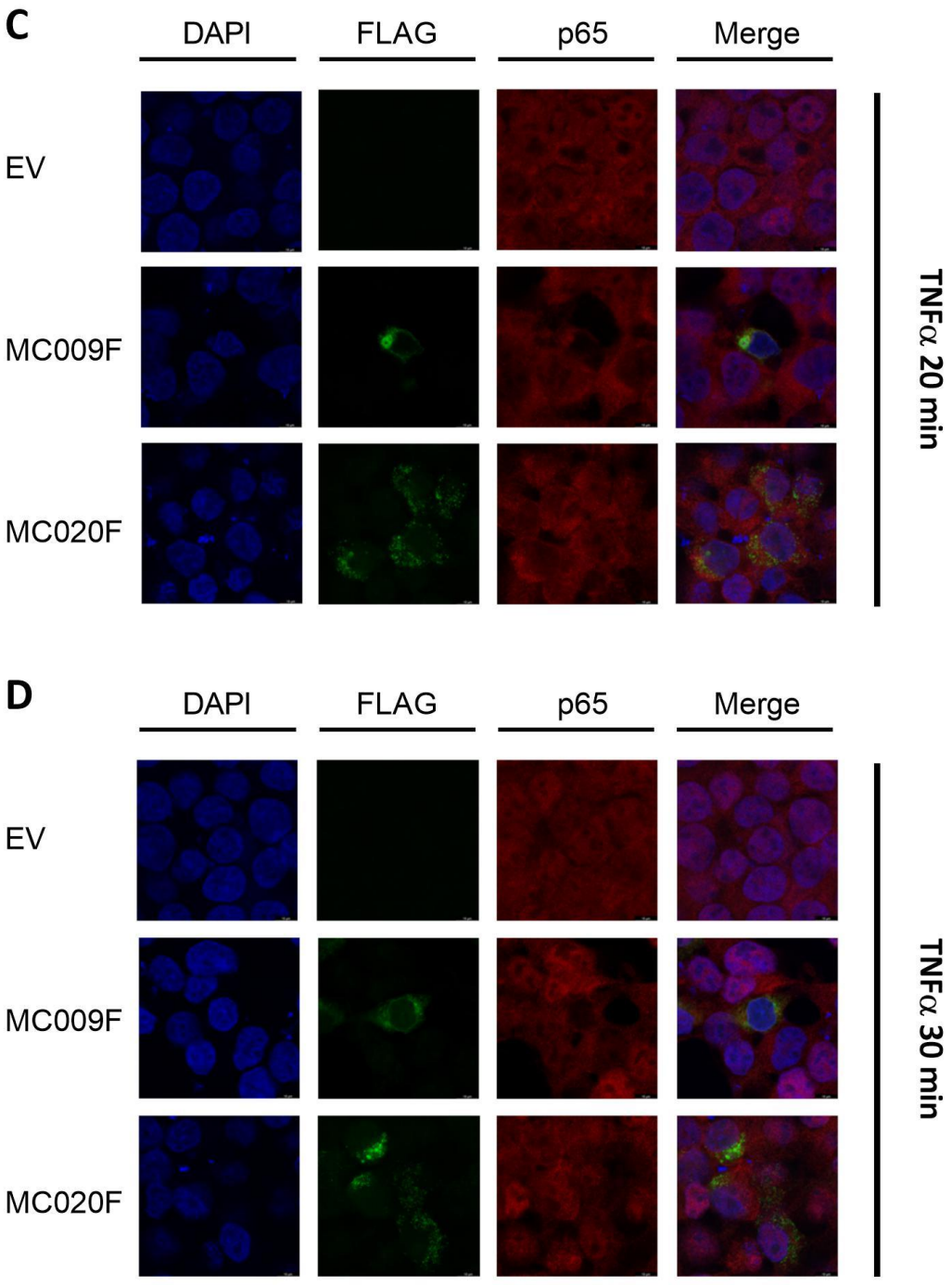
C
DAPI
FLAG
p65
Merge
EV
MC009F
MC020F
TNFα 20 min
D
DAPI
FLAG
p65
Merge
EV
MC009F
MC020F
TNFα 30 min

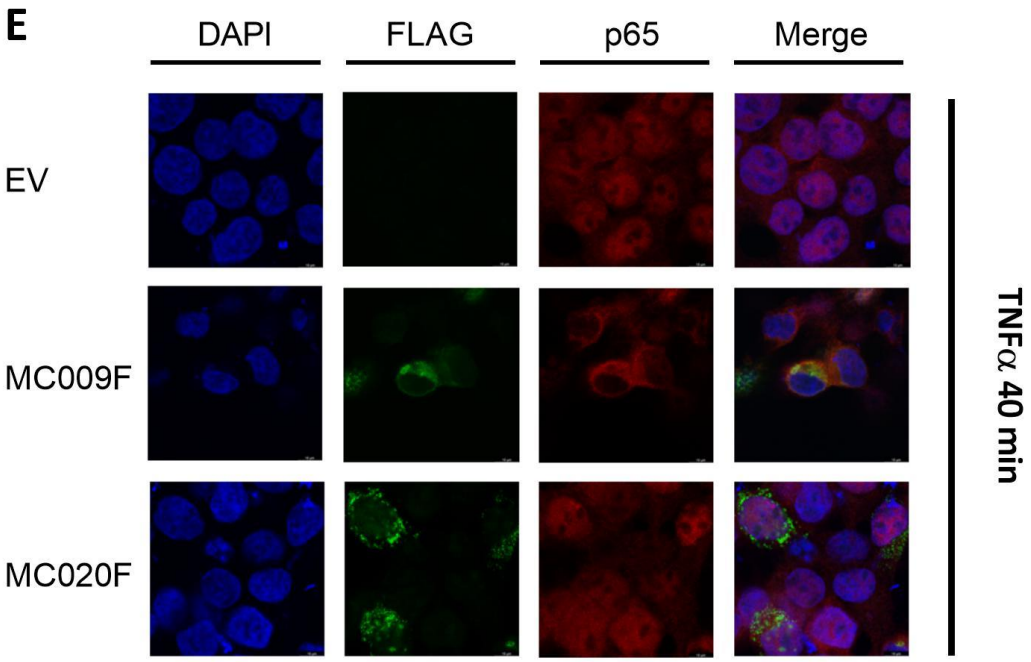
E
DAPI
FLAG
p65
Merge
EV
MC009F
MC020F
TNFα 40 min

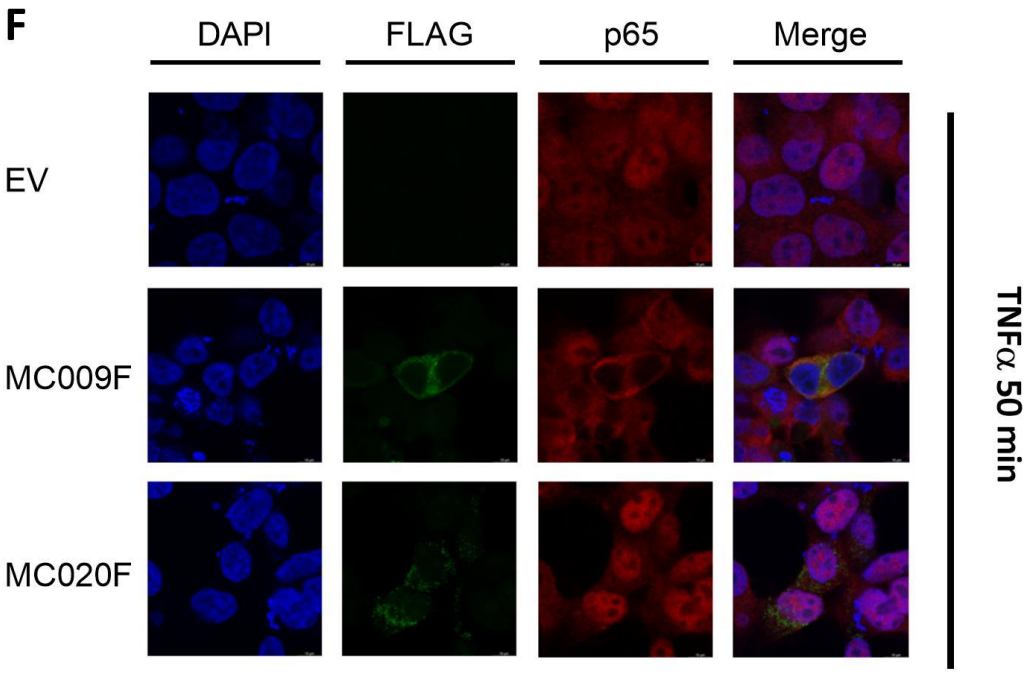
F
DAPI
FLAG
p65
Merge
EV
MC009F
MC020F
TNFα 50 min

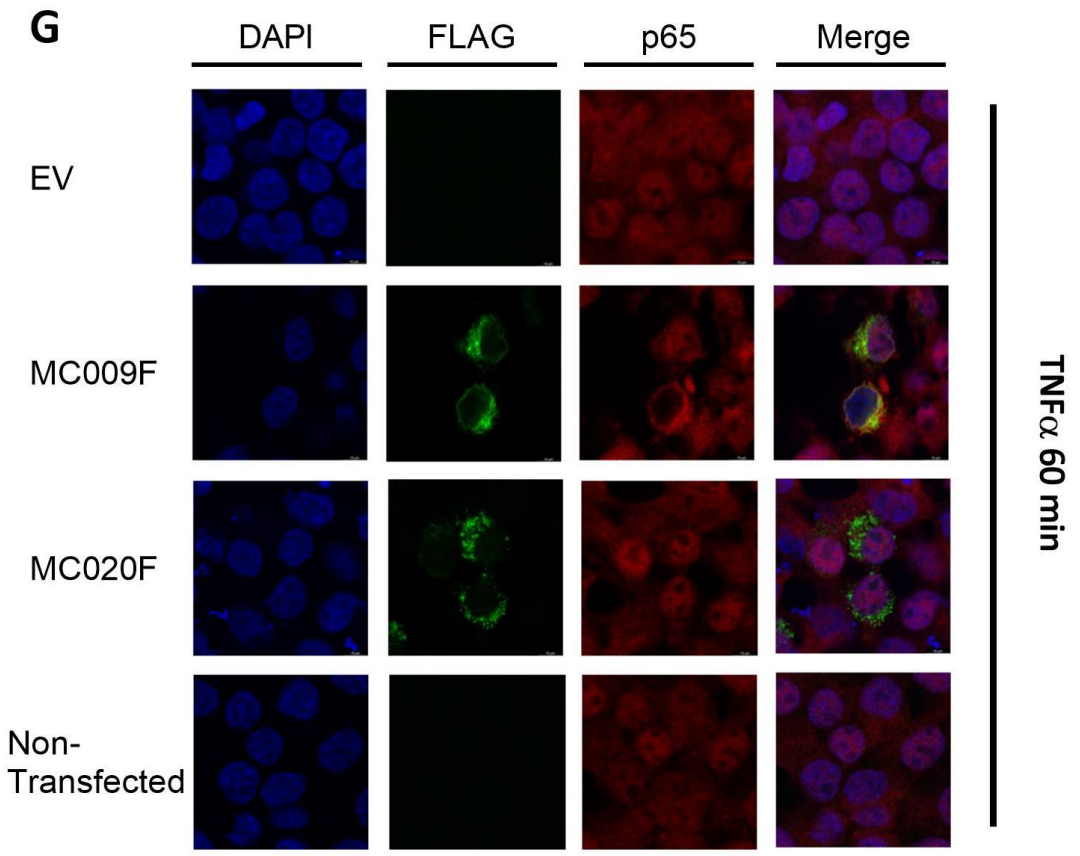

Figure 4.5. MC009 inhibits TNFα-induced p65 nuclear translocation. A-B. HEK293T cells were seeded at $1.8x10^5$ cells/mL in 8-well chamber slides. The wells were transfected with 1 µg MC009-FLAG, MC020-FLAG or CMV-HA. Cells were stimulated with 50 ng/mL TNFα over a 10-60-minute time course (**B**). The cells were stained for FLAG (488 nm) and p65 (647 nm). ProLong™ Gold DAPI mounting solution was used for nuclear staining. The images were taken with a 40x objective on a Leica SP8 scanning confocal microscope and LAS X software. This figure is representative of n=3.

4.4 MC009 does not inhibit NF-κB signalling through direct interaction with p65 or IκB degradation.

After observing that MC009 expression was correlated to p65 sequestering in the cytoplasm, the mechanism of inhibition was investigated. First, I examined whether MC009 was binding and potentially directly sequestering p65. HEK293T cells were transfected with MC009, MC020 or EV. It was noted that MC009-FLAG did not pull-down endogenous p65 suggesting that direct interaction was not responsible for inhibition of translocation (**Figure 4.6**).

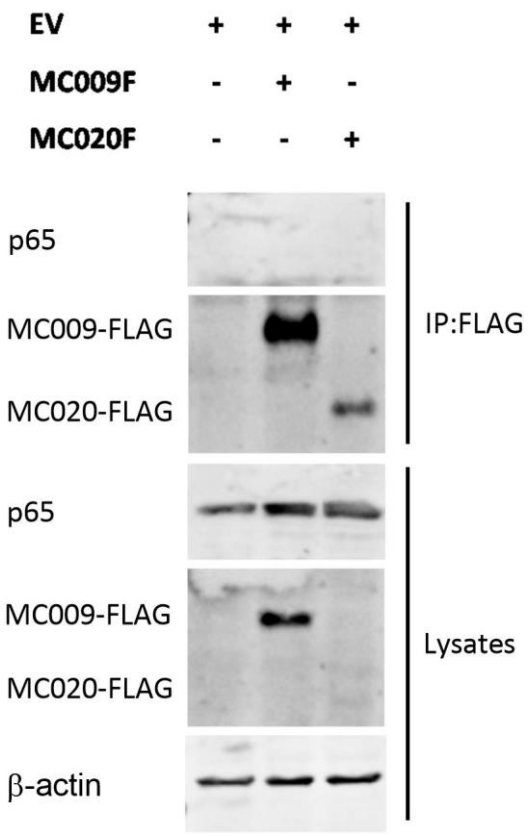

Figure 4.6. MC009 does not interact with endogenous p65. HEK293T cells were seeded at $4x10^6$ cells/mL in 10 cm. The wells were transfected with 4 µg MC009-FLAG or MC020-FLAG and 4 µg EV. Cells were lysed with a CO-IP lysis buffer containing phosphatase and protease inhibitors. Immunoprecipitants and control lysates were immunoblotted and imaged using the ChemiDoc Bio-Rad imaging system. This figure is representative of n=3.

Another potential mechanism of MC009 inhibition involved key events in NF-κB regulation such as p65 phosphorylation and IκBα degradation. To investigate this, MC009 expression was induced using stable-$CdCl_2$-inducible pMEP4-MC009-FLAG cells. Phosphorylation events were tested with a TNFα stimulation time-course. Interestingly, no inhibition was observed for TNFα-induced IκB degradation or p65 phosphorylation by MC009 (**Figure 4.7**).

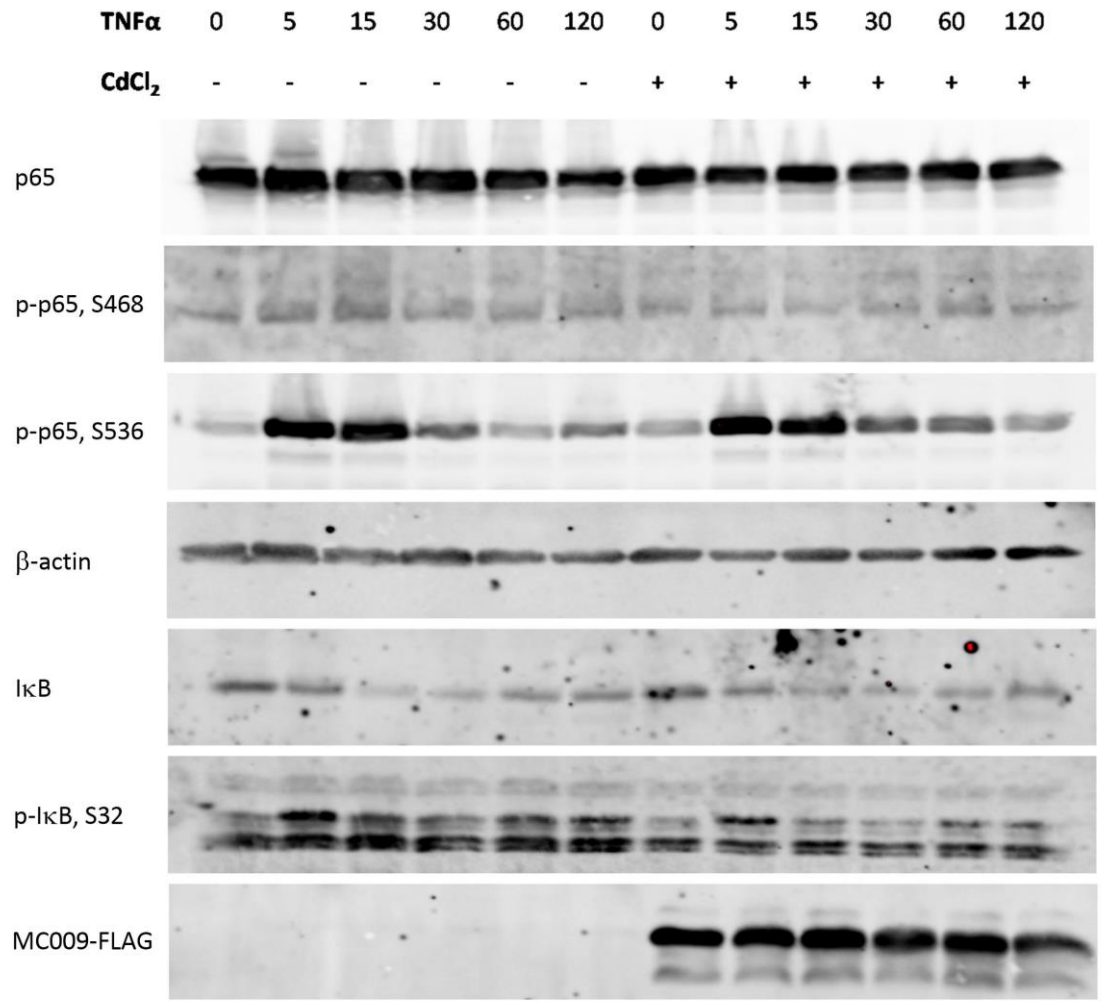

Figure 4.7. MC009 inhibits key upstream events in TNFα-induced NF-κB activation. Stable pMEP4-MC009-FLAG cells were seeded at $5x10^5$ cells/mL in 6-well plates. MC009 expression was induced with 1 µM $CdCl_2$ for 24h. Cells were stimulated with 50 ng/mL TNFα at 0, 5, 15,

30, 60 and 120 minutes. Cells were lysed and lysates were immunoblotted. Blots were imaged using ChemiDoc Bio-Rad imaging system. This figure is representative of n=3.

4.5 Discussion

Initial confocal microscopy MC009 localisation experiments presented flaws in the acquired protocol. HEK293T cells did not retain their standard morphology or growing pattern. Thus, the sample slides no longer represented the 2D *in vitro* cell culture model intended for this experiment. Furthermore, the overlapping of cells made it difficult to find MC009-FLAG expressing cells (**Figure 4.1**). Confocal microscopy optimisation examined optimal conditions for multiple steps of the protocol: cell culture optimisation, slide preparation optimisation and Leica SP8 scanning confocal microscope settings optimisation. Chamber slides and glass coverslips were tested for cell culture. HEK293T cells maintained a 2D *in vitro* model appearance when seeded on uncoated and untreated glass slides (**Figure 4.2**). Four out of nine conditions were used for confocal protocol optimisation. The raised cell growths on Poly-L-Lysine slides were not representative of standard 2D *in vitro* cell culture. It also prolonged the imaging process as multiple z-planes required to be observed for MC009-FLAG activity (**Figure 4.3E and G**). Changes in HEK293T cell growth on Poly-L-Lysine treated glass were not expected as it is a commonly used adhesion reagent (356). The difference observed could be a result of expired product or incorrect product storage. HEK293T cell growth on uncoated chamber slides and coverslips was the most reminiscent of standard cell morphology even after slide preparation for microscopy. The cell-surface adhesion was not as strong on these slides as on Poly-L-Lysine treated glass, however, all cells were present on the same z-plane making the imaging process more efficient (**Figure 4.3F and H**). Similar MC009-FLAG transfection levels were observed on both uncoated surfaces. The chamber slide system was chosen as the cell culture vessel for confocal microscopy for this project as

it required less space, less cells per well and allowed for 8 samples to be stored on the same slide.

MC009 and MC020 were found located in the cytoplasm of HEK293T cells (**Figure 4.4**). Expression pattern of MC009 was distinctly different from that of MC020. MC009 remained evenly spread throughout the cytoplasm whereas MC020 had a more granular manifestation. Transcription factor translocation is a vital step in any pathogen defence system as pro-inflammatory cytokine release and type I IFN production depend on it (335,357). Without an active cell stimulus, p65 remains bound to IκB retaining the protein in the cytoplasm. The IRF proteins, although not physically inhibited by a bound protein, require TBK1- or IKKε-mediated phosphorylation to drive dimer formation and later nuclear translocation (117,220,222). P65 translocation can be stimulated with TNFα over a short period of time. An acute stimulation for IRF signalling was not possible with Poly(dA:dT), the primary IRF stimulant used in the host lab. The dsDNA required to be transfected into the cell and later transcribed into 5'-triphhosphate dsRNA (244). Therefore, the project mainly focused on the NF-κB transcription factor. Groups such as Lin *et. al.* and Zhang *et. al.* have conducted IRF nuclear translocation experiments using Sendai virus (SeV), however, these experiments also required longer stimulation times, 8 hours and 12 hours respectively (358,359).

Intriguingly, MC009 inhibited p65 from translocating from the cytoplasm into the nucleus (**Figure 4.5**). The same effect was not observed in cells expressing MC020 or EV. Based on the confocal images, three hypotheses seemed plausible: MC009 was preventing p65 from being released by IκB, MC009 interacts with p65 forcing it to sequester in the cytoplasm or MC009 inhibits the mechanism by which nuclear

translocation occurs. All above hypotheses were investigated. It is not surprising that viruses would directly target p65 as it is a common point for most signalling cascades. Proteins such as EV71 2C protein and Measles Virus V (MVV) protein are just two examples of viral material designed to directly interact with p65 to block downstream pro-inflammatory gene regulation (360,361). Firstly, the interaction between MC009-p65 was examined, however, endogenous p65 was not co-immunoprecipitated with MC009-FLAG (**Figure 4.6**). The Co-IP was conducted on endogenous p65 without any prior cell stimulation similarly to experiments which confirmed EV71 2C- and MVV-p65 interactions (360,361). It would have been interesting to conduct the same experiment after a TNFα stimulation, testing if phosphorylation of p65 or IκBα release altered the co-immunoprecipitation result.

The inhibitor appeared to be disrupting p65 nuclear translocation indirectly. IκB levels were examined in cells expressing MC009 with no changes to IκB or pIκB observed (**Figure 4.7**). As a result, two out of the three previously stated hypotheses were refuted. The experiment design was influenced by MC005 and MC132 research papers (292,299). Unlike both studies, I tested two different p65 phosphorylation sites, S536 and S468. Site S536 is one of the most commonly used phosphorylation sites in literature examining p65 modification with almost 5000 citations using the same antibody as was used for this project (362). Residue S468 is more closely related with proteasomal degradation (363). Unfortunately, the latter did not give clear results (**Figure 4.7**). The antibody used for p-p65 S468 did not provide a strong signal therefore, if any changes occurred, they were not easily visible to the naked eye. Densitometry can be used to quantify changes observed on western blot images, however, in comparison to the other antibodies used

throughout the project, the antibody did not appear to work effectively or very low levels of p65 was phosphorylated at S468 in the samples.

4.6 Conclusion

Confocal microscopy protocol using chamber slide culture vessels without Poly-L-Lysine was shown to be most effective and beneficial for further confocal microscopy work. The optimisation set a strong foundation for p65 nuclear translocation experiments. MC009 was shown to inhibit TNFα-induced p65 nuclear translocation. This inhibitory effect corresponds to the reduced production levels of IL-8 and IP-10 observed in chapter 3. The MCV inhibitor does not block p65 translocation through directly interacting with p65 or by affecting p65-inhibitor IκB.

Chapter 5: MC009 Interacts with Karyopherin Proteins to Inhibit Signal Transduction.

5.1 Introduction

The importin family is divided into two arms subunit α and subunit β, also known as KPNA and KPNB/IPO proteins. The karyopherin family has become a more popular research topic in recent years, like their role in specific molecular processes or availability in different tissues (364). KPNA7, the most newly discovered KPNA member, functions mainly during early development (364). Furthermore, the α-subunits also hold varied importance in disease states. KPNA2 has been demonstrated to play a key role in oncogenesis whereas KPNA6 has been recently implicated in viral immune evasion (286,287,365,366).

KPNA1-7 are composed of an N-terminal importin β binding (IBB) region, armadillo (ARM) repeats and the C-terminal (272). The IBB domain is nuclear localisation sequence (NLS) specific to import-adaptor-proteins and is not considered a classic NLS (367). IBB domain competitive binding occurs between importin β proteins and RanGTP during nuclear cargo translocation (367). The KPNA members are largely composed of 42 amino acid-long ARM repeats (272). The motifs consist of three α-helices ultimately forming a superhelix structure (368,369). Each KPNA protein contains ten ARM motifs, however, sequence identity is not well conserved between the α subunit members (**Figure 5.5**). Nevertheless, ARM repeat proteins share a common structural similarity (370).

Chapter four focused on confocal microscopy protocol optimisation necessary for further MC009 investigation. The inhibitory effect of MC009 on p65 nuclear translocation was also discussed. As an interaction between MC009 and p65 was not observed, it was vital to determine which host protein(s) were involved in MC009-driven signal inhibition. This chapter focuses on the MCV protein interactions with human innate proteins.

Additionally, the effect of MC009 was investigated on complex formation between two host proteins, KPNA6 and p65.

5.2 MC009 does not interact with importin IPO5.

Prior to project commencement, affinity purification-mass spectrometry (AP-MS) was conducted on MC009-co-purifying proteins from stable inducible pMEP4-MC009-FLAG HEK293T cells. The results listed various proteins which immunoprecipitated with the inhibitor, although the inhibitor itself was not detected potentially due to the poor MC009 trypsin fragment enrichment. In contrast to the AP-MS results obtained for other MCV inhibitors investigated in the host lab, the number of proteins which immunoprecipitated with MC009 was larger than, for example, for MC132. The data showed a plethora of proteins, most of which were deemed 'false positive' interactions. However, two proteins were of particular interest, importin-5 (IPO5) and karyopherin subunit alpha 6 (KPNA6)(**Figure 5.1**). Both proteins are members of the importin family required for the translocation of transcription factors from the cytoplasm into the nucleus (277). As MC009 was inhibiting p65 translocation but not directly interacting with the transcription factor member nor affecting IκB degradation, interaction between IPO5 and KPNA6 with MC009 was investigated.

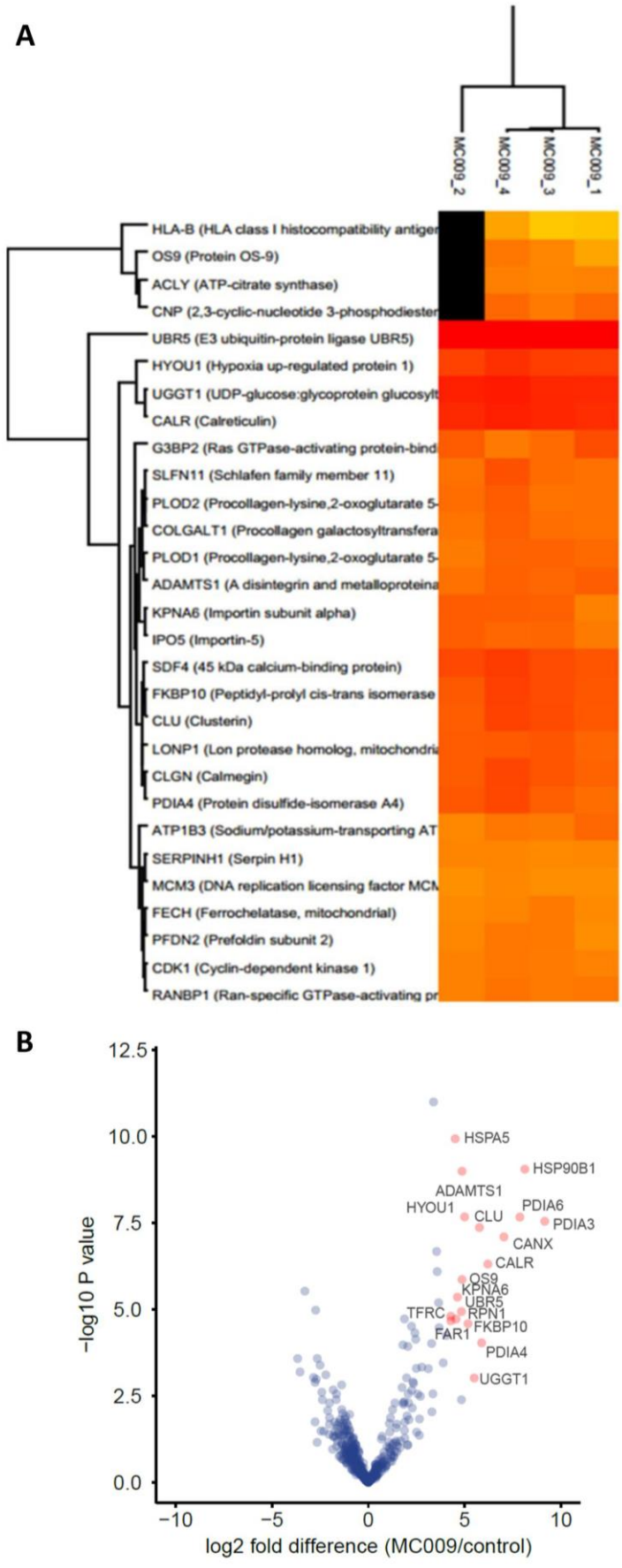
A
MC009_2
MC009_4
MC009_3
MC009_1
HLA-B (HLA class I histocompatibility antige
OS9 (Protein OS-9)
ACLY (ATP-citrate synthase)
CNP (2,3-cyclic-nucleotide 3-phosphodieste
UBR5 (E3 ubiquitin-protein ligase UBR5)
HYOU1 (Hypoxia up-regulated protein 1)
UGGT1 (UDP-glucose:glycoprotein glucosylt
CALR (Calreticulin)
G3BP2 (Ras GTPase-activating protein-bind
SLFN11 (Schlafen family member 11)
PLOD2 (Procollagen-lysine,2-oxoglutarate 5-
COLGALT1 (Procollagen galactosyltransfera
PLOD1 (Procollagen-lysine,2-oxoglutarate 5-
ADAMTS1 (A disintegrin and metalloproteina
KPNA6 (Importin subunit alpha)
IPO5 (Importin-5)
SDF4 (45 kDa calcium-binding protein)
FKBP10 (Peptidyl-prolyl cis-trans isomerase
CLU (Clusterin)
LONP1 (Lon protease homolog, mitochondri
CLGN (Calmegin)
PDIA4 (Protein disulfide-isomerase A4)
ATP1B3 (Sodium/potassium-transporting AT
SERPINH1 (Serpin H1)
MCM3 (DNA replication licensing factor MCM
FECH (Ferrochelatase, mitochondrial)
PFDN2 (Prefoldin subunit 2)
CDK1 (Cyclin-dependent kinase 1)
RANBP1 (Ran-specific GTPase-activating pr
B
12.5
10.0
7.5
5.0
2.5
0.0
−log10 P value
HSPA5
HSP90B1
ADAMTS1
HYOU1
CLU
PDIA6
PDIA3
CANX
CALR
OS9
KPNA6
UBR5
TFRC
RPN1
FAR1
FKBP10
PDIA4
UGGT1
−10
−5
0
5
10
log2 fold difference (MC009/control)

Figure 5.1. Affinity purification-mass spectrometry analysis of MC009 immunoprecipitants. A-B. Heatmap and volcano plot illustrating potential proteins interacting with MC009. This data was obtained by Dr. Andreas Pichlmair in collaboration with Prof. Gareth Brady and has been included in this thesis to give context to the initial course of investigation.

First, the interaction between endogenous IPO5 and MC009-FLAG was examined. IPO5 is a subunit β member of the importin family. These members often work alongside of the α subunit proteins to transport the cargo across the nuclear membrane as a complex (277,371). Once again, MC020 expression was not observed in the control lysate, however, MC020-FLAG was present in the immunoprecipitated lysates. Although, IPO5 was expressed in the HEK293T control lysates, the protein was not immunoprecipitated with MC009- or MC020-FLAG (**Figure 5.2**).

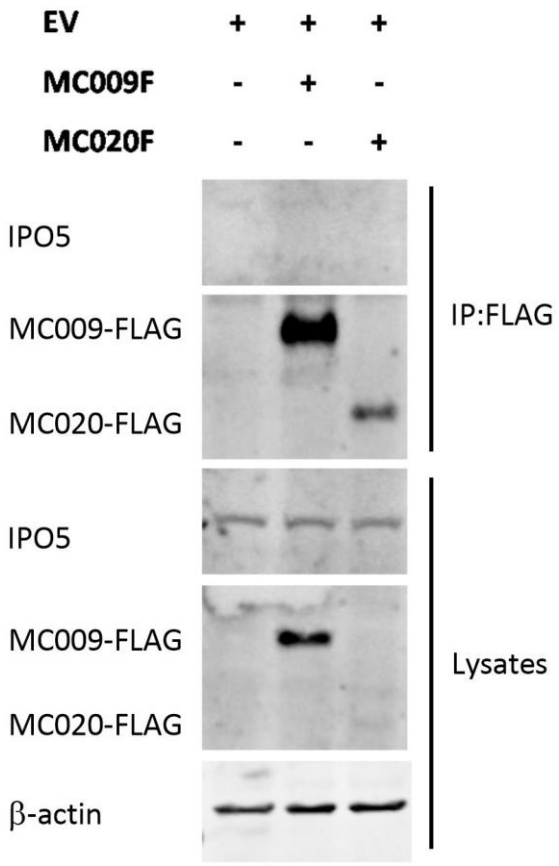

Figure 5.2. IPO5 does not interact with MC009. HEK293T cells were seeded at $4x10^6$ cells/mL in 10 cm dishes. The wells were transfected with 4 µg MC009-FLAG or MC020-FLAG and 4 µg EV. Cells were lysed with a CO-IP lysis buffer containing phosphatase and protease inhibitors. Immunoprecipitants and control lysates were immunoblotted and imaged using the ChemiDoc Bio-Rad imaging system. This figure is representative of n=3.

5.3 MC009 interacts with karyopherin KPNA6.

As MC009 was not shown to interact with a β subunit importin another avenue was investigated. Representative members of both subunit families, α and β, were noted in the AP-MS data received by the host lab. Thus, KPNA6 was investigated next. Recent studies have shown viruses, such as Influenza virus or SARS-CoV-2, to target KPNA6 in order to evade the host immune system (286,287). Thus far, no MCV proteins have been implicated in inhibiting nuclear cargo transport by members of the importin family, with only one known example of poxviral interaction with karyopherins (283).

Like p65 and IPO5, the cell lysates and immunoprecipitants were probed for FLAG or endogenous KPNA6. Strong expression of KPNA6 was noted in the control lysates for all three samples. Moreover, immunoprecipitation results indicated a clear interaction between MC009 and endogenous KPNA6 (**Figure 5.3**).

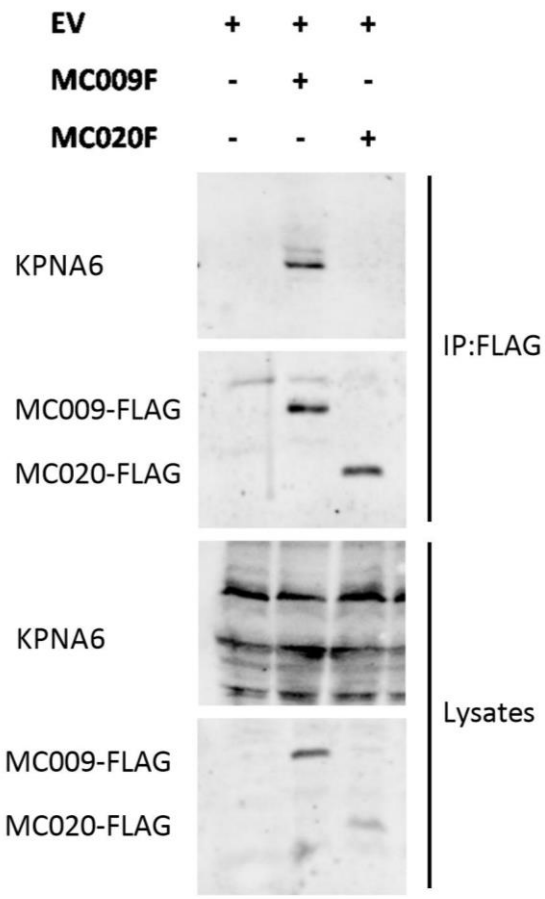

Figure 5.3. Endogenous KPNA6 interacts with MC009. HEK293T cells were seeded at $4x10^6$ cells/mL in 10 cm dishes. The wells were transfected with 4 µg MC009-FLAG or MC020-FLAG and EV, 8 µg DNA final. Cells were lysed with a CO-IP lysis buffer containing phosphatase and protease inhibitors. Immunoprecipitants and control lysates were immunoblotted for anti-FLAG and KPNA6. Images were taken using the ChemiDoc Bio-Rad imaging system. This figure is representative of n=3.

To further investigate the interaction between MC009 and KPNA6, MC009-HA was examined for interactions with overexpressed KPNA6-FLAG. Additionally, KPNA1-5 were examined alongside KPNA6 and were intended to serve as controls. KPNA5-FLAG expression was not detected in the control lysate, with the expression of all FLAG-tagged proteins being low. Nevertheless, strong levels of all KPNA proteins were observed in immunoprecipitant lysates. Control lysates showed strong MC009-HA expression.

Unexpectedly, MC009 not only immunoprecipitated with KPNA6, but it also showed a strong interaction with KPNA5. A weaker expression band was also seen with KPNA1. No interactions were observed with KPNA2, KPNA3 or KPNA4 with the MCV inhibitor (**Figure 5.4**).

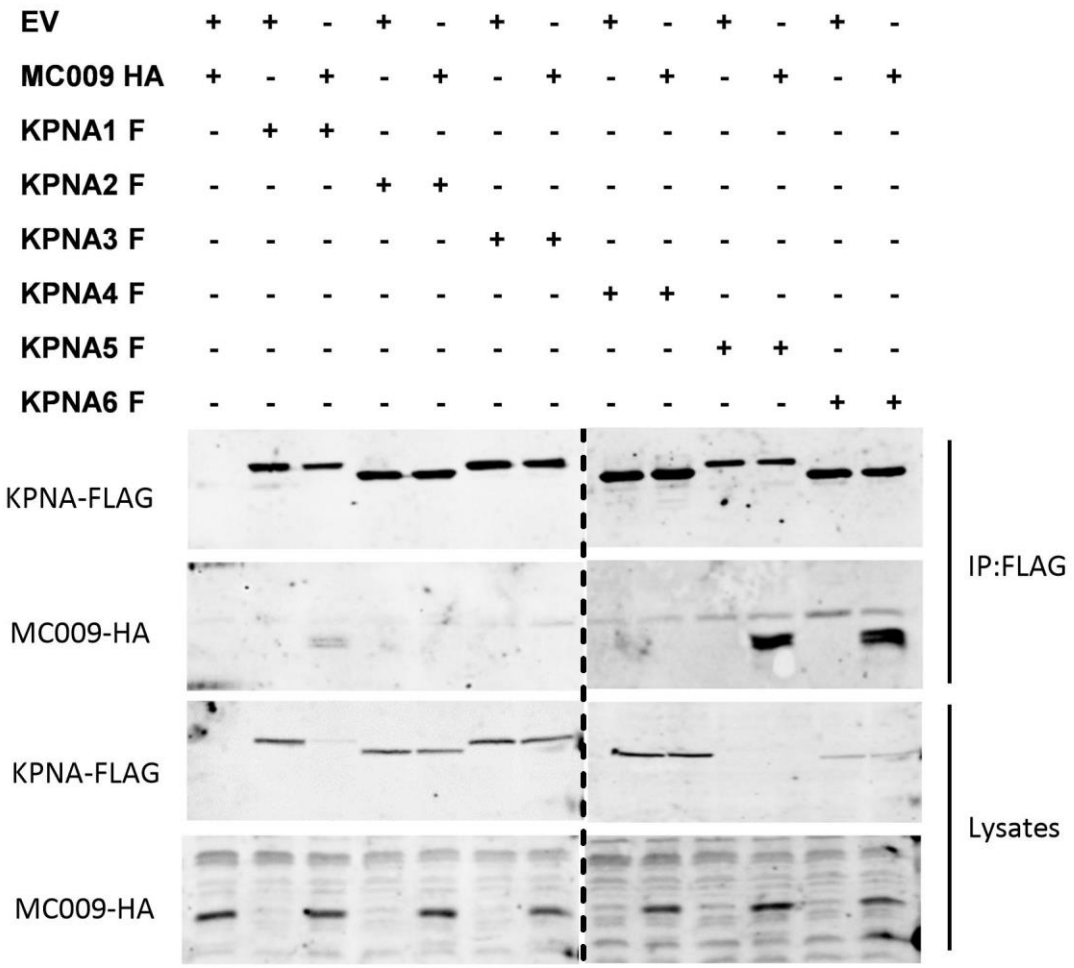

Figure 5.4. MC009 interacts with karyopherins KPNA1, KPNA5 and KPNA6. HEK293T cells were seeded at $4x10^6$ cells/mL in 10 cm dishes. The wells were transfected with 4 µg FLAG-tagged karyopherin (KPNA) plasmid and 4 µg MC009-HA or EV. Cells were lysed with a CO-IP lysis buffer containing phosphatase and protease inhibitors. Immunoprecipitants and control lysates were immunoblotted and imaged using the ChemiDoc Bio-Rad imaging system. This figure is representative of n=3.

Following the results observed in **Figure 5.4**, it was important to understand why MC009 could interact with KPNA1 and KPNA5 additionally to KPNA6. ClustalOmega was used to conduct a sequence alignment of all known human KPNA subunits, including KPNA7 which was not used experimentally as part of this thesis. The subunits, categorised into three subfamilies, are between 42.5% and 85.8% homologous with one another. The alignment in **Figure 5.5** showed conserved amino acids within all proteins as well as key sites where the proteins differ.

A

KPNA	Importin α	Subfamily	GenBank
KPNA1	Importin α5	α3	CAG33024.1
KPNA2	Importin α1	α1	NP_001307540.1
KPNA3	Importin α4	α2	NP_002258.2
KPNA4	Importin α3	α2	NP_002259.1
KPNA5	Importin α6	α3	NP_001353234.1
KPNA6	Importin α7	α3	NP_036448.1
KPNA7	Importin α8	α1	NP_001139187.1

B

```
CAG33024.1          ----------------------MTTPGKENFRLKSYKNKSLNPDEMRRRREEEGLQLRK   37
NP_001353234.1      MGRQRSRGRGSRTFPLRTRRRDAMASPGKDNYRMKSYKNKALNPQEMRRRREEEGIQLRK   60
NP_036448.1         --------------------METMASPGKDNYRMKSYKNNALNPEEMRRRREEEGIQLRK   40
NP_002258.2         --------------------MA--ENPSLENHRIKSFKNKGRDVETMRRHRNEVTVELRK   38
NP_002259.1         --------------------MA--DNEKLDNQRLKNFKNKGRDLETMRRQRNEVVVELRK   38
NP_001307540.1      --------------------MSTNENANTPAARLHRFKNKGKDSTEMRRRRIEVNVELRK   40
NP_001139187.1      ----------------------MPTLDAPEERRRKFKYRGKDVSLRRQQRMAVSLELRK   37
                                          .     * : :* .. :    *::*    ::***

CAG33024.1          QKREEQLFKRRNVATAEEETEEEVMSDGGFHEAQI-NNMEMAPGGVITSDMIEMIFSKSP   96
NP_001353234.1      QKREEQLFKRRNVYLPRNDE---SMLESPIQDPDISSTVPIPEEEVVTTDMVQMIFSNNA   117
NP_036448.1         QKREQQLFKRRNVELINEEA---AMFDSLLMDSYVSST---TGESVITREMVEMLFSDDS   94
NP_002258.2         NKRDEHLLKKRNVPQEESLEDSDV------------DADFKAQNVTLEAILQNATSDNP   85
NP_002259.1         NKRDEHLLKRRNVPHEDICEDSDI------------DGDYRVQNTSLEAIVQNASSDNQ   85
NP_001307540.1      AKKDDQMLKRRNVSSFPDDATSPLQEN----------RNNQGTVNWSVDDIVKGINSSNV   90
NP_001139187.1      AKKDEQTLKRRNITSFCPDTPSEK------------TAKGVAVSLTLGEIIKGVNSSDP   84
                     *:::: :*:**:                                  :::   *..
```

```
CAG33024.1          EQQLSATQKFRKLLSKEPNPPIDEVISTPGVVARFVEFLKRKENCTLQFESAWVLTNIAS      156
NP_001353234.1      DQQLTATQKFRKLLSKEPNPPIDQVIQKPGVVQRFVKFLERNENCTLQFEAAWALTNIAS      177
NP_036448.1         DLQLATTQKFRKLLSKEPSPPIDEVINTPRVVDRFVEFLKRNENCTLQFEAAWALTNIAS      154
NP_002258.2         VVQLSAVQAARKLLSSDRNPPIDDLIK-SGILPILVKCLERDDNPSLQFEAAWALTNIAS      144
NP_002259.1         GIQLSAVQAARKLLSSDRNPPIDDLIK-SGILPILVHCLERDDNPSLQFEAAWALTNIAS      144
NP_001307540.1      ENQLQATQAARKLLSREKQPPIDNIIR-AGLIPKFVSFLGRTDCSPIQFESAWALTNIAS      149
NP_001139187.1      VLCFQATQTARKMLSQEKNPPLKLVIE-AGLIPRMVEFLKSSLYPCLQFEAAWALTNIAS      143
                       : :.*  **:** : .**:. :*    ::  :*  *       :***:**.******

CAG33024.1          GNSLQTRIVIQAGAVPIFIELLSSEFEDVQEQAVWALGNIAGDSTMCRDYVLDCNILPPL      216
NP_001353234.1      GTFLHTKVVIETGAVPIFIKLLNSEHEDVQEQAVWALGNIAGDNAECRDFVLNCEILPPL      237
NP_036448.1         GTSQQTKIVIEAGAVPIFIELLNSDFEDVQEQAVWALGNIAGDSSVCRDYVLNCSILNPL      214
NP_002258.2         GTSAQTQAVVQSNAVPLFLRLLRSPHQNVCEQAVWALGNIIGDGPQCRDYVISLGVVKPL      204
NP_002259.1         GTSEQTQAVVQSNAVPLFLRLLHSPHQNVCEQAVWALGNIIGDGPQCRDYVISLGVVKPL      204
NP_001307540.1      GTSEQTKAVVDGGAIPAFISLLASPHAHISEQAVWALGNIAGDGSVFRDLVIKYGAVDPL      209
NP_001139187.1      GTSEQTRAVVEGGAIQPLIELLSSSNVAVCEQAVWALGNIAGDGPEFRDNVITSNAIPHL      203
                    *.  :*: *:: .*:  :: ** *    : ********** **.   ** *:    :  *

CAG33024.1          LQLFS----KQNRLTMTRNAVWALSNLCRGKSPPPEFAKVSPCLNVLSWLLFVSDTDVLA      272
NP_001353234.1      LELLT----NSNRLTTTRNAVWALSNLCRGKNPPPNFSKVSPCLNVLSRLLFSSDPDVLA      293
NP_036448.1         LTLLT----KSTRLTMTRNAVWALSNLCRGKNPPPEFAKVSPCLPVLSRLLFSSDSDLLA      270
NP_002258.2         LSFIS----PSIPITFLRNVTWVIVNLCRNKDPPPPMETVQEILPALCVLIYHTDINILV      260
NP_002259.1         LSFIS----PSIPITFLRNVTWVMVNLCRHKDPPPPMETIQEILPALCVLIHHTDVNILV      260
NP_001307540.1      LALLAVPDMSSLACGYLRNLTWTLSNLCRNKNPAPPIDAVEQILPTLVRLLHHDDPEVLA      269
NP_001139187.1      LALIS----PTLPITFLRNITWTLSNLCRNKNPYPCDTAVKQILPALLHLLQHQDSEVLS      259
                    * :::            ** .*.: **** *.* *    :.  * .*  *:   * ::*

CAG33024.1          DACWALSYLSDGPNDKIQAVIDAGVCRRLVELLMHNDYKVVSPALRAVGNIVTGDDIQTQ      332
NP_001353234.1      DVCWALSYLSDGPNDKIQAVIDSGVCRRLVELLMHNDYKVVSPALRAVGNIVTGDDIQTQ      353
NP_036448.1         DACWALSYLSDGPNEKIQAVIDSGVCRRLVELLMHNDYKVASPALRAVGNIVTGDDIQTQ      330
NP_002258.2         DTVWALSYLTDGGNEQIQMVIDSGVVPFLVPLLSHQEVKVQTAALRAVGNIVTGTDEQTQ      320
NP_002259.1         DTVWALSYLTDAGNEQIQMVIDSGIVPHLVPLLSHQEVKVQTAALRAVGNIVTGTDEQTQ      320
NP_001307540.1      DTCWAISYLTDGPNERIGMVVKTGVVPQLVKLLGASELPIVTPALRAIGNIVTGTDEQTQ      329
NP_001139187.1      DACWALSYLTDGSNKRIGQVVNTGVLPRLVVLMTSSELNVLTPSLRTVGNIVTGTDEQTQ      319
                    *. **:***:*. *.:*  *:.:*:   ** *:  .:  : : :**::****** * ***

CAG33024.1          VILNCSALQSLLHLLSSPKESIKKEACWTISNITAGNRAQIQTVIDANIFPALISILQTA      392
NP_001353234.1      VILNCSALPCLLHLLSSPKESIRKEACWTVSNITAGNRAQIQAVIDANIFPVLIEILQKA      413
NP_036448.1         VILNCSALPCLLHLLSSPKESIRKEACWTISNITAGNRAQIQAVIDANIFPVLIEILQKA      390
NP_002258.2         VVLNCDVLSHFPNLLSHPKEKINKEAVWFLSNITAGNQQQVQAVIDAGLIPMIIHQLAKG      380
NP_002259.1         VVLNCDALSHFPALLTHPKEKINKEAVWFLSNITAGNQQQVQAVIDANLVPMIIHLLDKG      380
NP_001307540.1      VVIDAGALAVFPSLLTNPKTNIQKEATWTMSNITAGRQDQIQQVVNHGLVPFLVSVLSKA      389
NP_001139187.1      MAIDAGMLNVLPQLLQHNKPSIQKEAAWALSNVAAGPCHHIQQLLAYDVLPPLVALLKNG      379
                    : ::.. *  :  **   * .*.*** * :**::**   ::* ::  .:.* ::  * ..

CAG33024.1          EFRTRKEAAWAITNATSGGSAEQIKYLVELGCIKPLCDLLTVMDSKIVQVALNGLENILR      452
NP_001353234.1      EFRTRKEAAWAITNATSGGTPEQIRYLVALGCIKPLCDLLTVMDSKIVQVALNGLENILR      473
NP_036448.1         EFRTRKEAAWAITNATSGGTPEQIRYLVSLGCIKPLCDLLTVMDSKIVQVALNGLENILR      450
NP_002258.2         DFGTQKEAAWAISNLTISGRKDQVEYLVQQNVIPPFCNLLSVKDSQVVQVVLDGLKNILI      440
NP_002259.1         DFGTQKEAAWAISNLTISGRKDQVAYLIQQNVIPPFCNLLTVKDAQVVQVVLDGLSNILK      440
NP_001307540.1      DFKTQKEAVWAVTNYTSGGTVEQIVYLVHCGIIEPLMNLLTAKDTKIILVILDAISNIFQ      449
NP_001139187.1      EFKVQKEAVWMVANFATGATMDQLIQLVHSGVLEPLVNLLTAPDVKIVLIILDVISCILQ      439
                    :* .:***.* ::* : ..  :*:  *:  . : *: :**:. * ::: : *: :. *:

CAG33024.1          LGEQEAKRNGTGINPYCALIEEAYGLDKIEFLQSHENQEIYQKAFDLIEHYFGTED--ED      510
NP_001353234.1      LGEQESKQNGIGINPYCALIEEAYGLDKIEFLQSHENQEIYQKAFDLIEHYFGVEE--DD      531
NP_036448.1         LGEQEGKRSGSGVNPYCGLIEEAYGLDKIEFLQSHENQEIYQKAFDLIEHYFGVED--DD      508
NP_002258.2         MAGD--EA-----STIAEIIEECGGLEKIEVLQQHENEDIYKLAFEIIDQYFSGDDIDED      493
NP_002259.1         MAED--EA-----ETIGNLIEECGGLEKIEQLQNHENEDIYKLAYEIIDQFFSSDDIDED      493
NP_001307540.1      AAEKLGET-----EKLSIMIEECGGLDKIEALQNHENESVYKASLSLIEKYFSVEE-EED      503
NP_001139187.1      AAEKRSEK-----ENLCLLIEELGGIDRIEALQLHENRQIGQSALNIIEKHFGEEE-DES      493
                     . .  :      .    :***  *:::** ** ***..: : : .:*::.*. ::  :.
```

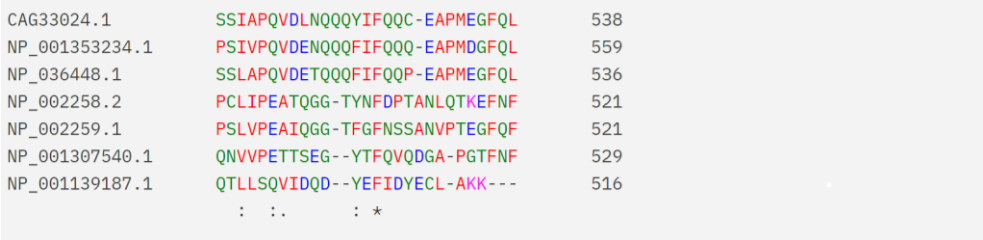

Figure 5.5. Multiple sequence alignment of human KPNA1-7 amino acid sequence. A. Importin α subunit nomenclature with the corresponding GenBank code used for sequence alignment. **B.** Karyopherin α subunit proteins were grouped based on the subfamily they are a part of. The proteins are listed in the following order: KPNA1, KPNA5, KPNA6, KPNA3, KPNA4, KPNA2, KPNA7. Key Legend: (-) gap in sequence, (.) amino acids of weakly similar properties, (:) amino acids of similar properties, (*) fully conserved amino acid. Sequence alignment was conducted using Clustal Omega (EBI-EMBL).

Next, confocal microscopy was used to investigate co-localisation of MC009 and KPNA family members. Endogenous KPNA6 and overexpressed KPNA1-6 were visualised to investigate potential co-localisation with MC009. Endogenous KPNA6 was first screened using FLAG-tagged MC009 with MC020-FLAG, EV and non-transfected cells operating as controls. During the screening process, KPNA6 was observed in the cytoplasm and the nucleus without any prior cell signal stimulation, therefore, MC009 localisation was observed in relation to both cytoplasmic and nuclear KPNA6 (**Figure 5.6**). In HEK293T cells where KPNA6 was present in the cytoplasm, MC009 also remained in the cytoplasm co-localising with the karyopherin (**Figure 5.6 'Cytoplasmic KPNA6' panel**). The same even distribution was not noted with MC020. Although MC009 and KPNA6 were not shown to co-localise in cells with nuclear KPNA6, MC009 was seen to tightly cluster around the nucleus. Nuclear localisation of KPNA6 did not influence MC020 localisation (**Figure 5.6 'Nuclear KPNA6' panel**).

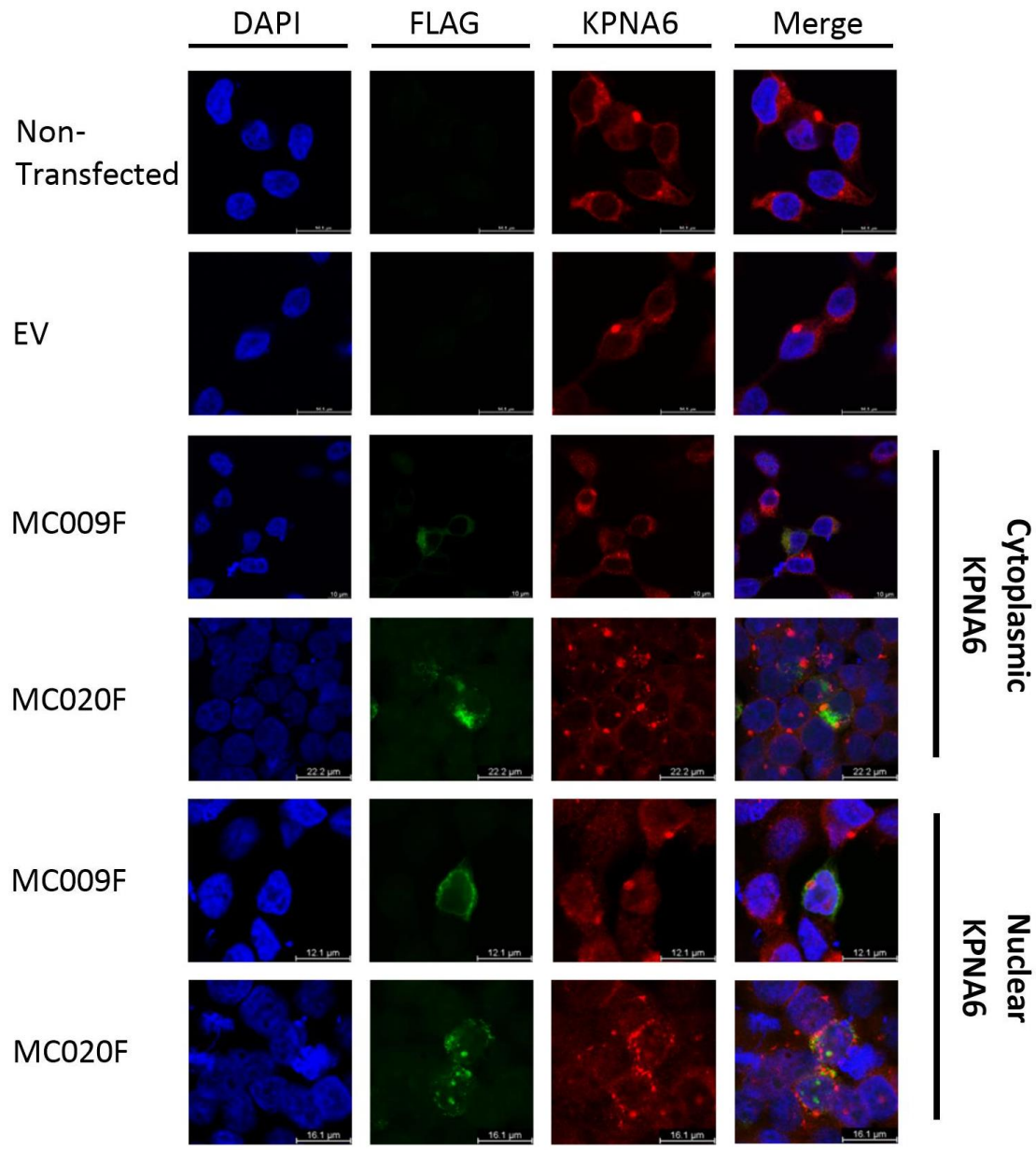

Figure 5.6. Confocal Microscopy visualising endogenous KPNA6 and MC009 or MC020. HEK293T cells were seeded at $1.8x10^5$ cells/mL in 8-well chamber slides. The wells were transfected with 1 µg MC009-FLAG, MC020-FLAG or EV. Slides were stained for KPNA6 (647 nm) and FLAG (488 nm). ProLong™ Gold DAPI mounting solution was used for nuclear staining. The images were taken with a 40x objective on a Leica SP8 scanning confocal microscope and LAS X software. This figure is representative of n=2.

MC009 was also examined for co-localisation with the previously tested six overexpressed KPNAs. In contrast, to the endogenous protein, the overexpressed KPNAs

exclusively localised in the nucleus of HEK293T cells. Interestingly, MC009 was also able to transport into the nucleus in cells expressing KPNA6 as well as KPNA1 and KPNA5. The nuclear translocation of the inhibitor was not observed with KPNA2, KPNA3 or KPNA4 for which MC009 remained in the cytoplasm (**Figure 5.7**).

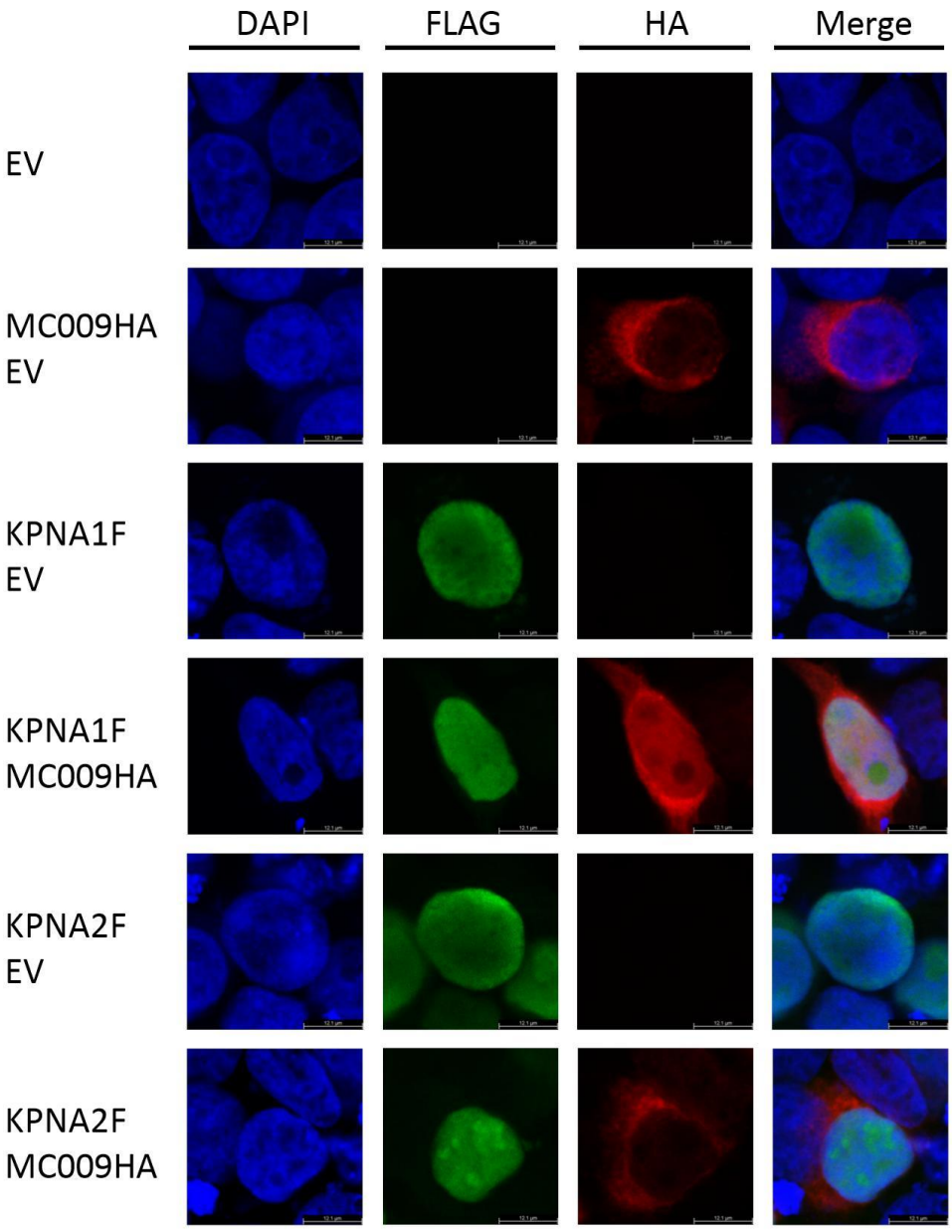

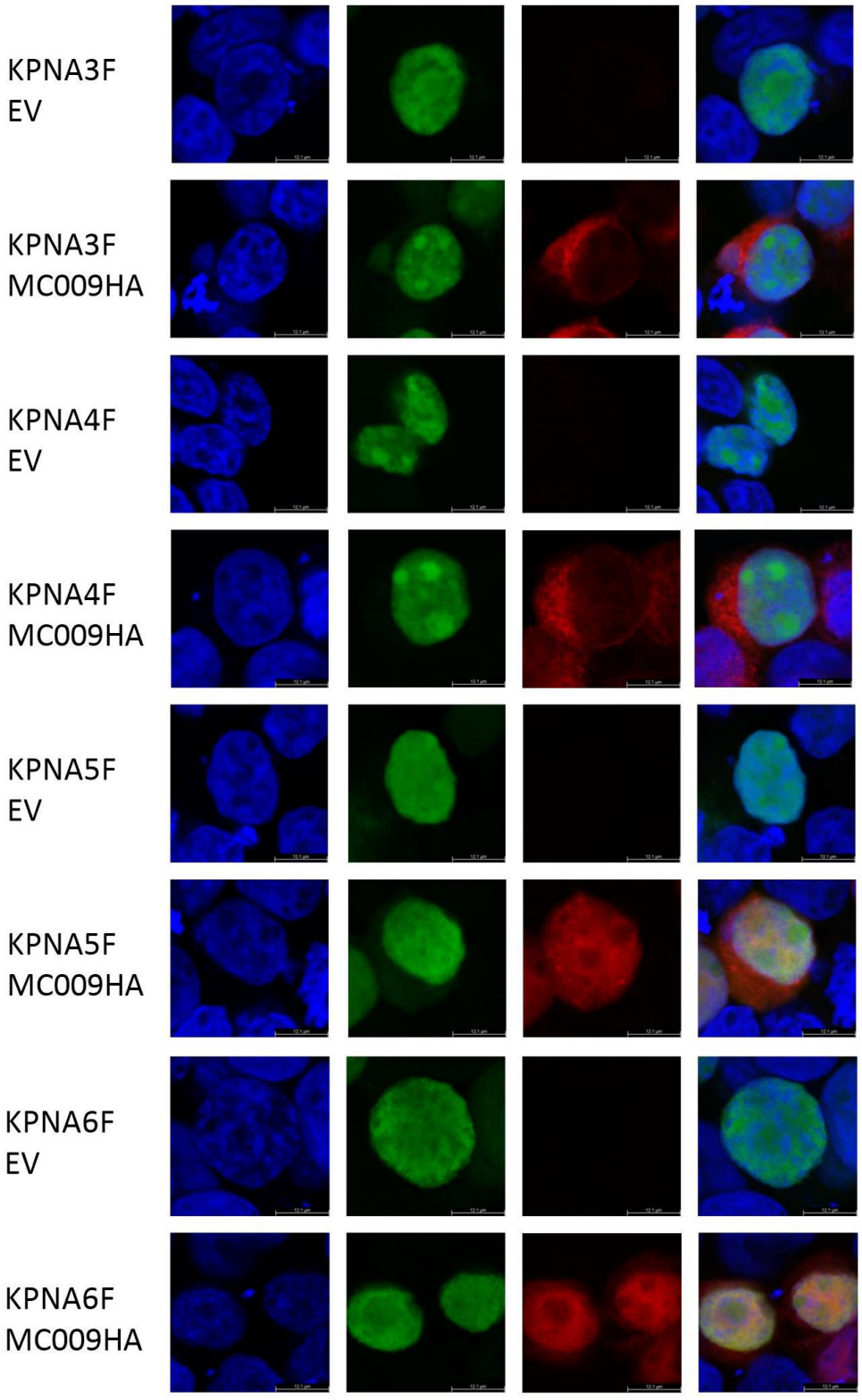

Figure 5.7. MC009 co-localises in HEK293T cell nucleus with overexpressed KPNA1, KPNA5 and KPNA6. HEK293T cells were seeded at 1.8x10^5 cells/mL in 8-well chamber slides. The wells were transfected with 1 µg FLAG-tagged karyopherins with/without MC009-HA. The

cells were stained for FLAG (488 nm) and HA (647 nm). ProLong™ Gold DAPI mounting solution was used for nuclear staining. The images were taken with a 40x objective on a Leica SP8 scanning confocal microscope and LAS X software. This figure is representative of n=3.

5.4 MC009 forms a complex with KPNA6 and p65.

Although MC009 did not interact with p65 directly, it was shown to bind with three karyopherin α proteins. Certain karyopherins have been shown to transport p65 or IRF3 into the nucleus (277,281,286,371–373). The interaction between KPNA6 and the two transcription factors, p65 and IRF3, was investigated using co-immunoprecipitation and confocal microscopy.

The potential interaction of endogenous p65 and IRF3 with overexpressed KPNA1-6 were investigated first. As seen in previous immunoprecipitation data, control lysate FLAG was not observed. Strong KPNA-FLAG expression was seen in immunoprecipitated lysates with low levels of p65 immunoprecipitation were visualised for all KPNA proteins (**Figure 5.8A**). However, no indication of KPNA-IRF3 interaction was observed (**Figure 5.8B**).

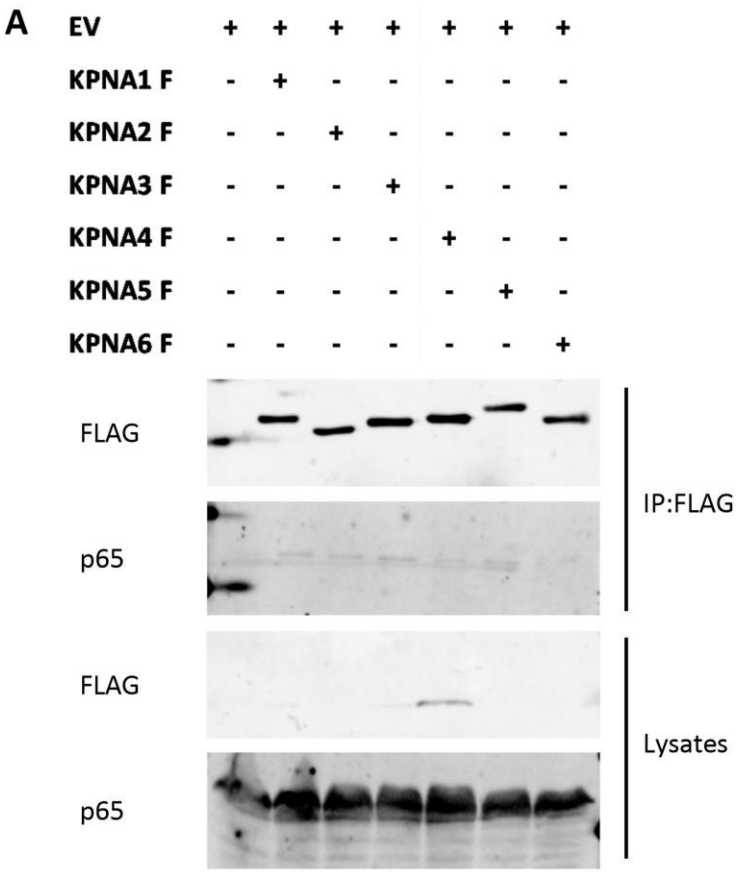
A
EV + + + + + + +
KPNA1 F - + - - - - -
KPNA2 F - - + - - - -
KPNA3 F - - - + - - -
KPNA4 F - - - - + - -
KPNA5 F - - - - - + -
KPNA6 F - - - - - - +
FLAG
p65
IP:FLAG
FLAG
p65
Lysates

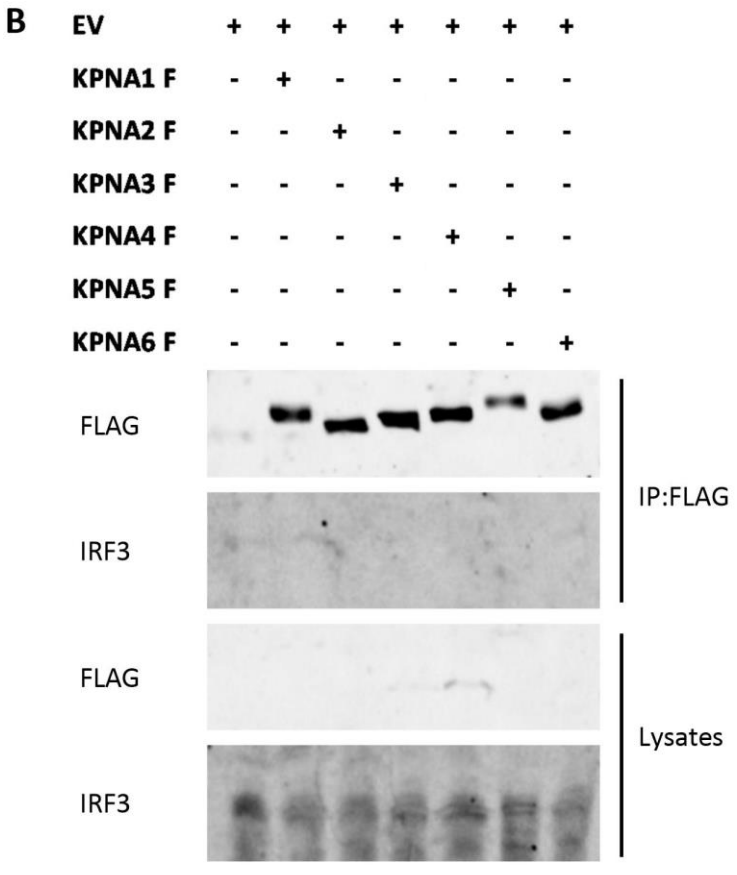
B
EV + + + + + + +
KPNA1 F - + - - - - -
KPNA2 F - - + - - - -
KPNA3 F - - - + - - -
KPNA4 F - - - - + - -
KPNA5 F - - - - - + -
KPNA6 F - - - - - - +
FLAG
IRF3
IP:FLAG
FLAG
IRF3
Lysates

Figure 5.8. Overexpressed KPNA proteins show weak interaction with unstimulated p65. **A-B.** HEK293T cells were seeded at $4x10^6$ cells/mL in 10 cm dishes. The wells were transfected with 4 µg KPNA6-FLAG and 4 µg EV. Cells were lysed with a CO-IP lysis buffer containing phosphatase and protease inhibitors. Immunoprecipitants and control lysates were immunoblotted for anti-FLAG and p65 or IRF3. Images were taken using the ChemiDoc Bio-Rad imaging system. Panel A is representative of n=3. Panel B is representative of n=1.

Stimulant-induced transcription factors were investigated next. Poly(dA:dT) was tested as a stimulant for IRF3 and KPNA6 interaction. The effect of MC009 on KPNA6 and IRF3 coupling was also examined. Unfortunately, no immunoprecipitation was observed between FLAG-tagged KPNA6 and Poly(dA:dT)-stimulated IRF3 (**Figure 5.9**).

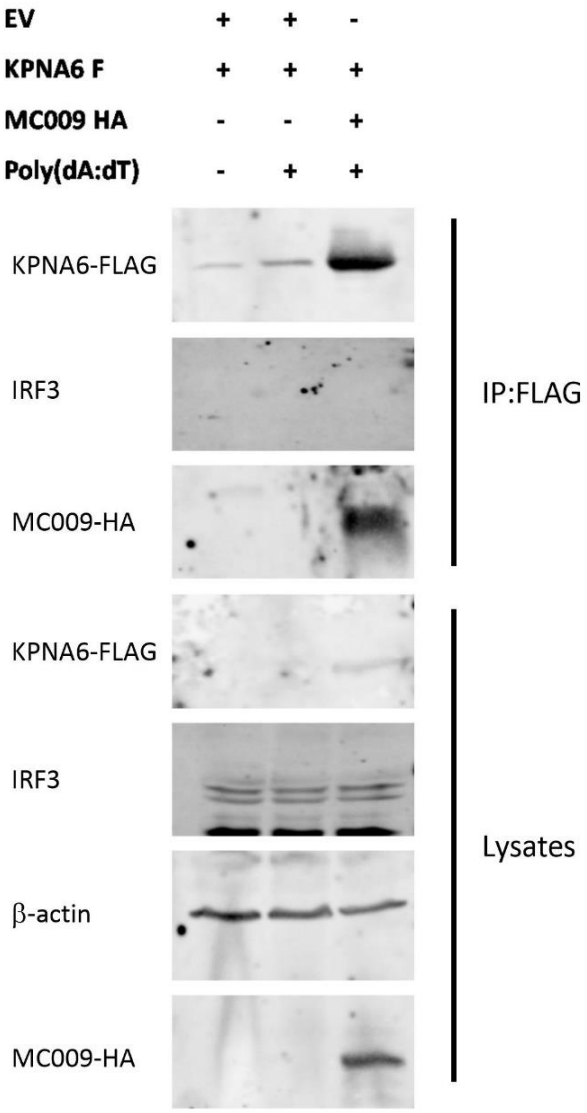

Figure 5.9. Poly(dA:dT) stimulation does not induce a KPNA6-IRF3 protein-protein interaction. HEK293T cells were seeded at $4x10^6$ cells/mL in 10 cm. The wells were transfected with 4 µg KPNA6-FLAG and MC009-HA or EV, 8 µg DNA final. Plates were stimulated with 1 µg Poly(dA:dT) for 24 hours. Cells were lysed with a CO-IP lysis buffer containing phosphatase and protease inhibitors. Immunoprecipitants and control lysates were immunoblotted. Images were taken using the ChemiDoc Bio-Rad imaging system. This figure is representative of n=1.

TNFα was used to stimulate HEK293T cell to investigate potential stimulus-dependant p65 and KPNA6 interaction. Although background p65 immunoprecipitation was observed, increased interaction between KPNA6 and p65 was seen after TNFα

stimulation (**Figure 5.10**). Interestingly, although MC009 immunoprecipitated in the same complex, it did not inhibit the association of KPNA6 with p65. Importin β 1 (KPNB1) shown to interact with KPNA6 (374), was also investigated to test KPNA6-p65-KPNB1-MC009 complex formation. Preliminary data suggested potential interaction between KPNB1 and KPNA6 without being disrupted by MC009 (**Figure 5.10**).

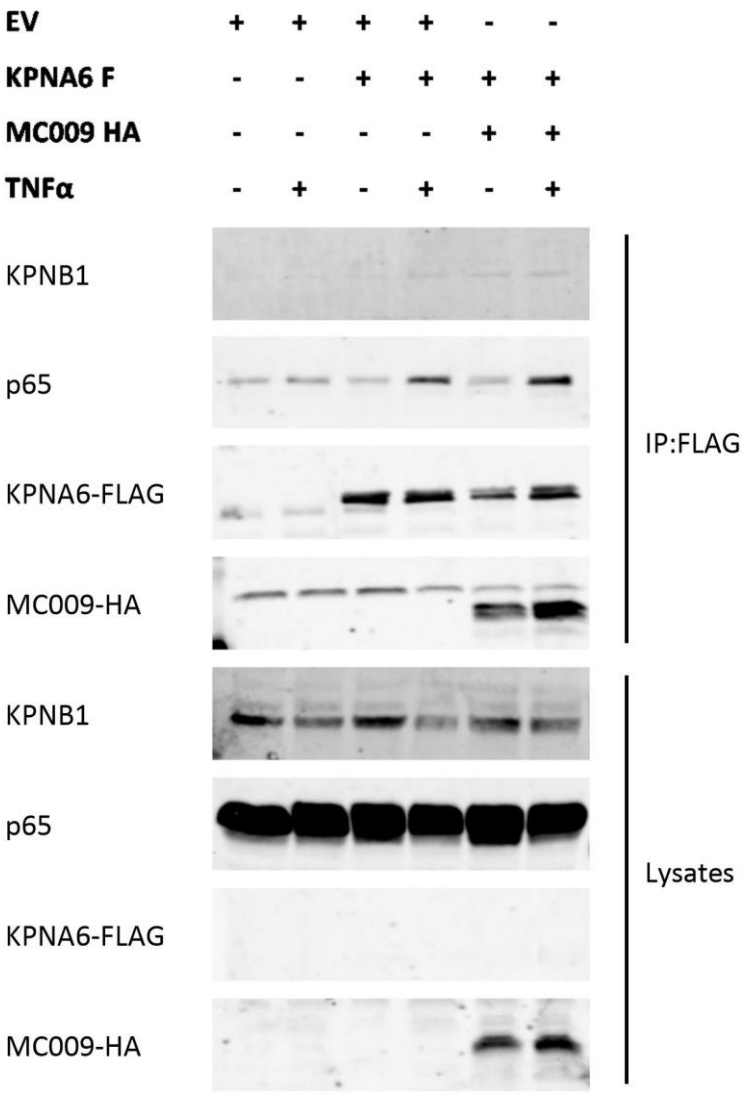

Figure 5.10. MC009 does not disrupt TNFα-induced KPNA6 and p65 interaction. HEK293T cells were seeded at $4x10^6$ cells/mL in 10 cm dishes. The wells were transfected with 4 µg KPNA6-FLAG and/or MC009-HA, 8 µg DNA final. P65 activity was stimulated with 50 ng/mL

TNFα for 20 min. Cells were lysed with a CO-IP lysis buffer containing phosphatase and protease inhibitors. Immunoprecipitants and control lysates were immunoblotted for anti-FLAG and KPNA6. Images were taken using the ChemiDoc Bio-Rad imaging system. This figure is representative of n=4 with the exception of KPNB1 which is representative of n=2.

As a TNFα-induced interaction was observed between KPNA6 and p65, the same stimulant was used to examine protein co-localisation. A 30-minute TNFα stimulation was conducted based on p65 nuclear translocation data (**Figure 4.5**). Both proteins were exclusively present in the cytoplasm in unstimulated HEK293T cells. The level of endogenous KPNA6 present in the nucleus post 30-minute TNFα -stimulation was not equivalent to that of p65 with the proteins still mainly co-localising in the cytoplasm of the cell (**Figure 5.11**).

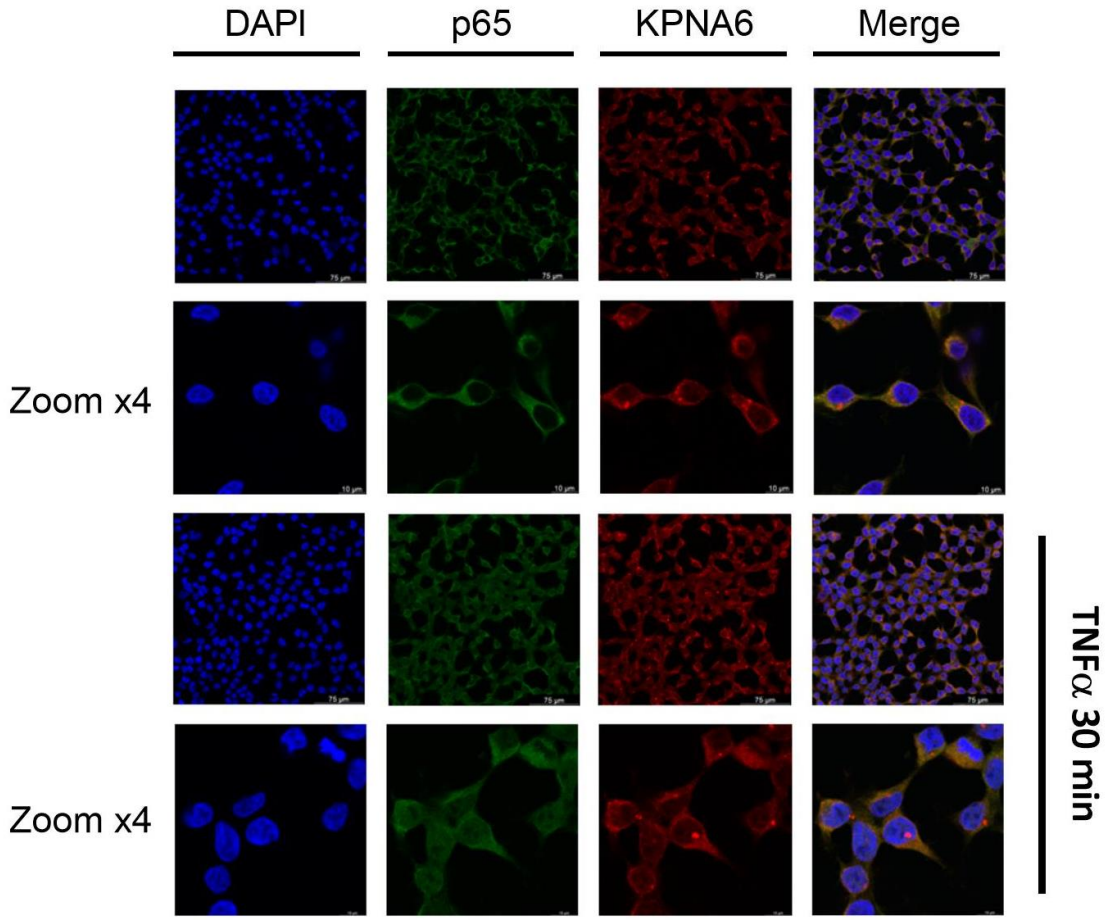

Figure 5.11. KPNA6 co-localises with p65 in HEK293T cell cytoplasm. HEK293T cells were seeded at $1.8x10^5$ cells/mL in 8-well chamber slides. Slides were stained for endogenous KPNA6 (647 nm) and p65 (488 nm). ProLong™ Gold DAPI mounting solution was used for nuclear staining. The images were taken with a 40x objective on a Leica SP8 scanning confocal microscope and LAS X software. This figure is representative of n=2.

The effect of MC009 on KPNA6-p65 was also examined using confocal microscopy. Two approaches were used for the examination. Firstly, the Leica SP8 scanning microscope (utilised throughout the project) was used. KPNA6 and p65 were both localised in the cytoplasm of TNFα-stimulated HEK293T cells transfected with MC009-FLAG (**Figure 5.12A**). A maximum of three lasers could be used at once on this microscope, thus, the expression of FLAG-tagged proteins could not be visualised. The protocol was therefore altered to stain the cells for p65, KPNA6, FLAG and DAPI. Additionally, a different confocal microscope was used allowing four lasers to be active simultaneously. Unfortunately, the addition of a fourth channel at 568 nm led to interference with the previously optimised 488 nm channel (**Figure 5.12B**). Furthermore, nuclear translocation of KPNA6 appeared to be independent of the 30-minute TNFα stimulation as the karyopherin was observed in the nucleus in unstimulated non-transfected cells (**Figure 5.12A and B**).

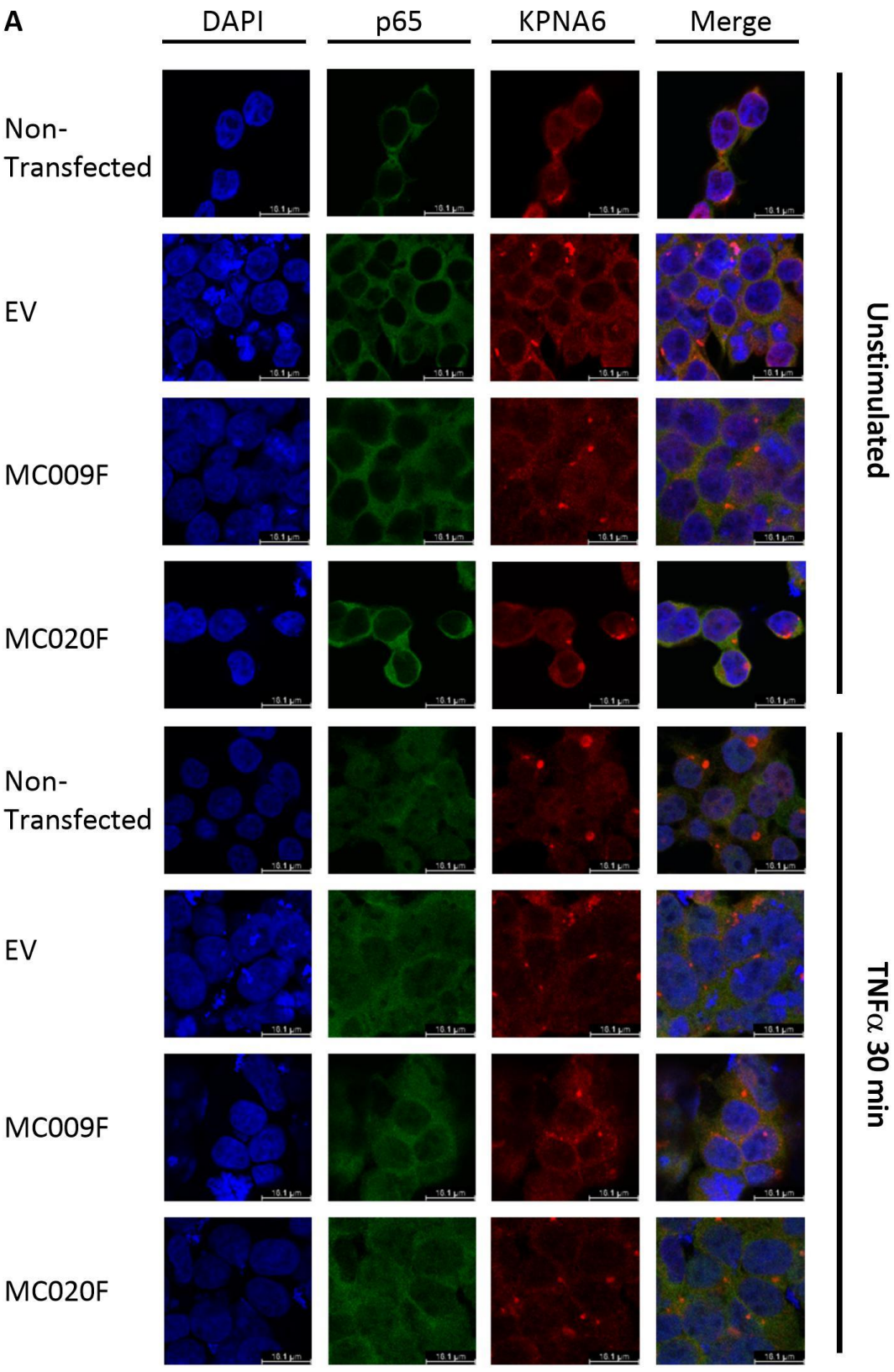
A
DAPI
p65
KPNA6
Merge
Non-Transfected
EV
MC009F
MC020F
Non-Transfected
EV
MC009F
MC020F
Unstimulated
TNFα 30 min

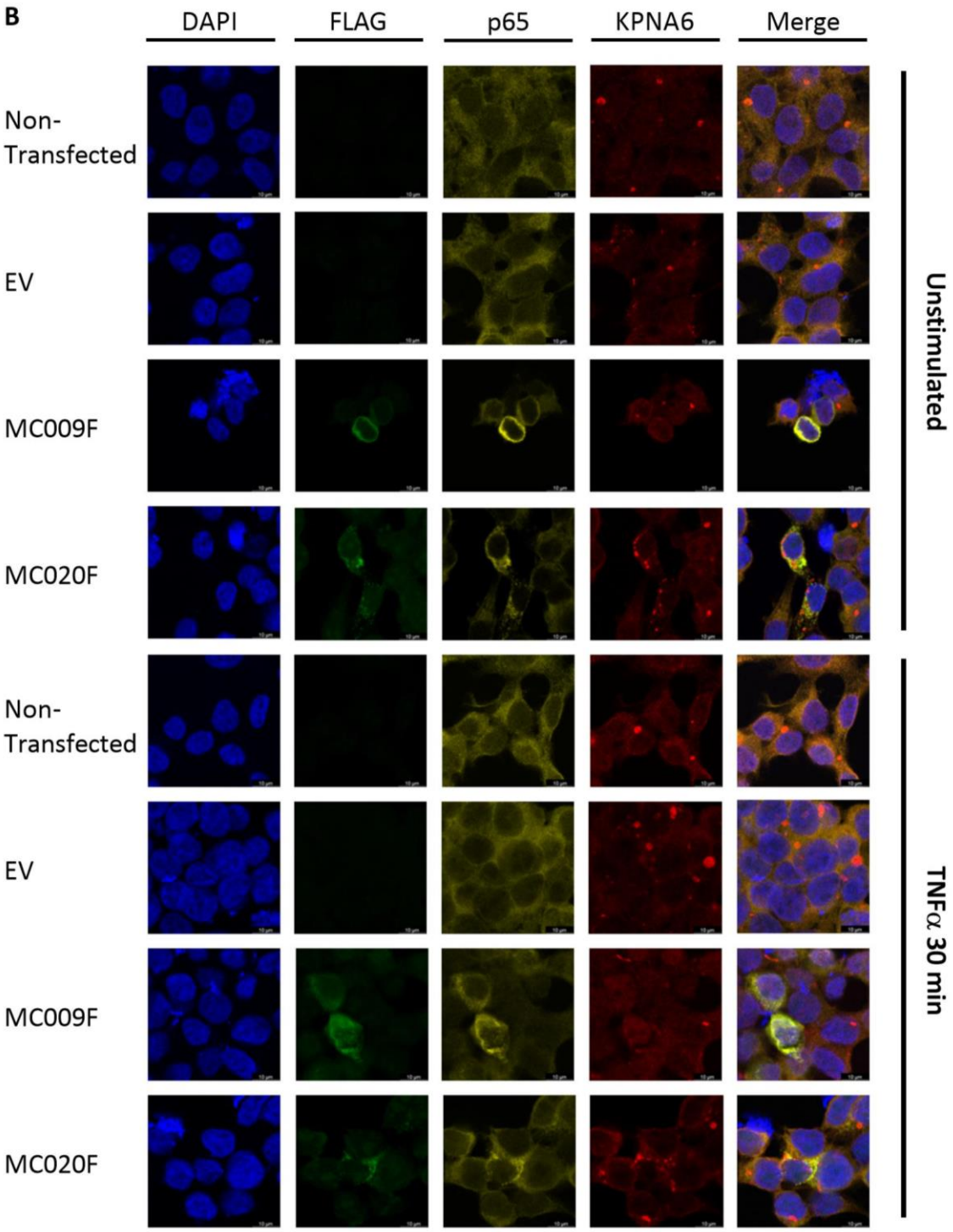

Figure 5.12. KPNA6 and p65 co-localise in the cytoplasm in MC009 expressing cells. A-B. HEK293T cells were seeded at $1.8x10^5$ cells/mL in 8-well chamber slides. The wells were transfected with 1 µg MC009-FLAG, MC020-FLAG or EV. **A.** Slides were stained for KPNA6 (647 nm) and p65 (488 nm). Transfected plasmids were not stained for. ProLong™ Gold DAPI

mounting solution was used for nuclear staining. The images were taken with a 40x objective on a Leica SP8 scanning confocal microscope and LAS X software. This figure is representative of n=1. **B.** Slides were stained for FLAG (488 nm), p65 (568 nm) and KPNA6 (647 nm). ProLong™ Gold DAPI mounting solution was used for nuclear staining. The images were taken with a 40x objective on a Leica SP8 Gated 'STED' confocal microscope with 5 lasers and LAS X software. This figure is representative of n=1.

5.5 KPNA6 siRNA knockdown optimisation.

Co-immunoprecipitation and confocal imaging provided evidence of MC009-KPNA6-p65 complex formation. Next, small interfering RNA (siRNA) were sought out to further investigate the involvement of KPNA6 in MCV immune system evasion. RNA interference is a common technique used to examine the effects of protein knockdowns in cell responses. Two KPNA6 siRNA peptides were tested along with a standard pre-designed siRNA negative control which were all inspected at three concentrations. Optimisation was initiated by determining the appropriate transfection duration, 24 hours versus 48 hours, and required siRNA concentration for KPNA6 knockdown (**Figure 5.13A**). Initial results showed no KPNA6 expression in HEK293T cells transfected with negative control siRNA and s41 siRNA. KPNA6 was also not present in non-transfected lysates. Changes in karyopherin levels were noted for s42 siRNA peptide with reduced expression with the highest peptide concentration and 48 hour incubation.

A

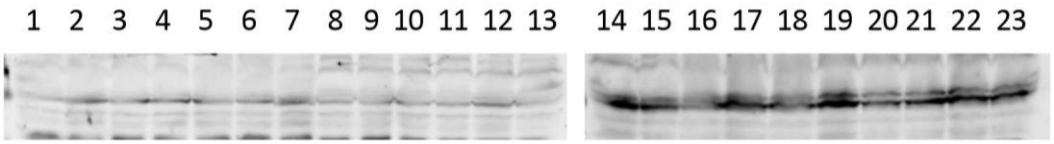

1. Non-transfected HEK293T cells
2. 2.5 pmol Negative control 48H
3. 5 pmol Negative control 48H
4. 10 pmol Negative control 48H
5. 2.5 pmol Negative control 24H
6. 5 pmol Negative control 24H
7. 10 pmol Negative control 24H
8. 2.5 pmol s41 KPNA6 48H
9. 5 pmol s41 KPNA6 48H
10. 10 pmol s41 KPNA6 48H
11. 2.5 pmol s41 KPNA6 24H
12. 5 pmol s41 KPNA6 24H
13. 10 pmol s41 KPNA6 24H
14. 2.5 pmol s42 KPNA6 48H
15. 5 pmol s42 KPNA6 48H
16. 10 pmol s42 KPNA6 48H
17. 2.5 pmol s42 KPNA6 24H
18. 5 pmol s42 KPNA6 24H
19. 10 pmol s42 KPNA6 24H
20. 2.5 pmol s41+s42 KPNA6 48H
21. 2.5 pmol s41+s42 KPNA6 24H
22. 5 pmol s41+s42 KPNA6 48H
23. 5 pmol s41+s42 KPNA6 24H

B

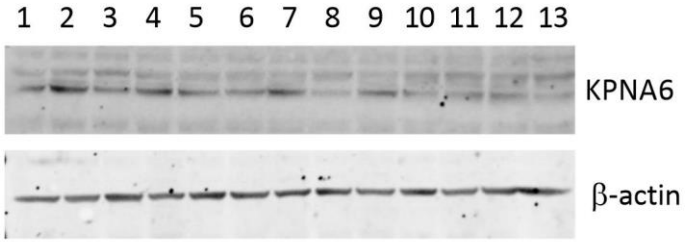

1. Non-transfected HEK293T cells
2. 5 pmol Negative control 48H
3. 10 pmol Negative control 48H
4. 40 pmol Negative control 48H
5. 5 pmol s41 KPNA6 48H
6. 10 pmol s41 KPNA6 48H
7. 40 pmol s41 KPNA6 48H
8. 5 pmol s42 KPNA6 48H
9. 10 pmol s42 KPNA6 48H
10. 40 pmol s42 KPNA6 48H
11. 5 pmol s41+s42 KPNA6 48H
12. 10 pmol s41+s42 KPNA6 48H
13. 40 pmol s41+s42 KPNA6 48H

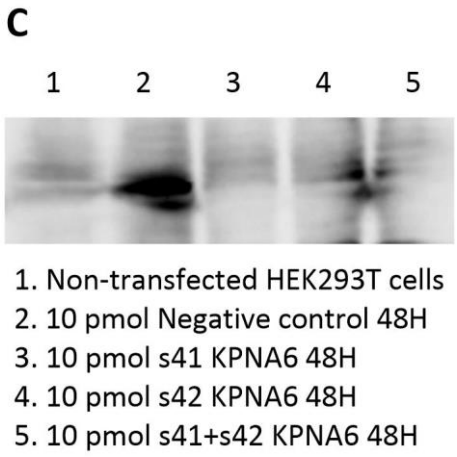

Figure 5.13. KPNA6 siRNA protocol optimisation. A. HEK293T cells were seeded at $1x10^5$ cells/mL in 24-well plates with DMEM media with 10% FBS and 1% Penicillin-Streptomycin. The wells were transfected with 2.5, 5 or 10 pmol siRNA peptide using Lipofectamine 2000 as a transfection reagent. Plates were incubated for 24 and 48 hours at 37°C and 5% CO_2. **A.** HEK293T cells were seeded at $1x10^5$ cells/mL in 24-well plates with DMEM media with 10% FBS and 1% Penicillin-Streptomycin. The wells were transfected with 5, 10 or 40 pmol siRNA peptide using Lipofectamine 2000 as a transfection reagent. Plates were incubated for 48 hours at 37°C and 5% CO_2. **C.** HEK293T cells were seeded at $1x10^5$ cells/mL in 24-well plates with DMEM media with 10% FBS. The wells were transfected with 10 pmol siRNA peptide using Lipofectamine 2000 as a transfection reagent and incubated for 48 hours at 37°C and 5% CO_2. **A-C.** Cells were lysed with a western blot sample buffer. Images were taken using the ChemiDoc Bio-Rad imaging system. All panels are representative of n=1.

The optimisation protocol was altered based on the previously obtained results. Transfection duration remained constant at 48 hours; however, the peptide concentration range was increased. KPNA6 knockdown was observed with both s41 and s42 at multiple concentrations (**Figure 5.13**). General expression levels of KPNA6 remained low. Use of antibiotics in cell culture media during siRNA transfections can lead to higher cell toxicity rates (375). Lastly, the protocol was repeated in cells cultured using only DMEM

with 10% FBS without Penicillin-Streptomycin. Strong KPNA6 expression was observed in cells treated with the negative control in contrast to little or no KPNA6 expression in s41, s42 and s41+s42 treated lysates (**Figure 5.13C**). Unfortunately, due to the time limitations, planned luciferase assays and confocal microscopy experiments using siRNA were not conducted.

5.6 Discussion

Data received from the AP-MS collaboration between the host lab and Dr. Andreas Pichlmair, provided a foundation for the next stage of the project (**Figure 5.1**). Firstly, a list of all potential MC009 interacting proteins was created and each individual protein was researched. Additionally, all proteins were searched for within a database of common AP-MS contaminants; Contaminant Repository for Affinity Purification (CRAPome). From the extensive list of probable MC009 targets, many appeared to be trivial, for example heat shock protein family α member 5 (HSPA5), HSP90B1 or protein disulfide isomerase family α member 6 (PDIA6). Nevertheless, potentially interesting hits were also obtained with possible links to our hypotheses, such as IPO5, KPNA6 and ubiquitin protein ligase E3 component n-recognin 5 (UBR5). Both IPO5 and KPNA6 are part of the importin family responsible for the transport of cargo from the cytoplasm to the nucleus (277). IPO5 is one of many subunit β members of the importin family and has been shown to play a role in porcine circovirus immune evasion (282,376). KPNA6, however, is one of seven known human importin α proteins. Recently, this karyopherin has been shown to be implicated in both Influenza virus and SARS-CoV-2 immune evasion strategies (286,287). KPNA6 is a known transporter of IRF3 (286). UBR5 is a E3 ubiquitin ligase involved in RIG-I-mediated anti-viral responses (377). The nuclear ligase was an interesting AP-MS hit as MCV has been previously shown to inhibit E3

ligases in order to stop NF-κB signalling (299). Furthermore, UBR5 has been shown to interact with KPNA1 a close homolog of KPNA6 marked as a likely target of MC009 (378). The totality of our data suggested that MC009 works at the transcription factor level of both NF-κB and IRF signalling and prevented p65 nuclear translocation. Therefore, the three aforementioned proteins were likely to be implicated in MCV-MC009 human immune system evasion. Multiple attempts were made at trialling a sample UBR5 antibody, however, endogenous UBR5 was not seen in control HEK293T lysates tested (data not shown). Ubiquitin protein ligases are common targets of viral inhibitors. UBR5 has been shown to interact with karyopherins, therefore, the AP-MS immunoprecipitation of UBR5 with MC009 could have been influenced by the UBR5-KPNA interaction. Thus, UBR5-MC009 was not further investigated.

Upon investigating IPO5, co-immunoprecipitation of MC009 was not detected (**Figure 5.2**). In contrast, a strong interaction was noted between endogenous and overexpressed KPNA6 with MC009 (**Figure 5.3 and Figure 5.4**). Unexpectedly, an interaction was also observed with close homologs of KPNA6, KPNA1 and KPNA5, which share 82.1% and 84.5% of the same sequence, respectively (272). The protein-protein interaction was not dependent on cell signal stimulation by TNFα or Poly(dA:dT). MC009 could therefore bind to the transporters prior to viral detection completely inhibiting gene regulation once MCV is exposed.

KPNA1, KPNA5, KPNA6 are all members of the α3 subfamily. The most recently discovered human KPNA protein (KPNA7) was not available to test for an MC009 interaction. KPNA7 has been shown to be the most distinct karyopherin α member from KPNA6 with only 42.5% shared sequence identity and is not classified to be part of the

same subfamily. Furthermore, KPNA7 and KPNA2 share subfamily α1 with 54.7% sequence homology. Based on this information, I did not seek out KPNA7 for MC009 investigation. The biggest variation between the amino acid identity of these proteins was shown to be in the N-terminal importin β binding (IBB) region, the ARM4 repeat and the C-terminal (**Figure 5.5**). Thus, the similarities of the α1 subfamily members and their differences from the other KPNA proteins could aid in deciphering the KPNA1/5/6-MC009 binding region. This could be further investigated with protein truncations similarly to MC009 peptide truncations. Protein-protein interaction could be tested with co-immunoprecipitation blots. The technique could prove difficult as very small proteins do not easily separate on SDS-PAGE gels. Nuclear translocation experiments using confocal microscopy could potentially visualise if the altered KPNA proteins behave in a similar manner to the parent protein.

Co-localisation of MC009 with endogenous KPNA6 was investigated in unstimulated cells first. Two main observations were made. Initially, MC009 and KPNA6 were seen to co-localise in the cytoplasm (**Figure 5.6**). Secondly, a handful of cells presented with nuclear KPNA6. Where karyopherin nuclear translocation was observed, MC009 tightly surrounded the nucleus unlike the normal even dispersion throughout the cytoplasm previously seen in localisation experiments. The full function of KPNA6 is not yet completely understood. KPNA proteins can hold a variety of roles outside of anti-viral signalling, as such the nuclear translocation in unstimulated cells could have been unrelated to innate signalling.

Interestingly, overexpressed KPNAs were not observed in the cytoplasm of HEK293T cells. Furthermore, MC009 was able to move across the nuclear membrane alongside

KPNA1, KPNA5 and KPNA6 (**Figure 5.7**). As mentioned before, nuclear translocation of MC009 was not observed previously during endogenous KPNA6 co-localisation experiments. As overexpression of proteins is a more artificial system than endogenous protein investigation, it is likely that the nuclear translocation of MC009 was forced by the abundancy of the overexpressed karyopherins. The translocation of MC009 also did not correlate with the previous data obtained from p65 nuclear translocation experiments where p65 and MC009 remained within the cytoplasm. Thus, the confocal images of overexpressed proteins support the immunoprecipitation data however, more work would be required to fully understand the movement of MC009. These changes could be investigated further with the addition of overexpressed p65 to observe if nuclear translocation of the artificial protein occurs.

KPNA6 has been shown to co-immunoprecipitate with overexpressed IRF3 (286). The interaction between KPNA6 and IRF3 was investigated examining the effect of MC009 on complex formation. However, immunoprecipitation was not observed between endogenous KPNA6 and Poly(dA:dT)-induced IRF3 in cell lysates with or without MC009 (**Figure 5.9**). Poly(dA:dT) was used as an IRF3-stimulant which does not convey an acute signalling response. As mentioned previously, the long incubation period and slow signal output proved to be difficult when working with karyopherin proteins.

KPNA6-p65 coupling was investigated after 10, 20 and 30 minutes of TNFα cell stimulation (data not shown). A link between the proteins was seen in as little as 10 minutes post signal induction. A stronger relationship was evident at the two longer timepoints (data not shown). As similar expression levels were observed at 20 and 30 minutes, the 20-minute timepoint was chosen for further immunoprecipitation

investigation. The interaction between KPNA6 and p65 was not disrupted by MC009. In contrast, p65 immunoprecipitation levels were moderately higher when present in the KPNA6-p65-MC009 complex (**Figure 5.10**). Complex formation supports previous p65 nuclear translocation data causing the three proteins to remain sequestered within the cytoplasm inhibiting gene regulation.

Co-localisation of endogenous KPNA6 and p65 was investigated next. The interaction was observed in unstimulated cells as well as TNFα-induced HEK293T cells. KPNA6 and p65 co-localised in the cytoplasm in both cases (**Figure 5.11**). A 30-minute TNFα stimulation was chosen for this experiment as clear p65 translocation was observed with this timepoint in previous data (**Figure 4.5**). However, as previously mentioned, co-immunoprecipitation results showed an interaction between the proteins after 10- and 20-minute stimulations. KPNA6-p65 binding could occur during the first 30 minutes of cell stimulation, however, the nuclear translocation potentially took place past this time-frame. As a result, KPNA6 was not present in the nucleus at the examined 30-minute TNFα timepoint.

Changes to KPNA6 and p65 co-localisation were also inspected in the presence of MC009. Firstly, this was attempted using the previously optimised confocal microscopy protocol using three lasers: 405 nm, 488 nm, and 647 nm. The effect of the inhibitor on KPNA6 and p65 was the focal point of this experiment, therefore, the cells were stained for p65 (488 nm) and KPNA6 (647 nm) (**Figure 5.12A**). Nuclear translocation of either protein was not observed in cells with MC009, however, MC009 expression could not be visually verified as only three lasers were available on the machine. The experiment was repeated, and cells were stained with four fluorophores. The staining procedure was more

complex as all antibodies had to be derived from various host animals and the fluorophore wavelengths could not strongly overlap. To allow for four lasers (405 nm, 488 nm, 568 nm, 647 nm) to scan the sample slide simultaneously a different confocal microscope was required. It is important to note that results obtained using the three-laser vs four-laser microscope were not directly comparable. Unlike previous TNFα stimulations, p65 did not translocate to the nucleus even in non-MC009 containing control cells (**Figure 5.12B**). Furthermore, channel interference was evident between the 488 nm and 568 nm channels which could have been a result of wavelength overlap or antibody hosts being closely related. The combination of channel feed-through and lack of p65 nuclear translocation ultimately rendered the results inconclusive. More optimisation experiments, such as antibody dilutions and microscope laser set-up, were necessary which was not possible due to time restraints.

Utilisation of siRNA has been proven to be an effective and advantageous tool in examining protein involvement in cell signalling. Peptide design and protocol optimisation require precision and practice. Pre-designed siRNA sequences were chosen for KPNA6 testing with '70% knockdown guarantee' by ThermoFisher. Pre-designed peptides were selected over manual peptide design as a commonly used KPNA6 siRNA or knockout sequence was not found in literature (273,287,379). Silencer Select® siRNA was picked over other ThermoFisher siRNA lines such as Stealth® siRNA as it was a more recently designed product line with higher potency rates, 5-100 fold, based on the information provided by the company (380). The optimisation experiments showed antibiotic culture media supplementation to significantly interfere with siRNA (**Figure 5.13**). Unfortunately, due to time sensitivity of the project siRNA luciferase assays, co-immunoprecipitations and confocal microscopy could not be conducted. It is unclear if

KPNA6 knockdown experiments would yield conclusive results as MC009 was shown to target other karyopherins, KPNA1 and KPNA5. Due to the lack of functional exclusivity, the effect of KPNA6 siRNA could have been bypassed through the use of KPNA1 or KPNA5. Each relevant KPNA would require siRNA testing to determine the order of importance during MC009 inhibition. Furthermore, experiments examining KPNA1, KPNA5 and KPNA6 knockdown in combination with each other would be necessary for comprehensive siRNA data.

5.7 Conclusion

The inhibitor interacts with members of the karyopherin subfamily α3: KPNA1, KPNA5 and KPNA6. I propose that MC009 blocks TNFα-induced p65 nuclear translocation through p65-KPNA6-MC009 complex formation. MC009 is the only MCV-derived immunomodulator currently known to impact the importin family. Furthermore, it is the second poxviral protein described to interact with karyopherin proteins. MC009 could provide insight into the utilisation of karyopherin proteins as part of poxviral immune evasion strategies.

Chapter 6: Discussion

Molluscum contagiosum infections occur around the world with limited treatment options available. MCV is estimated to constitute for 1% of all skin disorders (22). The virus is not yet fully understood in comparison to its poxviral relatives such as VAR or VACV. A lack of potential animal models significantly hinders MCV research as it is a human adapted pathogen. Nevertheless, cultured cell lines can help in understanding the virus one protein at a time. During this project I found MCV protein MC009 to be a novel inhibitor of human innate immune signalling. Results obtained not only expanded our knowledge about MCV but also broadened our understanding of innate immune signalling.

Five out of the eleven currently described MCV immunomodulators impede the IKK complex or the IKK related kinases where TLR, RLR and cGAS-STING pathways converge (60,292,293,306,309). With such a high proportion of the immunomodulators obstructing signal transduction upstream of the transcription factors, MC009 acts as a safety blanket. MC009 works at the final stage of signalling before nuclear transport and gene regulation. The inhibitor specifically targets the nuclear translocation of TNFα-induced p65. MC009 potentially works as a final barrier in instances where signal transduction was uninterrupted. Furthermore, MC009 is one of three known MCV-derived proteins capable of inhibiting PRR- and cytokine-induced NF-κB and IRF3 signalling. Poxviruses encode for large numbers of immunomodulators showing their ability to quickly adapt to their environment and surpass the host immune defences. They are also some of the oldest human infecting viruses described with evidence of smallpox-like rashes dating back to 900-1000 BCE (before common era) potentially accumulating new immunomodulators over long periods of time (381). The use of multi-faceted

immunomodulators, like MC009, shows the 'intelligence' of MCV and highlights the inherent drive for survival of the virus.

The order of MCV immunomodulator evolution remains unclear, however, MC009 can be hypothesised to have been developed at a later stage of viral evolution. MC009 has one characterised homolog found in EMCVL, a close relative of MCV and the only other member of the *Molluscipoxvirus* genera (44). This project revealed MC009 as the first MCV protein to interact with karyopherins KPNA6, along with weaker interactions with KPNA1 and KPNA5. Surprisingly, it is only the second known poxviral protein which specifically targets nuclear transporters (283). Low occurrence rate of KPNA-interacting proteins could indicate the necessary development of these proteins as a bypass system when other evasion strategies were ineffective. Recent studies have shown other viruses such as SARS-CoV-2 and influenza virus to also target KPNA6 (286,287). Tissue type and molecular events influence the demand for particular KPNA family members (364). Viral protein interactions with KPNA6 could signify the importance of KPNA6 in anti-viral responses. Additionally, MC009 could be utilised as a KPNA6 inhibitor in studies focusing on the karyopherin's role in viral infections.

Lastly, MC009 significantly impacted pro-inflammatory and type I IFN responses examined during this project. MC009 would not be a good treatment target for MCV infection therapies due to the range of immunomodulators encoded by MCV. However, it could be utilised as a treatment to target dysregulated responses occurring in autoimmune diseases. Studies focusing on systemic lupus erythematosus (SLE), dermatomyositis and rheumatoid arthritis present with an imbalanced type I IFN response (382). I show MC009 to significantly reduce IFNα/β production which can be

upregulated in autoimmune disorders. Furthermore, pro-inflammatory chemokines such as IL-8 and IP-10 have been associated with inflammatory bowel disease (IBD; Crohn's disease and ulcerative colitis) and experimental autoimmune encephalomyelitis (EAE; disease model for multiple sclerosis [MS]), respectively (383). The production of both chemokines was reduced in cells expressing MC009. Cell penetrating peptides (CPPs) containing the 11 amino acid-long functional region of MC009 could be utilised to develop topical treatments for autoimmune disorders such as psoriasis where type I IFN responses and IL-8 production are dysregulated (384,385).

This thesis established a strong foundation for further MC009 research progression. Future work should focus on establishing the mechanism of function during MC009-induced IRF3 inhibition. Similarly to other MCV inhibitors, MC009 functionality should be investigated in additional cell lines such as HaCaT or HeLa cells (292,293). Animal virulence impact of MC009 can be examined using vaccinia virus vector in mouse models (60). Future research could determine if MC009 functions independently or in combination with other MCV signal inhibitors as it is currently unknown if MCV-encoded immunomodulators are expressed equally at the early stage of viral replication.

In conclusion, MCV is a master of immune system evasion. Eleven MCV immunomodulators have been identified, multiple of which target similar points of innate signalling or the cell cycle. MC009 is a novel inhibitor of PRR- and cytokine-mediated NF-κB and IRF signalling. The MCV-derived inhibitor emphasises the importance of KPNA research and could be utilised as tool to further examine the role of KPNA6 in anti-viral immunity. MC009 provides novel insights necessary for the development of new therapeutic agents for autoimmune diseases and inflammatory disorders. This thesis

demonstrates that MCV is a strong model of human immune system regulation while also broadening our understanding of MCV immune evasion strategies.

References

1. Moss B. Poxvirus DNA Replication. Cold Spring Harb Perspect Biol [Internet]. 2013 Sep;5(9). Available from: /pmc/articles/PMC3753712/

2. Shisler JL. Chapter Four: Immune Evasion Strategies of Molluscum Contagiosum Virus. Vol. 92, Advances in Virus Research. Academic Press; 2015. 201–252 p.

3. Srinivasan Rajsri K, Rao M. Poxvirus-driven human diseases and emerging therapeutics. Ther Adv Infect Dis [Internet]. 2022;9. Available from: /pmc/articles/PMC9666863/

4. MacLachlan NJ, Dubovi EJ, editors. Fenner's Veterinary Virology [Internet]. Fifth Edit. American Press. Academic Press; 2017. 157–174 p. Available from: https://linkinghub.elsevier.com/retrieve/pii/B9780128009468000076

5. Institute of Medicine (US) Board on Health Promotion and Disease Prevention. Scientific and policy considerations in developing smallpox vaccination options [Internet]. National Academies Press (US); 2002. Available from: https://www.ncbi.nlm.nih.gov/books/NBK221063/

6. Kondas A V., Olson VA. Poxviruses. Clin Virol Manual, Fifth Ed [Internet]. 2023 May 29 [cited 2024 Mar 29];457–71. Available from: https://www.ncbi.nlm.nih.gov/books/NBK558959/

7. Smith GL, McFadden G. Smallpox: anything to declare? Nat Rev Immunol [Internet]. 2002;2(7):521–7. Available from: https://pubmed.ncbi.nlm.nih.gov/12094226/

8. Janoff EN, Lynfield R. Smallpox: Remembrance of things past, or the coming plague? J Lab Clin Med [Internet]. 2003;142(4):211–5. Available from: https://pubmed.ncbi.nlm.nih.gov/14625525/

9. Bray M, Buller M. Looking back at smallpox. Clin Infect Dis [Internet]. 2004 Mar 15;38(6):882–9. Available from: https://dx.doi.org/10.1086/381976

10. Centres for Disease Control and Prevention (CDC) [Internet]. Smallpox. Available from: https://www.cdc.gov/smallpox/index.html

11. Riedel S. Edward Jenner and the history of smallpox and vaccination. Proc (Bayl Univ Med Cent) [Internet]. 2005 Jan 1;18(1):21. Available from:

/pmc/articles/PMC1200696/

12. World Health Organisation (WHO) [Internet]. Smallpox. Available from: https://www.who.int/health-topics/smallpox#tab=tab_1

13. Verardi PH, Titong A, Hagen CJ. A vaccinia virus renaissance: New vaccine and immunotherapeutic uses after smallpox eradication. Hum Vaccin Immunother [Internet]. 2012 Jul 7;8(7):961. Available from: /pmc/articles/PMC3495727/

14. Moss B. Vaccinia Virus: A Tool for Research and Vaccine Development. Science (80-) [Internet]. 1991;252(5013):1662–7. Available from: https://www.science.org/doi/10.1126/science.2047875

15. Centers for Disease Control and Prevention C. Molluscum Contagiosum [Internet]. Available from: https://www.cdc.gov/poxvirus/molluscum-contagiosum/index.html

16. Badri T, Gandhi GR. Molluscum Contagiosum - NCBI Bookshelf [Internet]. 2023. Available from: https://www.ncbi.nlm.nih.gov/books/NBK441898/

17. Clebak KT, Malone MA. Skin Infections. Prim Care [Internet]. 2018 Sep 1;45(3):433–54. Available from: https://pubmed.ncbi.nlm.nih.gov/30115333/

18. Nyati A, Gupta S, Jain SK, Yadav D, Patidar BL, Sharma M. A retrospective study of the pattern of sexually transmitted infections from a tertiary care hospital of Rajasthan. Indian J Sex Transm Dis AIDS [Internet]. 2017 Jul 1;38(2):147–51. Available from: https://pubmed.ncbi.nlm.nih.gov/30148268/

19. Vora RV, Pilani AP, Kota RK. Extensive Giant Molluscum Contagiosum in a HIV Positive Patient. J Clin Diagn Res [Internet]. 2015 Nov 1;9(11):WD01. Available from: /pmc/articles/PMC4668510/

20. Katzman M, Carey JT, Elmets CA, Jacobs GH, Lederman MM. Molluscum contagiosum and the acquired immunodeficiency syndrome: clinical and immunological details of two cases. Br J Dermatol [Internet]. 1987;116(1):131. Available from: /pmc/articles/PMC7161859/

21. Vozmediano JM, Manrique A, Petraglia S, Romero MA, Nieto I. Giant molluscum contagiosum in AIDS. Int J Dermatol [Internet]. 1996;35(1):45–7. Available from: https://pubmed.ncbi.nlm.nih.gov/8838930/

22. Hebert AA, Bhatia N, Del Rosso JQ. Molluscum Contagiosum: Epidemiology, Considerations, Treatment Options, and Therapeutic Gaps. J Clin Aesthet Dermatol [Internet]. 2023 Aug 1;16(8 Suppl 1):S4. Available from: /pmc/articles/PMC10453394/

23. Molluscum Contagiosum - Dermatology - Medbullets Step 2/3 [Internet]. Available from: https://step2.medbullets.com/dermatology/120053/molluscum-contagiosum

24. A Collection of Surgical Pathology Images: Molluscum contagiosum [Internet]. Available from: https://www.webpathology.com/image.asp?case=1099&n=54

25. Thompson CH, De Zwart-Steffe RT, Donovan B. Clinical and molecular aspects of molluscum contagiosum infection in HIV-1 positive patients. Int J STD AIDS [Internet]. 1992;3(2):101–6. Available from: https://pubmed.ncbi.nlm.nih.gov/1571379/

26. Dohil MA, Lin P, Lee J, Lucky AW, Paller AS, Eichenfield LF. The epidemiology of molluscum contagiosum in children. J Am Acad Dermatol [Internet]. 2006 Jan 1;54(1):47–54. Available from: http://www.jaad.org/article/S0190962205026502/fulltext

27. Matis WL, Triana A, Shapiro R, Eldred L, Frank Polk B, Hood AF. Dermatologic findings associated with human immunodeficiency virus infection. J Am Acad Dermatol [Internet]. 1987;17(5 Pt 1):746–51. Available from: https://pubmed.ncbi.nlm.nih.gov/3680653/

28. Olsen JR, Gallacher J, Piguet V, Francis NA. Epidemiology of molluscum contagiosum in children: a systematic review. Fam Pract [Internet]. 2014 Apr;31(2):130–6. Available from: https://pubmed.ncbi.nlm.nih.gov/24297468/

29. Poojary SA, Kokane PT. Giant molluscum contagiosum with granulomatous inflammation and panniculitis: An unusual clinical and histopathological pattern in an HIV seropositive child. Indian J Sex Transm Dis AIDS [Internet]. 2015;36(1):95. Available from: /pmc/articles/PMC4555913/

30. Uzuncakmak TK, Kuru BC, Zemheri EI, Zindanci I, Turkoglu Z, Kavala M. Isolated giant molluscum contagiosum mimicking epidermoid cyst. Dermatol

Pract Concept [Internet]. 2016 Jul 31;6(3):71. Available from: /pmc/articles/PMC5006558/

31. Molluscum contagiosum - Treatment - NHS [Internet]. [cited 2022 Feb 25]. Available from: https://www.nhs.uk/conditions/molluscum-contagiosum/treatment/

32. Somogyi A, Becker M, Gugler R. Cimetidine pharmacokinetics and dosage requirements in children. Eur J Pediatr [Internet]. 1985 May;144(1):72–6. Available from: https://pubmed.ncbi.nlm.nih.gov/4018106/

33. van der Wouden JC, van der Sande R, Kruithof EJ, Sollie A, van Suijlekom-Smit LWA, Koning S. Interventions for cutaneous molluscum contagiosum. Cochrane Database Syst Rev [Internet]. 2017 May 17;5(5). Available from: https://www.cochranelibrary.com/cdsr/doi/10.1002/14651858.CD004767.pub4/full

34. Hughes CM, Damon IK, Reynolds MG. Understanding U.S. healthcare providers' practices and experiences with molluscum contagiosum. PLoS One [Internet]. 2013 Oct 14;8(10). Available from: https://pubmed.ncbi.nlm.nih.gov/24155912/

35. Metkar A, Pande S, Khopkar U. An open, nonrandomized, comparative study of imiquimod 5% cream versus 10% potassium hydroxide solution in the treatment of molluscum contagiosum. Indian J Dermatol Venereol Leprol [Internet]. 2008 Nov 1;74(6):614–8. Available from: https://pubmed.ncbi.nlm.nih.gov/19171985/

36. Silverberg NB, Sidbury R, Mancini AJ. Childhood molluscum contagiosum: experience with cantharidin therapy in 300 patients. J Am Acad Dermatol [Internet]. 2000;43(3):503–7. Available from: https://pubmed.ncbi.nlm.nih.gov/10954663/

37. Syed TA, Lundin S, Alimad M. Topical 0.3% and 0.5% podophyllotoxin cream for self-treatment of molluscum contagiosum in males. A placebo-controlled, double-blind study. Dermatology [Internet]. 1994;189(1):65–8. Available from: https://pubmed.ncbi.nlm.nih.gov/8003791/

38. Chapa PJ, Mavura DR, Philemon R, Kini L, Masenga EJ. Contributing Factors and Outcome after Cryotherapy of Molluscum Contagiosum among Patients Attending

Tertiary Hospital, Northern Tanzania: A Descriptive Prospective Cohort Study. Dermatol Res Pract [Internet]. 2021;2021. Available from: /pmc/articles/PMC8266469/

39. Simonart T, De Maertelaer V. Curettage treatment for molluscum contagiosum: a follow-up survey study. Br J Dermatol [Internet]. 2008 Nov;159(5):1144–7. Available from: https://pubmed.ncbi.nlm.nih.gov/18795919/

40. Griffith RD, Yazdani Abyaneh MA, Falto-Aizpurua L, Mouri K. Pulsed Dye Laser Therapy for Molluscum Contagiosum: A Systematic Review. J Drugs Dermatology [Internet]. 2014;13(11). Available from: https://jddonline.com/articles/pulsed-dye-laser-therapy-for-molluscum-contagiosum-a-systematic-review-S1545961614P1349X

41. Weller R, O'Callaghan CJ, MacSween RM, White MI. Scarring in molluscum contagiosum: comparison of physical expression and phenol ablation. BMJ Br Med J [Internet]. 1999 Dec 12;319(7224):1540. Available from: /pmc/articles/PMC28297/

42. Sen S, Bhaumik P. Resolution of giant Molluscum contagiosum with antiretroviral therapy. Indian J Dermatol Venereol Leprol [Internet]. 2008 May 1;74(3):267–8. Available from: https://pubmed.ncbi.nlm.nih.gov/18583804/

43. Meza-Romero R, Navarrete-Dechent C, Downey C. Molluscum contagiosum: an update and review of new perspectives in etiology, diagnosis, and treatment. Clin Cosmet Investig Dermatol [Internet]. 2019;12:373. Available from: /pmc/articles/PMC6553952/

44. Ehmann R, Brandes K, Antwerpen M, Walter M, Schlippenbach K V, Stegmaier E, et al. Molecular and genomic characterization of a novel equine molluscum contagiosum-like virus. J Gen Virol. 2021;102(3):1357.

45. Chen X, Anstey A V., Bugert JJ. Molluscum contagiosum virus infection. Lancet Infect Dis. 2013 Oct 1;13(10):877–88.

46. Trčko K, Hošnjak L, Kušar B, Zorec TM, Kocjan BJ, Križmarić M, et al. Clinical, Histopathological, and Virological Evaluation of 203 Patients With a Clinical Diagnosis of Molluscum Contagiosum. Open Forum Infect Dis [Internet]. 2018

Nov 1;5(11). Available from: /pmc/articles/PMC6284465/

47. Leung AK., Barankin B, Hon KL. Molluscum Contagiosum: An Update. Recent Pat Inflamm Allergy Drug Discov. 2017 May 18;11(1).

48. Trama JP, Adelson ME, Mordechai E. Identification and genotyping of molluscum contagiosum virus from genital swab samples by real-time PCR and Pyrosequencing. J Clin Virol. 2007 Dec 1;40(4):325–9.

49. Hošnjak L, Kocjan BJ, Kušar B, Seme K, Poljak M. Rapid detection and typing of Molluscum contagiosum virus by FRET-based real-time PCR. J Virol Methods [Internet]. 2013 Feb;187(2):431–4. Available from: https://pubmed.ncbi.nlm.nih.gov/23174165/

50. Senkevich TG, Bugert JJ, Sisler JR, Koonin E V., Darai G, Moss B. Genome sequence of a human tumorigenic poxvirus: prediction of specific host response-evasion genes. Science [Internet]. 1996;273(5276):813–6. Available from: https://pubmed.ncbi.nlm.nih.gov/8670425/

51. Senkevich TG, Koonin E V., Bugert JJ, Darai G, Moss B. The genome of molluscum contagiosum virus: analysis and comparison with other poxviruses. Virology [Internet]. 1997 Jun 23;233(1):19–42. Available from: https://pubmed.ncbi.nlm.nih.gov/9201214/

52. Moyer RW, Graves RL. The mechanism of cytoplasmic orthopoxvirus DNA replication. Cell [Internet]. 1981;27(2 Pt 1):391–401. Available from: https://pubmed.ncbi.nlm.nih.gov/6277506/

53. Bugert JJ, Ehmann R. Viruses as Infectious Agents: Human and Animal Viruses. Encycl Virol Vol 1-5, Fourth Ed. 2021 Jan 1;1–5:629–33.

54. Katsafanas GC, Moss B. Colocalization of Transcription and Translation within Cytoplasmic Poxvirus Factories Coordinates Viral Expression and Subjugates Host Functions.

55. Fernández de Castro I, Tenorio R, Risco C. Virus Factories. Encycl Virol [Internet]. 2021 Jan 1;1–5:495. Available from: /pmc/articles/PMC7329290/

56. Hyun J. Poxvirus under the eyes of electron microscope. Appl Microsc [Internet]. 2022 Dec 1;52(1). Available from: /pmc/articles/PMC9659681/

57. Neva FA. Studies on molluscum contagiosum. Observations on the cytopathic effect of molluscum suspensions in vitro. Arch Intern Med [Internet]. 1962;110(5):720–5. Available from: https://pubmed.ncbi.nlm.nih.gov/13938198/

58. Burnett JW, Neva FA. Studies on the mechanism of molluscum contagiosum cytotoxicity. J Invest Dermatol [Internet]. 1966;46(1):76–83. Available from: https://pubmed.ncbi.nlm.nih.gov/5910975/

59. Bugert JJ, Melquiot N, Kehm R. Molluscum contagiosum virus expresses late genes in primary human fibroblasts but does not produce infectious progeny. Virus Genes [Internet]. 2001;22(1):27–33. Available from: https://pubmed.ncbi.nlm.nih.gov/11210936/

60. Biswas S, Smith GL, Roy EJ, Ward B, Shisler JL. A comparison of the effect of molluscum contagiosum virus MC159 and MC160 proteins on vaccinia virus virulence in intranasal and intradermal infection routes. J Gen Virol [Internet]. 2018 Feb 1;99(2):246. Available from: /pmc/articles/PMC5884965/

61. Prose PH, Friedman-Kien AE, Viliek J. Molluscum Contagiosum Virus in Adult Human Skin Cultures: An Electron Microscopic Study. Am J Pathol. 1969;55(3).

62. Alberts B, Johnson A, Lewis J, Raff M, Roberts K, Walter P. Innate Immunity. In: Molecular Biology of the Cell, 4th Edition [Internet]. 4th ed. Garland Science; 2002. Available from: https://www.ncbi.nlm.nih.gov/books/NBK26846/

63. Innate Immunity - Molecular Biology of the Cell - NCBI Bookshelf [Internet]. [cited 2021 Feb 8]. Available from: https://www.ncbi.nlm.nih.gov/books/NBK26846/

64. Mogensen TH. Pathogen Recognition and Inflammatory Signaling in Innate Immune Defenses. Clin Microbiol Rev [Internet]. 2009 Apr [cited 2022 Jan 20];22(2):240. Available from: /pmc/articles/PMC2668232/

65. Schleimer RP, Kato A, Kern R, Kuperman D, Avila PC. Epithelium: At the interface of innate and adaptive immune responses. J Allergy Clin Immunol [Internet]. 2007 Dec [cited 2022 Jan 20];120(6):1279. Available from: /pmc/articles/PMC2810155/

66. Bautista-Hernández LA, Gómez-Olivares JL, Buentello-Volante B, Lucio VMB

de. Fibroblasts: The Unknown Sentinels Eliciting Immune Responses Against Microorganisms. Eur J Microbiol Immunol (Bp) [Internet]. 2017 Sep [cited 2022 Jan 20];7(3):151. Available from: /pmc/articles/PMC5632742/

67. Medzhitov R, Janeway CA. Innate immune recognition and control of adaptive immune responses. Semin Immunol [Internet]. 1998 [cited 2022 Jan 20];10(5):351–3. Available from: https://pubmed.ncbi.nlm.nih.gov/9799709/

68. Bianchi ME. DAMPs, PAMPs and alarmins: all we need to know about danger. J Leukoc Biol [Internet]. 2007 Jan [cited 2022 Jan 20];81(1):1–5. Available from: https://www.researchgate.net/publication/6761949_DAMPs_PAMPs_and_alarmins_all_we_need_to_know_about_danger

69. Tang D, Kang R, Coyne CB, Zeh HJ, Lotze MT. PAMPs and DAMPs: signal 0s that spur autophagy and immunity. Immunol Rev [Internet]. 2012 Sep 1 [cited 2022 Jan 20];249(1):158–75. Available from: https://onlinelibrary.wiley.com/doi/full/10.1111/j.1600-065X.2012.01146.x

70. Heise MT. Viral Pathogenesis. Ref Modul Biomed Sci. 2014 Jan 1;

71. Lawler C, Brady G. Poxviral Targeting of Interferon Regulatory Factor Activation. Viruses [Internet]. 2020 Oct 20 [cited 2021 Oct 10];12(10):1191. Available from: https://www.mdpi.com/1999-4915/12/10/1191/htm

72. Carty M, Guy C, Bowie AG. Detection of Viral Infections by Innate Immunity. Vol. 183, Biochemical Pharmacology. Elsevier Inc.; 2021. p. 114316.

73. Vénéreau E, Ceriotti C, Bianchi ME. DAMPs from cell death to new life. Front Immunol. 2015;6(AUG):422.

74. Roh JS, Sohn DH. Damage-Associated Molecular Patterns in Inflammatory Diseases. Immune Netw [Internet]. 2018 Aug 1 [cited 2022 Jan 20];18(4). Available from: /pmc/articles/PMC6117512/

75. Schaefer L. Complexity of Danger: The Diverse Nature of Damage-associated Molecular Patterns. J Biol Chem [Internet]. 2014 Dec 19 [cited 2022 Jan 20];289(51):35237. Available from: /pmc/articles/PMC4271212/

76. Newton K, Dixit VM. Signaling in Innate Immunity and Inflammation. Cold Spring Harb Perspect Biol [Internet]. 2012 Mar 1 [cited 2022 Jan

20];4(3):a006049. Available from: http://cshperspectives.cshlp.org/content/4/3/a006049.full

77. Liu J, Qian C, Cao X. Post-Translational Modification Control of Innate Immunity. Immunity. 2016 Jul 19;45(1):15–30.

78. Liu S, Cai X, Wu J, Cong Q, Chen X, Li T, et al. Phosphorylation of innate immune adaptor proteins MAVS, STING, and TRIF induces IRF3 activation. Science (80-) [Internet]. 2015 Mar 13 [cited 2022 Jan 20];347(6227). Available from: https://www.science.org/doi/abs/10.1126/science.aaa2630

79. Hu H, Sun SC. Ubiquitin signaling in immune responses. Cell Res 2016 264 [Internet]. 2016 Mar 25 [cited 2022 Jan 20];26(4):457–83. Available from: https://www.nature.com/articles/cr201640

80. Iwanaszko M, Kimmel M. NF-κB and IRF pathways: cross-regulation on target genes promoter level. BMC Genomics [Internet]. 2015 Dec 17;16(1):307. Available from: https://bmcgenomics.biomedcentral.com/articles/10.1186/s12864-015-1511-7

81. Lawrence T. The Nuclear Factor NF-kB Pathway in Inflammation. Cold Spring Harb Perspect Biol [Internet]. 2009;1(6). Available from: http://cshperspectives.cshlp.org/

82. Hayden MS, Ghosh S. Shared principles in NF-kappaB signaling. Cell [Internet]. 2008 Feb 8;132(3):344–62. Available from: https://pubmed.ncbi.nlm.nih.gov/18267068/

83. Chen FE, Huang D Bin, Chen YQ, Ghosh G. Crystal structure of p50/p65 heterodimer of transcription factor NF-kappaB bound to DNA. Nature [Internet]. 1998 Jan 22 [cited 2022 Jun 16];391(6665):410–2. Available from: https://pubmed.ncbi.nlm.nih.gov/9450761/

84. Albensi BC. What Is Nuclear Factor Kappa B (NF-κB) Doing in and to the Mitochondrion? Front Cell Dev Biol. 2019;0(JULY):154.

85. Bagaev A V., Garaeva AY, Lebedeva ES, Pichugin A V., Ataullakhanov RI, Ataullakhanov FI. Elevated pre-activation basal level of nuclear NF-κB in native macrophages accelerates LPS-induced translocation of cytosolic NF-κB into the

cell nucleus. Sci Rep [Internet]. 2019 Dec 1 [cited 2022 Jun 16];9(1). Available from: /pmc/articles/PMC6418260/

86. Tak PP, Firestein GS. NF-κB: a key role in inflammatory diseases. J Clin Invest. 2001 Jan 1;107(1):7–11.

87. Fallahi-Sichani M, Kirschner DE, Linderman JJ. NF-κB Signaling Dynamics Play a Key Role in Infection Control in Tuberculosis. Front Physiol [Internet]. 2012 [cited 2022 Apr 5];3. Available from: /pmc/articles/PMC3368390/

88. Naumann M, Weßler S, Bartsch C, Wieland B, Meyer TF. Neisseria gonorrhoeae epithelial cell interaction leads to the activation of the transcription factors nuclear factor kappaB and activator protein 1 and the induction of inflammatory cytokines. J Exp Med [Internet]. 1997 Jul 21 [cited 2022 Apr 5];186(2):247–58. Available from: https://pubmed.ncbi.nlm.nih.gov/9221754/

89. Brady G, Bowie AG. Innate immune activation of NFkB and its antagonism by poxviruses. 2014 [cited 2022 Apr 5]; Available from: http://dx.doi.org/10.1016/j.cytogfr.2014.07.004

90. Hiscott J, Kwon H, Génin P. Hostile takeovers: viral appropriation of the NF-kB pathway. J Clin Invest [Internet]. 2001 [cited 2021 Oct 27];107(2):143. Available from: /pmc/articles/PMC199181/

91. Hall BS, Tam W, Sen R, Pereira MEA. Cell-specific Activation of Nuclear Factor-κB by the Parasite Trypanosoma cruzi Promotes Resistance to Intracellular Infection. Mol Biol Cell [Internet]. 2000 [cited 2022 Apr 5];11(1):153. Available from: /pmc/articles/PMC14764/

92. Harte MT, Haga IR, Maloney G, Gray P, Reading PC, Bartlett NW, et al. The Poxvirus Protein A52R Targets Toll-like Receptor Signaling Complexes to Suppress Host Defense. J Exp Med [Internet]. 2003 Feb 2 [cited 2022 Jun 14];197(3):343. Available from: /pmc/articles/PMC2193841/

93. Liu T, Zhang L, Joo D, Sun SC. NF-κB signaling in inflammation [Internet]. Vol. 2, Signal Transduction and Targeted Therapy. Springer Nature; 2017. p. 1–9. Available from: www.nature.com/sigtrans

94. Monaco C, Andreakos E, Kiriakidis S, Mauri C, Bicknell C, Foxwell B, et al.

Canonical pathway of nuclear factor kappa B activation selectively regulates proinflammatory and prothrombotic responses in human atherosclerosis. Proc Natl Acad Sci U S A [Internet]. 2004 Apr 13 [cited 2021 Oct 25];101(15):5634–9. Available from: https://pubmed.ncbi.nlm.nih.gov/15064395/

95. Beg AA, Sha WC, Bronson RT, Ghosh S, Baltimore D. Embryonic lethality and liver degeneration in mice lacking the RelA component of NF-kappa B. Nature [Internet]. 1995 Jul 13 [cited 2022 Jun 15];376(6536):167–70. Available from: https://pubmed.ncbi.nlm.nih.gov/7603567/

96. Sun SC. The non-canonical NF-κB pathway in immunity and inflammation. Nat Rev Immunol 2017 179 [Internet]. 2017 Jun 5 [cited 2021 Oct 24];17(9):545–58. Available from: https://www.nature.com/articles/nri.2017.52

97. Zandi E, Rothwarf DM, Delhase M, Hayakawa M, Karin M. The IkB kinase complex (IKK) contains two kinase subunits, IKKalpha and IKKbeta, necessary for IkappaB phosphorylation and NF-kappaB activation. Cell [Internet]. 1997 Oct 17 [cited 2021 Oct 25];91(2):243–52. Available from: https://pubmed.ncbi.nlm.nih.gov/9346241/

98. Sen R, Baltimore D. Multiple nuclear factors interact with the immunoglobulin enhancer sequences. Cell [Internet]. 1986 Aug 29 [cited 2022 Mar 31];46(5):705–16. Available from: https://pubmed.ncbi.nlm.nih.gov/3091258/

99. Mellits KH, Hay RT, Goodbourn S. Proteolytic degradation of MAD3 (I kappa B alpha) and enhanced processing of the NF-kappa B precursor p105 are obligatory steps in the activation of NF-kappa B. Nucleic Acids Res [Internet]. 1993 Nov 11 [cited 2022 Mar 31];21(22):5059. Available from: /pmc/articles/PMC310617/?report=abstract

100. Baeuerle PA, Baltimore D. Activation of DNA-binding activity in an apparently cytoplasmic precursor of the NF-kappa B transcription factor. Cell [Internet]. 1988 Apr 22 [cited 2022 Mar 31];53(2):211–7. Available from: https://pubmed.ncbi.nlm.nih.gov/3129195/

101. Sun SC, Ganchi PA, Ballard DW, Greene WC. NF-kappa B controls expression of inhibitor I kappa B alpha: evidence for an inducible autoregulatory pathway. Science [Internet]. 1993 [cited 2022 Mar 31];259(5103):1912–5. Available from:

https://pubmed.ncbi.nlm.nih.gov/8096091/

102. Senftleben U, Cao Y, Xiao G, Greten FR, Krähn G, Bonizzi G, et al. Activation by IKKalpha of a second, evolutionary conserved, NF-kappa B signaling pathway. Science [Internet]. 2001 Aug 24 [cited 2021 Oct 25];293(5534):1495–9. Available from: https://pubmed.ncbi.nlm.nih.gov/11520989/

103. Tripathi P, Aggarwal A. NF-kB transcription factor: a key player in the generation of immune response on JSTOR. Curr Sci [Internet]. 2006 Feb 25 [cited 2021 Oct 27];90(4):519–31. Available from: https://www-jstor-org.elib.tcd.ie/stable/24088944?seq=7#metadata_info_tab_contents

104. Tian B, Nowak DE, Brasier AR. A TNF-induced gene expression program under oscillatory NF-κB control. BMC Genomics [Internet]. 2005 Sep 28 [cited 2022 Jun 20];6:137. Available from: /pmc/articles/PMC1262712/

105. Tian B, Nowak DE, Jamaluddin M, Wang S, Brasier AR. Identification of Direct Genomic Targets Downstream of the Nuclear Factor-κB Transcription Factor Mediating Tumor Necrosis Factor Signaling *. J Biol Chem [Internet]. 2005 Apr 29 [cited 2022 Jun 20];280(17):17435–48. Available from: http://www.jbc.org/article/S0021925820659257/fulltext

106. Garofalo R, Sabry M, Jamaluddin M, Yu RK, Casola A, Ogra PL, et al. Transcriptional activation of the interleukin-8 gene by respiratory syncytial virus infection in alveolar epithelial cells: nuclear translocation of the RelA transcription factor as a mechanism producing airway mucosal inflammation. J Virol [Internet]. 1996 Dec [cited 2022 Jun 20];70(12):8773–81. Available from: https://pubmed.ncbi.nlm.nih.gov/8971006/

107. Tian B, Zhang Y, Luxon BA, Garofalo RP, Casola A, Sinha M, et al. Identification of NF-κB-Dependent Gene Networks in Respiratory Syncytial Virus-Infected Cells. J Virol [Internet]. 2002 Jul [cited 2022 Jun 20];76(13):6800. Available from: /pmc/articles/PMC136270/

108. Lawrence T, Gilroy DW, Colville-Nash PR, Willoughby DA. Possible new role for NF-κB in the resolution of inflammation. Nat Med 2001 712 [Internet]. 2001 [cited 2021 Oct 27];7(12):1291–7. Available from: https://www.nature.com/articles/nm1201-1291

109. Tamura T, Yanai H, Savitsky D, Taniguchi T. The IRF family transcription factors in immunity and oncogenesis. Annu Rev Immunol [Internet]. 2008;26:535–84. Available from: https://pubmed.ncbi.nlm.nih.gov/18303999/

110. Fujii Y, Shimizu T, Kusumoto M, Kyogoku Y, Taniguchi T, Hakoshima T. Crystal structure of an IRF-DNA complex reveals novel DNA recognition and cooperative binding to a tandem repeat of core sequences. EMBO J [Internet]. 1999 Sep 15 [cited 2022 Apr 5];18(18):5028–41. Available from: https://onlinelibrary.wiley.com/doi/full/10.1093/emboj/18.18.5028

111. Arakura F, Hida S, Ichikawa E, Yajima C, Nakajima S, Saida T, et al. Genetic control directed toward spontaneous IFN-alpha/IFN-beta responses and downstream IFN-gamma expression influences the pathogenesis of a murine psoriasis-like skin disease. J Immunol [Internet]. 2007 Sep 1 [cited 2022 Apr 5];179(5):3249–57. Available from: https://pubmed.ncbi.nlm.nih.gov/17709541/

112. Honda K, Sakaguchi S, Nakajima C, Watanabe A, Yanai H, Matsumoto M, et al. Selective contribution of IFN-alpha/beta signaling to the maturation of dendritic cells induced by double-stranded RNA or viral infection. Proc Natl Acad Sci U S A [Internet]. 2003 Sep 16 [cited 2022 Apr 5];100(19):10872–7. Available from: https://pubmed.ncbi.nlm.nih.gov/12960379/

113. Pestka S, Krause CD, Walter MR. Interferons, interferon-like cytokines, and their receptors. Immunol Rev [Internet]. 2004 Dec 1 [cited 2021 Nov 1];202(1):8–32. Available from: https://onlinelibrary.wiley.com/doi/full/10.1111/j.0105-2896.2004.00204.x

114. Taniguchi T, Mantei N, Schwarzstein M, Nagata S, Muramatsu M, Weissmann C. Human leukocyte and fibroblast interferons are structurally related. Nat 1980 2855766 [Internet]. 1980 [cited 2021 Nov 1];285(5766):547–9. Available from: https://www.nature.com/articles/285547a0

115. Veer MJ de, Holko M, Frevel M, Walker E, Der S, Paranjape JM, et al. Functional classification of interferon-stimulated genes identified using microarrays. J Leukoc Biol [Internet]. 2001 Jun 1 [cited 2022 Jan 20];69(6):912–20. Available from: https://onlinelibrary.wiley.com/doi/full/10.1189/jlb.69.6.912

116. Der SD, Zhou A, Williams BRG, Silverman RH. Identification of genes

differentially regulated by interferon α, β, or γ using oligonucleotide arrays. Proc Natl Acad Sci U S A [Internet]. 1998 Dec 22 [cited 2022 Jan 20];95(26):15623. Available from: /pmc/articles/PMC28094/

117. McNab F, Mayer-Barber K, Sher A, Wack A, O'Garra A. Type I interferons in infectious disease. Nat Rev Immunol 2015 152 [Internet]. 2015 Jan 23 [cited 2021 Oct 24];15(2):87–103. Available from: https://www.nature.com/articles/nri3787

118. Honda K, Takaoka A, Taniguchi T. Type I Inteferon Gene Induction by the Interferon Regulatory Factor Family of Transcription Factors. Immunity [Internet]. 2006 Sep 1 [cited 2021 Nov 1];25(3):349–60. Available from: http://www.cell.com/article/S1074761306003943/fulltext

119. Au WC, Moore PA, LaFleur DW, Tombal B, Pitha PM. Characterization of the Interferon Regulatory Factor-7 and Its Potential Role in the Transcription Activation of Interferon A Genes. TheJournal Biol Chem [Internet]. 1998;273(44):p29210-29217. Available from: https://www.jbc.org/article/S0021-9258(19)59512-6/pdf

120. Kumagai Y, Takeuchi O, Kato H, Kumar H, Matsui K, Morii E, et al. Alveolar Macrophages Are the Primary Interferon-α Producer in Pulmonary Infection with RNA Viruses. Immunity [Internet]. 2007 Aug 24 [cited 2022 Jun 16];27(2):240–52. Available from: http://www.cell.com/article/S1074761307003779/fulltext

121. Fejer G, Drechsel L, Liese J, Schleicher U, Ruzsics Z, Imelli N, et al. Key Role of Splenic Myeloid DCs in the IFN-αβ Response to Adenoviruses In Vivo. PLOS Pathog [Internet]. 2008 [cited 2022 Jun 16];4(11):e1000208. Available from: https://journals.plos.org/plospathogens/article?id=10.1371/journal.ppat.1000208

122. Brewitz A, Eickhoff S, Dähling S, Quast T, Bedoui S, Kroczek RA, et al. CD8+ T Cells Orchestrate pDC-XCR1+ Dendritic Cell Spatial and Functional Cooperativity to Optimize Priming. Immunity [Internet]. 2017 Feb 21 [cited 2022 Jun 16];46(2):205–19. Available from: http://www.cell.com/article/S1074761317300250/fulltext

123. Barbalat R, Lau L, Locksley RM, Barton GM. Toll-like receptor 2 on inflammatory monocytes induces type I interferon in response to viral but not bacterial ligands. Nat Immunol 2009 1011 [Internet]. 2009 Oct 4 [cited 2022 Jun

16];10(11):1200–7. Available from: https://www.nature.com/articles/ni.1792

124. Bauer J, Dress RJ, Schulze A, Dresing P, Ali S, Deenen R, et al. Cutting Edge: IFN-β Expression in the Spleen Is Restricted to a Subpopulation of Plasmacytoid Dendritic Cells Exhibiting a Specific Immune Modulatory Transcriptome Signature. J Immunol [Internet]. 2016 Jun 1 [cited 2022 Jun 16];196(11):4447–51. Available from: https://www.jimmunol.org/content/196/11/4447

125. Scheu S, Dresing P, Locksley RM. Visualization of IFNβ production by plasmacytoid versus conventional dendritic cells under specific stimulation conditions in vivo. Proc Natl Acad Sci U S A [Internet]. 2008 Dec 23 [cited 2022 Jun 16];105(51):20416–21. Available from: www.pnas.org/cgi/content/full/

126. Schneider K, Loewendorf A, De Trez C, Fulton J, Rhode A, Shumway H, et al. Lymphotoxin-Mediated Crosstalk between B Cells and Splenic Stroma Promotes the Initial Type I Interferon Response to Cytomegalovirus. Cell Host Microbe [Internet]. 2008 Feb 14 [cited 2022 Jun 16];3(2):67–76. Available from: http://www.cell.com/article/S1931312808000280/fulltext

127. Dai J, Megjugorac NJ, Amrute SB, Fitzgerald-Bocarsly P. Regulation of IFN regulatory factor-7 and IFN-alpha production by enveloped virus and lipopolysaccharide in human plasmacytoid dendritic cells. J Immunol [Internet]. 2004 Aug 1 [cited 2022 Apr 5];173(3):1535–48. Available from: https://pubmed.ncbi.nlm.nih.gov/15265881/

128. Ning S, Pagano JS, Barber GN. IRF7: activation, regulation, modification and function. Genes Immun 2011 126 [Internet]. 2011 Apr 14;12(6):399–414. Available from: https://www.nature.com/articles/gene201121

129. Andrilenas KK, Ramlall V, Kurland J, Leung B, Harbaugh AG, Siggers T. DNA-binding landscape of IRF3, IRF5 and IRF7 dimers: implications for dimer-specific gene regulation. Nucleic Acids Res [Internet]. 2018 Mar 16 [cited 2022 Apr 1];46(5):2509–20. Available from: https://academic.oup.com/nar/article/46/5/2509/4816212

130. Yoneyama M, Suhara W, Fujita T. Control of IRF-3 activation by phosphorylation. J Interferon Cytokine Res [Internet]. 2002 [cited 2022 Apr 5];22(1):73–6. Available from: https://pubmed.ncbi.nlm.nih.gov/11846977/

131. Smith EJ, Marié I, Prakash A, García-Sastre A, Levy DE. IRF3 and IRF7 phosphorylation in virus-infected cells does not require double-stranded RNA-dependent protein kinase R or Ikappa B kinase but is blocked by Vaccinia virus E3L protein. J Biol Chem [Internet]. 2001 Mar 23 [cited 2022 Apr 5];276(12):8951–7. Available from: https://pubmed.ncbi.nlm.nih.gov/11124948/

132. Rubio D, Xu RH, Remakus S, Krouse TE, Truckenmiller ME, Thapa RJ, et al. Crosstalk between the Type 1 Interferon and Nuclear Factor Kappa B Pathways Confers Resistance to a Lethal Virus Infection. Cell Host Microbe. 2013 Jun 12;13(6):701–10.

133. Panne D, Maniatis T, Harrison SC. An Atomic Model of the Interferon-β Enhanceosome. Cell [Internet]. 2007 Jun 15 [cited 2022 Jan 31];129(6):1111–23. Available from: http://www.cell.com/article/S0092867407006563/fulltext

134. Kim TK, Maniatis T. The mechanism of transcriptional synergy of an in vitro assembled interferon-beta enhanceosome. Mol Cell [Internet]. 1997 [cited 2022 Apr 4];1(1):119–29. Available from: https://pubmed.ncbi.nlm.nih.gov/9659909/

135. Ryals J, Dierks P, Ragg H, Weissmann C. A 46-nucleotide promoter segment from an IFN-alpha gene renders an unrelated promoter inducible by virus. Cell [Internet]. 1985 [cited 2022 Apr 4];41(2):497–507. Available from: https://pubmed.ncbi.nlm.nih.gov/3986909/

136. Balachandran S, Beg AA. Defining Emerging Roles for NF-κB in Antivirus Responses: Revisiting the Interferon-β Enhanceosome Paradigm. PLOS Pathog [Internet]. 2011 Oct [cited 2022 Apr 4];7(10):e1002165. Available from: https://journals.plos.org/plospathogens/article?id=10.1371/journal.ppat.1002165

137. Bertolusso R, Tian B, Zhao Y, Vergara L, Sabree A, Iwanaszko M, et al. Dynamic Cross Talk Model of the Epithelial Innate Immune Response to Double-Stranded RNA Stimulation: Coordinated Dynamics Emerging from Cell-Level Noise. PLoS One [Internet]. 2014 Apr 7 [cited 2022 Apr 4];9(4):e93396. Available from: https://journals.plos.org/plosone/article?id=10.1371/journal.pone.0093396

138. Barnes BJ, Moore PA, Pitha PM. Virus-specific Activation of a Novel Interferon Regulatory Factor, IRF-5, Results in the Induction of Distinct Interferon a Genes. J Biol Chem [Internet]. 2001;276(26):p23382--23390. Available from:

https://www.jbc.org/action/showPdf?pii=S0021-9258%2820%2978325-0

139. Yanai, Negishi, Taniguchi. The IRF family of transcription factors. 2012; Available from: http://dx.doi.org/10.4161/onci.22475

140. Armstrong MJ, Stang MT, Liu Y, Yan J, Pizzoferrato E, Yim JH. IRF-1 inhibits NF-κB activity, suppresses TRAF2 and cIAP1 and induces breast cancer cell specific growth inhibition. Cancer Biol Ther [Internet]. 2015 Jan 1 [cited 2021 Oct 24];16(7):1029. Available from: /pmc/articles/PMC4622679/

141. Joly S, Rhea L, Volk P, Moreland JG, Dunnwald M. Interferon Regulatory Factor 6 Has a Protective Role in the Host Response to Endotoxic Shock. PLoS One [Internet]. 2016 Apr 1 [cited 2022 Apr 1];11(4). Available from: /pmc/articles/PMC4817988/

142. Panda D, Gjinaj E, Bachu M, Squire E, Novatt H, Ozato K, et al. IRF1 maintains optimal constitutive expression of antiviral genes and regulates the early antiviral response. Front Immunol. 2019;10(MAY):1019.

143. Cai YJ, Wang WS, Yang Y, Sun LH, Teitelbaum DH, Yang H. Up-regulation of intestinal epithelial cell derived IL-7 expression by keratinocyte growth factor through STAT1/IRF-1, IRF-2 pathway. PLoS One [Internet]. 2013 Mar 12 [cited 2022 Jun 20];8(3). Available from: https://pubmed.ncbi.nlm.nih.gov/23554911/

144. Yanai H, Chiba S, Hangai S, Kometani K, Inoue A, Kimura Y, et al. Revisiting the role of IRF3 in inflammation and immunity by conditional and specifically targeted gene ablation in mice. Proc Natl Acad Sci U S A [Internet]. 2018 May 15 [cited 2022 Jun 20];115(20):5253–8. Available from: www.pnas.org/cgi/doi/10.1073/pnas.1803936115

145. Krishnamoorthy V, Kannanganat S, Maienschein-Cline M, Cook SL, Chen J, Bahroos N, et al. The IRF4 Gene Regulatory Module Functions as a Read-Write Integrator to Dynamically Coordinate T Helper Cell Fate. Immunity. 2017 Sep 19;47(3):481-497.e7.

146. Li C, Ying W, Huang Z, Brehm T, Morin A, Vella AT, et al. IRF6 Regulates Alternative Activation by Suppressing PPARγ in Male Murine Macrophages. Endocrinology [Internet]. 2017 Sep 9 [cited 2022 Jun 20];158(9):2837. Available

from: /pmc/articles/PMC5659664/

147. Daffis S, Samuel MA, Suthar MS, Keller BC, Gale M, Diamond MS. Interferon Regulatory Factor IRF-7 Induces the Antiviral Alpha Interferon Response and Protects against Lethal West Nile Virus Infection. J Virol [Internet]. 2008 Sep [cited 2022 Jun 20];82(17):8465–75. Available from: https://journals.asm.org/doi/full/10.1128/JVI.00918-08

148. Wang H, Lee CH, Qi C, Tailor P, Feng J, Abbasi S, et al. IRF8 regulates B-cell lineage specification, commitment, and differentiation. Blood [Internet]. 2008 Nov 11 [cited 2022 Jun 20];112(10):4028. Available from: /pmc/articles/PMC2581985/

149. Suprunenko T, Hofer MJ. The emerging role of interferon regulatory factor 9 in the antiviral host response and beyond. Cytokine Growth Factor Rev. 2016 Jun 1;29:35–43.

150. McWhirter SM, Fitzgerald KA, Rosains J, Rowe DC, Golenbock DT, Maniatis T. IFN-regulatory factor 3-dependent gene expression is defective in Tbk1-deficient mouse embryonic fibroblasts. Proc Natl Acad Sci U S A [Internet]. 2004 Jan;101(1):233–8. Available from: https://pubmed.ncbi.nlm.nih.gov/14679297/

151. Ozato K, Tsujimura H, Tamura T. Toll-like receptor signaling and regulation of cytokine gene expression in the immune system. Biotechniques. 2002;70(72 passim.):Suppl:66-68.

152. Doyle SE, Vaidya SA, O'Connell R, Dadgostar H, Dempsey PW, Wu TT, et al. IRF3 Mediates a TLR3/TLR4-Specific Antiviral Gene Program. Immunity. 2002 Sep 1;17(3):251–63.

153. Mukherjee S, Karmakar S, Babu SPS. TLR2 and TLR4 mediated host immune responses in major infectious diseases: a review. Brazilian J Infect Dis. 2016 Mar 1;20(2):193–204.

154. Civril F, Deimling T, De Oliveira Mann CC, Ablasser A, Moldt M, Witte G, et al. Structural mechanism of cytosolic DNA sensing by cGAS. Nature [Internet]. 2013 [cited 2022 Feb 25];498(7454):332–7. Available from: https://pubmed.ncbi.nlm.nih.gov/23722159/

155. Li X, Shu C, Yi G, Chaton CT, Shelton CL, Diao J, et al. Cyclic GMP-AMP synthase is activated by double-stranded DNA-induced oligomerization. Immunity [Internet]. 2013 Dec 12 [cited 2022 Feb 25];39(6):1019–31. Available from: https://pubmed.ncbi.nlm.nih.gov/24332030/

156. Kato H, Takahasi K, Fujita T. RIG-I-like receptors: cytoplasmic sensors for non-self RNA. Immunol Rev [Internet]. 2011 Sep;243(1):91–8. Available from: https://pubmed.ncbi.nlm.nih.gov/21884169/

157. Yoneyama M, Fujita T. RNA recognition and signal transduction by RIG-I-like receptors. Immunol Rev [Internet]. 2009 Jan [cited 2022 Apr 4];227(1):54–65. Available from: https://pubmed.ncbi.nlm.nih.gov/19120475/

158. Matsushima N, Tanaka T, Enkhbayar P, Mikami T, Taga M, Yamada K, et al. Comparative sequence analysis of leucine-rich repeats (LRRs) within vertebrate toll-like receptors. BMC Genomics [Internet]. 2007 May 21 [cited 2022 Apr 6];8:124. Available from: /pmc/articles/PMC1899181/

159. Bell JK, Mullen GED, Leifer CA, Mazzoni A, Davies DR, Segal DM. Leucine-rich repeats and pathogen recognition in Toll-like receptors. Trends Immunol. 2003 Oct 1;24(10):528–33.

160. Ozinsky A, Underhill DM, Fontenot JD, Hajjar AM, Smith KD, Wilson CB, et al. The repertoire for pattern recognition of pathogens by the innate immune system is defined by cooperation between Toll-like receptors. Proc Natl Acad Sci U S A [Internet]. 2000 Dec 5 [cited 2022 Apr 7];97(25):13766–71. Available from: www.pnas.orgcgidoi10.1073pnas.250476497

161. Lee BL, Moon JE, Shu JH, Yuan L, Newman ZR, Schekman R, et al. UNC93B1 mediates differential trafficking of endosomal TLRs. Elife [Internet]. 2013 Feb 19 [cited 2022 Apr 6];2(2):291. Available from: /pmc/articles/PMC3576711/

162. O'Neill LAJ, Bowie AG. The family of five: TIR-domain-containing adaptors in Toll-like receptor signalling. Nat Rev Immunol [Internet]. 2007 May [cited 2021 Oct 23];7:353–64. Available from: https://pubmed.ncbi.nlm.nih.gov/17457343/

163. Toshchakov VY, Neuwald AF. A survey of TIR domain sequence and structure divergence. Immunogenetics [Internet]. 2020 Apr 1 [cited 2022 Jun

16];72(3):181–203. Available from: https://link.springer.com/article/10.1007/s00251-020-01157-7

164. Francisco S, Billod JM, Merino J, Punzón C, Gallego A, Arranz A, et al. Induction of TLR4/TLR2 Interaction and Heterodimer Formation by Low Endotoxic Atypical LPS. Front Immunol. 2022 Jan 24;12:5951.

165. Stewart CR, Stuart LM, Wilkinson K, van Gils JM, Deng J, Halle A, et al. CD36 ligands promote sterile inflammation through assembly of a Toll-like receptor 4 and 6 heterodimer. Nat Immunol 2009 112 [Internet]. 2009 Dec 27 [cited 2021 Oct 24];11(2):155–61. Available from: https://www.nature.com/articles/ni.1836

166. Shimazu R, Akashi S, Ogata H, Nagai Y, Fukudome K, Miyake K, et al. MD-2, a Molecule that Confers Lipopolysaccharide Responsiveness on Toll-like Receptor 4. J Exp Med [Internet]. 1999 [cited 2021 Oct 21];189(11):1777–82. Available from: http://www.jem.org

167. Kang JY, Lee JO. Structural biology of the Toll-like receptor family. Annu Rev Biochem [Internet]. 2011 Jul 7;80:917–41. Available from: https://pubmed.ncbi.nlm.nih.gov/21548780/

168. Botos I, Segal DM, Davies DR. The Structural Biology of Toll-like Receptors. Structure [Internet]. 2011 Apr 13 [cited 2021 Oct 20];19(4):447–59. Available from: http://www.cell.com/article/S0969212611000724/fulltext

169. Fore F, Indriputri C, Mamutse J, Nugraha J. TLR10 and Its Unique Anti-Inflammatory Properties and Potential Use as a Target in Therapeutics. Immune Netw [Internet]. 2020 Jun 1 [cited 2021 Oct 21];20(3):e21. Available from: /pmc/articles/PMC7327153/

170. Chockalingam A, Brooks JC, Cameron JL, Blum LK, Leifer CA. TLR9 traffics through the Golgi complex to localize to endolysosomes and respond to CpG DNA. Immunol Cell Biol [Internet]. 2009 Mar 1 [cited 2022 Apr 6];87(3):209–17. Available from: https://onlinelibrary.wiley.com/doi/full/10.1038/icb.2008.101

171. Latz E, Schoenemeyer A, Visintin A, Fitzgerald KA, Monks BG, Knetter CF, et al. TLR9 signals after translocating from the ER to CpG DNA in the lysosome. Nat Immunol 2004 52 [Internet]. 2004 Jan 11 [cited 2022 Apr 6];5(2):190–8.

Available from: https://www.nature.com/articles/ni1028

172. Park B, Brinkmann MM, Spooner E, Lee CC, Kim YM, Ploegh HL. Proteolytic cleavage in an endolysosomal compartment is required for activation of Toll-like receptor 9. Nat Immunol 2008 912 [Internet]. 2008 Oct 19 [cited 2022 Apr 6];9(12):1407–14. Available from: https://www.nature.com/articles/ni.1669

173. Funami K, Matsumoto M, Oshiumi H, Akazawa T, Yamamoto A, Seya T. The cytoplasmic 'linker region' in Toll-like receptor 3 controls receptor localization and signaling. Int Immunol [Internet]. 2004 Aug 1 [cited 2022 Apr 6];16(8):1143–54. Available from: https://academic.oup.com/intimm/article/16/8/1143/865669

174. Tanji H, Ohto U, Shibata T, Miyake K, Shimizu T. Structural reorganization of the Toll-like receptor 8 dimer induced by agonistic ligands. Science [Internet]. 2013 Mar 22 [cited 2022 Mar 31];339(6126):1426–9. Available from: https://pubmed.ncbi.nlm.nih.gov/23520111/

175. Latz E, Verma A, Visintin A, Gong M, Sirois CM, Klein DCG, et al. Ligand-induced conformational changes allosterically activate Toll-like receptor 9. Nat Immunol [Internet]. 2007 [cited 2022 Mar 31];8(7):772–9. Available from: https://pubmed.ncbi.nlm.nih.gov/17572678/

176. Liu L, Botos I, Wang Y, Leonard JN, Shiloach J, Segal DM, et al. Structural basis of toll-like receptor 3 signaling with double-stranded RNA. Science [Internet]. 2008 Apr 18;320(5874):379–81. Available from: https://pubmed.ncbi.nlm.nih.gov/18420935/

177. Hemmi H, Kaisho T, Takeuchi O, Sato S, Sanjo H, Hoshino K, et al. Small anti-viral compounds activate immune cells via the TLR7 MyD88-dependent signaling pathway. Nat Immunol [Internet]. 2002 [cited 2022 Mar 31];3(2):196–200. Available from: https://pubmed.ncbi.nlm.nih.gov/11812998/

178. Gantier MP, Tong S, Behlke MA, Irving AT, Lappas M, Nilsson UW, et al. Rational design of immunostimulatory siRNAs. Mol Ther [Internet]. 2010 Apr [cited 2022 Mar 31];18(4):785–95. Available from: https://pubmed.ncbi.nlm.nih.gov/20125126/

179. Nikolova EN, Goh GB, Brooks CL, Al-Hashimi HM. Characterizing the

protonation state of cytosine in transient G·C hoogsteen base pairs in duplex DNA. J Am Chem Soc [Internet]. 2013 May 8 [cited 2022 Mar 31];135(18):6766–9. Available from: https://pubs.acs.org/doi/abs/10.1021/ja400994e

180. Park C, Lee S, Cho IH, Lee HK, Kim D, Choi SY, et al. TLR3-mediated signal induces proinflammatory cytokine and chemokine gene expression in astrocytes: Differential signaling mechanisms of TLR3-induced IP-10 and IL-8 gene expression. Glia [Internet]. 2006 Feb 1 [cited 2022 Jun 17];53(3):248–56. Available from: https://onlinelibrary.wiley.com/doi/full/10.1002/glia.20278

181. Wang Q, Miller DJ, Bowman ER, Nagarkar DR, Schneider D, Zhao Y, et al. MDA5 and TLR3 Initiate Pro-Inflammatory Signaling Pathways Leading to Rhinovirus-Induced Airways Inflammation and Hyperresponsiveness. PLoS Pathog [Internet]. 2011 May [cited 2022 Jun 17];7(5):1002070. Available from: /pmc/articles/PMC3102730/

182. Li Wang X, Thomas J, Sen GC, Stark GR, Yamashita M, Kang Z, et al. The Dual Functions of IL-1 Receptor-Associated Kinase 2 in TLR9-Mediated IFN and Proinflammatory Cytokine Production. 2022 [cited 2022 Jun 17]; Available from: http://www.jimmunol.org/content/186/5/3006

183. Triantafilou K, Orthopoulos G, Vakakis E, Ahmed MAE, Golenbock DT, Lepper PM, et al. Human cardiac inflammatory responses triggered by Coxsackie B viruses are mainly Toll-like receptor (TLR) 8-dependent. Cell Microbiol. 2005 Aug;7(8):1117–26.

184. Fitzgerald KA, Rowe DC, Barnes BJ, Caffrey DR, Visintin A, Latz E, et al. LPS-TLR4 signaling to IRF-3/7 and NF-kappaB involves the toll adapters TRAM and TRIF. J Exp Med [Internet]. 2003 Oct 6 [cited 2022 Jun 17];198(7):1043–55. Available from: https://pubmed.ncbi.nlm.nih.gov/14517278/

185. Yamamoto M, Sato S, Hemmi H, Uematsu S, Hoshino K, Kaisho T, et al. TRAM is specifically involved in the Toll-like receptor 4-mediated MyD88-independent signaling pathway. Nat Immunol [Internet]. 2003 Nov [cited 2022 Jun 17];4(11):1144–50. Available from: https://pubmed.ncbi.nlm.nih.gov/14556004/

186. Medzhitov R, Preston-Hurlburt P, Kopp E, Stadlen A, Chen C, Ghosh S, et al. MyD88 Is an Adaptor Protein in the hToll/IL-1 Receptor Family Signaling

Pathways. Mol Cell. 1998 Aug 1;2(2):253–8.

187. Clabbers MTB, Holmes S, Muusse TW, Vajjhala PR, Thygesen SJ, Malde AK, et al. MyD88 TIR domain higher-order assembly interactions revealed by microcrystal electron diffraction and serial femtosecond crystallography. Nat Commun 2021 121 [Internet]. 2021 May 10 [cited 2022 Apr 7];12(1):1–14. Available from: https://www.nature.com/articles/s41467-021-22590-6

188. Loiarro M, Gallo G, Fantò N, Santis R De, Carminati P, Ruggiero V, et al. Identification of Critical Residues of the MyD88 Death Domain Involved in the Recruitment of Downstream Kinases. J Biol Chem [Internet]. 2009 Oct 9 [cited 2021 Oct 23];284(41):28093. Available from: /pmc/articles/PMC2788860/

189. Hardiman G, Rock FL, Balasubramanian S, Kastelein RA, Bazan JF. Molecular characterization and modular analysis of human MyD88. Oncogene [Internet]. 1996 Dec 1 [cited 2022 Apr 7];13(11):2467–75. Available from: https://europepmc.org/article/med/8957090

190. Lin SC, Lo YC, Wu H. Helical assembly in the MyD88–IRAK4–IRAK2 complex in TLR/IL-1R signalling. Nature [Internet]. 2010 May 19 [cited 2021 Oct 23];465(7300):885–90. Available from: https://www.nature.com/articles/nature09121

191. Motshwene PG, Moncrieffe MC, Grossmann JG, Kao C, Ayaluru M, Sandercock AM, et al. An Oligomeric Signaling Platform formed by the toll-like receptor signal transducers MyD88 and IRAK-4. J Biol Chem [Internet]. 2009 Sep 11 [cited 2022 Apr 7];284(37):25404–11. Available from: http://www.jbc.org/article/S0021925820306268/fulltext

192. Horng T, Barton GM, Medzhitov R. TIRAP: an adapter molecule in the Toll signaling pathway. Nat Immunol [Internet]. 2001 [cited 2021 Oct 24];2(9):835–41. Available from: https://pubmed.ncbi.nlm.nih.gov/11526399/

193. Yamamoto M, Sato S, Hemmi H, Sanjo H, Uematsu S, Kaisho T, et al. Essential role for TIRAP in activation of the signalling cascade shared by TLR2 and TLR4. Nat 2002 4206913 [Internet]. 2002 Nov 21 [cited 2021 Oct 24];420(6913):324–9. Available from: https://www.nature.com/articles/nature01182

194. Fitzgerald KA, Palsson-McDermott EM, Bowie AG, Jefferies CA, Mansell AS, Brady G, et al. Mal (MyD88-adapter-like) is required for Toll-like receptor-4 signal transduction. Nat 2001 4136851 [Internet]. 2001 Sep 6 [cited 2021 Oct 24];413(6851):78–83. Available from: https://www.nature.com/articles/35092578

195. Choi YJ, Jung J, Chung HK, Im E, Rhee SH. PTEN regulates TLR5-induced intestinal inflammation by controlling Mal/TIRAP recruitment. FASEB J [Internet]. 2013 Jan [cited 2022 Apr 7];27(1):243–54. Available from: https://pubmed.ncbi.nlm.nih.gov/23038756/

196. Uematsu S, Sato S, Yamamoto M, Hirotani T, Kato H, Takeshita F, et al. Interleukin-1 receptor-associated kinase-1 plays an essential role for Toll-like receptor (TLR)7- and TLR9-mediated interferon-{alpha} induction. J Exp Med [Internet]. 2005 Mar 21 [cited 2022 Mar 31];201(6):915–23. Available from: https://pubmed.ncbi.nlm.nih.gov/15767370/

197. Kawai T, Sato S, Ishii KJ, Coban C, Hemmi H, Yamamoto M, et al. Interferon-α induction through Toll-like receptors involves a direct interaction of IRF7 with MyD88 and TRAF6. Nat Immunol 2004 510 [Internet]. 2004 Sep 7 [cited 2021 Oct 24];5(10):1061–8. Available from: https://www.nature.com/articles/ni1118

198. Keating SE, Maloney GM, Moran EM, Bowie AG. IRAK-2 Participates in Multiple Toll-like Receptor Signaling Pathways to NFκB via Activation of TRAF6 Ubiquitination *. J Biol Chem [Internet]. 2007 Nov 16 [cited 2022 Apr 7];282(46):33435–43. Available from: http://www.jbc.org/article/S0021925820716777/fulltext

199. Deng L, Wang C, Spencer E, Yang L, Braun A, You J, et al. Activation of the IkappaB kinase complex by TRAF6 requires a dimeric ubiquitin-conjugating enzyme complex and a unique polyubiquitin chain. Cell [Internet]. 2000 Oct 13 [cited 2022 Mar 31];103(2):351–61. Available from: https://pubmed.ncbi.nlm.nih.gov/11057907/

200. Chen ZJ. Ubiquitination in Signaling to and Activation of IKK. Immunol Rev [Internet]. 2012 Mar [cited 2021 Oct 24];246(1):95. Available from: /pmc/articles/PMC3549672/

201. Hayden MS, Ghosh S. Shared Principles in NF-κB Signaling. Cell [Internet]. 2008

Feb 8 [cited 2021 Oct 24];132(3):344–62. Available from: http://www.cell.com/article/S0092867408001207/fulltext

202. Karin M, Ben-Neriah Y. Phosphorylation Meets Ubiquitination: The Control of NF-κB Activity. http://dx.doi.org/101146/annurev.immunol181621 [Internet]. 2003 Nov 28 [cited 2022 Jan 19];18:621–63. Available from: https://www.annualreviews.org/doi/abs/10.1146/annurev.immunol.18.1.621

203. Honda K, Yanai H, Mizutani T, Negishi H, Shimada N, Suzuki N, et al. Role of a transductional-transcriptional processor complex involving MyD88 and IRF-7 in Toll-like receptor signaling. Proc Natl Acad Sci [Internet]. 2004 Oct 26 [cited 2021 Oct 24];101(43):15416–21. Available from: https://www.pnas.org/content/101/43/15416

204. Schoenemeyer A, Barnes BJ, Mancl ME, Latz E, Goutagny N, Pitha PM, et al. The Interferon Regulatory Factor, IRF5, Is a Central Mediator of Toll-like Receptor 7 Signaling *. J Biol Chem [Internet]. 2005 Apr 29 [cited 2021 Oct 24];280(17):17005–12. Available from: http://www.jbc.org/article/S0021925820658720/fulltext

205. Siegal FP, Kadowaki N, Shodell M, Fitzgerald-Bocarsly PA, Shah K, Ho S, et al. The nature of the principal type 1 interferon-producing cells in human blood. Science [Internet]. 1999 Jun 11 [cited 2022 Jan 19];284(5421):1835–7. Available from: https://pubmed.ncbi.nlm.nih.gov/10364556/

206. Paludan SR, Bowie AG. Immune sensing of DNA. Immunity [Internet]. 2013 May 23 [cited 2021 Oct 24];38(5):870. Available from: /pmc/articles/PMC3683625/

207. Hoebe K, Du X, Georgel P, Janssen E, Tabeta K, Kim SO, et al. Identification of Lps2 as a key transducer of MyD88-independent TIR signalling. Nat 2003 4246950 [Internet]. 2003 Jul 20 [cited 2022 Jun 17];424(6950):743–8. Available from: https://www.nature.com/articles/nature01889

208. Oshiumi H, Matsumoto M, Funami K, Akazawa T, Seya T. TICAM-1, an adaptor molecule that participates in Toll-like receptor 3–mediated interferon-β induction. Nat Immunol 2003 42 [Internet]. 2003 Jan 21 [cited 2022 Jun 17];4(2):161–7. Available from: https://www.nature.com/articles/ni886

209. Choi YJ, Im E, Chung HK, Pothoulakis C, Rhee SH. TRIF Mediates Toll-like Receptor 5-induced Signaling in Intestinal Epithelial Cells. J Biol Chem [Internet]. 2010 Nov 11 [cited 2022 Aug 29];285(48):37570. Available from: /pmc/articles/PMC2988362/

210. Gay NJ, Symmons MF, Gangloff M, Bryant CE. Assembly and localization of Toll-like receptor signalling complexes. Nat Rev Immunol 2014 148 [Internet]. 2014 Jul 25 [cited 2021 Oct 24];14(8):546–58. Available from: https://www.nature.com/articles/nri3713

211. Kagan JC, Su T, Horng T, Chow A, Akira S, Medzhitov R. TRAM couples endocytosis of Toll-like receptor 4 to the induction of interferon-β. Nat Immunol 2008 94 [Internet]. 2008 Feb 24 [cited 2021 Oct 26];9(4):361–8. Available from: https://www.nature.com/articles/ni1569

212. Ullah MO, Sweet MJ, Mansell A, Kellie S, Kobe B. TRIF-dependent TLR signaling, its functions in host defense and inflammation, and its potential as a therapeutic target. [cited 2021 Oct 26]; Available from: www.jleukbio.org

213. Fochi S, Bergamo E, Serena M, Mutascio S, Journo C, Mahieux R, et al. TRAF3 is required for NF-κB pathway activation mediated by HTLV tax proteins. Front Microbiol. 2019;10(JUN):1302.

214. He JQ, Oganesyan G, Saha SK, Zarnegar B, Cheng G. TRAF3 and its biological function. Adv Exp Med Biol [Internet]. 2007 [cited 2022 Jan 19];597:48–59. Available from: https://pubmed.ncbi.nlm.nih.gov/17633016/

215. Häcker H, Redecke V, Blagoev B, Kratchmarova I, Hsu LC, Wang GG, et al. Specificity in Toll-like receptor signalling through distinct effector functions of TRAF3 and TRAF6. Nature [Internet]. 2006 Jan 12 [cited 2022 Feb 1];439(7073):204–7. Available from: https://pubmed.ncbi.nlm.nih.gov/16306937/

216. Oganesyan G, Saha SK, Guo B, He JQ, Shahangian A, Zarnegar B, et al. Critical role of TRAF3 in the Toll-like receptor-dependent and -independent antiviral response. Nat 2005 4397073 [Internet]. 2005 Nov 23 [cited 2022 Feb 1];439(7073):208–11. Available from: https://www.nature.com/articles/nature04374

217. Dietrich N, Lienenklaus S, Weiss S, Gekara NO. Murine Toll-Like Receptor 2 Activation Induces Type I Interferon Responses from Endolysosomal Compartments. PLoS One [Internet]. 2010 [cited 2022 Apr 1];5(4):e10250. Available from: https://journals.plos.org/plosone/article?id=10.1371/journal.pone.0010250

218. Stack J, Doyle SL, Connolly DJ, Reinert LS, O'Keeffe KM, McLoughlin RM, et al. TRAM Is Required for TLR2 Endosomal Signaling to Type I IFN Induction. J Immunol [Internet]. 2014 Dec 15 [cited 2022 Apr 1];193(12):6090–102. Available from: https://www.jimmunol.org/content/193/12/6090

219. Perkins DJ, Polumuri SK, Pennini ME, Lai W, Xie P, Vogel SN. Reprogramming of Murine Macrophages through TLR2 Confers Viral Resistance via TRAF3-Mediated, Enhanced Interferon Production. PLoS Pathog [Internet]. 2013 Jul [cited 2022 Apr 1];9(7):1003479. Available from: /pmc/articles/PMC3708851/

220. Fitzgerald KA, McWhirter SM, Faia KL, Rowe DC, Latz E, Golenbock DT, et al. IKKepsilon and TBK1 are essential components of the IRF3 signaling pathway. Nat Immunol [Internet]. 2003 May 1 [cited 2022 Jan 19];4(5):491–6. Available from: https://pubmed.ncbi.nlm.nih.gov/12692549/

221. Tojima Y, Fujimoto A, Delhase M, Chen Y, Hatekeyama S, Nakayama KI, et al. NAK is an IκB kinase-activating kinase. Nat 2000 4046779 [Internet]. 2000 Apr 13 [cited 2022 Jan 19];404(6779):778–82. Available from: https://www.nature.com/articles/35008109

222. Hiscott J. Triggering the Innate Antiviral Response through IRF-3 Activation *. J Biol Chem [Internet]. 2007 May 25 [cited 2021 Oct 24];282(21):15325–9. Available from: http://www.jbc.org/article/S0021925820874055/fulltext

223. Perry AK, Chow EK, Goodnough JB, Yeh WC, Cheng G. Differential Requirement for TANK-binding Kinase-1 in Type I Interferon Responses to Toll-like Receptor Activation and Viral Infection. J Exp Med [Internet]. 2004 Jun 21 [cited 2022 Jan 21];199(12):1651–8. Available from: http://www.jem.org/cgi/doi/10.1084/jem.20040528

224. Sharma S, TenOever BR, Grandvaux N, Zhou GP, Lin R, Hiscott J. Triggering the interferon antiviral response through an IKK-related pathway. Science [Internet].

2003 May 16 [cited 2022 Jan 31];300(5622):1148–51. Available from: https://pubmed.ncbi.nlm.nih.gov/12702806/

225. Bouwmeester T, Bauch A, Ruffner H, Angrand PO, Bergamini G, Croughton K, et al. A physical and functional map of the human TNF-alpha/NF-kappa B signal transduction pathway. Nat Cell Biol [Internet]. 2004 Feb [cited 2022 Jan 31];6(2):97–105. Available from: https://pubmed.ncbi.nlm.nih.gov/14743216/

226. Sasai M, Shingai M, Funami K, Yoneyama M, Fujita T, Matsumoto M, et al. NAK-Associated Protein 1 Participates in Both the TLR3 and the Cytoplasmic Pathways in Type I IFN Induction. J Immunol [Internet]. 2006 Dec 15 [cited 2022 Feb 1];177(12):8676–83. Available from: https://www.jimmunol.org/content/177/12/8676

227. Guo B, Cheng G. Modulation of the interferon antiviral response by the TBK1/IKKi adaptor protein TANK. J Biol Chem [Internet]. 2007 Apr 20 [cited 2022 Feb 1];282(16):11817–26. Available from: https://pubmed.ncbi.nlm.nih.gov/17327220/

228. Ryzhakov G, Randow F. SINTBAD, a novel component of innate antiviral immunity, shares a TBK1-binding domain with NAP1 and TANK. EMBO J [Internet]. 2007 Jul 11 [cited 2022 Jan 31];26(13):3180. Available from: /pmc/articles/PMC1914091/

229. Goncalves A, Bürckstümmer T, Dixit E, Scheicher R, Górna MW, Karayel E, et al. Functional dissection of the TBK1 molecular network. PLoS One. 2011;6(9).

230. Chau TL, Gioia R, Gatot JS, Patrascu F, Carpentier I, Chapelle JP, et al. Are the IKKs and IKK-related kinases TBK1 and IKK-ε similarly activated? Trends Biochem Sci. 2008 Apr 1;33(4):171–80.

231. Sasai M, Matsumoto M, Seya T. The kinase complex responsible for IRF-3-mediated IFN-beta production in myeloid dendritic cells (mDC). J Biochem [Internet]. 2006 Feb [cited 2022 Apr 4];139(2):171–5. Available from: https://pubmed.ncbi.nlm.nih.gov/16452304/

232. Kawagoe T, Takeuchi O, Takabatake Y, Kato H, Isaka Y, Tsujimura T, et al. TANK is a negative regulator of Toll-like receptor signaling and is critical for the

prevention of autoimmune nephritis. Nat Immunol [Internet]. 2009 [cited 2022 Feb 1];10(9):965–72. Available from: https://pubmed.ncbi.nlm.nih.gov/19668221/

233. Ermolaeva MA, Michallet MC, Papadopoulou N, Utermöhlen O, Kranidioti K, Kollias G, et al. Function of TRADD in tumor necrosis factor receptor 1 signaling and in TRIF-dependent inflammatory responses. Nat Immunol [Internet]. 2008 [cited 2022 Apr 4];9(9):1037–46. Available from: https://pubmed.ncbi.nlm.nih.gov/18641654/

234. Sharma S, Garg I, Ashraf MZ. TLR signalling and association of TLR polymorphism with cardiovascular diseases. Vascul Pharmacol. 2016 Dec 1;87:30–7.

235. He M, Wang M, Huang Y, Peng W, Zheng Z, Xia N, et al. The ORF3 Protein of Genotype 1 Hepatitis E Virus Suppresses TLR3-induced NF-κB Signaling via TRADD and RIP1. Sci Rep [Internet]. 2016 Jun 8 [cited 2022 Apr 4];6. Available from: https://pubmed.ncbi.nlm.nih.gov/27270888/

236. Cusson-Hermance N, Khurana S, Lee TH, Fitzgerald KA, Kelliher MA. Rip1 mediates the Trif-dependent toll-like receptor 3- and 4-induced NF-{kappa}B activation but does not contribute to interferon regulatory factor 3 activation. J Biol Chem [Internet]. 2005 Nov 4 [cited 2022 Apr 4];280(44):36560–6. Available from: https://pubmed.ncbi.nlm.nih.gov/16115877/

237. Rehwinkel J, Gack MU. RIG-I-like receptors: their regulation and roles in RNA sensing. Nat Rev Immunol 2020 209 [Internet]. 2020 Mar 13 [cited 2021 Oct 27];20(9):537–51. Available from: https://www.nature.com/articles/s41577-020-0288-3

238. Stok JE, Quiroz MEV, Veen AG van der. Self RNA Sensing by RIG-I–like Receptors in Viral Infection and Sterile Inflammation. J Immunol [Internet]. 2020 Aug 15 [cited 2022 Jun 16];205(4):883–91. Available from: https://www.jimmunol.org/content/205/4/883

239. Lee JH, Chiang C, Gack MU. Endogenous Nucleic Acid Recognition by RIG-I-Like Receptors and cGAS. J Interf Cytokine Res [Internet]. 2019 Aug 1 [cited 2022 Jun 16];39(8):450–8. Available from: https://www.liebertpub.com/doi/10.1089/jir.2019.0015

240. Devarkar SC, Schweibenz B, Wang C, Marcotrigiano J, Patel SS. RIG-I Uses an ATPase-Powered Translocation-Throttling Mechanism for Kinetic Proofreading of RNAs and Oligomerization. Mol Cell. 2018 Oct 18;72(2):355-368.e4.

241. Züst R, Cervantes-Barragan L, Habjan M, Maier R, Neuman BW, Ziebuhr J, et al. Ribose 2′-O-methylation provides a molecular signature for the distinction of self and non-self mRNA dependent on the RNA sensor Mda5. Nat Immunol 2011 122 [Internet]. 2011 Jan 9 [cited 2022 Jun 16];12(2):137–43. Available from: https://www.nature.com/articles/ni.1979

242. Gack MU, Shin YC, Joo CH, Urano T, Liang C, Sun L, et al. TRIM25 RING-finger E3 ubiquitin ligase is essential for RIG-I-mediated antiviral activity. Nat 2007 4467138 [Internet]. 2007 Mar 28 [cited 2022 Apr 4];446(7138):916–20. Available from: https://www.nature.com/articles/nature05732

243. Oshiumi H, Matsumoto M, Hatakeyama S, Seya T. Riplet/RNF135, a RING finger protein, ubiquitinates RIG-I to promote interferon-β induction during the early phase of viral infection. J Biol Chem [Internet]. 2009 Jan 9 [cited 2022 Apr 4];284(2):807–17. Available from: http://www.jbc.org/article/S0021925820710951/fulltext

244. Ablasser A, Bauernfeind F, Hartmann G, Latz E, Fitzgerald KA, Hornung V. RIG-I-dependent sensing of poly(dA:dT) through the induction of an RNA polymerase III–transcribed RNA intermediate. Nat Immunol 2009 1010 [Internet]. 2009 Jul 16;10(10):1065–72. Available from: https://www.nature.com/articles/ni.1779

245. Kawai T, Takahashi K, Sato S, Coban C, Kumar H, Kato H, et al. IPS-1, an adaptor triggering RIG-I- and Mda5-mediated type I interferon induction. Nat Immunol 2005 610 [Internet]. 2005 Aug 28 [cited 2022 Apr 4];6(10):981–8. Available from: https://www.nature.com/articles/ni1243

246. Meylan E, Curran J, Hofmann K, Moradpour D, Binder M, Bartenschlager R, et al. Cardif is an adaptor protein in the RIG-I antiviral pathway and is targeted by hepatitis C virus. Nat 2005 4377062 [Internet]. 2005 Sep 21 [cited 2022 Apr 4];437(7062):1167–72. Available from: https://www.nature.com/articles/nature04193

247. Xu LG, Wang YY, Han KJ, Li LY, Zhai Z, Shu HB. VISA Is an Adapter Protein

Required for Virus-Triggered IFN-β Signaling. Mol Cell. 2005 Sep 16;19(6):727–40.

248. Seth RB, Sun L, Ea CK, Chen ZJ. Identification and Characterization of MAVS, a Mitochondrial Antiviral Signaling Protein that Activates NF-κB and IRF3. Cell. 2005 Sep 9;122(5):669–82.

249. Seth RB, Sun L, Ea CK, Chen ZJ. Identification and characterization of MAVS, a mitochondrial antiviral signaling protein that activates NF-κB and IRF3. Cell [Internet]. 2005 Sep 9 [cited 2022 Feb 24];122(5):669–82. Available from: http://www.cell.com/article/S0092867405008160/fulltext

250. Potter JA, Randall RE, Taylor GL. Crystal structure of human IPS-1/MAVS/VISA/Cardif caspase activation recruitment domain. BMC Struct Biol [Internet]. 2008 [cited 2022 Apr 4];8:11. Available from: /pmc/articles/PMC2291057/

251. Sun Q, Sun L, Liu HH, Chen X, Seth RB, Forman J, et al. The Specific and Essential Role of MAVS in Antiviral Innate Immune Responses. Immunity. 2006 May 1;24(5):633–42.

252. Saha SK, Pietras EM, He JQ, Kang JR, Liu SY, Oganesyan G, et al. Regulation of antiviral responses by a direct and specific interaction between TRAF3 and Cardif. EMBO J [Internet]. 2006 Jul 26 [cited 2022 Apr 4];25(14):3257–63. Available from: https://onlinelibrary.wiley.com/doi/full/10.1038/sj.emboj.7601220

253. Kayagaki N, Phung Q, Chan S, Chaudhari R, Quan C, O'Rourke KM, et al. DUBA: A deubiquitinase that regulates type I interferon production. Science (80-) [Internet]. 2007 Dec 7 [cited 2022 Apr 4];318(5856):1628–32. Available from: https://www.science.org/doi/full/10.1126/science.1145918

254. Sharma S, TenOever BR, Grandvaux N, Zhou GP, Lin R, Hiscott J. Triggering the interferon antiviral response through an IKK-related pathway. Science (80-) [Internet]. 2003 May 16 [cited 2022 Apr 4];300(5622):1148–51. Available from: https://www.science.org/doi/full/10.1126/science.1081315

255. Yoshida R, Takaesu G, Yoshida H, Okamoto F, Yoshioka T, Choi Y, et al. TRAF6 and MEKK1 Play a Pivotal Role in the RIG-I-like Helicase Antiviral Pathway *.

J Biol Chem [Internet]. 2008 Dec 26 [cited 2022 Apr 4];283(52):36211–20. Available from: http://www.jbc.org/article/S0021925820496279/fulltext

256. Theofilopoulos AN, Baccala R, Beutler B, Kono DH. TYPE I INTERFERONS (α/β) IN IMMUNITY AND AUTOIMMUNITY. http://dx.doi.org/101146/annurev.immunol23021704115843 [Internet]. 2004 Nov 16 [cited 2022 Apr 4];23:307–36. Available from: https://www.annualreviews.org/doi/abs/10.1146/annurev.immunol.23.021704.115843

257. Zhao T, Yang L, Sun Q, Arguello M, Ballard DW, Hiscott J, et al. The NEMO adaptor bridges the nuclear factor-κB and interferon regulatory factor signaling pathways. Nat Immunol 2007 86 [Internet]. 2007 Apr 29 [cited 2022 Apr 4];8(6):592–600. Available from: https://www.nature.com/articles/ni1465

258. Michallet MC, Meylan E, Ermolaeva MA, Vazquez J, Rebsamen M, Curran J, et al. TRADD Protein Is an Essential Component of the RIG-like Helicase Antiviral Pathway. Immunity. 2008 May 16;28(5):651–61.

259. Balachandran S, Thomas E, Barber GN. A FADD-dependent innate immune mechanism in mammalian cells. Nat 2004 4327015 [Internet]. 2004 Nov 18 [cited 2022 Apr 4];432(7015):401–5. Available from: https://www.nature.com/articles/nature03124

260. Balachandran S, Roberts PC, Kipperman T, Bhalla KN, Compans RW, Archer DR, et al. Alpha/beta interferons potentiate virus-induced apoptosis through activation of the FADD/Caspase-8 death signaling pathway. J Virol [Internet]. 2000 Feb [cited 2022 Apr 4];74(3):1513–23. Available from: https://pubmed.ncbi.nlm.nih.gov/10627563/

261. Kranzusch PJ, Lee ASY, Berger JM, Doudna JA. Structure of human cGAS reveals a conserved family of second-messenger enzymes in innate immunity. Cell Rep [Internet]. 2013 May 30 [cited 2022 Feb 25];3(5):1362–8. Available from: https://pubmed.ncbi.nlm.nih.gov/23707061/

262. Gao P, Ascano M, Wu Y, Barchet W, Gaffney BL, Zillinger T, et al. Cyclic [G(2',5')pA(3',5')p] is the metazoan second messenger produced by DNA-activated cyclic GMP-AMP synthase. Cell [Internet]. 2013 May 23 [cited 2022

Feb 25];153(5):1094–107. Available from: https://pubmed.ncbi.nlm.nih.gov/23647843/

263. Seo GJ, Kim C, Shin WJ, Sklan EH, Eoh H, Jung JU. TRIM56-mediated monoubiquitination of cGAS for cytosolic DNA sensing. Nat Commun 2018 91 [Internet]. 2018 Feb 9 [cited 2022 Jun 16];9(1):1–13. Available from: https://www.nature.com/articles/s41467-018-02936-3

264. Abe T, Barber GN. Cytosolic-DNA-Mediated, STING-Dependent Proinflammatory Gene Induction Necessitates Canonical NF-κB Activation through TBK1. J Virol [Internet]. 2014 May 15 [cited 2022 Apr 4];88(10):5328. Available from: /pmc/articles/PMC4019140/

265. Zhao B, Shu C, Gao X, Sankaran B, Du F, Shelton CL, et al. Structural basis for concerted recruitment and activation of IRF-3 by innate immune adaptor proteins. Proc Natl Acad Sci U S A [Internet]. 2016 Jun 14 [cited 2022 Apr 4];113(24):E3403–12. Available from: /pmc/articles/PMC4914169/

266. Tanaka Y, Chen ZJ. STING specifies IRF3 phosphorylation by TBK1 in the cytosolic DNA signaling pathway. Sci Signal [Internet]. 2012 Mar 6 [cited 2022 Apr 4];5(214). Available from: https://pubmed.ncbi.nlm.nih.gov/22394562/

267. Ishikawa H, Barber GN. STING is an endoplasmic reticulum adaptor that facilitates innate immune signalling. Nature [Internet]. 2008 Oct 2 [cited 2022 Feb 25];455(7213):674–8. Available from: https://pubmed.ncbi.nlm.nih.gov/18724357/

268. Zhang C, Shang G, Gui X, Zhang X, Bai X chen, Chen ZJ. Structural basis of STING binding with and phosphorylation by TBK1. Nature [Internet]. 2019 Mar 21 [cited 2022 Apr 4];567(7748):394–8. Available from: https://pubmed.ncbi.nlm.nih.gov/30842653/

269. Larabi A, Devos JM, Ng SL, Nanao MH, Round A, Maniatis T, et al. Crystal Structure and Mechanism of Activation of TANK-Binding Kinase 1. Cell Rep. 2013 Mar 28;3(3):734–46.

270. Decout A, Katz JD, Venkatraman S, Ablasser A. The cGAS–STING pathway as a therapeutic target in inflammatory diseases. Nat Rev Immunol 2021 219 [Internet].

2021 Apr 8 [cited 2021 Oct 28];21(9):548–69. Available from: https://www.nature.com/articles/s41577-021-00524-z

271. Quan Y, Ji ZL, Wang X, Tartakoff AM, Tao T. Evolutionary and Transcriptional Analysis of Karyopherin β Superfamily Proteins. Mol Cell Proteomics. 2008 Jul 1;7(7):1254–69.

272. Kelley JB, Talley AM, Spencer A, Gioeli D, Paschal BM. Karyopherin α7 (KPNA7), a divergent member of the importin α family of nuclear import receptors. BMC Cell Biol [Internet]. 2010 Aug 11;11. Available from: https://www.researchgate.net/publication/45628652_Karyopherin_a7_KPNA7_a_divergent_member_of_the_importin_a_family_of_nuclear_import_receptors

273. Gabriel G, Klingel K, Otte A, Thiele S, Hudjetz B, Arman-Kalcek G, et al. Differential use of importin-α isoforms governs cell tropism and host adaptation of influenza virus. Nat Commun [Internet]. 2011;2(1):156. Available from: /pmc/articles/PMC3105303/

274. Miyamoto Y, Hieda M, Harreman MT, Fukumoto M, Saiwaki T, Hodel AE, et al. Importin α can migrate into the nucleus in an importin β- and Ran-independent manner. EMBO J [Internet]. 2002 Nov 11;21(21):5833. Available from: /pmc/articles/PMC131066/

275. Kimura M, Okumura N, Kose S, Takao T, Imamoto N. Identification of Cargo Proteins Specific for Importin-β with Importin-α Applying a Stable Isotope Labeling by Amino Acids in Cell Culture (SILAC)-based in Vitro Transport System. J Biol Chem [Internet]. 2013 Aug 8;288(34):24540. Available from: /pmc/articles/PMC3750152/

276. Vogel OA, Forwood JK, Leung DW, Amarasinghe GK, Basler CF. Viral Targeting of Importin Alpha-Mediated Nuclear Import to Block Innate Immunity. Cells [Internet]. 2024 Jan 1;13(1). Available from: /pmc/articles/PMC10778312/

277. Oka M, Yoneda Y. Importin α: functions as a nuclear transport factor and beyond. Proc Jpn Acad Ser B Phys Biol Sci [Internet]. 2018 Aug 8 [cited 2024 Mar 18];94(7):259. Available from: /pmc/articles/PMC6117492/

278. Sorokin A V., Kim ER, Ovchinnikov LP. Nucleocytoplasmic transport of proteins.

Biochem [Internet]. 2007;72(13):1439–57. Available from: https://link.springer.com/article/10.1134/S0006297907130032

279. Cavazza T, Vernos I. The RanGTP pathway: From nucleo-cytoplasmic transport to spindle assembly and beyond. Front Cell Dev Biol. 2016 Jan 11;3(JAN):169805.

280. Lu J, Wu T, Zhang B, Liu S, Song W, Qiao J, et al. Types of nuclear localization signals and mechanisms of protein import into the nucleus. Cell Commun Signal [Internet]. 2021 Dec 1;19(1):1–10. Available from: https://biosignaling.biomedcentral.com/articles/10.1186/s12964-021-00741-y

281. Liang P, Zhang H, Wang G, Li S, Cong S, Luo Y, et al. KPNB1, XPO7 and IPO8 mediate the translocation ofNF-κB/p65 into the nucleus. Traffic [Internet]. 2013 Nov;14(11):1132–43. Available from: https://pubmed.ncbi.nlm.nih.gov/23906023/

282. Lin C, Hu J, Dai Y, Zhang H, Xu K, Dong W, et al. Porcine Circovirus Type 2 Hijacks Host IPO5 to Sustain the Intracytoplasmic Stability of Its Capsid Protein. J Virol [Internet]. 2022 Dec 14;96(23). Available from: https://journals.asm.org/journal/jvi

283. Pallett MA, Ren H, Zhang RY, Scutts SR, Gonzalez L, Zhu Z, et al. Vaccinia Virus BBK E3 Ligase Adaptor A55 Targets Importin-Dependent NF-κB Activation and Inhibits CD8+ T-Cell Memory. J Virol [Internet]. 2019 May 15;93(10). Available from: https://pubmed.ncbi.nlm.nih.gov/30814284/

284. Zhuo Y, Guo Z, Ba T, Zhang C, He L, Zeng C, et al. African Swine Fever Virus MGF360-12L Inhibits Type I Interferon Production by Blocking the Interaction of Importin α and NF-κB Signaling Pathway. Virol Sin [Internet]. 2021 Apr 1;36(2):176–86. Available from: https://link.springer.com/article/10.1007/s12250-020-00304-4

285. Kamata M, Nitahara-Kasahara Y, Miyamoto Y, Yoneda Y, Aida Y. Importin-α Promotes Passage through the Nuclear Pore Complex of Human Immunodeficiency Virus Type 1 Vpr. J Virol [Internet]. 2005 Mar 15;79(6):3557. Available from: /pmc/articles/PMC1075686/

286. Zhang Q, Chen Z, Huang C, Sun J, Xue M, Feng T, et al. Severe Acute Respiratory Syndrome Coronavirus 2 (SARS-CoV-2) Membrane (M) and Spike (S) Proteins Antagonize Host Type I Interferon Response. 2021; Available from: www.frontiersin.org

287. Yu M, Sun L, Zhang Z, Zhang Y, Zhang H, Na L, et al. KPNA6 is a Cofactor of ANP32A/B in Supporting Influenza Virus Polymerase Activity. 2022;

288. Price C, Nguyen AD. Latent Tuberculosis. Rev Chil Enfermedades Respir [Internet]. 2024 Jan 11;28(1):61–8. Available from: https://www.ncbi.nlm.nih.gov/books/NBK599527/

289. Jr JM, Sapra A. Herpes Simplex Type 2. StatPearls [Internet]. 2023 Aug 7; Available from: https://www.ncbi.nlm.nih.gov/books/NBK554427/

290. DiPerna G, Stack J, Bowie AG, Boyd A, Kotwal G, Zhang Z, et al. Poxvirus protein N1L targets the I-κB kinase complex, inhibits signaling to NF-κB by the tumor necrosis factor superfamily of receptors, and inhibits NF-κB and IRF3 signaling by toll-like receptors. J Biol Chem [Internet]. 2004 Aug 27;279(35):36570–8. Available from: http://www.jbc.org/article/S0021925820859031/fulltext

291. Afonso CL, Tulman ER, Lu Z, Zsak L, Osorio FA, Balinsky C, et al. The Genome of Swinepox Virus. J Virol [Internet]. 2002 Jan 15;76(2):783–90. Available from: https://journals.asm.org/doi/10.1128/jvi.76.2.783-790.2002

292. Brady G, Haas DA, Farrell PJ, Pichlmair A, Bowie AG, Mcfadden G. Molluscum Contagiosum Virus Protein MC005 Inhibits NF-B Activation by Targeting NEMO-Regulated IB Kinase Activation Downloaded from. 2017;91:2020. Available from: http://jvi.asm.org/

293. Phelan T, Lawler C, Pichlmair A, Little MA, Bowie AG, Brady G. Molluscum Contagiosum Virus Protein MC008 Targets NF-κB Activation by Inhibiting Ubiquitination of NEMO. J Virol [Internet]. 2023 Mar 30;97(3). Available from: https://journals.asm.org/doi/10.1128/jvi.00108-23

294. Mohr S, Grandemange S, Massimi P, Darai G, Banks L, Martinou JC, et al. Targeting the retinoblastoma protein by MC007L, gene product of the molluscum

contagiosum virus: Detection of a novel virus-cell interaction by a member of the poxviruses. J Virol. 2008 Nov 1;82(21):10625–33.

295. Xiang Y, Moss B. IL-18 binding and inhibition of interferon gamma induction by human poxvirus-encoded proteins. Proc Natl Acad Sci U S A [Internet]. 1999 Sep 28;96(20):11537–42. Available from: https://pubmed.ncbi.nlm.nih.gov/10500212/

296. Xiang Y, Moss B. Molluscum Contagiosum Virus Interleukin-18 (IL-18) Binding Protein Is Secreted as a Full-Length Form That Binds Cell Surface Glycosaminoglycans through the C-Terminal Tail and a Furin-Cleaved Form with Only the IL-18 Binding Domain. J Virol [Internet]. 2003 Feb 15;77(4):2623. Available from: /pmc/articles/PMC141116/

297. Elasifer H, Wang EC, Prod V, Davies J, Forbes S, Stanton RJ, et al. Downregulation of HLA-I by the molluscum contagiosum virus mc080 impacts NK-cell recognition and promotes CD8 + T-cell evasion. J Gen Virol. 2020;101:863–72.

298. Harvey IB, Wang X, Fremont DH. Molluscum contagiosum virus MC80 sabotages MHC-I antigen presentation by targeting tapasin for ER-associated degradation. PLOS Pathog [Internet]. 2019 Apr 1;15(4):e1007711. Available from: https://journals.plos.org/plospathogens/article?id=10.1371/journal.ppat.1007711

299. Brady G, Haas DA, Farrell PJ, Pichlmair A, Bowie AG. Poxvirus Protein MC132 from Molluscum Contagiosum Virus Inhibits NF-B Activation by Targeting p65 for Degradation. 2015; Available from: http://jvi.asm.org/

300. Jin Q, Altenburg JD, Hossain MM, Alkhatib G. Role for the Conserved N-terminal Cysteines in the Anti-Chemokine Activities by the Chemokine-like Protein MC148R1 Encoded by Molluscum Contagiosum Virus. Virology [Internet]. 2011 Sep 9;417(2):449. Available from: /pmc/articles/PMC3760151/

301. Krathwohl MD, Hromas R, Brown DR, Broxmeyer HE, Fife KH. Functional characterization of the C—C chemokine-like molecules encoded by molluscum contagiosum virus types 1 and 2. Proc Natl Acad Sci U S A [Internet]. 1997 Sep 9;94(18):9875. Available from: /pmc/articles/PMC23285/

302. Lüttichau HR, Stine J, Bocsen TP, Johnsen AH, Chantry D, Gerstoft J, et al. A Highly Selective Cc Chemokine Receptor (Ccr)8 Antagonist Encoded by the Poxvirus Molluscum Contagiosum. J Exp Med [Internet]. 2000 Jan 1;191(1):171. Available from: /pmc/articles/PMC2195798/

303. Biswas S, Shisler JL. Molluscum Contagiosum Virus MC159 Abrogates cIAP1-NEMO Interactions and Inhibits NEMO Polyubiquitination. J Virol [Internet]. 2017 Aug;91(15). Available from: https://journals.asm.org/doi/10.1128/jvi.00276-17

304. Randall CMH, Jokela JA, Shisler JL. The MC159 protein from the molluscum contagiosum poxvirus inhibits NF-κB activation by interacting with the IκB kinase complex. J Immunol [Internet]. 2012 Mar 1;188(5):2371–9. Available from: https://pubmed.ncbi.nlm.nih.gov/22301546/

305. Park HH, Lo YC, Lin SC, Wang L, Yang JK, Wu H. The Death Domain Superfamily in Intracellular Signaling of Apoptosis and Inflammation. Annu Rev Immunol [Internet]. 2007 [cited 2021 Oct 23];25:561. Available from: /pmc/articles/PMC2904440/

306. Randall CMH, Biswas S, Selen C V., Shisler JL. Inhibition of interferon gene activation by death-effector domain-containing proteins from the molluscum contagiosum virus. Proc Natl Acad Sci U S A [Internet]. 2014 Jan 14;111(2):E265–72. Available from: https://www.pnas.org/doi/abs/10.1073/pnas.1314569111

307. Nichols DB, Shisler JL. Poxvirus MC160 Protein Utilizes Multiple Mechanisms To Inhibit NF-κB Activation Mediated via Components of the Tumor Necrosis Factor Receptor 1 Signal Transduction Pathway. J Virol [Internet]. 2009 Apr;83(7):3162–74. Available from: https://journals.asm.org/doi/10.1128/jvi.02009-08

308. De Martini W, Coutu J, Bugert J, Iversen T, Cottrell J, Nichols DB. The molluscum contagiosum virus protein MC163 inhibits TNF-α-induced NF-κB activation. https://doi.org/102217/fvl-2019-0018 [Internet]. 2019 May 31;14(5):319–33. Available from: https://www.futuremedicine.com/doi/abs/10.2217/fvl-2019-0018

309. Coutu J, Ryerson MR, Bugert J, Nichols DB. The Molluscum Contagiosum Virus protein MC163 localizes to the mitochondria and dampens mitochondrial mediated apoptotic responses. 2017; Available from: http://dx.doi.org/10.1016/j.virol.2017.02.017

310. Nichols DB, Shisler JL. The MC160 Protein Expressed by the Dermatotropic Poxvirus Molluscum Contagiosum Virus Prevents Tumor Necrosis Factor Alpha-Induced NF-κB Activation via Inhibition of I Kappa Kinase Complex Formation. J Virol [Internet]. 2006 Jan 15;80(2):578–86. Available from: https://journals.asm.org/doi/10.1128/jvi.80.2.578-586.2006

311. Gao C, Pallett MA, Croll TI, Smith GL, Graham SC. Molecular basis of cullin-3 (Cul3) ubiquitin ligase subversion by vaccinia virus protein A55. J Biol Chem [Internet]. 2019 Apr 4;294(16):6416. Available from: /pmc/articles/PMC6484134/

312. McFadden G. Smallpox: An ancient disease enters the modern era of virogenomics. Proc Natl Acad Sci U S A [Internet]. 2004 Oct 10;101(42):14994. Available from: /pmc/articles/PMC524071/

313. Lalani AS, Ness TL, Singh R, Harrison JK, Seet BT, Kelvin DJ, et al. Functional comparisons among members of the poxvirus T1/35kDa family of soluble CC-chemokine inhibitor glycoproteins. Virology [Internet]. 1998 Oct 10;250(1):173–84. Available from: https://pubmed.ncbi.nlm.nih.gov/9770431/

314. Graham KA, Lalani AS, Macen JL, Ness TL, Barry M, Liu LY, et al. The T1/35kDa family of poxvirus-secreted proteins bind chemokines and modulate leukocyte influx into virus-infected tissues. Virology [Internet]. 1997 Mar 3;229(1):12–24. Available from: https://pubmed.ncbi.nlm.nih.gov/9123853/

315. Phelan T, Little MA, Brady G. Targeting of the cGAS-STING system by DNA viruses. Vol. 174, Biochemical Pharmacology. Elsevier Inc.; 2020.

316. Unterholzner L, Keating SE, Baran M, Horan KA, Jensen SB, Sharma S, et al. IFI16 is an innate immune sensor for intracellular DNA. Nat Immunol 2010 1111 [Internet]. 2010 Oct 3;11(11):997–1004. Available from: https://www.nature.com/articles/ni.1932

317. Carty M, Goodbody R, Schröder M, Stack J, Moynagh PN, Bowie AG. The human

adaptor SARM negatively regulates adaptor protein TRIF–dependent Toll-like receptor signaling. Nat Immunol 2006 710 [Internet]. 2006 Sep 10;7(10):1074–81. Available from: https://www.nature.com/articles/ni1382

318. Kaiser WJ, Sridharan H, Huang C, Mandal P, Upton JW, Gough PJ, et al. Toll-like Receptor 3-mediated Necrosis via TRIF, RIP3, and MLKL. J Biol Chem [Internet]. 2013 Oct 25;288(43):31268. Available from: /pmc/articles/PMC3829437/

319. Chen X, Chen Y. Ubiquitination of cGAS by TRAF6 regulates anti-DNA viral innate immune responses. Biochem Biophys Res Commun. 2019 Jun 30;514(3):659–64.

320. Duan T, Du Y, Xing C, Wang HY, Wang RF. Toll-Like Receptor Signaling and Its Role in Cell-Mediated Immunity. Front Immunol [Internet]. 2022 Mar 3;13:812774. Available from: www.frontiersin.org

321. Xie X, Jin J, Zhu L, Jie Z, Li Y, Zhao B, et al. Cell type-specific function of TRAF2 and TRAF3 in regulating type I IFN induction. Cell Biosci 2019 91 [Internet]. 2019 Jan 3 [cited 2021 Oct 24];9(1):1–10. Available from: https://cellandbioscience.biomedcentral.com/articles/10.1186/s13578-018-0268-5

322. Chen F, Chen L, Li Y, Sang H, Zhang C, Yuan S, et al. TRAF3 Positively Regulates Host Innate Immune Resistance to Influenza A Virus Infection. Available from: www.frontiersin.org

323. Chen X, Yang X, Zheng Y, Yang Y, Xing Y, Chen Z. SARS coronavirus papain-like protease inhibits the type I interferon signaling pathway through interaction with the STING-TRAF3-TBK1 complex. Protein Cell [Internet]. 2014 May 1;5(5):369–81. Available from: https://pubmed.ncbi.nlm.nih.gov/24622840/

324. Unterholzner L, Sumner RP, Baran M, Ren H, Mansur DS, Bourke NM, et al. Vaccinia Virus Protein C6 Is a Virulence Factor that Binds TBK-1 Adaptor Proteins and Inhibits Activation of IRF3 and IRF7. PLOS Pathog [Internet]. 2011 Sep;7(9):e1002247. Available from: https://journals.plos.org/plospathogens/article?id=10.1371/journal.ppat.1002247

325. Miyahira AK, Shahangian A, Hwang S, Sun R, Cheng G. TANK-Binding Kinase-1 Plays an Important Role during In Vitro and In Vivo Type I IFN Responses to DNA Virus Infections. J Immunol [Internet]. 2009 Feb 15 [cited 2022 Jan 31];182(4):2248–57. Available from: https://www.jimmunol.org/content/182/4/2248

326. Chen Q, Sun L, Chen ZJ. Regulation and function of the cGAS–STING pathway of cytosolic DNA sensing. Nat Immunol 2016 1710 [Internet]. 2016 Sep 20;17(10):1142–9. Available from: https://www.nature.com/articles/ni.3558

327. Hollenhorst PC. RAS/ERK pathway transcriptional regulation through ETS/AP-1 binding sites. Small GTPases [Internet]. 2012 Jul 7;3(3):154. Available from: /pmc/articles/PMC3442800/

328. Soares-Silva M, Diniz FF, Gomes GN, Bahia D. The Mitogen-Activated Protein Kinase (MAPK) Pathway: Role in Immune Evasion by Trypanosomatids. Front Microbiol [Internet]. 2016 Feb 24;7(FEB). Available from: /pmc/articles/PMC4764696/

329. Newbatt Y, Burns S, Hayward R, Whittaker S, Kirk R, Marshall C, et al. Identification of inhibitors of the kinase activity of oncogenic V600EBRAF in an enzyme cascade high-throughput screen. J Biomol Screen [Internet]. 2006 Mar;11(2):145–54. Available from: https://www.researchgate.net/publication/7408222_Identification_of_Inhibitors_of_the_Kinase_Activity_of_Oncogenic_V600EBRAF_in_an_Enzyme_Cascade_High-Throughput_Screen

330. Margolis B, Skolnik EY. Activation of Ras by receptor tyrosine kinases. J Am Soc Nephrol [Internet]. 1994;5(6):1288–99. Available from: https://pubmed.ncbi.nlm.nih.gov/7893993/

331. Besnard A, Galan-Rodriguez B, Vanhoutte P, Caboche J. Elk-1 a Transcription Factor with Multiple Facets in the Brain. Front Neurosci [Internet]. 2011;5(MAR). Available from: /pmc/articles/PMC3060702/

332. Mayo MW, Norris JL, Baldwin AS. Ras regulation of NF-KB and apoptosis. Methods Enzymol. 2001 Jan 1;333:73–87.

333. Chen GA, Lin YR, Chung HT, Hwang LH. H-Ras exerts opposing effects on type I interferon responses depending on its activation status. Front Immunol [Internet]. 2017 Aug 11;8(AUG):11. Available from: /pmc/articles/PMC5554495/

334. Loo YM, Gale M. Immune signaling by RIG-I-like receptors. Immunity [Internet]. 2011 May 27 [cited 2022 Apr 4];34(5):680–92. Available from: https://pubmed.ncbi.nlm.nih.gov/21616437/

335. Liu T, Zhang L, Joo D, Sun SC. NF-κB signaling in inflammation. Signal Transduct Target Ther 2017 21 [Internet]. 2017 Jul 14;2(1):1–9. Available from: https://www.nature.com/articles/sigtrans201723

336. Takeuchi O, Akira S. Pattern recognition receptors and inflammation. Cell [Internet]. 2010 [cited 2022 Apr 4];140(6):805–20. Available from: https://pubmed.ncbi.nlm.nih.gov/20303872/

337. Valentine R, Smith GL. Inhibition of the RNA polymerase III-mediated dsDNA-sensing pathway of innate immunity by vaccinia virus protein E3. Available from: http://vir.sgmjournals.org

338. Shi JH, Sun SC. Tumor Necrosis Factor Receptor-Associated Factor Regulation of Nuclear Factor κB and Mitogen-Activated Protein Kinase Pathways. Front Immunol. 2018 Aug 9;0(AUG):1849.

339. Xu YR, Lei CQ. TAK1-TABs Complex: A Central Signalosome in Inflammatory Responses. Front Immunol. 2021 Jan 5;11:3208.

340. Peters RT, Maniatis T. A new family of IKK-related kinases may function as IκB kinase kinases. Biochim Biophys Acta - Rev Cancer. 2001 Jan 26;1471(2):M57–62.

341. Hamrashdi M Al, Brady G. Regulation of IRF3 activation in human antiviral signaling pathways. Biochem Pharmacol [Internet]. 2022;200:115026. Available from: http://creativecommons.org/licenses/by/4.0/

342. Quintero-Barceinas RS, Gehringer F, Ducker C, Saxton J, Shaw PE. ELK-1 ubiquitination status and transcriptional activity are modulated independently of F-Box protein FBXO25. J Biol Chem [Internet]. 2021 Jan 1;296. Available from: https://pubmed.ncbi.nlm.nih.gov/33428929/

343. Repasky GA, Cox AD, Hanker AB, Mitin N, Der CJ. Role of R-Ras in Cell Growth. Handb Cell Signaling, 2/e. 2010 Jan 1;2:1753–62.

344. Israël A. The IKK Complex, a Central Regulator of NF-κB Activation. Cold Spring Harb Perspect Biol [Internet]. 2010;2(3). Available from: /pmc/articles/PMC2829958/

345. Bloor S, Ryzhakov G, Wagner S, Butler PJG, Smith DL, Krumbach R, et al. Signal processing by its coil zipper domain activates IKK gamma. Proc Natl Acad Sci U S A [Internet]. 2008 Jan 23;105(4):1279–84. Available from: http://www.pnas.org/cgi/content/full/105/4/1279

346. Beg AA, Baldwin Jr. AS. The IKB proteins: multifunctional regulators of Rel/NF-KB transcription factors. Genes Dev. 1993;7:2064–70.

347. Andersen J, VanScoy S, Cheng TF, Gomez D, Reich NC. IRF-3-dependent and augmented target genes during viral infection. Genes Immun 2008 92 [Internet]. 2007 Dec 20;9(2):168–75. Available from: https://www.nature.com/articles/6364449

348. Traenckner EBM, Pahl HL, Henkel T, Schmidt KN, Wilk S, A.baeuerle P. Phosphorylation of human IκB-α on serines 32 and 36 controls IκB-α proteolysis and NF-κB activation in response to diverse stimuli. EMBO J [Internet]. 1995;14(12):2876–83. Available from: https://www.researchgate.net/publication/15402020_Phosphorylation_of_human_IkB-a_on_serines_32_and_36_controls_IkB-a_proteolysis_and_NF-kB_activation_in_response_to_diverse_stimuli

349. Lu B, Ren Y, Sun X, Han C, Wang H, Chen Y, et al. Induction of INKIT by Viral Infection Negatively Regulates Antiviral Responses through Inhibiting Phosphorylation of p65 and IRF3. Cell Host Microbe. 2017 Jul 12;22(1):86-98.e4.

350. Diel DG, Luo S, Delhon G, Peng Y, Flores EF, Rock DL. A Nuclear Inhibitor of NF-κB Encoded by a Poxvirus. J Virol [Internet]. 2011 Jan;85(1):264. Available from: /pmc/articles/PMC3014193/

351. Siow WX, Chang YT, Babič M, Lu YC, Horák D, Ma YH. Interaction of poly-l-lysine coating and heparan sulfate proteoglycan on magnetic nanoparticle uptake

by tumor cells. Int J Nanomedicine [Internet]. 2018 Mar 20;13:1693. Available from: /pmc/articles/PMC5866726/

352. Hayden MS, Ghosh S. Regulation of NF-κB by TNF Family Cytokines. Semin Immunol [Internet]. 2014;26(3):253. Available from: /pmc/articles/PMC4156877/

353. Moreno R, Sobotzik JM, Schultz C, Schmitz ML. Specification of the NF-κB transcriptional response by p65 phosphorylation and TNF-induced nuclear translocation of IKKε. Nucleic Acids Res [Internet]. 2010 Oct 1;38(18):6029–44. Available from: https://dx.doi.org/10.1093/nar/gkq439

354. Wang D, Westerheide SD, Hanson JL, Baldwin AS. Tumor Necrosis Factor-induced Phosphorylation of RelA/p65 on Ser 529 Is Controlled by Casein Kinase II*. 2000; Available from: http://www.jbc.org

355. Sakurai H, Suzuki S, Kawasaki N, Nakano H, Okazaki T, Chino A, et al. Tumor Necrosis Factor-induced IKK Phosphorylation of NF-B p65 on Serine 536 Is Mediated through the TRAF2, TRAF5, and TAK1 Signaling Pathway*. J Biol Chem [Internet]. 2003;278(38):36916–23. Available from: http://www.jbc.org

356. Zhu H, Liu R, Shang Y, Sun L. Polylysine complexes and their biomedical applications. Eng Regen. 2023 Mar 1;4(1):20–7.

357. Honda K, Takaoka A, Taniguchi T. Type I Inteferon Gene Induction by the Interferon Regulatory Factor Family of Transcription Factors. Immunity [Internet]. 2006 Sep 1;25(3):349–60. Available from: http://www.cell.com/article/S1074761306003943/fulltext

358. Lin R, Heylbroeck C, Pitha PM, Hiscott J. Virus-dependent phosphorylation of the IRF-3 transcription factor regulates nuclear translocation, transactivation potential, and proteasome-mediated degradation. Mol Cell Biol [Internet]. 1998 May 1;18(5):2986–96. Available from: https://pubmed.ncbi.nlm.nih.gov/9566918/

359. Zhang D, Ji L, Chen X, He Y, Sun Y, Ji L, et al. SARS-CoV-2 Nsp15 suppresses type I interferon production by inhibiting IRF3 phosphorylation and nuclear translocation. iScience [Internet]. 2023 Sep 15;26(9):107705. Available from: http://www.cell.com/article/S2589004223017820/fulltext

360. Du H, Yin P, Yang X, Zhang L, Jin Q, Zhu G. Enterovirus 71 2C Protein Inhibits NF-κB Activation by Binding to RelA(p65). Sci Reports 2015 51 [Internet]. 2015 Sep 23;5(1):1–8. Available from: https://www.nature.com/articles/srep14302

361. Schuhmann KM, Pfaller CK, Conzelmann KK. The Measles Virus V Protein Binds to p65 (RelA) To Suppress NF-κB Activity. J Virol [Internet]. 2011 Apr;85(7):3162. Available from: /pmc/articles/PMC3067892/

362. Phospho-NF-κB p65 (Ser536) (93H1) Rabbit mAb | Cell Signaling Technology [Internet]. Available from: https://www.cellsignal.com/products/primary-antibodies/phospho-nf-kb-p65-ser536-93h1-rabbit-mab/3033

363. Geng H, Wittwer T, Dittrich-Breiholz O, Kracht M, Schmitz ML. Phosphorylation of NF-κB p65 at Ser468 controls its COMMD1-dependent ubiquitination and target gene-specific proteasomal elimination. EMBO Rep [Internet]. 2009;10(4):381. Available from: /pmc/articles/PMC2672889/

364. Oostdyk LT, McConnell MJ, Paschal BM. Characterization of the Importin-β binding domain in nuclear import receptor KPNA7. Biochem J [Internet]. 2019 Nov 15;476(21):3413–34. Available from: /biochemj/article/476/21/3413/220914/Characterization-of-the-Importin-binding-domain-in

365. Alshareeda AT, Negm OH, Green AR, Nolan CC, Tighe P, Albarakati N, et al. KPNA2 is a nuclear export protein that contributes to aberrant localisation of key proteins and poor prognosis of breast cancer. Br J Cancer 2015 11212 [Internet]. 2015 May 19;112(12):1929–37. Available from: https://www.nature.com/articles/bjc2015165

366. Christiansen A, Dyrskjøt L. The functional role of the novel biomarker karyopherin α 2 (KPNA2) in cancer. Cancer Lett [Internet]. 2013 Apr 4;331(1):18. Available from: /pmc/articles/PMC7126488/

367. Lott K, Cingolani G. The importin β binding domain as a master regulator of nucleocytoplasmic transport. Biochim Biophys Acta - Mol Cell Res. 2011 Sep 1;1813(9):1578–92.

368. Striegl H, Andrade-Navarro MA, Heinemann U. Armadillo Motifs Involved in

Vesicular Transport. PLoS One [Internet]. 2010 Feb 1;5(2):e8991. Available from: https://journals.plos.org/plosone/article?id=10.1371/journal.pone.0008991

369. Kidd AR, Miskowski JA, Siegfried KR, Sawa H, Kimble J. A β-Catenin Identified by Functional Rather Than Sequence Criteria and Its Role in Wnt/MAPK Signaling. Cell. 2005 Jun 3;121(5):761–72.

370. Tewari R, Bailes E, Bunting KA, Coates JC. Armadillo-repeat protein functions: questions for little creatures. Trends Cell Biol. 2010 Aug 1;20(8):470–81.

371. Kimura M, Imamoto N. Biological Significance of the Importin-β Family-Dependent Nucleocytoplasmic Transport Pathways. Traffic. 2014;15(7):727–48.

372. Tao R, Xu X, Sun C, Wang Y, Wang S, Liu Z, et al. KPNA2 interacts with P65 to modulate catabolic events in osteoarthritis. 2015; Available from: http://dx.doi.org/10.1016/j.yexmp.2015.07.007

373. Rolhion N, Furniss RCD, Grabe G, Ryan A, Liu M, Matthews SA, et al. Inhibition of Nuclear Transport of NF-κB p65 by the Salmonella Type III Secretion System Effector SpvD. PLoS Pathog [Internet]. 2016 May 1;12(5). Available from: /pmc/articles/PMC4883751/

374. Köhler M, Speck C, Christiansen M, Bischoff FR, Prehn S, Haller H, et al. Evidence for Distinct Substrate Specificities of Importin α Family Members in Nuclear Protein Import. Mol Cell Biol [Internet]. 1999 Nov 1;19(11):7782–91. Available from: https://www.tandfonline.com/doi/abs/10.1128/MCB.19.11.7782

375. Top Ten Ways to Optimize siRNA Delivery in Cultured Cells | Thermo Fisher Scientific - IE [Internet]. Available from: https://www.thermofisher.com/ie/en/home/references/ambion-tech-support/rnai-sirna/general-articles/top-ten-ways-to-optimize-sirna-delivery-in-cultured-cells.html

376. Clerman A, Noor Z, Fishelevich R, Lockatell V, Hampton BS, Shah NG, et al. The full-length interleukin-33 (FLIL33)–importin-5 interaction does not regulate nuclear localization of FLIL33 but controls its intracellular degradation. J Biol Chem [Internet]. 2017 Dec 29 [cited 2021 Nov 18];292(52):21653. Available from: /pmc/articles/PMC5766934/

377. Yang D, Geng T, Harrison AG, Cahoon JG, Xing J, Jiao B, et al. UBR5 promotes antiviral immunity by disengaging the transcriptional brake on RIG-I like receptors. Available from: https://doi.org/10.1038/s41467-024-45141-1

378. Henderson MJ, Russell AJ, Hird S, Muñ Oz M, Clancy JL, Lehrbach GM, et al. EDD, the Human Hyperplastic Discs Protein, Has a Role in Progesterone Receptor Coactivation and Potential Involvement in DNA Damage Response*. J Biol Chem [Internet]. 2002;277:26468–78. Available from: http://www.jbc.org

379. Hudjetz B, Lsah Gabriel G. Human-like PB2 627K Influenza Virus Polymerase Activity Is Regulated by Importin-a1 and-a7. 2012; Available from: www.plospathogens.org

380. ThermoFisher. Silencer Select FAQs Thermo Fisher Scientific - IE [Internet]. Available from: https://www.thermofisher.com/ie/en/home/life-science/rnai/synthetic-rnai-analysis/ambion-silencer-select-sirnas/silencer-select-faqs.html

381. Centers for Disease Control and Prevention C. History of Smallpox | Smallpox | CDC [Internet]. Available from: https://www.cdc.gov/smallpox/history/history.html

382. Carolina Londe A, Fernandez-Ruiz R, Rogério Julio P, Appenzeller S, Niewold TB, Londe A, et al. Type I Interferons in Autoimmunity: Implications in Clinical Phenotypes and Treatment Response. J Rheumatol [Internet]. 2023 Sep 1;50(9):1103–13. Available from: https://www.jrheum.org/content/50/9/1103

383. Santamaria P. Advances in Experimental Medicine and Biology: Cytokines and Chemokines in Autoimmune Disease. 2003;520. Available from: www.Eurekah.com;

384. Gu H, Zhang Y, Zeng W, Xia Y. Participation of interferons in psoriatic inflammation. Cytokine Growth Factor Rev. 2022 Apr 1;64:12–20.

385. Lemster BH, Carroll PB, Rilo HR, Johnson N, Nikaein A, Thomson AW. IL-8/IL-8 receptor expression in psoriasis and the response to systemic tacrolimus (FK506) therapy. Clin Exp Immunol [Internet]. 1995;99(2):148. Available from: /pmc/articles/PMC1534299/?report=abstract